

**THE UNIVERSITY OF ALBERTA**

**THE BEHAVIOUR OF A REINFORCED SOIL SLOPE**

**by**

**RICHARD JOHN CHALATURNYK**

**A THESIS**

**SUBMITTED TO THE FACULTY OF GRADUATE STUDIES AND RESEARCH**

**IN PARTIAL FULFILMENT OF THE REQUIREMENTS FOR THE DEGREE**

**OF MASTER OF SCIENCE**

**DEPARTMENT OF CIVIL ENGINEERING**

**EDMONTON, ALBERTA**

**SPRING 1988**



## ABSTRACT

The objective of the research program was to study the factor of safety against shear failure for a nonreinforced and a multilayer reinforced soil slope constructed on a competent foundation.

An 18 m high nonreinforced and reinforced cohesive soil embankment with side slopes of 1:1 was analyzed using the limit equilibrium and the finite element methods of analysis. Bishop's Modified Method, which uses circular slip surfaces and includes the effects of reinforcement, was used to conduct the limit equilibrium analyses. A total stress, plane strain, nonlinear elastic finite element analysis was used to study the stress-deformation behaviour of the slopes. The factor of safety against shear failure, computed from the results of the limit equilibrium and the finite element analyses served as the basis for comparison between the two analytical methods as well as between the nonreinforced and reinforced embankment behaviour. The finite element analysis results are used to show how the reinforcement affects the stress-deformation behaviour of the reinforced soil embankment and to study the partial factors of safety for the soil and the reinforcement.

Comparisons between the safety factors computed from the limit equilibrium and the finite element analyses indicate that Bishop's Modified Method provides conservative factors of safety. The modification of the state of stress

within the soil mass of the reinforced soil slope was found to be a major factor in increasing the factor of safety above that of the nonreinforced slope. A significant difference between the partial safety factors for the soil and the reinforcement indicated that the strain incompatibility between the soil and the reinforcement must be considered in order to select an appropriate overall factor of safety for a reinforced slope.

The finite element analysis results revealed that for reinforced embankments constructed on rigid foundations, the maximum reinforcement load does not occur in the lowest reinforcing layer. As well, two unique relationships between the mobilized reinforcement loads and the position of the reinforcing layers within the embankment were found.

## ACKNOWLEDGEMENTS

The financial support provided by Alberta Transportation and Utilities to the author for the initial period of the research is gratefully acknowledged. The interest and support of the Research and Development Department and the Geotechnical Services Section of the Materials Engineering Branch are appreciated.

The extensive computing work performed on the CDC Cyber 205 at the University of Calgary was made possible by the Department of Civil Engineering, University of Alberta. The Department's patience and understanding concerning the large amount of computing funds spent during this research is gratefully acknowledged.

This research was performed under the supportive guidance of Dr. J.D. Scott. His knowledgeable advice, his sense of right and wrong and his approachability are all warmly acknowledged.

I also wish to acknowledge the support provided by Professor E.A. Richards. Her patient scrutiny of my apparently "written in English" thesis has improved it's quality tremendously. Thank you.

The assistance provided by Dr. D. Chan is immensely appreciated. Without his knowledgeable advice and enthusiasm for the intricacies and complexities of the finite element method, this research would not have been possible.

To my fellow colleagues, especially Linda Bobey and Sangeeta Prasad, a note of thanks for the encouragement and support provided throughout the years of research on this thesis.

A special acknowledgement for my wife, Tracy, who has patiently supported the time required in completing this thesis. As well, I wish to acknowledge her love and courage in allowing me to continue on with my academic endeavours.

To my father, John, I dedicate this thesis. From his love, support and encouragement grew a sense of respect for the pursuit of knowledge and the worth of "getting an education".

## Table of Contents

Chapter	Page
1. INTRODUCTION .....	1
1.1 Statement of Problem .....	1
1.2 Objective of Thesis .....	4
1.3 Organization of Thesis .....	5
2. LITERATURE REVIEW .....	7
2.1 Introduction .....	7
2.2 Stress-Strain Behaviour of Reinforced Soil .....	7
2.2.1 Model Studies .....	7
2.2.2 Interface Behaviour .....	9
2.3 Limit Equilibrium Design Methods .....	12
2.3.1 Current Methods of Analysis .....	12
2.3.2 Summary of Limit Equilibrium Methods .....	23
2.4 Finite Element Analysis of Reinforced Soil .....	23
2.4.1 Discrete Finite Element Methods .....	25
2.4.2 Soil-Reinforcement Interaction .....	28
3. FINITE ELEMENT ANALYSIS OF REINFORCED SOIL .....	31
3.1 Introduction .....	31
3.2 Reinforcement Element .....	32
3.2.1 Introduction .....	32
3.2.2 Reinforcement Element Formulation .....	33
3.2.3 Reinforcement Element Load-Strain Models ..	45
3.2.3.1 Linear Elastic Model .....	45
3.2.3.2 Nonlinear Quadratic Model .....	46
3.2.3.3 Polynomial Elastic Model .....	49
3.3 Verification of Reinforcement Element .....	50
4. FINITE ELEMENT ANALYSIS OF A REINFORCED SOIL SLOPE ..	61

4.1	Introduction .....	61
4.2	Analysis Procedure .....	62
4.3	Material Properties .....	67
4.3.1	Soil .....	67
4.3.2	Reinforcement .....	68
4.4	Nonreinforced Slope Analysis Results .....	70
4.4.1	Stresses .....	73
4.4.2	Strains .....	75
4.4.3	Deformations .....	79
4.5	Reinforced Slope Analysis Results .....	83
4.5.1	Stresses .....	83
4.5.2	Strains .....	84
4.5.3	Deformation .....	88
4.5.4	Reinforcement Loads .....	93
4.6	Discussion on the Influence of the Soil-Reinforcement Interface .....	100
4.7	Comparison of the Nonreinforced and Reinforced Slope Behavior .....	106
4.7.1	Stresses .....	107
4.7.2	Strains .....	109
4.7.3	Deformations .....	117
4.8	Summary and Conclusions .....	117
5.	LIMIT EQUILIBRIUM ANALYSIS OF A REINFORCED SOIL SLOPE .....	122
5.1	Introduction .....	122
5.2	Bishops Modified Method .....	122
5.2.1	Reinforcement Acting as a Free Body Force	126
5.2.2	Reinforcement Acting to Increase the Soil Shear Strength .....	128



5.3	Limit Equilibrium Analysis of a Reinforced Slope .....	133
5.3.1	Introduction .....	133
5.3.2	Reinforced Embankment Geometry .....	134
5.3.3	Soil and Reinforcement Characteristics ...	136
5.3.4	Limit Equilibrium Analysis Results .....	140
5.3.5	Location of Critical Slip Surfaces .....	146
5.4	Summary and Conclusions .....	152
6.	COMPARISON BETWEEN THE LIMIT EQUILIBRIUM AND FINITE ELEMENT ANALYSES .....	154
6.1	Introduction .....	154
6.2	Definition of Safety Factors used in the Comparisons .....	155
6.2.1	Finite Element Safety Factors: Nonreinforced Slope .....	156
6.2.2	Finite Element Safety Factors: Reinforced Slope .....	158
6.2.3	Partial Factor of Safety .....	163
6.3	Comparison of the Nonreinforced Embankment Analyses .....	164
6.4	Comparison of the Reinforced Embankment Analyses .....	168
6.4.1	Reinforced Slope Safety Factors .....	169
6.4.2	Limit Equilibrium Safety Factors .....	171
6.4.3	Improvement in Factor of Safety Due to Reinforcement .....	178
6.4.4	State of Stress Within the Soil of the Reinforced Slope .....	183
6.5	Partial Factors of Safety of the Soil and Reinforcement .....	187
6.6	Verification of Circular Slip Surface Assumption .....	192
6.7	Summary and Conclusions .....	197

7.	CONCLUSIONS AND RECOMMENDATIONS .....	200
7.1	General .....	200
7.2	Conclusions .....	201
7.2.1	Nonreinforced Slope Factors of Safety ....	201
7.2.2	Reinforced Slope Factors of Safety .....	201
7.2.3	Shape of Slip Surfaces Within the Reinforced Slope .....	203
7.2.4	Partial Safety Factor of Soil and Reinforcement .....	203
7.2.5	Load Distribution in Reinforcement .....	204
7.2.6	Stress-Deformation Behaviour .....	206
7.3	Recommendations for Future Research .....	208
	REFERENCES .....	211
	APPENDIX A: General Description of SAFE .....	217
	APPENDIX B: Finite Element Formulation for an Interface Element .....	224
B.1	Introduction .....	224
B.2	Interface Element Formulation .....	225
B.3	Interface Element Constitutive Models .....	234
B.3.1	Linear Elastic Model .....	234
B.3.2	Hyperbolic Model with Linear Failure Envelope .....	235
B.3.3	Hyperbolic Model with Curved Failure Envelope .....	239
	APPENDIX C: Nonreinforced Embankment Finite Element Results .....	242
	APPENDIX D: Embankment Finite Element Results .....	258
	APPENDIX E: Reinforcement Load Distributions from Finite Element Analysis of the Reinforced Embankment .....	274
	APPENDIX F: Factor of Safety Calculations using the Finite Element Results .....	292

F.1 Nonreinforced Slope .....	293
F.2 Reinforced Slope .....	295

## List of Tables

Table	Page
2.1	Limit Equilibrium Methods Applied to Reinforced Soil Systems .....24
4.1	Parameters for the Hyperbolic Elastic Soil Model .....71
4.2	Parameters for the Nonlinear Quadratic Reinforcement Model .....71
5.1	Limit Equilibrium Analysis Results .....141
6.1	Factors of Safety of Nonreinforced and Reinforced Slope .....165
6.2	Partial Factors of Safety for the Soil and Reinforcement .....190
F.1	Stress Distribution Values Along Slip Surface in Nonreinforced Embankment, H = 15 m .....297
F.2	Stress Distribution Values Along Slip Surface in Reinforced Embankment, H = 15 m .....298
F.3	Stress Distribution Values Along Slip Surface in Nonreinforced Embankment, H = 5 m .....299
F.4	Stress Distribution Values Along Slip Surface in Nonreinforced Embankment, H = 10 m .....300
F.5	Stress Distribution Values Along Slip Surface in Nonreinforced Embankment, H = 18 m .....301
F.6	Stress Distribution Values Along Slip Surface in Reinforced Embankment, H = 5 m .....302
F.7	Stress Distribution Values Along Slip Surface in Reinforced Embankment, H = 10 m .....303
F.8	Stress Distribution Values Along Slip Surface in Reinforced Embankment, H = 18 m .....304

## List of Figures

Figure	Page
1.1 Examples of Multilayer Reinforced Slopes (modified from Bonaparte et al. 1986) .....	3
3.1 Degrees of Freedom for Reinforcement Element .....	34
3.2 Geometry for Global to Local Displacement Transformations .....	41
3.3 Linear Elastic Load-Strain Model .....	48
3.4 Nonlinear Quadratic Load-Strain Model .....	48
3.5 Unloading Characteristics of HDPE Geogrid .....	51
3.6 Polynomial Load-Strain Model .....	51
3.7 Element Assemblages for Patch Tests .....	53
3.8 Data for Reinforcement Element Eigenproblem Solution .....	57
3.9 Eigenvectors and Eigenvalues for the Reinforcement Element .....	59
4.1 Nonreinforced and Reinforced Embankment Configurations .....	63
4.2 Finite Element Idealization of the Embankments .....	65
4.3 Embankment Construction Sequences used in Finite Element Analysis .....	66
4.4 Hyperbolic Stress-Strain Relationship used in Modelling Soil Behaviour .....	69
4.5 Nonlinear Quadratic Load-Strain Relationship used in Modelling Reinforcement Behaviour .....	72
4.6 Mobilized Soil Strength (%) in Nonreinforced Embankment, H = 18 m .....	74
4.7 Tensile Stress Zones in Nonreinforced Embankment, H = 18 m .....	76
4.8 Maximum Shear Strains, $\gamma_{max}$ , in Nonreinforced Embankment, H = 18 m .....	77
4.9 Horizontal Strain, $\epsilon_x$ , in Nonreinforced Embankment, H = 18 m .....	78

Figure	Page
4.10 Vertical Strain, $\epsilon_y$ , in Nonreinforced Embankment, H = 18 m .....	80
4.11 Principal Tensile Strains, $\epsilon_3$ , in Nonreinforced Embankment, H = 18 m .....	81
4.12 Velocity Field for Nonreinforced Embankment, H = 18 m, (Scale: 1 cm = .5 m) .....	82
4.13 Mobilized Soil Strength (%) in Reinforced Embankment, H = 18 m .....	85
4.14 Tensile Stress Zones in Reinforced Embankment, H = 18 m .....	86
4.15 Maximum Shear Strain, $\gamma_{max}$ , in Reinforced Embankment, H = 18 m .....	87
4.16 Horizontal Strain, $\epsilon_x$ , in Reinforced Embankment, H = 18 m .....	89
4.17 Vertical Strain, $\epsilon_y$ , in Reinforced Embankment, H = 18 m .....	90
4.18 Principal Tensile Strains, $\epsilon_3$ , in Reinforced Embankment, H = 18 m .....	91
4.19 Velocity Field for Reinforced Embankment, H = 18 m, (Scale: 1 cm = .5 m) .....	92
4.20 Mobilized Loads Along Reinforcement Layer Located 4 m Above the Foundation .....	95
4.21 Parameters used in Defining the Relationship Between $h_i/H$ and $T_i/T_{max}$ .....	96
4.22 Relationship Between the Level of the Reinforcing Layer Within the Embankment and the Mobilized Load in the Reinforcement .....	97
4.23 Relationship Between the Maximum Load and its Location Relative of the Face of the Embankment for any Reinforcing Layer .....	99
4.24 Shear Stress - Displacement Behaviour of Soil-Reinforcement Interface (modified from Bobey, 1988) .....	102
4.25 Shear Stress, $\tau_{xy}$ (kPa), Developed in Reinforced Embankment, H = 18 m .....	105

Figure	Page
4.26 Vertical Stress, $\sigma_y$ (kPa), Developed in Reinforced Embankment, H = 18 m .....	105
4.27 Comparison of Mobilized Soil Strengths in Nonreinforced and Reinforced Embankments, H = 18 m .....	108
4.28 Comparison of Maximum Shear Strains in Nonreinforced and Reinforced Embankments, H = 18 m .....	110
4.29 Comparison of Horizontal Strains in Nonreinforced and Reinforced Embankments, H = 18 m .....	112
4.30 Comparison of Vertical Strains in Nonreinforced and Reinforced Embankments, H = 18 m .....	113
4.31 Reduction in $\epsilon_x$ due to Reinforcement, H = 18 m .....	115
4.32 Reduction in $\epsilon_y$ due to Reinforcement, H = 18 m .....	115
4.33 Comparison of Tensile Strains, $\epsilon_3$ , in Nonreinforced and Reinforced Embankments, H = 18 m .....	116
4.34 Comparison Between Nonreinforced and Reinforced Embankment Deformations, H = 18 m .....	118
5.1 Comparison of Bishop's Simplified Method with other Limit Equilibrium Methods (modified from Fredlund and Krahn, 1976) .....	124
5.2 Slice Forces used in Bishop's Simplified Method .....	125
5.3 Horizontal Reinforcement Force Orientation .....	127
5.4 Tangential Reinforcement Force Orientation .....	127
5.5 Reinforcement Force Orientation assumed by Schmertmann et al. (1987) .....	130
5.6 Geometry for Comparing Reinforcement Force Assumptions .....	130

Figure	Page
5.7	Variation in the Reinforcement Resisting Moment for Different Force Orientation Assumptions .....132
5.8	Reinforced Slope Geometry .....135
5.9	Hyperbolic Stress Strain Curves of Embankment Soil .....137
5.10	Total Stress, Mohr-Coulomb Failure Envelope for Soil .....138
5.11	Load-Strain Relationship of Reinforcement .....138
5.12	Limit Equilibrium Results .....142
5.13	Effect of $F_o$ on the Additional Factor of Safety Provided by the Reinforcement .....144
5.14	Effect of the Nonreinforced Slope Safety Factor, $F_o$ , on the Difference Between Safety Factors Computed for Horizontal and Tangential Reinforcement Force Orientations, $\Delta F_{th}$ .....145
5.15	Critical Slip Surfaces for H = 5 m .....147
5.16	Critical Slip Surfaces for H = 10 m .....147
5.17	Critical Slip Surfaces for H = 15 m .....148
5.18	Critical Slip Surfaces for H = 18 m .....149
5.19	Location of Critical Slip Surface Centers .....151
6.1	Deformed Shape of Reinforcement within the Reinforced Embankment, H = 18 m .....160
6.2	Relationship Between the Level of Reinforcing Layer Within the Embankment and the Mobilized Load in the Reinforcement .....162
6.3	Variation in Nonreinforced Embankment Safety Factors Computed from the Limit Equilibrium and Finite Element Analyses .....167
6.4	Variation in the Reinforced Embankment Safety Factors Computed From the Limit Equilibrium and the Finite Element Analyses .....170



Figure	Page
6.5 Potential Reinforcement Load Distribution for a Slope Height of 5 m .....	172
6.6 Potential Reinforcement Load Distribution for a Slope Height of 10 m .....	172
6.7 Potential Reinforcement Load Distribution for a Slope Height of 15 m .....	173
6.8 Potential Reinforcement Load Distribution for a Slope Height of 18 m .....	174
6.9 Constant Reinforcement Load Distribution for a Slope Height of 18 m .....	176
6.10 Variation in Limit Equilibrium Safety Factors, $F_{r1}$ and $F_{r2}$ .....	177
6.11 Variation in the Nonreinforced and Reinforced Slope Safety Factors, $F_{fe}$ and $F_r$ , Calculated Using the Finite Element Analysis Results .....	179
6.12 Variation in the Nonreinforced and Reinforced Slope Safety Factors, $F_{1e}$ and $F_{r1}$ , Calculated Using the Limit Equilibrium Analysis Results .....	180
6.13 Variation in the Improvement Ratio for the Reinforced Slope .....	182
6.14 Variation in the Nonreinforced Slope Safety Factor, $F_{fe}$ , and $F_{ro}$ .....	184
6.15 Relative Improvement in the Safety Factor due to a Modification of the Soil Stresses by the Reinforcement .....	186
6.16 Variation in the Partial Factors of Safety for the Soil and Reinforcement .....	191
6.17 Comparison Between the Position of the Maximum Reinforcement Loads and Critical Slip Surfaces, $H = 5$ m .....	194
6.18 Comparison Between the Position of the Maximum Reinforcement Loads and Critical Slip Surfaces, $H = 10$ m .....	194
6.19 Comparison Between the Position of the Maximum Reinforcement Loads and Critical Slip Surfaces, $H = 15$ m .....	195

Figure	Page
6.20 Comparison Between the Position of the Maximum Reinforcement Loads and Critical Slip Surfaces, H = 18 m .....	196
7.1 Relationship Between the Level of the Reinforcing Layer within the Embankment and the Mobilized Load in the Reinforcement .....	205
7.2 Relationship Between the Maximum Load and its Location Relative to the Face of the Embankment for any Reinforcing Layer .....	207
A.1 Types of Elements Available in SAFE .....	218
A.2 Material Models Available in SAFE .....	220
A.3 Solution Schemes used in SAFE .....	222
B.1 Interface Element Degrees of Freedom .....	226
B.2 Role of Interface Element in Finite Element Mesh Assemblage .....	226
B.3 Coordinate Transformation Geometry for Interface Element .....	230
B.4 Linear Elastic $\tau$ - $\Delta u$ Model for Interface Element .....	236
B.5 Hyperbolic Elastic $\tau$ - $\Delta u$ Model for Interface Element .....	237
B.6 Hyperbolic Model with Curved Failure Envelope .....	241
C.1 Mobilized Soil Strength (%), H = 5 m .....	243
C.2 Mobilized Soil Strength (%), H = 10 m .....	244
C.3 Mobilized Soil Strength (%), H = 15 m .....	245
C.4 Maximum Shear Strains, H = 5 m .....	246
C.5 Maximum Shear Strains, H = 10 m .....	247
C.6 Maximum Shear Strains, H = 15 m .....	248
C.7 Horizontal Strains, H = 5 m .....	249
C.8 Horizontal Strains, H = 10 m .....	250
C.9 Horizontal Strains, H = 15 m .....	251

Figure	Page
C.10 Vertical Strains, H = 5 m .....	252
C.11 Vertical Strains, H = 10 m .....	253
C.12 Vertical Strains, H = 15 m .....	254
C.13 Velocity Field, H = 5 m, (Scale: 1 cm = .5 m) .....	255
C.14 Velocity Field, H = 10 m, (Scale: 1 cm = .5 m) .....	256
C.15 Velocity Field, H = 15 m, (Scale: 1 cm = .5 m) .....	257
D.1 Mobilized Soil Strength (%), H = 5 m .....	259
D.2 Mobilized Soil Strength (%), H = 10 m .....	260
D.3 Mobilized Soil Strength (%), H = 15 m .....	261
D.4 Maximum Shear Strains, H = 5 m .....	262
D.5 Maximum Shear Strains, H = 10 m .....	263
D.6 Maximum Shear Strains, H = 15 m .....	264
D.7 Horizontal Strains, H = 5 m .....	265
D.8 Horizontal Strains, H = 10 m .....	266
D.9 Horizontal Strains, H = 15 m .....	267
D.10 Vertical Strains, H = 5 m .....	268
D.11 Vertical Strains, H = 10 m .....	269
D.12 Vertical Strains, H = 15 m .....	270
D.13 Velocity Field, H = 5 m, (Scale: 1 cm = .5 m) .....	271
D.14 Velocity Field, H = 10 m, (Scale: 1 cm = .5 m) .....	272
D.15 Velocity Field, H = 15 m, (Scale: 1 cm = .5 m) .....	273
E.1 Load in Reinforcing Layer 1 m Above the Foundation .....	275
E.2 Load in Reinforcing Layer 2 m Above the Foundation .....	276

Figure	Page
E.3 Load in Reinforcing Layer 3 m Above the Foundation .....	277
E.4 Load in Reinforcing Layer 4 m Above the Foundation .....	278
E.5 Load in Reinforcing Layer 5 m Above the Foundation .....	279
E.6 Load in Reinforcing Layer 6 m Above the Foundation .....	280
E.7 Load in Reinforcing Layer 7 m Above the Foundation .....	281
E.8 Load in Reinforcing Layer 8 m Above the Foundation .....	282
E.9 Load in Reinforcing Layer 9 m Above the Foundation .....	283
E.10 Load in Reinforcing Layer 10 m Above the Foundation .....	284
E.11 Load in Reinforcing Layer 11 m Above the Foundation .....	285
E.12 Load in Reinforcing Layer 12 m Above the Foundation .....	286
E.13 Load in Reinforcing Layer 13 m Above the Foundation .....	287
E.14 Load in Reinforcing Layer 14 m Above the Foundation .....	288
E.15 Load in Reinforcing Layer 15 m Above the Foundation .....	289
E.16 Load in Reinforcing Layer 16 m Above the Foundation .....	290
E.17 Load in Reinforcing Layer 17 m Above the Foundation .....	291
F.1 Horizontal Stress, $\sigma_x$ (kPa), Contours Within the Nonreinforced Embankment, H = 15 m .....	305
F.2 Vertical Stress, $\sigma_v$ (kPa), Contours Within the Nonreinforced Embankment, H = 15 m .....	306

Figure	Page
F.3 Shear Stress, $\tau_{xy}$ (kPa), Contours Within the Nonreinforced Embankment, H = 15 m .....	307
F.4 Horizontal Stress, $\sigma_x$ (kPa), Distribution Along the Slip Surface in Nonreinforced Embankment, H = 15 m .....	308
F.5 Vertical Stress, $\sigma_y$ (kPa), Distribution Along Slip Surface in Nonreinforced Embankment, H = 15 m .....	309
F.6 Shear Stress, $\tau_{xy}$ (kPa), Distribution Along Slip Surface in Nonreinforced Embankment, H = 15 m .....	310
F.7 Normal Stress, $\sigma_n$ (kPa), Distribution Along Slip Surface in Nonreinforced Embankment, H = 15 m .....	311
F.8 Mobilized Shear Stress, $\tau$ (kPa), Distribution Along Slip Surface in Nonreinforced Embankment, H = 15 m .....	312
F.9 Horizontal Stress, $\sigma_x$ (kPa), Contours Within the Reinforced Embankment, H = 15 m .....	313
F.10 Vertical Stress, $\sigma_y$ (kPa), Contours Within the Reinforced Embankment, H = 15 m .....	314
F.11 Shear Stress, $\tau_{xy}$ (kPa), Contours Within the Reinforced Embankment, H = 15 m .....	315
F.12 Horizontal Stress, $\sigma_x$ (kPa), Distribution Along the Slip Surface in Reinforced Embankment, H = 15 m .....	316
F.13 Vertical Stress, $\sigma_y$ (kPa), Distribution Along Slip Surface in Reinforced Embankment, H = 15 m .....	317
F.14 Shear Stress, $\tau_{xy}$ (kPa), Distribution Along Slip Surface in Reinforced Embankment, H = 15 m .....	318
F.15 Normal Stress, $\sigma_n$ (kPa), Distribution Along Slip Surface in Reinforced Embankment, H = 15 m .....	319
F.16 Mobilized Shear Stress, $\tau$ (kPa), Distribution Along Slip Surface in Reinforced Embankment, H = 15 m .....	320

## LIST OF SYMBOLS

The following list of symbols is included to assist the interpretation of the equations within the text:

<b>SYMBOL</b>	<b>MEANING</b>
$\sigma_{ij}$	Stress tensor
$\epsilon_{ij}$	Strain tensor
$T_i$	Surface traction tensor
$F_i$	Body force tensor
$\delta q_i$	Virtual displacements
$\int_v dv$	Volume integral
$\int_s ds$	Surface integral
$\int_l dl$	Length integral
$\sigma_a$	Axial stress in reinforcement
$\epsilon_a$	Axial strain in reinforcement
A	Cross sectional area
l	Length
r	Local coordinate axis, ranges from -1 to +1
D	Slope of reinforcement load-strain curve

$\{q_i\}$	Displacements of nodes in global coordinate system
$\{\delta q_i\}$	Virtual displacements of nodes in global coordinate system
[B]	Strain transformation matrix
$Q_i$	Nodal forces
$q_x, q_y$	Nodal displacements in global coordinate system
[N]	Interpolation (shape) function $[N] = [ .5(r^2-r) \quad .5(r^2+r) \quad (1-r^2) ]$
$\bar{l}$	Unit vector defining the orientation of the reinforcement element
$\frac{dx}{dr}$	Variation in x coordinates of element nodes along the element local coordinate system, r
$\frac{dy}{dr}$	Variation in y coordinates of element nodes along the element local coordinate system, r
$q_1$	Nodal displacement obtained by resolving $q_x$ and $q_y$ along $\bar{l}$
[K]	Stiffness matrix
[NR]	$\frac{d[N]}{dr}$ , derivative of [N] with respect to r, the local coordinate axis
$w_i$	Gaussian weighting factors
$r_i$	Gaussian sampling points

[T]	Transformation matrix. Converts global nodal displacements into axial displacements of the reinforcement element
E	Young's modulus
$\nu$	Poisson's ratio
$\gamma_{\max}$	Maximum shear strain
$\epsilon_x$	Horizontal strain
$\epsilon_y$	Vertical strain
$\epsilon_3$	Minor principal strain
$\tau_{\text{mob}}$	Mobilized shear stress
$\sigma_1, \sigma_3$	Major and minor principal stresses
$\sigma_n$	Normal stress
$\tau_{xy}$	Shear stress
$\tau_f$	Shear stress at failure
S	Soil shear strength
C	Cohesion (total stress)
$\phi$	Friction angle (total stress)
$F_0$	Factor of safety of a nonreinforced slope
$F_r$	Factor of safety of a reinforced slope



$\Delta F_r$	Component of $F_r$ provided by the reinforcement
$F_{fe}$	Factor of safety of nonreinforced slope calculated from a finite element analysis
$F_{le}$	Factor of safety of nonreinforced slope calculated from a limit equilibrium analysis
$F_{ro}$	Factor of safety of reinforced slope based on soil stresses only; the resistance moment provided by the reinforcement is neglected in the safety factor calculation
$F_{r1}$	Factor of safety of reinforced slope calculated from a limit equilibrium analysis assuming a reinforcement load distribution from a finite element analysis
$F_{r2}$	Factor of safety of reinforced slope calculated from a limit equilibrium analysis assuming a constant reinforcement design load
$F_{rr}$	Partial factor of safety of the reinforcement alone
$F_{rs}$	Partial factor of safety of the soil alone
$H$	Height of embankment
$h_i$	Height above foundation of reinforcing layer $i$
$M_{ST}$	Resisting moment provided by the soil shear strength

$M_R$	Resisting moment provided by the reinforcement
$M_O$	Overturning or disturbing moment due to soil self weight
$M_{sm}$	Mobilized soil resisting moment under working load conditions
$M_{rm}$	Mobilized reinforcement resisting moment under working load conditions
$R$	Radius of circular slip surface
$T_i$	Force in reinforcing layer $i$
$T_{max}$	Maximum force in any reinforcing layer $i$

# 1. INTRODUCTION

## 1.1 Statement of Problem

The concept of earth reinforcement is not a modern development. Early examples of soil reinforcement, where woven mats of reeds or branches served to reinforce clay brick structures, are known to have existed before the birth of Christ. The best known example of these early reinforced soil structures is the Great Wall of China.

The modern development of earth reinforcement was pioneered by Vidal in the 1960's. Vidal developed the concept of "Reinforced Earth" where flat metal strips are laid horizontally in a frictional soil to provide the means of reinforcement. Due to the success of the "Reinforced Earth" concept, rapid development in the area of soil reinforcement technology has occurred. The reasons for this rapid development are due to inexpensive and uncomplicated construction procedures, tolerance of reinforced soil structures to ground movements and the economy achieved in using soil reinforcement technology (Mitchell, 1987). Presently, the most common applications of reinforced soil technology are in the construction of reinforced walls, slopes and embankments.

This thesis focuses on one aspect of soil reinforcement: the application of planar reinforcement in the construction of steep, multilayer reinforced soil

embankment slopes on competent foundations. The reinforcement permits construction of stable slopes at angles steeper than would be possible without reinforcement. Reinforcement also permits the use of weaker soils for slope construction. The ability to use relatively weak soils for constructing stable soil slopes, the decrease in the required volume of soil and the reduction in the required right-of-way all provide an economic advantage for reinforced soil slope construction. Figure 1.1 illustrates typical examples of multilayer reinforced soil slopes.

The stability of these slopes can be analyzed using limit equilibrium or stress-deformation analyses. Presently, limit equilibrium methods are the most common analytical procedures used in designing reinforced slopes. Satisfactory performance of thousands of reinforced soil structures constructed worldwide suggests that the current design procedures are conservative (Mitchell, 1987). The reason for the conservatism in design lies in the fact that several areas of uncertainty exist regarding the behaviour of reinforced soil. Concerning reinforced slopes, Schneider and Holtz (1986) list as uncertainties the stress field within reinforced slopes, the influence of the reinforcement on the stress field and the selection of appropriate failure mechanisms in reinforced soil slopes. Mitchell (1987) states that research is required on the effects of non-uniform reinforcement lengths, the effects of reinforcement extensibility on the shape and location of failure surfaces,

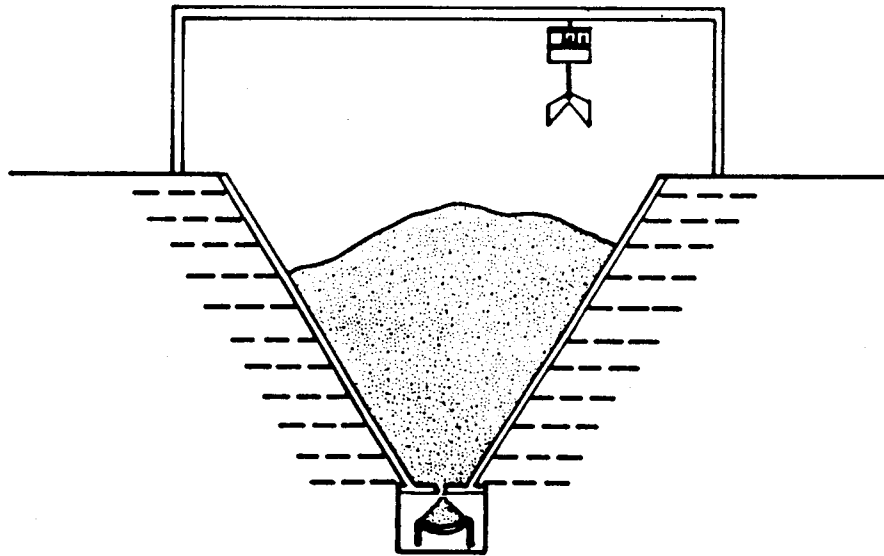
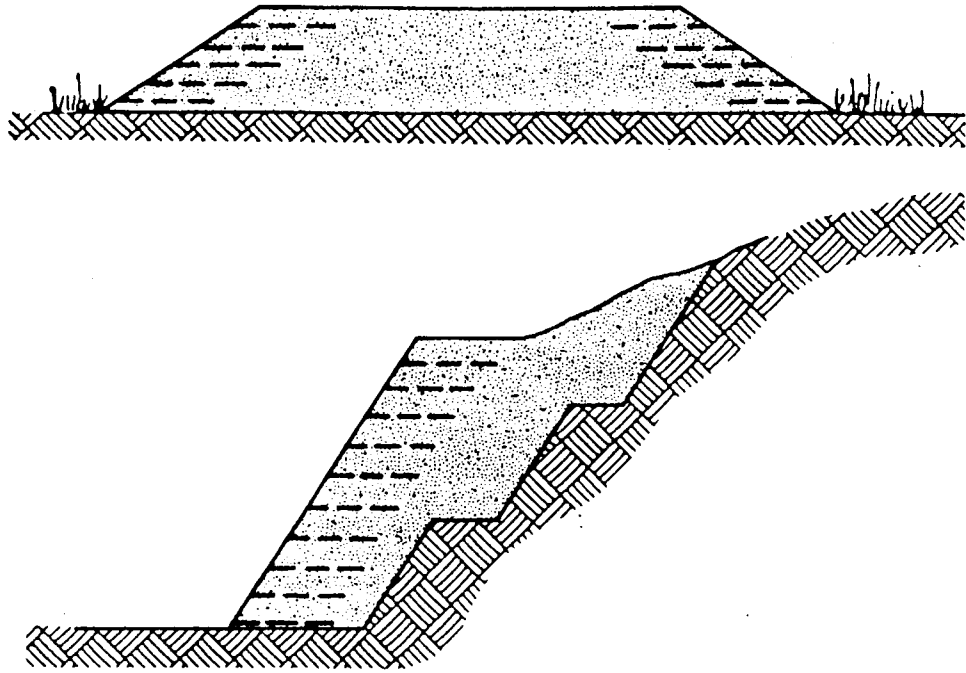


Figure 1.1 Examples of Multilayer Reinforced Slopes  
(modified from Bonaparte et al. 1986)

pullout resistance, internal stress distribution and the behaviour of reinforced cohesive soil structures.

## 1.2 Objective of Thesis

The objective of the research documented in this thesis is to study the factor of safety against shear failure for a nonreinforced and reinforced soil slope constructed on a competent foundation. The reinforcement within the reinforced soil slope is planar or "sheet" reinforcement and should not be confused with reinforcing "strips" as used in the Reinforced Earth concept. The safety factors for the slopes will be computed using the limit equilibrium and the finite element method of analysis.

Comparisons between these safety factors calculated for the nonreinforced slope will be used to gain confidence in the methods of analysis and the techniques used in calculating the factor of safety of the reinforced slope. Extensive experience with the limit equilibrium method of analysis for nonreinforced slopes has demonstrated its reliability and effectiveness which makes it useful for confirming the results of the finite element method of analysis.

Factors of safety computed from the limit equilibrium and finite element analyses of the reinforced soil slope will be compared. Favorable comparisons in the reinforced slope safety factors will provide a measure of confidence in

the results of the analyses. Partial factors of safety for the soil and the reinforcement, determined from the finite element analysis of the reinforced slope, will be calculated.

As a consequence of the wealth of information that can be obtained from a finite element analysis, a secondary objective of the research will be the presentation of the stresses, strains, deformations and reinforcement loads within the reinforced slope. A comparison between the nonreinforced and reinforced slope finite element analyses results will be presented in order to assess how reinforcement affects the stress-deformation behaviour of a reinforced soil slope. This comparison also allows an evaluation of how reinforcement improves the stability or factor of safety of the reinforced soil slope.

### **1.3 Organization of Thesis**

The rapid increase in the development of earth reinforcement technology and its practical application has led to a parallel increase in the volume of literature dealing with reinforced soil. Chapter 2 introduces and discusses selected concepts specific to the areas of reinforced soil pertinent to this thesis.

Chapter 3 presents the finite element formulation of a reinforcement element suitable for modelling the behaviour of planar reinforcement under plane strain loading

conditions. Several load-strain models are developed and tested.

The stress-deformation results from a finite element analysis of a constructed nonreinforced and reinforced soil slope are presented in Chapter 4. Chapter 5 presents the results of a limit equilibrium analysis of the same nonreinforced and reinforced slope.

Chapter 6 provides a comparison between the nonreinforced and reinforced slope safety factors calculated from the limit equilibrium and finite element analyses. Partial factors of safety and possible slip surface shapes are also discussed. Chapter 7 provides the conclusions derived from the research and recommendations for further research.



## **2. LITERATURE REVIEW**

### **2.1 Introduction**

The purpose of this chapter is to present a summary of published literature pertaining to the analysis of reinforced soil structures. A distinction is made between the concept of Reinforced Earth as first proposed by Vidal (1969) and the concept of reinforced soil which will be used to refer to any soil reinforced with planar reinforcement such as geotextiles and polymeric or steel geogrids. The effects of reinforcement on the stress-strain behaviour of soil are described. Limit equilibrium methods that have been developed for analyzing reinforced soils are presented. The use of the finite element method in analyzing reinforced soil structures is discussed.

### **2.2 Stress-Strain Behaviour of Reinforced Soil**

The effects of reinforcing inclusions on the stress-strain behaviour of a soil mass have been studied using several techniques. Laboratory scale models, full scale models, direct shear tests, pullout tests and numerical studies have been conducted in order to study the mechanisms involved in reinforced soil.

#### **2.2.1 Model Studies**

McGown and Andrawes (1977) conducted plane strain, confined compression tests on a unit cell of sand with and

without a fabric inclusion. From these unit cell tests, a general increase in the strength of the unit cell system was achieved when non-woven fabric inclusions were placed along the major principal stress plane. They also found that the strain required to attain peak strength was increased and the brittleness of the system was markedly reduced. Anisotropic patterns of behaviour resulted when the inclusions were inclined to the horizontal. At inclinations close to the angle of shear failure in the unit cell, a weakening of the system over that of soil alone was observed.

McGown et al. (1978) present further results from plane strain unit cell tests. Additional attention was given to the inclusion properties: physical shape and dimension, frictional and adhesional characteristics, load deformation behaviour and environmental stability. In realizing the difference in behaviour between reinforced soil incorporating inextensible inclusions (Vidal, 1969) or extensible inclusions such as geotextiles, the authors state " the postulated behaviour of systems with extensible inclusions does not fall within the concepts presented by Vidal and as such, requires the development of a separate design technique"(p.331). The authors also state that to optimize the improvement derived from inclusions, they must be placed along the directions of principal tensile strain.

As a continuation of their research, McGown et al. (1981) constructed soil-fabric model embankments to further study the strain behaviour of reinforced soil systems. Model embankments were constructed from coarse Leighton Buzzard sand, with and without inclusions, on a compressible rubber foundation. Measurements of boundary displacements and internal embankment strains were made. Construction of the nonreinforced embankment indicated the zone of maximum tensile strain was at or close to the toe and the tensile principal strain directions were significantly inclined to the horizontal. The reinforced embankment clearly indicated a reduction in the horizontal displacements and differential settlements occurring at the embankment foundation interface.

### **2.2.2 Interface Behaviour**

An inherent complexity in the analysis of reinforced soil structures is the soil-reinforcement interaction. In order to adequately design a reinforced soil structure, the relative behaviour between the soil and the reinforcement must be considered.

A general discussion on the various types of direct shear tests and their limitations can be found in Bobey (1988). Richards and Scott (1985) evaluate five types of modified direct shear tests commonly used to determine the soil-reinforcement interface behaviour. Jewell (1980) conducted a comprehensive study on the effects of

reinforcement on the mechanical response of soils. Using large scale direct shear tests on Leighton Buzzard sand for a wide range of different reinforcement cases, several important patterns of behaviour were discovered.

Reinforcement locally modifies the state of stress and strain in sand and causes a significant reorientation of the principal axes of stress and strain over a well defined zone of the sand. Changing the orientation of the reinforcement can either increase or decrease the shear strength of the sand. As the spacing between separate reinforcement layers is reduced, the increase in the shear strength that each can provide is also reduced. Jewell also found that the relationship between the increase in the shear strength of the sand and the reinforcement orientation may be successfully predicted using the concepts of limit equilibrium.

Jewell et al. (1984), in attempting to quantify the interaction between soil and geogrids, identified three mechanisms of soil-reinforcement interaction:

- 1) soil shearing on plane surfaces of the reinforcement,
- 2) soil normal stresses on surfaces of the reinforcement and
- 3) soil shearing over soil through the apertures in a reinforcement grid.

Equations were derived which allow a simplified evaluation of the resistance to direct sliding of soil over a

reinforcement grid embedded in soil with the bond strength for a grid.

The bond strength of reinforcement within a soil mass is usually assessed using the pullout test. The pullout test can yield the load-displacement behaviour and the peak pullout force that can be generated by reinforcement embedded in soil. A great deal of work has been done on the pullout resistance of steel strip and mesh reinforcement (Chang et al., 1977b). Jewell (1980) and Ingold (1981) tested polymeric grid reinforcement for its pullout resistance in both cohesionless and cohesive soils.

Beech (1987) in attempting to incorporate the concept of strain compatibility into "limit equilibrium" design methods, developed an analytical method which predicts the pullout curve based on the soil and on the reinforcement properties. The analytical approach is based on the load-transfer method, a concept originally developed for pile design.

Mowafy (1986) found that two different mechanisms contribute to the pullout resistance of mesh materials embedded in granular soils. The primary mechanisms consisted of tensile strength mobilized within the reinforcement, the mesh-soil interlock and the soil confinement within the mesh openings. The secondary mechanism is the surface friction between the mesh material and the soil. These mechanisms are very similar to those found by Jewell et al. (1984) who used

direct shear tests to study the soil-reinforcement interaction.

### **2.3 Limit Equilibrium Design Methods**

The limit equilibrium method has become one of the most useful design tools available to geotechnical engineers. Its use for slope stability analyses is routinely employed in design practice and extensive experience has demonstrated its effectiveness and reliability for the analysis and design of nonreinforced slopes. The development of reinforced earth concepts in the 1960's (Vidal, 1969), however, resulted in the adoption of these classical limit equilibrium methods for the analysis of reinforced soils. The application of the limit equilibrium method to the analysis of reinforced soil structures is a function of the relatively complex behaviour of reinforced soils. Reinforced soil exhibits significant anisotropic behaviour due to the planar reinforcement, involves complex load transfer mechanisms and displays strain incompatibility between the soil and the reinforcement. Limit equilibrium methods are able to account for some of these inherent complexities by analyzing the reinforced soil mass at a state of impending failure.

#### **2.3.1 Current Methods of Analysis**

In an examination of some present limit equilibrium methods used for analyzing reinforced soil, Bonaparte et

al.(1986) state that the external stability of a reinforced soil mass can be checked using classical limit equilibrium methods and the internal stability can be analyzed using either a global or discrete approach. External stability refers to stability along failure surfaces which do not intersect reinforcement layers whereas internal stability is concerned with failure surfaces which pass through reinforcing layers. The global approach involves defining the reinforced soil mass as an equivalent continuum having definable mechanical properties. Stability analyses in a global approach can now be made using classical limit equilibrium methods. The global approach is deemed unfeasible when soil structures are reinforced with strips, bars, grids or fabrics due to difficulties in defining an equivalent continuum. The discrete approach, which involves analyzing the stress transfer between the soil and reinforcement, is recommended for these structures. With this approach, classical limit equilibrium methods are employed with appropriate modifications to include the effects of the reinforcement. At present, several methods of analysis have been developed which utilize circular, wedge, bilinear and log-spiral failure surfaces with differing assumptions as to the effect of the reinforcement.

The selection of an appropriate factor of safety is another area of debate in the analysis of reinforced soil systems using limit equilibrium methods. For reinforced soil structures, the markedly different stress-strain behaviour

of the soil and the reinforcement creates difficulty in defining an overall factor of safety. Bonaparte et al. (1986) present guidelines for the selection and use of partial factors of safety in reinforced soil design.

Ingold (1982) presents results of an analytical study on the stability of a geotextile reinforced embankment using an infinite slope analysis and Bishop's Modified Method. Bishop's Modified Method was developed by modifying Bishop's Simplified Method to include the effects of discrete layers of continuous horizontal reinforcement. The infinite slope analysis was used for checking shallow slope instability in the embankment and Bishop's Modified Method is used for the main slope design. Ingold's approach involves determining the difference between the factor of safety for a reinforced slope and the factor of safety of a nonreinforced slope with the same soils and geometry. By assuming the reinforcement provides the additional factor of safety,  $\Delta F$ , a design curve is produced relating the slope geometry to  $\Delta F$ . The spacing of the reinforcement is included in the analysis by creating a normalized parameter,  $\Delta F/N$ , where  $N$  is the spacing. The major assumption made in the analysis was that for a given factor of safety, the restoring force provided by the reinforcement is proportional to  $1/H^2$ , where  $H$  is the height of the embankment. Using this simple approach gives a factor of safety for the reinforced slope very close to the factor of safety calculated using Bishop's Modified Method. Ingold also offers recommendations for designing the length of the



reinforcement to prevent bond failure and for checking the external stability of the slope. Unfortunately, Ingold only demonstrates the design method for one slope geometry and one set of effective stress soil strength properties. The effects of the pore pressure ratio, soil cohesion, and soil friction angle have not been identified.

The development of limit equilibrium design methods for analyzing the stability of reinforced embankments constructed over weak foundations have dominated the literature. The reason for concentration in this area is due to the economic advantages created when using reinforcement for constructing embankments over weak soils.

Fowler(1982) presented one of the first design concepts used in analyzing fabric reinforced embankments. Three failure modes were examined; 1) horizontal sliding/lateral spreading, 2) rotational slope/foundation failure and 3) excessive foundation displacement. A Simplified Bishop slope stability analysis was used in the investigation. The reinforcement was incorporated into the analysis by assuming the fabric strength was equivalent to the strength of a cohesive layer uniformly distributed along the failure plane. From his studies, Fowler concluded that the horizontal force inducing the lateral spreading of the embankment could be approximated by a Mohr-Coulomb active earth pressure. The ultimate stress in the fabric would provide the horizontal sliding resistance necessary to

resist this active pressure. Fowler also presents a simple empirical method for calculating the minimum required fabric tensile modulus.

Jewell (1982) presents a limit equilibrium design method for reinforced embankments on soft foundations. Jewell considers the case of a low embankment reinforced by one layer of reinforcement placed between the embankment and the soft foundation. Only short term stability is considered in the design method. The design method separates the reinforcement forces required to provide equilibrium with a specified factor of safety from the reinforcement forces which could be generated and which are available to provide stability. The design criteria is based on two conditions:

- 1) the required force at any point along the reinforcement must not exceed the profile of available force for all limit states examined and
- 2) the reinforcement design strength must exceed the maximum value of force that could be realistically generated in the reinforcement.

If these two criteria are satisfied, then the reinforced embankment has a minimum overall safety factor not less than the value specified in the calculation of required reinforcement forces at the working limit state. Jewell assumes that the reinforcement force acts horizontally for horizontally placed reinforcement and the reinforcement only reduces the overall shear stresses carried by the soil (that is, increases in normal stress due to reinforcement is

ignored in the slope stability calculations).

Rowe and Soderman (1985) have developed an approximate method for estimating the stability of geotextile reinforced embankments from extensive parametric finite element studies. Their method of analysis is an extension of Bishop's Simplified Method but includes consideration of strain compatibility between the fabric and the soil. The analysis establishes an allowable compatible strain criteria to limit the strains beneath a reinforced embankment to those which would be obtained just prior to collapse in an unreinforced embankment. Design curves illustrating the relationship between allowable compatible strain and a dimensionless parameter containing embankment strength and geometric factors is presented by the authors. Unfortunately, these design curves are only applicable to the embankment geometry analyzed in their study and interpolation of the data to other geometries may be subject to error.

The limit equilibrium method proposed by Rowe and Soderman was used to analyze the behaviour of two test embankments constructed in the vicinity of Highway 6 at Almere in the Netherlands (SCRC, 1979). The proposed method calculated the collapse height to be 2.55 m while the actual embankment collapse occurred at 2.75 m indicating the method does provide reasonable and conservative predictions of collapse height. The authors' suggest that further testing

of the proposed technique is warranted.

Ingold and Miller(1986) present an analytical discussion on the inclusion of reinforcement creep and foundation consolidation phenomena into an analysis of the intermediate stability of a reinforced embankment built over soft clays. Intermediate stability refers to the embankment stability during a period between the end of construction and the end of consolidation. The authors have developed several design curves illustrating the relationship between geotextile strain and time and required restoring force and porewater pressure. By applying classical theories of consolidation, curves are also presented illustrating the qualitative variation of required restoring force and time. The authors assume that as the foundation materials consolidate and gain strength, the load in the geotextile will decrease proportionally. Using isochronous curves to describe the creep phenomena in the geotextile reinforcement, the authors develop a relationship which describes the variation of the required geotextile load and the geotextile creep load as a function of time. The primary criteria for satisfactory long term performance of the embankment consists of ensuring that at any time, the geotextile creep strength exceeds the required geotextile load.

In contrast to a stability analysis of fabric reinforced embankments constructed on weak foundations is

the stability analysis of multilayer reinforced embankment slopes constructed on competent foundations. The stress regime in a multilayer reinforced slope is much more complex to analyze and the effects of the reinforcement on the behaviour of the embankment are more difficult to quantify. Relatively few design methods have been developed for this case and even fewer have been calibrated against field or extensive numerical studies.

Murray (1982) presented one of the first comprehensive methods of design for slopes reinforced with several layers of reinforcement. The design method assumes a simple bilinear slip plane and takes into account the adherence and tensile resistance of the fabric. An extension of the design approach of Murray is presented by Schneider and Holtz (1986). The factor of safety in the bilinear method is defined as the ratio of resisting forces to disturbing forces. The most significant difference between Murray's approach and Schneider and Holtz's approach is how the contribution of the adherence resistance provided by the geotextile, in terms of effective stress, is considered. Recommendations are provided for selecting parameters relating to the initial state of stress in the slope, soil strengths, geotextile tensile strength, soil-geotextile friction, reinforcement spacing and selection of trial failure surfaces. At present, this method has not been calibrated against field studies.

Jewell et al. (1984) outline a design method for steep reinforced slopes and present charts suitable for preliminary design calculations. A limit equilibrium method based on two part wedge failure surfaces was employed. The main emphasis of the paper is on the development of design charts. These design charts were derived for the following conditions:

- 1) competent foundation and uniform slope with horizontal upper surface
- 2) uniform surcharge along slope crest
- 3) slope angles in the range of  $30^\circ$  to  $80^\circ$
- 4) soil strengths of  $c'=0$  and  $\phi' = 20^\circ$  to  $40^\circ$
- 5) pore pressure ratio  $r_u$  in the range 0.0 to 0.5
- 6) horizontal, constant length for each layer of reinforcement.

Several assumptions concerning the mechanisms occurring in reinforced soil slopes were made by Jewell in order to develop the design charts: 1) the reinforcement bond angle of friction was assumed conservatively to be equal to half the design friction angle of the soil, 2) the value of frictional resistance to direct sliding over grid reinforcement was assumed equal to 80% of the design friction angle of the soil, and 3) spacing of the reinforcement is based on the assumption that each layer may locally have to support the horizontal stresses in the soil. Caution should be exercised when using the design charts for analyzing slopes not reinforced with geogrids as many of the

above assumptions are based on the premise that a geogrid, in particular, Tensar SR2, is being used as the reinforcing material.

Schmertmann et al. (1987) have produced design charts applicable to the design of geogrid reinforced soil slopes. The design charts are developed using Jewell's et al. (1984) design method but specific attention is placed on the calculation of the lengths of the reinforcement layers. A separate wedge analysis is performed in order to compute the required lengths of reinforcement. Their design method is based on a two part wedge slope stability analysis. It assumes the interface shear strength is 90% of the internal soil shear strength, no pore pressures exist in the slope,  $c'=0$  only analysis, the reinforcement is spaced inversely to its height within the embankment and the embankment is constructed on a competent foundation. It must be noted however, that the design charts have been developed through the synthesis of different analysis methods and as such, careful examination of the effects of the chart parameters in a particular design is warranted.

Leschinsky and Volk (1986) have developed a slope stability analysis method based on a limiting equilibrium approach combined with variational extremization. A log-spiral slip surface is the assumed failure mechanism and the geotextile restoring force is positioned orthogonally to the radii defining the log spiral. The analytical approach

developed by Leschinsky and Volk satisfies all equations of equilibrium. One important inclusion in this design method is the allowance for non-equal tensile forces in each reinforcing layer at the point of collapse. It is assumed that once the lowest reinforcing layer reaches its ultimate strength and fails, " a collapse, resembling a row of dominoes falling down will occur; that is, all other geotextiles will fail one after the other in an upward orderly manner". If one assumes that the soil reaches failure at the same time, this process of "progressive failure" seems intuitively possible. This process is incorporated into their design method by assuming a linear load-elongation relationship for the reinforcement and adjusting the reinforcement forces relative to the lowest reinforcement force using a mechanism defining the virtual rotation of any point along the log-spiral slip surface. Some of the important conclusions drawn from Leschinsky and Volk's analytical study are:

- 1) as the geotextile strength increases, the extent of the critical slip surface increases and
- 2) as the geotextile's tensile strength increases, the compressive stress normal to the critical slip surface increases.

The latter conclusion is significant considering that all previously developed limit equilibrium methods ignored the capability of the reinforcement to increase the normal stress component on the slip surface. A favourable



comparison was achieved between the log-spiral method and a Fellenius limit equilibrium method which was modified to include the reinforcement.

### **2.3.2 Summary of Limit Equilibrium Methods**

Many limit equilibrium methods have been developed in order to analyze the stability of reinforced soil slopes. Methods employing wedge or circular slip surfaces are the most common limit equilibrium methods applied to reinforced soil structures. Table 5.1 summarizes some of these methods.

Judging from the numerous types of methods adopted for reinforced soils, no one method has been shown to provide the best answer. As with the classical nonreinforced slope limit equilibrium methods, only through experience and comparisons with case histories will confidence in any one type of reinforced soil limit equilibrium method be established. Given the number of investigators who have used Bishop's Modified Method (Ingold, Duncan and Schmertmann) and the availability of a computer program to perform the analysis, Bishop's Modified Method will be used for the stability analyses of the reinforced soil slope presented in Chapter 5.

### **2.4 Finite Element Analysis of Reinforced Soil**

The application of the finite element method to the analysis of reinforced earth and soil structures has received a great deal of attention in the past decade. The

Table 2.1 Limit Equilibrium Methods Applied to Reinforced Soil Systems

INVESTIGATOR	LIMIT EQUILIBRIUM MODEL	SOIL TYPE	PORE PRESSURES	LENGTH OF REINFORCEMENT
Duncan, et al. 1985	Circular	$c'$ $\phi'$	$r_u$ or p.p. contours	n/a
Ingold, T.S. 1982	Infinite Slope Circular	$\phi'$ $c' = 0.0$ $c'$ $\phi'$	n/a $r_u$	n/a
Jewell, et al. 1984	Two Part Wedge	$\phi'$ $c' = 0.0$	$r_u$	Parallel Truncation
Leschinsky and Reinschmidt, 1985	Log Spiral	$c$ $\phi$ (total stress)	n/a	n/a
Murray, R.T. 1982	Two or Three Part Wedge	$c'$ $\phi'$	$r_u$	n/a
Schmertmann, et al. 1987	Two Part Wedge Circular	$\phi'$ $c' = 0.0$ $\phi'$ $c' = 0.0$	n/a $r_u$	General Truncation n/a
Schneider and Holtz, 1986	Two or Three Part Wedge (extension Murray's Work)	$c'$ $\phi'$	$r_u$	n/a

\* n/a ... not available

analysis has followed both a discrete approach and a composite approach. The discrete approach involves modelling each component of a reinforced soil structure separately; the soil, the reinforcement and the soil-reinforcement interaction. In the composite approach, the reinforced soil is modelled as a locally homogeneous, orthotropic material. The application of the composite approach has mainly been in the area of "Reinforced Earth". The placement of strips in the soil rather than sheets makes the idealization of plane strain conditions difficult so an equivalent continuum or composite approach has been adopted. An excellent discussion on the discrete and composite finite element methods of analysis as they relate to the concept of "Reinforced Earth" can be found in Al-Yassin (1979). Chang and Forsyth (1977), Al-Hussaini and Johnsson (1978) and Al-Yassin and Herrmann (1979) describe the application of the composite finite element approach to the analysis of reinforced earth structures.

#### **2.4.1 Discrete Finite Element Methods**

Andrawes et al. (1980) utilized the discrete approach in developing a finite element model capable of handling the response of the soil, the reinforcement and, through use of spring elements, the soil-reinforcement interaction. Duncan and Chang's (1970) hyperbolic elastic model was used to represent the nonlinear stress-strain behaviour of the soil. Hyperbolic curves were also used to model the nonlinear

shear stress-deformation characteristics of the soil-reinforcement interface. The interface elements were formulated using spring elements of zero thickness which connect the nodes of reinforcement elements to adjacent soil element nodes. The reinforcing elements are straight line elements with no bending stiffness. The behaviour of the reinforcement is modelled by a hyperbolic relationship with an option for confining pressure dependent load-elongation behaviour. Their finite element model was calibrated using the results of a laboratory plane strain model of a sand embankment built over a compressible strata. In general, the deformation predictions using the finite element method showed good agreement with the measured values.

A detailed presentation of the above finite element model is given by Andrawes et al. (1982). Derivation of the finite element equations is presented for the reinforcing elements, interface elements and soil elements. The accuracy and limitations of the model is assessed by making comparisons between finite element model predictions and laboratory observations for strip footing load tests. The major problem in analyzing the reinforced soil structure was found to be in adequately modelling the soil behaviour. A history matching of the laboratory test results to the finite element model predictions indicated that an increase of  $\approx 12\%$  in the triaxial soil strengths was required to obtain satisfactory results. Preceding failure conditions, the finite element model provided a good prediction of the

footing system behaviour.

Rowe (1984) outlines a comprehensive finite element model which permits consideration of soil reinforcement interaction, slip at the soil-fabric interface, plastic failure within the soil and large deformations. The geotextile is treated as a structural membrane with axial stiffness but negligible flexural rigidity. The soil is assumed to be a nonlinear elastic-plastic material. The validity of the finite element program was assessed using the results of the behaviour of an instrumented geotextile reinforced embankment constructed over peat. A more detailed presentation on the use of the finite element program for analyzing geotextile reinforced embankments constructed on peat is presented by Rowe and Soderman (1985).

Brown and Poulos (1984) have developed a finite element model which can be used to predict the failure of reinforced soil structures. The program allows for incremental construction, slip between the soil and reinforcement and elastic-plastic modelling of the soil. The analysis of two full scale experimental reinforced embankments using this program illustrated the ability of the finite element method to predict the collapse mechanisms occurring within reinforced soil structures.

The finite element analysis of a geotextile reinforced embankment constructed on soft ground is given by Boutrup and Holtz (1983). Their analysis included large

displacements, elastic-plastic behaviour of the soil and the nonlinear behaviour of the reinforcement. Interface elements appear to have been used to model the soil-reinforcement interaction but no explanation of these elements are provided in their paper.

Details of the development of a finite element procedure to discretely model a reinforced soil system is presented by Zeevaert (1980). Formulations for soil elements, interface elements, and reinforcing elements are outlined as well as discussions on nonlinear analysis, large displacement formulations, soil plasticity and no-tension analysis. Zeevaert applies his finite element program to the analysis of geotextile reinforced subgrades and generally found excellent agreement between laboratory test results and his finite element predictions.

#### **2.4.2 Soil-Reinforcement Interaction**

The complex phenomenon of stress transfer between the soil and the reinforcement is dependent on the soil-reinforcement characteristics. In order to adequately model the stress-strain behaviour of a reinforced soil structure, the soil-reinforcement interaction must be included in the analysis. In terms of a finite element analysis, interface elements must be employed in order to model the relative behaviour between the soil and the reinforcement.

Most interface elements have been developed to effectively model the behaviour of rock joints ( Ghaboussi et al. (1973), Heuze and Barbour (1982), Goodman (1977) ). The majority of these joint or interface elements utilized relative displacements as the independent degrees of freedom which eliminated some of the numerical difficulties that were common with the "spring" interface element approach.

Desai et al. (1984) suggested using a thin solid element for modelling soil-structure interaction. Through special treatment of the constitutive laws of the thin-layer element, the various modes of deformation such as no-slip, slip, debonding, and rebonding can be modelled. Katona (1983) developed a simple friction contact interface element by utilizing constraint equations to control the relative displacements between nodes pairs of the element. The use of constraint equations avoids numerical roundoff problems, allows for direct control of interface forces and relative movements and allows easy implementation into any finite element program.

The previous discussions have shown that a number of finite element methods have been developed or modified in order to analyze reinforced soil structures. It would have been advantageous and expedient if one of these methods could have been adopted for the present research. Unfortunately, insufficient information was available in the literature in order to use the aforementioned methods. The

following chapter provides the formulation of a reinforcement element which was incorporated into a geotechnical finite element program to allow finite element analyses of a reinforced soil slope to be conducted.



### 3. FINITE ELEMENT ANALYSIS OF REINFORCED SOIL

#### 3.1 Introduction

In the area of reinforced soil structures, design methods have focused on the utilization of limit equilibrium methods due to the inherent complexities of reinforced soil and the finite element method. Presently, however, increased emphasis is being placed on the evaluation of stresses and strains within a reinforced soil mass. The effects of soil-reinforcement strain compatibility and reinforcement stiffness on the stability of a reinforced soil structure have become important design considerations. The limit equilibrium method will not yield information on the deformations of the structure. The application of the finite element method to the analysis of reinforced soil structures can yield information on the stresses and strains within a reinforced soil mass as well as reveal the effects of soil-reinforcement interaction. A finite element analysis may also indicate soil-reinforcement load transfer mechanisms occurring within a reinforced soil mass.

The finite element method is utilized in the present research program to calculate the stresses, strains and deformations of the soil and the reinforcement loads for a nonreinforced and reinforced soil slope constructed on a competent foundation. In order to perform the finite element analyses, an element suitable for modelling the behaviour of planar reinforcement within a soil slope had to be

incorporated into a finite element program. The following sections describe the formulation of a reinforcement element which was incorporated into the finite element program SAFE to enable the modelling of geosynthetic reinforcement. A general description of the capabilities of SAFE are presented in Appendix A.

### **3.2 Reinforcement Element**

#### **3.2.1 Introduction**

A two dimensional, plane strain isoparametric bar (reinforcement) element has been incorporated into SAFE for the purpose of modelling the behaviour of planar reinforcement. The use of bar elements in modelling structural supports such as tie-backs or rock bolts is quite common (Lightner, 1981 and Bathe, 1982). Andrawes et al. (1982) were among the first researchers to utilize a bar element for modelling the load-strain response of polymeric reinforcement.

The reinforcement element implemented in this study required that it be fully compatible with the two dimensional element types available within SAFE and be fully capable of modelling the behaviour of polymeric reinforcement. The following sections present the reinforcement element formulation, the constitutive models used in modelling the load-strain behaviour of geosynthetic reinforcement and element tests performed in order to verify

the reinforcement element formulation and the computer code.

### 3.2.2 Reinforcement Element Formulation

A conventional displacement formulation (Bathe, 1982) based on the principle of virtual displacements was utilized in developing the reinforcement element. The reinforcement element is defined by a variable number of nodes (2 or 3) and is capable of resisting axial loads only; the flexural stiffness of the element is neglected. Figure 3.1 illustrates the degrees of freedom for the element in both the global (x,y) coordinate system and the local (r) coordinate system.

The formulation of this reinforcement element differs from that of a typical bar element in two respects. Firstly, the configuration and the displacement field of the element are defined using quadratic polynomial interpolation functions. Most bar elements are formulated using linear interpolation functions which allow the element orientation in the global coordinate system to be defined using the angle the element forms with respect to the horizontal axis. This results in a straightforward coordinate transformation process but limits the usefulness of the element in modelling curved surfaces. The use of higher order interpolation functions for the reinforcement element allows greater accuracy in modelling curved surfaces. The second difference is the constitutive models for the reinforcement elements are based on load-strain relationships; not

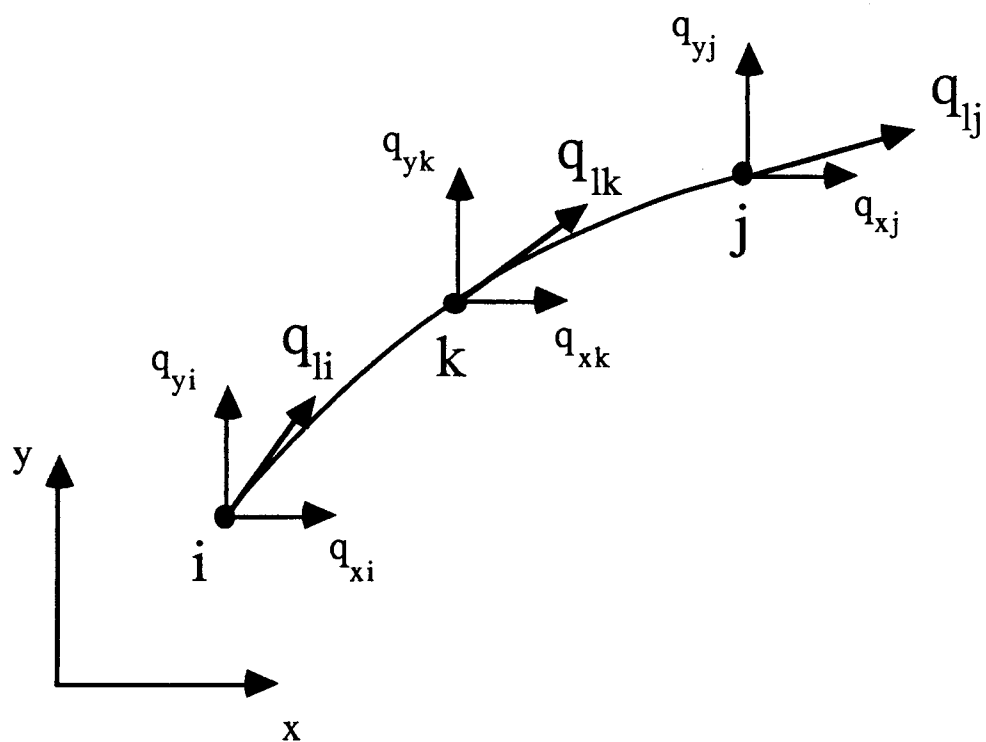


Figure 3.1 Degrees of Freedom for Reinforcement Element

stress-strain relationships. The generally accepted method of presenting tensile test results on geosynthetic materials is a load-strain curve and consequently, the reinforcement element derivation is based on the load-strain response.

In order to ensure compatibility between the reinforcement element and the soil elements, which are based on stress-strain relationships, a confirmation of the virtual work formulation for the element was performed.

The principle of virtual work can be stated as:

$$\text{Internal Work (IW)} = \text{External Work (EW)}$$

$$\int_V \sigma_{ij} \delta \epsilon_{ij} dV = \int_S T_i \delta q_i dS + \int_V F_i \delta q_i dV \quad [3.1]$$

Dealing first with the internal work expression, the tensorial notation can be expanded to give:

$$\int_V \sigma_{ij} \delta \epsilon_{ij} dV = \int_V (\sigma_x \delta \epsilon_x + \sigma_y \delta \epsilon_y + \sigma_z \delta \epsilon_z + \sigma_{xy} \delta \epsilon_{xy} + \sigma_{yz} \delta \epsilon_{yz} + \sigma_{xz} \delta \epsilon_{xz}) dV \quad [3.2]$$

The following formulation assumes incremental quantities of stress and strain. For plane strain conditions,  $\delta \epsilon_z = \delta \epsilon_{xz} = \delta \epsilon_{yz} = 0$ . As well, the internal virtual work due to  $\sigma_y \delta \epsilon_y$  and  $\sigma_{xy} \delta \epsilon_{xy}$  for the reinforcement element are neglected. Therefore the internal virtual work expression simplifies to:

$$\int_V \sigma_{ij} \delta \epsilon_{ij} dV = \int_V \sigma_x \delta \epsilon_x dV \quad [3.3]$$

The subscript "x" in Equation 3.3 refers to axial stresses and strains hence a change in notation to subscripts of "a" are made in order to identify the internal work done by "axial" stress. Since the reinforcement element is assumed to perform internal virtual work along its length only, the volume integral in Equation 3.3 can be reduced to an integration along the element length, assuming no change in cross sectional area of the element occurs during straining. The internal virtual work expression now becomes:

$$\int_V \sigma_{ij} \delta \epsilon_{ij} dV = \int_l \sigma_a \delta \epsilon_a A dl \quad [3.4]$$

From Hooke's Law it is known that  $\sigma_a = (\partial \sigma_a / \partial \epsilon_a) \epsilon_a$  and from the results of a wide strip tensile test on a reinforcing material, it can be shown that  $(\partial \sigma_a / \partial \epsilon_a) = D_t / A$ , where  $D_t / A$  is the incremental slope along the load-strain curve and  $A$  is the cross sectional area of the reinforcement. Note that since this is an incremental formulation,  $D_t$  represents a tangential reinforcement stiffness value and is not a constant value except for linear elastic analyses. Substituting these expressions into Equation 3.4, the internal virtual work equation reduces to:

$$\int_V \sigma_{ij} \delta \epsilon_{ij} dV = \int_l D_t \epsilon_a \delta \epsilon_a dl \quad [3.5]$$

Using a strain transformation procedure, the axial strains can be related to nodal displacements of the element by:

$$\epsilon_a = [B] \{q_i\} \quad [3.6]$$

$$\delta\epsilon_a = [B] \{\delta q_i\} \quad [3.7]$$

Substituting these two equations into Equation 3.5 yields:

$$\int_V \sigma_{ij} \delta\epsilon_{ij} dV = \int_l D_t [B] \{q_i\} [B] \{\delta q_i\} dl \quad [3.8]$$

The integral along the element length,  $l$ , can be transformed into an integral along the local coordinate axis,  $r$ , by using the chain rule of differentiation:

$$dl = \frac{dl}{dr} \times dr \quad [3.9]$$

$$\text{where } \frac{dl}{dr} = J = \text{Jacobian Matrix}$$

Using the Jacobian matrix and integrating from  $r = -1$  to  $r = +1$ , the final expression for the internal virtual work of the reinforcement element becomes:

$$IW = \langle \delta q_i \rangle \left[ \int_{-1}^{+1} [B]^T D_t [B] J dr \right] \{q_i\} \quad [3.10]$$

As presented in Equation 3.1, the external virtual work for the reinforcement element is defined as:

$$EW = \int_S T_i \delta q_i dS + \int_V F_i \delta q_i dV \quad [3.11]$$

Since the weight of the reinforcement element is negligible

in comparison with the weight of the soil, the body forces,  $F_i$ , are set equal to zero. Expanding the tensorial notation of Equation 3.11, the external virtual work equation becomes:

$$EW = \int_S (T_x \delta q_x + T_y \delta q_y + T_z \delta q_z) dS \quad [3.12]$$

Again, since the reinforcement element is a plane strain, one dimensional element,  $\delta q_y = \delta q_z = 0$  and changing the "x" subscript to "a" to represent axial work, the external virtual work expression can be rewritten as:

$$EW = \int_l T_a \delta q_a dl \quad [3.13]$$

Using an interpolation function to define the axial tractions,  $T_a$ , and the axial virtual displacements,  $\delta q_a$ , at any point along the reinforcement element, Equation 3.13 becomes:

$$EW = \int_l [N] \{T_i\} [N] \{\delta q_i\} dl \quad [3.14]$$

Using the same Jacobian matrix to transform the integration from global to local coordinates and rearranging terms, Equation 3.14 can be rewritten as:

$$EW = \int_{-1}^{+1} \langle T_i \rangle [N]^T [N] J dr \{\delta q_i\} \quad [3.15]$$



Assuming the same amount of external virtual work is done by the nodal tractions as the nodal forces (Bathe, 1982):

$$\int_{-1}^{+1} \langle T_i \rangle [N]^T [N] J dr \{ \delta q_i \} = \langle Q_i \rangle \{ \delta q_i \} \quad [3.16]$$

Equation 3.1 stated that the internal virtual work must equal the external virtual work. Therefore, using Equation 3.10 and 3.16:

$$\langle \delta q_i \rangle \int_{-1}^{+1} [B]^T D_t [B] J dr \{ q_i \} = \langle \delta q_i \rangle \{ Q_i \} \quad [3.17]$$

Rewriting this equation as:

$$\langle \delta q_i \rangle \left( \int_{-1}^{+1} [B]^T D_t [B] J dr \{ q_i \} - \{ Q_i \} \right) = 0 \quad [3.18]$$

and since  $\langle \delta q_i \rangle \neq 0$ ,

$$[K]_t \{ q_i \} = \{ Q_i \} \quad [3.19]$$

$$\text{where } [K]_t = \int_{-1}^{+1} [B]^T D_t [B] J dr$$

The stiffness matrix derived for the reinforcement element has the same form as the conventional stiffness matrix derived for solid elements. The interpretation and form of the strain transformaton matrix,  $[B]$ , and the Jacobian matrix,  $J$ , are different however. The reasons for the difference rests in the requirement that while each node of

the reinforcement element is permitted two global degrees of freedom,  $q_x$  and  $q_y$ , it is only the changes in the axial deformations of the element that are of concern. Equation 3.6 stated that the strains in the element are defined as:

$$\varepsilon_a = [B] \{ q_i \} \quad [3.20]$$

At any node, two global displacements occur;  $q_x$  and  $q_y$ . A global nodal displacement along the element length,  $q_1$ , can be obtained at any node using the geometry illustrated in Figure 3.2. A unit vector,  $\bar{l}$ , defining the slope of the element at a node can be defined as:

$$\bar{l} = \frac{(dx/dr) i + (dy/dr) j}{\sqrt{(dx/dr)^2 + (dy/dr)^2}} \quad [3.21]$$

where  $i, j$  are unit vectors defining the  $x$  and  $y$  coordinate directions

The direction of the unit vector,  $\bar{l}$ , is based on the original configuration of the element not the displaced configuration, therefore all displacements are referenced to the original element configuration in determining axial element displacements. The axial nodal displacement,  $q_1$ , is defined as:

$$q_1 = q_x \cdot \bar{l} + q_y \cdot \bar{l} \quad [3.22]$$

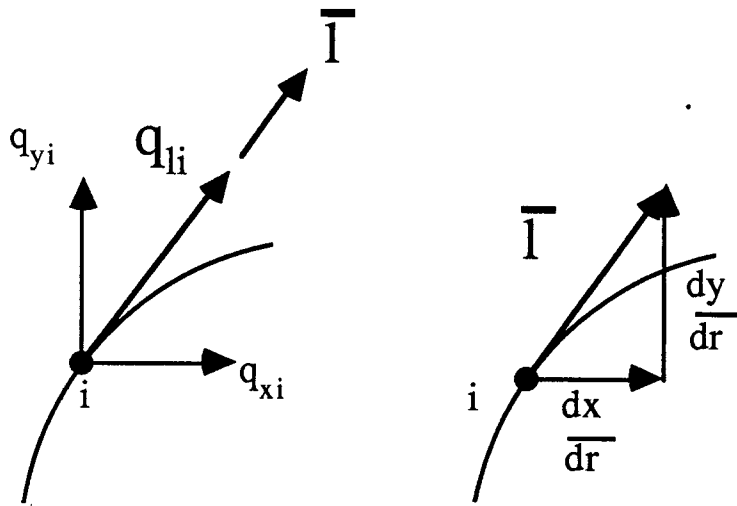


Figure 3.2 Geometry for Global to Local Displacement Transformations

By defining the axial displacements of the reinforcement element in this manner, a limitation is placed on the degree of element rotation during displacement. Since the axial displacements are referenced to the initial or original configuration of the element, a displacement field exhibiting rigid body rotation will result in straining of the element. This is clearly a limitation in the element formulation and subsequent development work should endeavour to define the axial displacements in a more rigorous manner than that presented in Equation 3.22.

Performing the dot product operation and simplifying the expression,  $q_1$ , the axial displacement at any node, becomes:

$$q_1 = \frac{1}{\sqrt{\left(\frac{dx}{dr}\right)^2 + \left(\frac{dy}{dr}\right)^2}} \left\langle \frac{dx}{dr} \quad \frac{dy}{dr} \right\rangle \begin{Bmatrix} q_x \\ q_y \end{Bmatrix} \quad [3.23]$$

This global displacement transformation allows the global nodal displacements,  $q_x$  and  $q_y$ , to be transformed into a axial nodal displacement,  $q_1$ . This transformation is performed at each node, so in terms of the element notation in Figure 3.1, the axial nodal displacements for each node are determined using the following equation:

$$\begin{Bmatrix} q_{1i} \\ q_{1j} \\ q_{1k} \end{Bmatrix} = [T] \{q_i\} \quad [3.24]$$

where  $\{q_i\} = \langle q_{xi} \ q_{yi} \ q_{xj} \ q_{yj} \ q_{xk} \ q_{yk} \rangle^T$

$$[T] = \begin{bmatrix} J^{-1} \frac{dx}{dr} \Big|_{r=-1} & J^{-1} \frac{dy}{dr} \Big|_{r=-1} & 0 & 0 & 0 & 0 \\ 0 & 0 & J^{-1} \frac{dx}{dr} \Big|_{r=1} & J^{-1} \frac{dy}{dr} \Big|_{r=1} & 0 & 0 \\ 0 & 0 & 0 & 0 & J^{-1} \frac{dx}{dr} \Big|_{r=0} & J^{-1} \frac{dy}{dr} \Big|_{r=0} \end{bmatrix}$$

Knowing  $q_{1i}$ ,  $q_{1j}$  and  $q_{1k}$ , the axial nodal displacement at any point along the element can be approximated by using the interpolation function  $[N]$ ,

$$\therefore q_1 = [N] [T] \{q_i\} \quad [3.25]$$

The strain in the reinforcement element is defined as the rate of change in length along the length of the element or:

$$\epsilon_a = \frac{d(q_1)}{dl} \quad [3.26]$$

In terms of the local coordinate axis,  $r$ :

$$\epsilon_a = \frac{d(q_1)}{dr} \times \frac{dr}{dl} \quad [3.27]$$

The expression  $dr/dl$  can be evaluated by first determining  $dl/dr$  and inverting the matrix. Using the geometry

illustrated in Figure 3.2,  $dl/dr$  is defined as:

$$\frac{dl}{dr} = \sqrt{\left(\frac{dx}{dr}\right)^2 + \left(\frac{dy}{dr}\right)^2} = J \quad [3.28]$$

Substituting Equation 3.25 into Equation 3.27 and using  $J^{-1}=dr/dl$ , the axial strain in the reinforcement element is defined as:

$$\epsilon_a = [NR] [T] J^{-1} \{ q_i \} \quad [3.29]$$

$$\text{where } [NR] = \frac{d([N])}{dr}$$

So now the strain transformation matrix,  $[B]$ , is:

$$[B] = [NR] [T] J^{-1} \quad [3.30]$$

Substituting Equation 3.30 into Equation 3.19, the expression for the tangent stiffness matrix,  $[K]_t$ , becomes:

$$[K]_t = \int_{-1}^{+1} J^{-1} [T]^T [NR]^T D_t [NR] [T] dr \quad [3.31]$$

In order to avoid the complexities of integrating the stiffness matrix, Gaussian Quadrature is used to evaluate  $[K]_t$ . Using Gauss-Legendre polynomials, the numerical integration form of the stiffness matrix is:

$$[K]_t = \sum_{i=1}^n w_i J^{-1}(r_i) [T]^T [NR(r_i)]^T D_t [NR(r_i)] [T] \quad [3.32]$$

### 3.2.3 Reinforcement Element Load-Strain Models

The models developed for representing the load-strain behaviour of geosynthetics are curve fitting methods; they employ an equation which "fits" the load-strain relationships developed from appropriate tensile tests conducted on the geosynthetic reinforcement. Three curve fitting techniques have been implemented in SAFE; 1) linear elastic, 2) nonlinear quadratic and 3) polynomial elastic. These three models are described in the following sections.

#### 3.2.3.1 Linear Elastic Model

The linear elastic model assumes a linear relationship between the strain in the reinforcement and the load development. Figure 3.3 illustrates the form of this relationship. The equation between the load and strain is simply:

$$F = D \epsilon_a \quad [3.33]$$

where  $F$  = tensile load, kN / m

$\epsilon_a$  = axial strain

$D$  = load modulus, kN/m

The failure load of the reinforcement is specified as an input parameter for the model. Once the current load exceeds the failure load, at any integration point, the incremental stiffness at that integration point is set to zero for the remainder of the analysis.

In most cases, a linear elastic model is suitable only for preliminary studies of a problem. For geosynthetic reinforcement such as geogrids or high strength geotextiles, however, the load-strain relationships generally remain linear. Geogrids such as Tensar SR2 and Signode TNX5001 typically exhibit a 10 to 15% decrease between the 2% and 5% secant modulus indicating strong linearity between load and strain. The linear elastic model may be suitable for modeling the response of these high strength geosynthetic materials.

### 3.2.3.2 Nonlinear Quadratic Model

In order to model the nonlinear load-strain response of a geosynthetic, a quadratic equation has been employed which relates the load to the strain using the following relationship:

$$F = D_i \left( \epsilon_a - \frac{\epsilon_a^2}{2\epsilon_f} \right) \quad [3.34]$$

where  $D_i$  = initial load modulus, kN/m

$\epsilon_a$  = axial strain

$\epsilon_f$  = axial strain at failure

The general form of the relationship is illustrated in Figure 3.4. The geogrid element formulation is based on the direct stiffness method so a tangential stiffness (modulus) is required at each step in a finite element analysis. By differentiating Equation 3.34 with respect to  $\epsilon$ , the tangent reinforcement



modulus can be expressed as:

$$D_i = D_i \left(1 - \frac{\epsilon}{\epsilon_f}\right) \quad [3.35]$$

Based on preliminary wide width tensile tests conducted at the University of Alberta on a high density polyethylene geogrid, the unloading response differed substantially from its loading behaviour. Figure 3.5 illustrates a typical loading-unloading-reloading cycle during a wide width tension test. In order to incorporate this behaviour into the model, an unloading modulus,  $D_{un}$ , has been introduced. The unloading modulus reflects the rate at which a geogrid will contract with a reduction in load. Typical of most plastic materials, significant hysteresis and plastic strains occur during unloading-reloading cycles. In the quadratic model, the unloading response in any load step  $i$  is controlled by storing the  $(i-1)^{th}$  strain value and comparing it with the  $i^{th}$  strain value at each integration point. If the  $i^{th}$  strain is less, then unloading has occurred. The unloading modulus is used to recalculate the load for the  $i^{th}$  strain and the unbalanced loads are computed and reapplied to the system.

The failure of a geogrid is determined by a strain value in excess of the failure strain. Once a

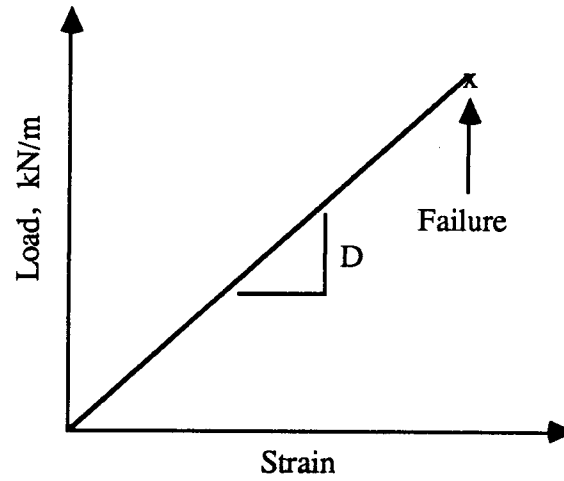


Figure 3.3 Linear Elastic Load-Strain Model

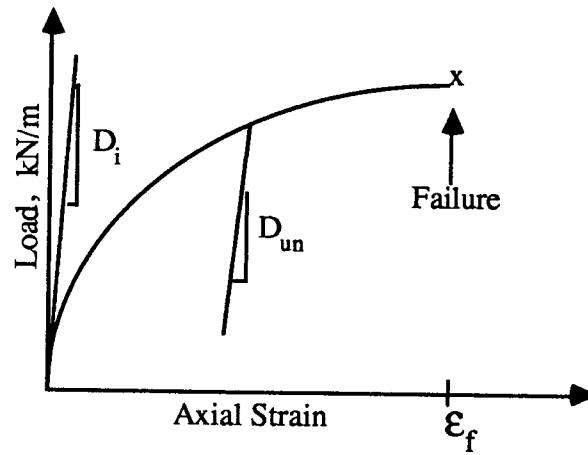


Figure 3.4 Nonlinear Quadratic Load-Strain Model

failure condition at any integration point is achieved, the incremental stiffness for that integration point is set to zero for the remainder of the analysis.

### 3.2.3.3 Polynomial Elastic Model

The polynomial model was implemented in order to model any general form of load-strain relationship. In particular, the polynomial equation is ideally suited to modelling the load-strain behaviour of geotextile reinforcement. The polynomial equation used for this model has the form:

$$F = a_0 + a_1\varepsilon + a_2\varepsilon^2 + a_3\varepsilon^3 + a_4\varepsilon^4 + a_5\varepsilon^5 + a_6\varepsilon^6 + a_7\varepsilon^7 + a_8\varepsilon^8 + a_9\varepsilon^9 + a_{10}\varepsilon^{10} \quad [3.36]$$

where  $F$  = tensile load, kN/m

$\varepsilon$  = axial strain

$a_0, a_1, \dots, a_{10}$  = polynomial coefficients

An expression for the tangent modulus is obtained by differentiating Equation 3.36 with respect to strain:

$$D_t = a_1 + 2a_2\varepsilon + 3a_3\varepsilon^2 + 4a_4\varepsilon^3 + 5a_5\varepsilon^4 + 6a_6\varepsilon^5 + 7a_7\varepsilon^6 + 8a_8\varepsilon^7 + 9a_9\varepsilon^8 + 10a_{10}\varepsilon^9 \quad [3.37]$$

The polynomial model is an elastic model; the loading and unloading response will follow the same curve.

Figure 3.6 illustrates the general form of the load-strain relationship for which the polynomial model is ideally suited for modelling. The quadratic equation can be obtained from the polynomial expression but the polynomial model is intended for more general forms of load-strain relationships.

### 3.3 Verification of Reinforcement Element

In order to confirm the validity of the reinforcement element formulation and the programming of the computer codes, several element tests have been performed. Several criteria must be satisfied if an element is to meet convergence requirements which define conditions that guarantee that exact answers will be approached as more and more elements are used to model an arbitrary structure (Cook, 1981). If these requirements are satisfied, the validity of the element is ensured.

The first requirement is that the displacement field within the element must be continuous. This has been easily met in the reinforcement element through the use of a polynomial displacement field. The displacements at any point along the element are defined using a one dimensional polynomial interpolation function and are expressed as:

$$q_1 = [N] \begin{Bmatrix} q_{1i} \\ q_{1j} \\ q_{1k} \end{Bmatrix} \quad [3.38]$$

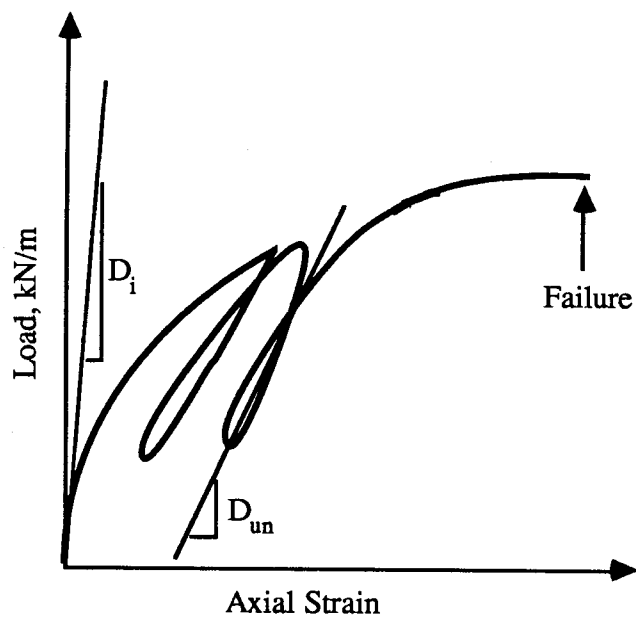


Figure 3.5 Unloading Characteristics of HDPE Geogrid

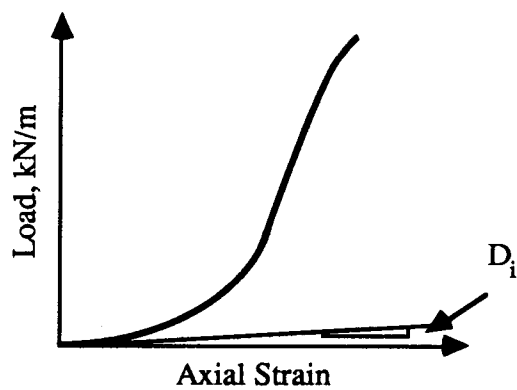


Figure 3.6 Polynomial Load-Strain Model

The second requirement is that the element must be able to assume a state of constant strain. To assess the constant strain states for the element, a series of "patch tests" and loading tests were performed. In the patch test, a patch of elements are subjected to boundary nodal point forces or nodal point displacements which correspond to a state of constant strain. Figure 3.7 illustrates the different element assemblages used in the patch tests. The elastic load-strain model was used with a modulus,  $D$ , of 1000 kN/m.

For the vertical arrangement, a load of  $F = 30$  kN was applied at node #7 which corresponds to a constant strain condition in each element of  $\epsilon_a = 0.030$  or 3.0%. The finite element results produced strains at the three integration points in element #2 of;

$$\epsilon_i = 0.030$$

$$\epsilon_{ii} = 0.030$$

$$\epsilon_{iii} = 0.030$$

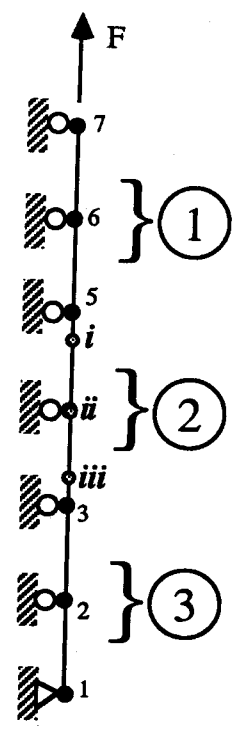
Using the same configuration, a displacement of 0.030 m was prescribed for node #7 which corresponds to a constant strain in each element of  $\epsilon_a = 0.010$  or 1.0%. The finite element results in element #2 were;

$$\epsilon_i = 0.010$$

$$\epsilon_{ii} = 0.010$$

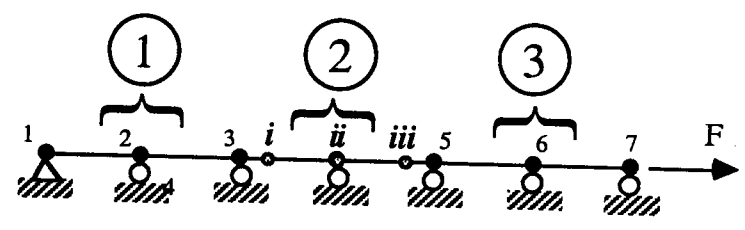
$$\epsilon_{iii} = 0.010$$

For the horizontal element configuration, the same nodal force and prescribed displacement was applied. For a

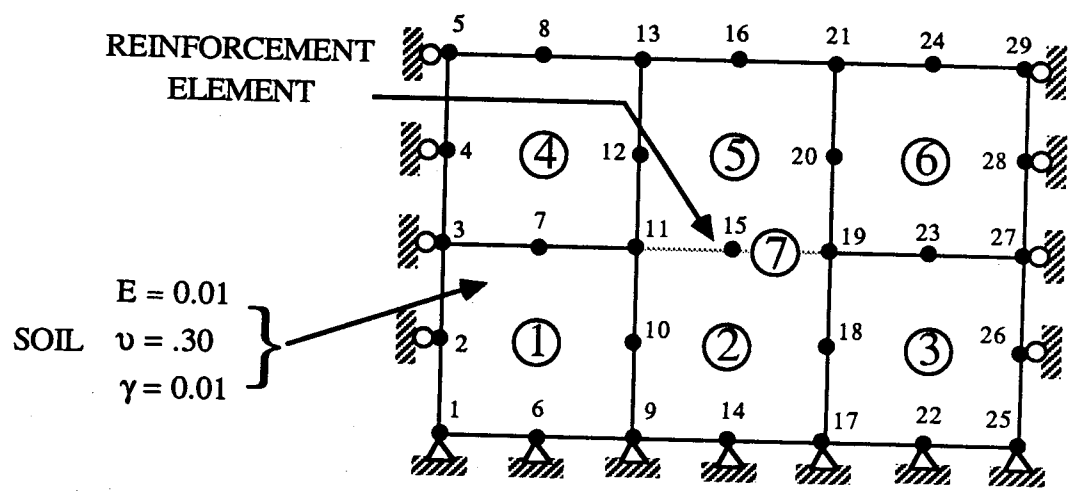


a) VERTICAL

● indicates an integration point



b) HORIZONTAL



c) EMBEDDED

Figure 3.7 Element Assemblages for Patch Tests

load of 30 kN, the strains in element #2 were;

$$\epsilon_i = 0.030$$

$$\epsilon_{ii} = 0.030$$

$$\epsilon_{iii} = 0.030$$

For a prescribed displacement of 0.030 m for node #7, the resulting strains were;

$$\epsilon_i = 0.010$$

$$\epsilon_{ii} = 0.010$$

$$\epsilon_{iii} = 0.010$$

Thus it can be seen the element satisfies the condition of constant strain under conditions of boundary nodal forces and displacements. Unfortunately, a single patch test as those just performed is not sufficient to guarantee convergence to the correct results. One additional requirement must be met in order to strictly satisfy the convergence requirements.



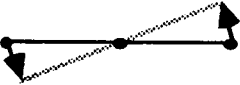
The third and final requirement of completeness for the reinforcement element states that for rigid body motions, the element must exhibit zero strain and zero nodal forces. The "embedded" reinforcement element assemblage shown in Figure 3.7 was used to test the constant strain requirement of the element for rigid body displacements. The nodal displacements corresponding to the rigid body motions of vertical translational (vt), horizontal translation (ht) and rotation (r) which were prescribed to the reinforcement element are:



$$\{q_i\}_{vt} = \begin{Bmatrix} 0.0 \\ 0.010 \\ 0.0 \\ 0.010 \\ 0.0 \\ 0.010 \end{Bmatrix}, \quad \{q_i\}_{ht} = \begin{Bmatrix} 0.010 \\ 0.0 \\ 0.0 \\ 0.010 \\ 0.0 \end{Bmatrix}, \quad \{q_i\}_r = \begin{Bmatrix} .007596 \\ -.086824 \\ -.007596 \\ .086824 \\ 0.0 \\ 0.0 \end{Bmatrix}$$

where  $\{q_i\} = \langle q_x^{11} \ q_y^{11} \ q_x^{19} \ q_y^{19} \ q_x^{15} \ q_y^{15} \rangle^T$

The strains and forces at each integration point within the reinforcement element when subjected to the above rigid body displacements are:

$\{\epsilon\}_{vt} = \begin{Bmatrix} 0.0 \\ 0.0 \\ 0.0 \end{Bmatrix}$	$\{F\}_{vt} = \begin{Bmatrix} 0.0 \\ 0.0 \\ 0.0 \end{Bmatrix}$	
		Vertical Translation
$\{\epsilon\}_{ht} = \begin{Bmatrix} .26 \times 10^{-17} \\ 0.0 \\ .26 \times 10^{-17} \end{Bmatrix}$	$\{F\}_{ht} = \begin{Bmatrix} .26 \times 10^{-14} \\ 0.0 \\ .26 \times 10^{-14} \end{Bmatrix}$	
		Horizontal Translation
$\{\epsilon\}_r = \begin{Bmatrix} -.0152 \\ -.0152 \\ -.0152 \end{Bmatrix}$	$\{F\}_r = \begin{Bmatrix} -15.2 \\ -15.2 \\ -15.2 \end{Bmatrix}$	
		Rotation

The finite element results from the rigid body displacement modes show that the reinforcement element does exhibit zero strain for rigid body translation but violates the zero strain requirement for rigid body rotation.

In order to further study the rigid body displacement modes and assess the nonzero strain result associated with rotation of the element, the following eigenproblem was solved:

$$[K] \{\phi_i\} = \lambda_i \{\phi_i\} \quad [3.39]$$

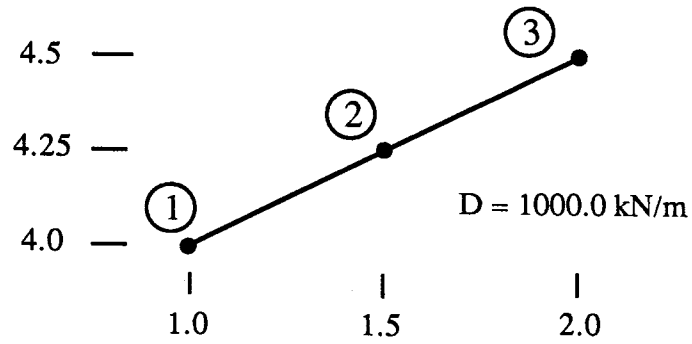
where  $[K]$  = stiffness matrix of element

$\{\phi_i\}$  = eigenvector defining the characteristic modes of deformation of the element

$\lambda_i$  = eigenvalues which represent the amount of strain energy required to attain the deformed shape defined by  $\{\phi_i\}$

The number of zero eigenvalues,  $\lambda_i$ , are equal to the number of rigid body modes of the element. As noted by Bathe (1982), the number of element rigid body modes and hence zero eigenvalues, is equal to the number of element degrees of freedom minus the number of element straining modes. A three noded reinforcement element will have two straining modes; a constant strain mode and a linear varying strain mode. Since each node of the element has two degrees of freedom in two dimensional space, the number of zero eigenvalues which can be expected from the solution of the eigenproblem will be four.

A general orientation of the reinforcement element, as shown in Figure 3.8, was used for the determination of the element stiffness matrix  $[K]$ . The values in the stiffness matrix are also given in Figure 3.8. Using the stiffness matrix, Equation 3.39 was solved to find  $\{\phi_i\}$  and  $\lambda_i$ . These quantities are also given in Figure 3.8. Figure 3.9 illustrates the modes of deformation of the element given by the eigenvectors  $\{\phi_i\}$ .



$$[K] = \begin{bmatrix} 1669.5974 & 834.7987 & 238.5139 & 119.2570 & -1908.1113 & -954.0557 \\ & 417.3994 & 119.2570 & 59.6285 & -954.0557 & -477.0278 \\ & & 1669.5974 & 834.7987 & -1908.1113 & -954.0557 \\ & & & 417.3994 & -954.0557 & -477.0278 \\ & \text{Symmetric} & & & 3816.2227 & -1908.1113 \\ & & & & & 954.0557 \end{bmatrix}$$

From the solution of Equation 3.39:

$$\{\phi_i\} = \begin{bmatrix} -.076 & .0311 & .4144 & -.5639 & -.6235 & .3651 \\ -.1077 & .0491 & .4070 & .8289 & -.3162 & .1826 \\ -.057 & -.3973 & .5453 & -.0908 & .6325 & .3651 \\ -.1453 & .906 & .1451 & -.0634 & .3162 & .1826 \\ -.5384 & -.0113 & .4062 & -.1078 & 0.0 & -.703 \\ .8175 & .1349 & .4234 & -.0293 & 0.0 & -.3651 \end{bmatrix}$$

$\phi_1 \quad \phi_2 \quad \phi_3 \quad \phi_4 \quad \phi_5 \quad \phi_6$

$$\lambda_i = \langle -.0024 \quad -.00066 \quad .0002 \quad .0009 \quad 1800.0 \quad 7200.0 \rangle^T$$

Figure 3.8 Data for Reinforcement Element Eigenproblem Solution

Four zero eigenvalues and two nonzero eigenvalues have been obtained. The fifth eigenvalue,  $\lambda_5 = 1800$ , represents a state of constant strain while  $\lambda_6 = 7200$  represents the condition of linear varying strain within the element. The first four eigenvalues show that conditions of translation of the element nodes perpendicular to or along the element direction do not cause straining in the element. The rotational rigid body displacement mode however, does not appear in the eigenproblem solution.

It appears the reinforcement element violates the third convergence or completeness requirement which states that an element must be able to represent the rigid body displacements. Although the reinforcement element develops zero strain during rigid body translation, rigid body rotation results in element strains. The violation of the rotation criteria does not, however, invalidate the reinforcement element formulation. It does show that during a finite element analysis of a reinforced soil structure, strains may develop within the reinforcement element if it undergoes significant rigid body rotation. In the problem analyzed for the present research, it will be seen that small rotations of the element occur. The strains induced in the reinforcement element will develop mainly from a lateral extension of the element due to the lateral movement of the slope. Testing of the element on small scale problems has indicated that for this class of problems (reinforced soil slope on a rigid foundation), the element performs

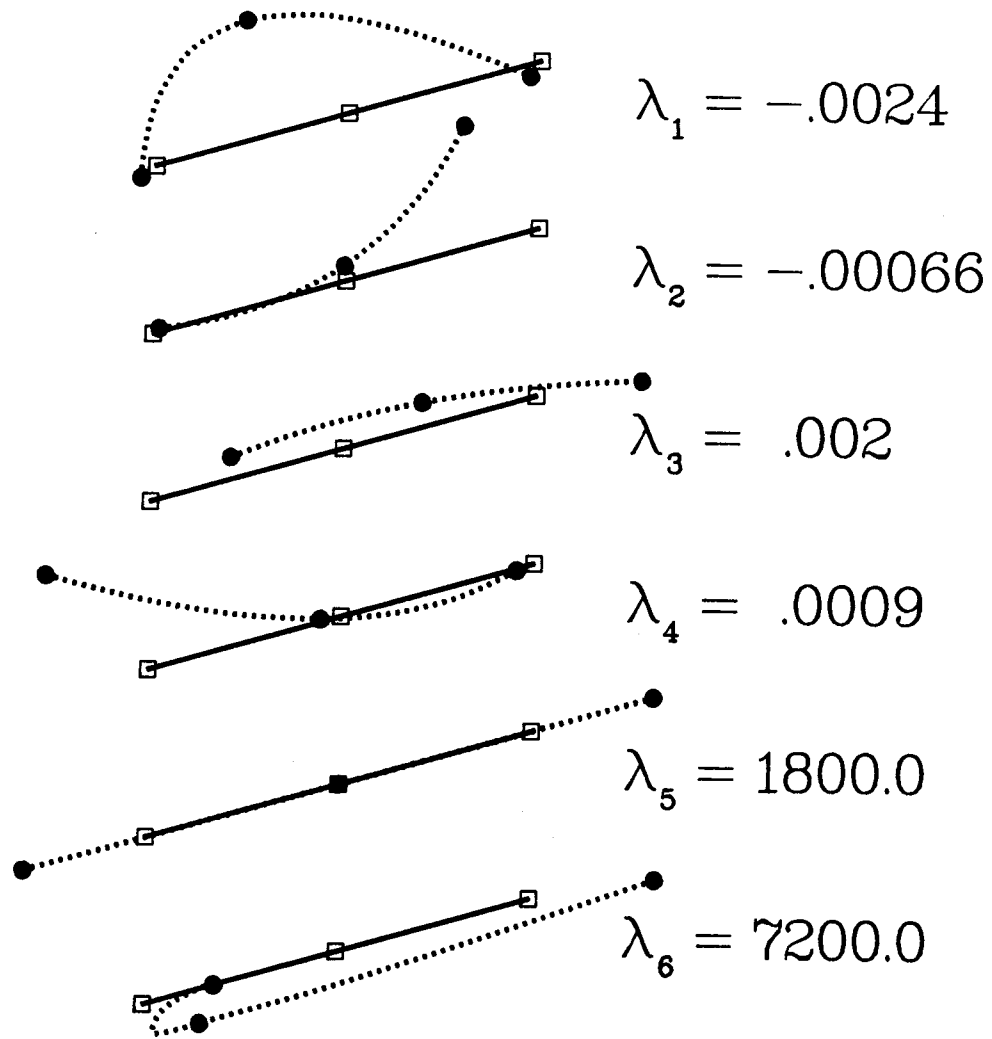


Figure 3.9 Eigenvectors and Eigenvalues for the Reinforcement Element

satisfactorily. It is realized however, that future development and implementation of the element in the solution of reinforced soil problems will require that the nonzero strain condition due to rigid body rotation of the element be corrected.

## 4. FINITE ELEMENT ANALYSIS OF A REINFORCED SOIL SLOPE

### 4.1 Introduction

The finite element method has been used to study the behaviour of a reinforced slope constructed on a rigid foundation. A finite element analysis allows for full consideration of the strength-deformation characteristics of the slope's constituents: the soil and the reinforcement. Unlike limit equilibrium methods which can not provide an engineer with information on the deformations, mobilized stresses within a soil slope or the loads developed within reinforcing layers, the finite element method provides these parameters by accounting for the stress-strain characteristics of the soil and the load-strain behaviour of the reinforcement. The finite element method has been used for the analysis of reinforced soil structures (Andrawes et al. (1980), Rowe et al. (1983), Brown and Poulos (1984) and Low and Duncan (1985)). The soil structures most commonly analyzed are reinforced walls or embankments constructed on soft/weak foundations.

This chapter presents the results of a nonlinear finite element analysis of a nonreinforced and reinforced embankment constructed on a rigid foundation. The nonreinforced and reinforced analyses are compared in order to show the effects due to the presence of the reinforcement. The finite element analysis yields the stresses, strains, deformations and reinforcement loads in

the slope. These values are subsequently used in Chapter 6 for calculating the factor of safety of the nonreinforced and reinforced slopes.

#### 4.2 Analysis Procedure

The embankment configurations analyzed in this research are illustrated in Figure 4.1. The embankment is constructed to a maximum height of 18 m with side slopes of 1:1. Slopes of 1:1 are considered a limit for practical construction of reinforced slopes when not using a "wrap around" construction technique. The reinforcement layers are placed horizontally with vertical spacings of 1 m. The lengths of each reinforcement layer were determined in part by a requirement to reduce the possibility of reinforcement pullout and by the finite element mesh design. The foundation soil is assumed to be rigid and behave elastically under embankment loading. The stiffness of the foundation was selected to be approximately 500 times larger than the embankment soil stiffness. A foundation approximately 500 to 1000 times stiffer than the embankment is considered to be a rigid foundation (Kulhawy, 1977).

The geometry selected for the embankment was not intended to model any particular embankment configuration but rather to represent a general design case for which the effects of the reinforcement on slope behaviour could be examined. Since the effects of reinforcement spacing on slope behaviour is not of concern in the present research, a



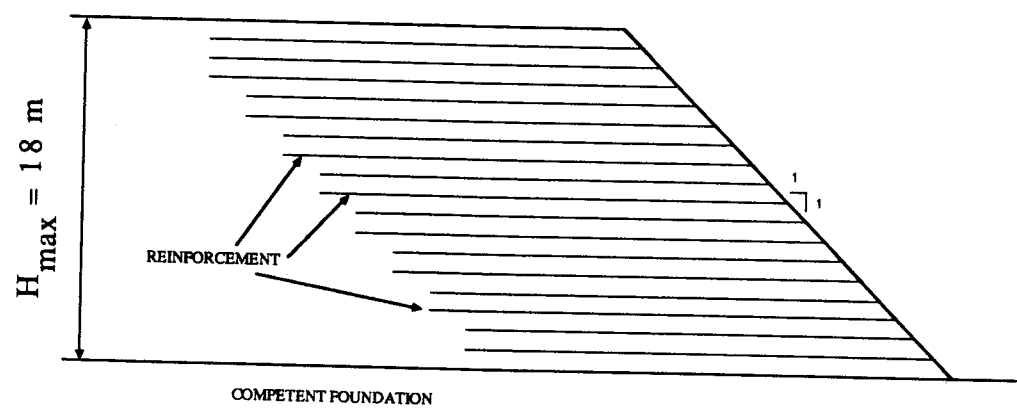
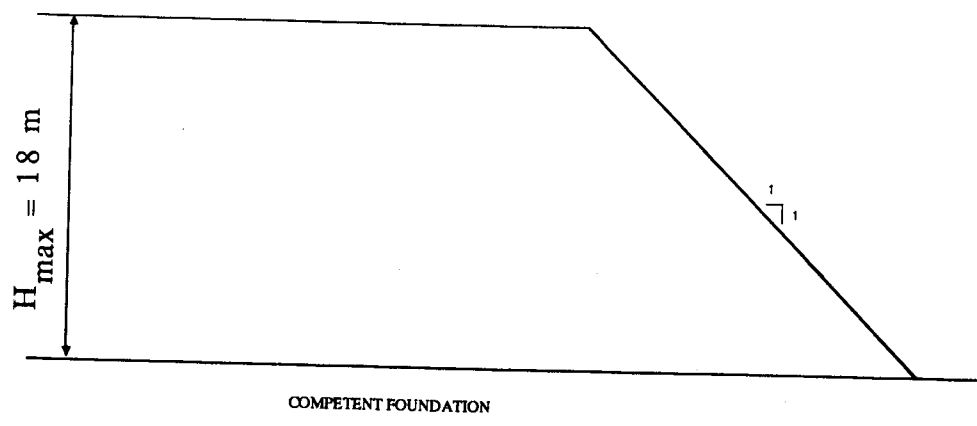


Figure 4.1 Nonreinforced and Reinforced Embankment Configurations

uniform vertical spacing of the reinforcement was chosen.

The finite element mesh is illustrated in Figure 4.2. The nonreinforced slope mesh constitutes 369 embankment elements and 133 foundation elements using a total of 1652 nodes. The reinforced slope mesh utilizes the same number of nodes and foundation elements but requires an additional 205 elements to model the reinforcement within the embankment. The soil is modelled using 6 and 8 node isoparametric elements. The reinforcement is modelled using the reinforcement element derived in Chapter 3.

The base of the foundation is assumed to be fixed. The left boundary represents a line of symmetry or the centerline of the embankment which restricts horizontal movements but permits free movement vertically. The right boundary restricts horizontal movements but allows vertical movements. The stages of embankment construction modelled in the finite element analysis are illustrated in Figure 4.3. The first step in the analysis involves placing the initial stresses in the foundation material using the "turn-on gravity" method. Successive load steps consist of placing 1 m lifts of soil and reinforcement (for the reinforced slope case) until the maximum embankment height of 18 m is achieved.

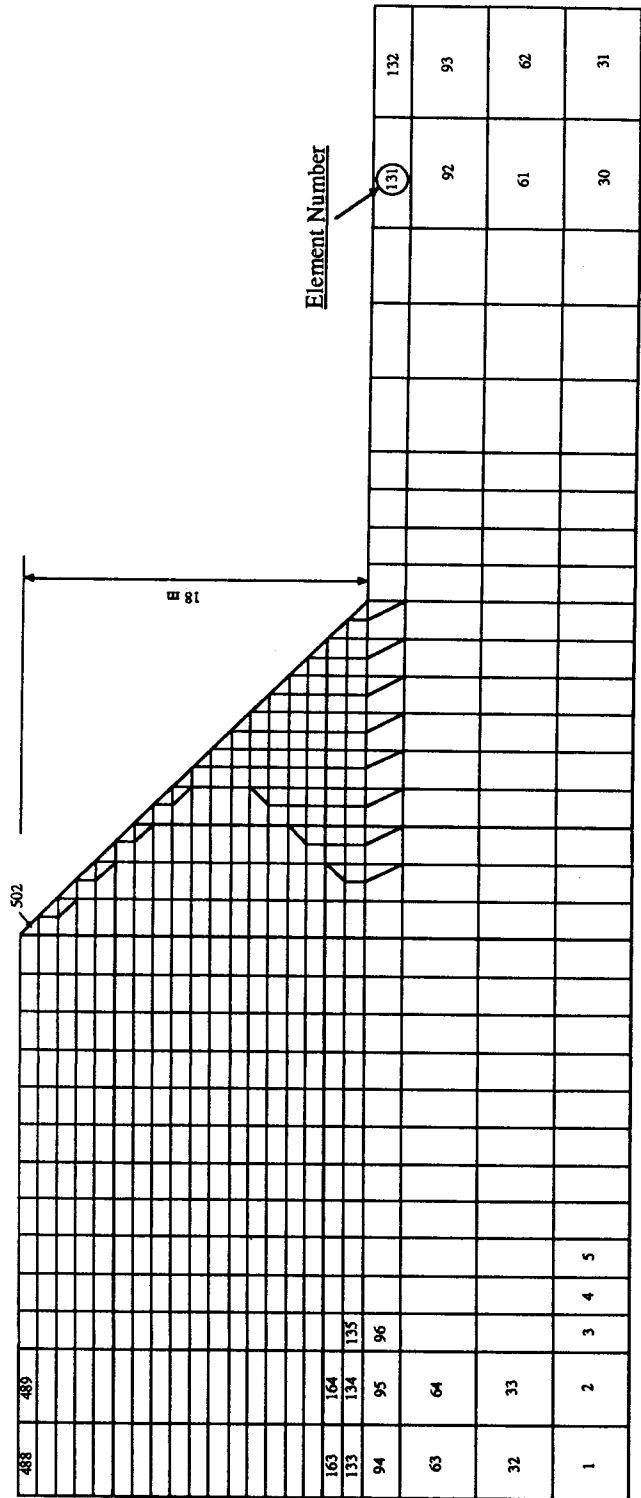


Figure 4.2 Finite Element Idealization of the Embankments

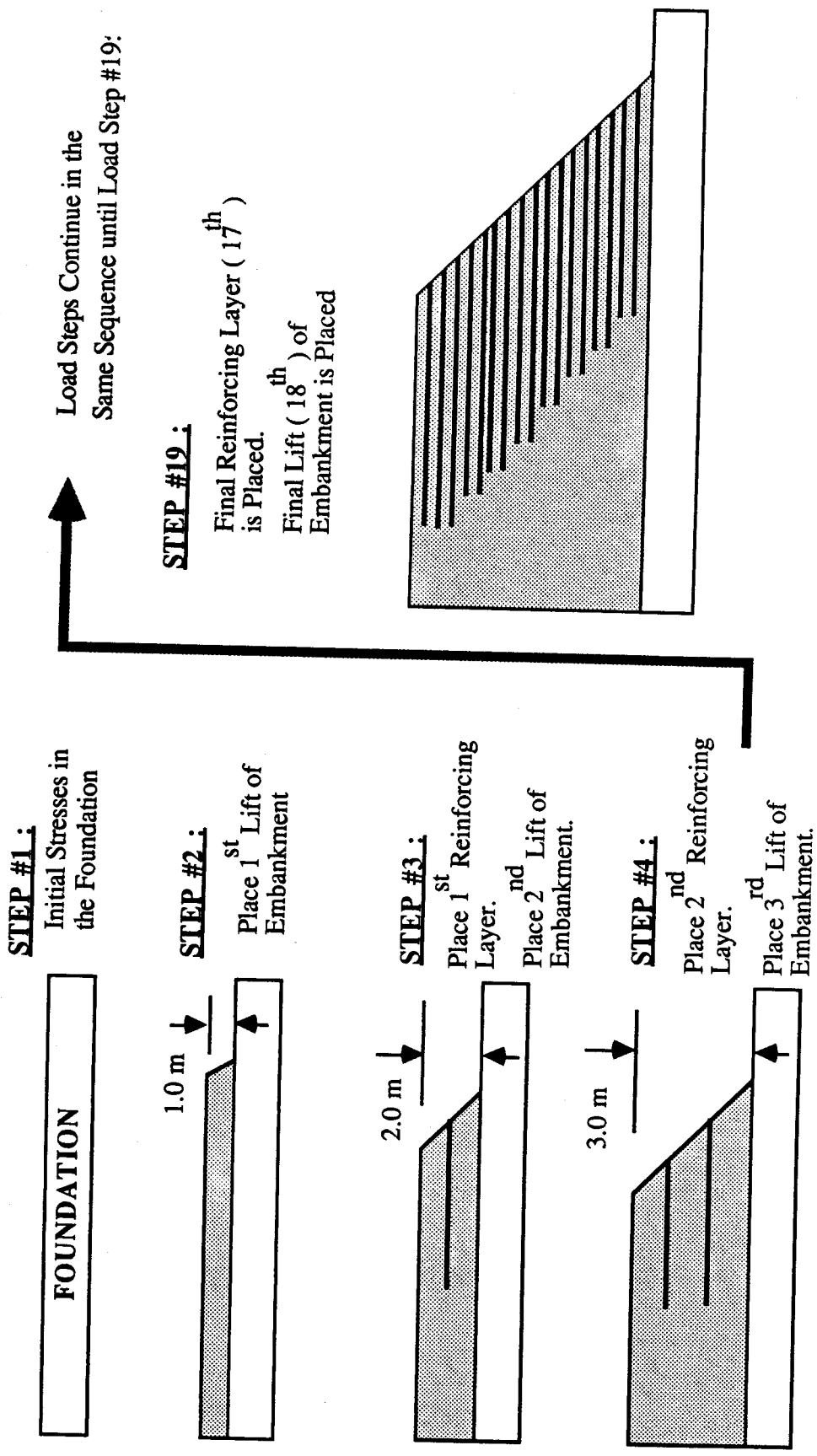


Figure 4.3 Embankment Construction Sequences used in Finite Element Analysis

### 4.3 Material Properties

#### 4.3.1 Soil

The soil type selected for the finite element analysis is a clayey silt of low to medium plasticity. This soil type is presently being used in the construction of the Devon Geogrid Test Fill (Scott et al, 1987). The soil is being recompacted at a moisture content approximately 3% above its optimum moisture content. Consequently, the soil exhibits strain hardening behaviour with failure strains of approximately 9% under consolidated undrained triaxial loading conditions. The soil also exhibits moderately rapid consolidation characteristics indicating that consolidation of each lift of embankment soil will likely occur prior to the application of the next lift of soil. Assuming each consolidated lift of soil acts in an undrained manner to the loading provided by subsequent lifts of soil, isotropically consolidated undrained triaxial test results have been selected for modelling the stress-strain behaviour of the soil. Details of the soil testing program and the test results can be found in Hofmann(1988).

A secondary reason for choosing the Devon Geogrid Test Fill soil for this analytical study is that as a part of the test fill project, an extensive soil-reinforcement interaction study with several geosynthetics using a direct shear apparatus and the test fill soil was undertaken (Bobey, 1988). These results will allow for an assessment of

the soil-reinforcement interface behaviour and its corresponding effect on the behaviour of the reinforced slope.

The stress-strain model selected for modelling the behaviour of the soil is the hyperbolic elastic model originally developed by Chang and Duncan (1969). Many versions of the hyperbolic elastic model have been developed with the most common versions based on Young's Modulus and Poisson's ratio or due to the need to model the volume change behaviour of soil, Young's modulus and the bulk modulus,  $B$ . Detailed description of the hyperbolic model used for finite analyses of stress and movement in soil masses can be found in Duncan et al., (1980). The hyperbolic model version used in the present study is based on the instantaneous Young's Modulus,  $E_t$ , which varies with confining pressure, and a constant Poisson's ratio. The model parameters derived from consolidated undrained triaxial test results are listed in Table 4.1. Figure 4.4 illustrates the stress-strain curves as given by the hyperbolic elastic model.

#### **4.3.2 Reinforcement**

The geosynthetic selected for the slope reinforcement is Tensar SR2. Tensar SR2 is a uniaxial, high strength geogrid constructed of high density polyethylene. Since the present analysis is concerned only with the short term, end of construction behaviour of the reinforced embankment, the

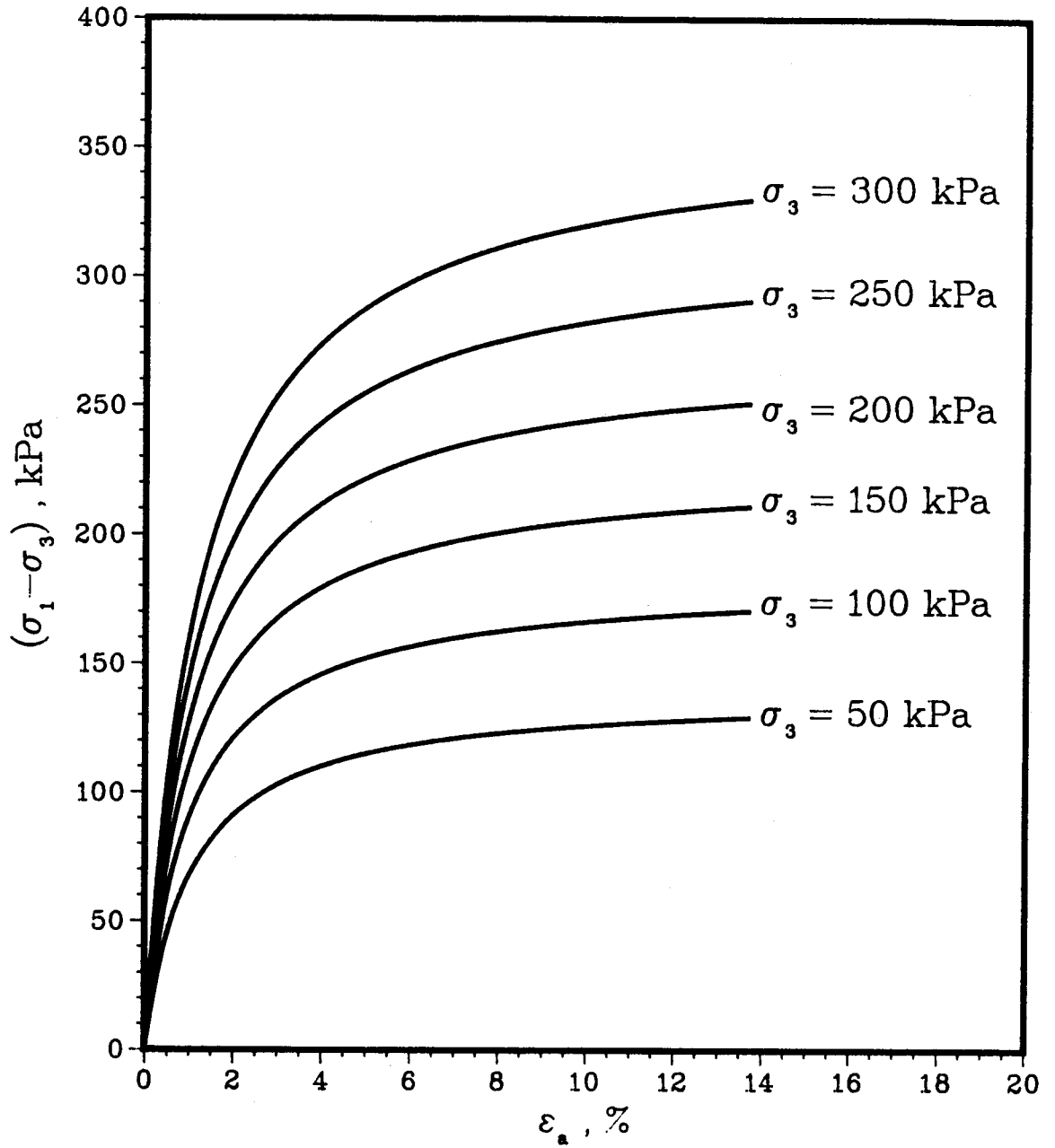


Figure 4.4 Hyperbolic Stress-Strain Relationship used in Modelling Soil Behaviour

creep, stress relaxation and temperature characteristics of Tensar SR2 are not incorporated in the analysis. An excellent summary of the effects of creep, stress relaxation and temperature on the behaviour of Tensar SR2 can be found in Andrawes et al. (1986). The load-strain behaviour of Tensar SR2 under standard test conditions of 20°C and a strain rate of 2% per minute are used to model the reinforcement.

The nonlinear quadratic reinforcement model developed in Chapter 3 is used to represent the load-strain behaviour of Tensar SR2. The model parameters used for the analysis are listed in Table 4.2. Figure 4.5 illustrates the load-strain curve given by the model along with a typical load-strain curve from a wide width tensile test on a Tensar SR2 specimen.

**4.4 Nonreinforced Slope Analysis Results**

In order to assess the effect of reinforcement on the behaviour of a reinforced embankment, it is necessary to understand the behaviour of its nonreinforced counterpart. This section presents the results of a nonlinear finite element analysis of a nonreinforced embankment with a geometry identical to that of the reinforced embankment. The analysis was conducted in terms of total stress and proceeded incrementally with each load step representing the placement of a 1 m lift of soil. The following results examine the stresses, strains and deformations for the final



Table 4.1 Parameters for the Hyperbolic Elastic Soil Model

PARAMETER	SYMBOL	Embankment Values	Foundation Values
Modulus of Elasticity	E	.....	3400 Mpa
Modulus Number	K	177	.....
Unloading Modulus No.	$K_{un}$	354	.....
Modulus Exponent	n	.43	.....
Cohesion	c	33 kPa	.....
Friction Angle	$\phi$	$17^{\circ}$	.....
Failure Ratio	$R_f$	.94	.....
Poisson's Ratio	$\nu$	.4	.49
Unit Weight	$\gamma$	20 kN/m <sup>3</sup>	20 kN/m <sup>3</sup>

Table 4.2 Parameters for the Nonlinear Quadratic Reinforcement Model

PARAMETER	SYMBOL	Reinforcement Values
Initial Modulus	$D_i$	778
Unloading Modulus	$D_{un}$	1556
Failure Strain	$\epsilon_f$	18 %

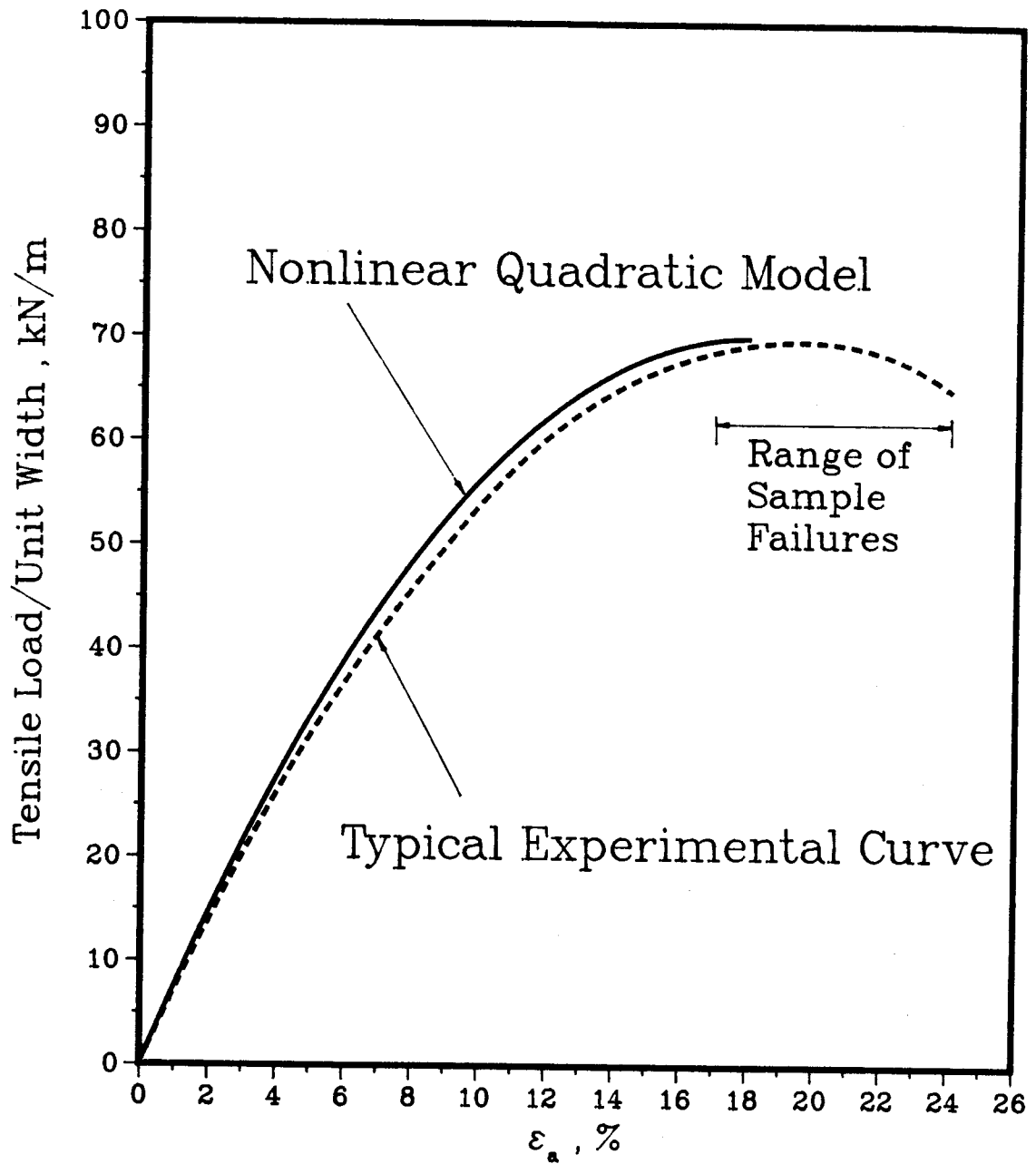


Figure 4.5 Nonlinear Quadratic Load-Strain Relationship used in Modelling Reinforcement Behaviour

embankment height of 18 m. The results for embankment heights of 5 m, 10 m and 15 m are included in Appendix C.

#### 4.4.1 Stresses

A straightforward manner of assessing the state of stress within the embankment can be accomplished by examining the degree of soil strength mobilized in order to maintain embankment stability. For the present analysis, the strength mobilized by the soil will be defined as:

$$\% \text{ Strength Mobilized} = \frac{(\sigma_1 - \sigma_3)_{\text{mobilized}}}{(\sigma_1 - \sigma_3)_{\text{failure}}} \times 100 \quad [4.1]$$

The contours representing the magnitudes of strength mobilized for the embankment at the end of construction are illustrated in Figure 4.6. It is clear from this graph that a "band" of soil has mobilized greater than 95% of its strength. This band represents the development of a failure zone within the slope. Note the circular arc followed by the "yield" band indicating the possible formation of a circular failure surface passing through the toe of the slope. The compact contour lines in the upper portion of the embankment are the result of tensile stresses.

The distribution of tensile stresses within the embankment are illustrated in Figure 4.7. In general, most of the tensile stresses can be attributed to the boundary condition imposed by the left centerline boundary. Horizontal movement is restricted along this boundary and

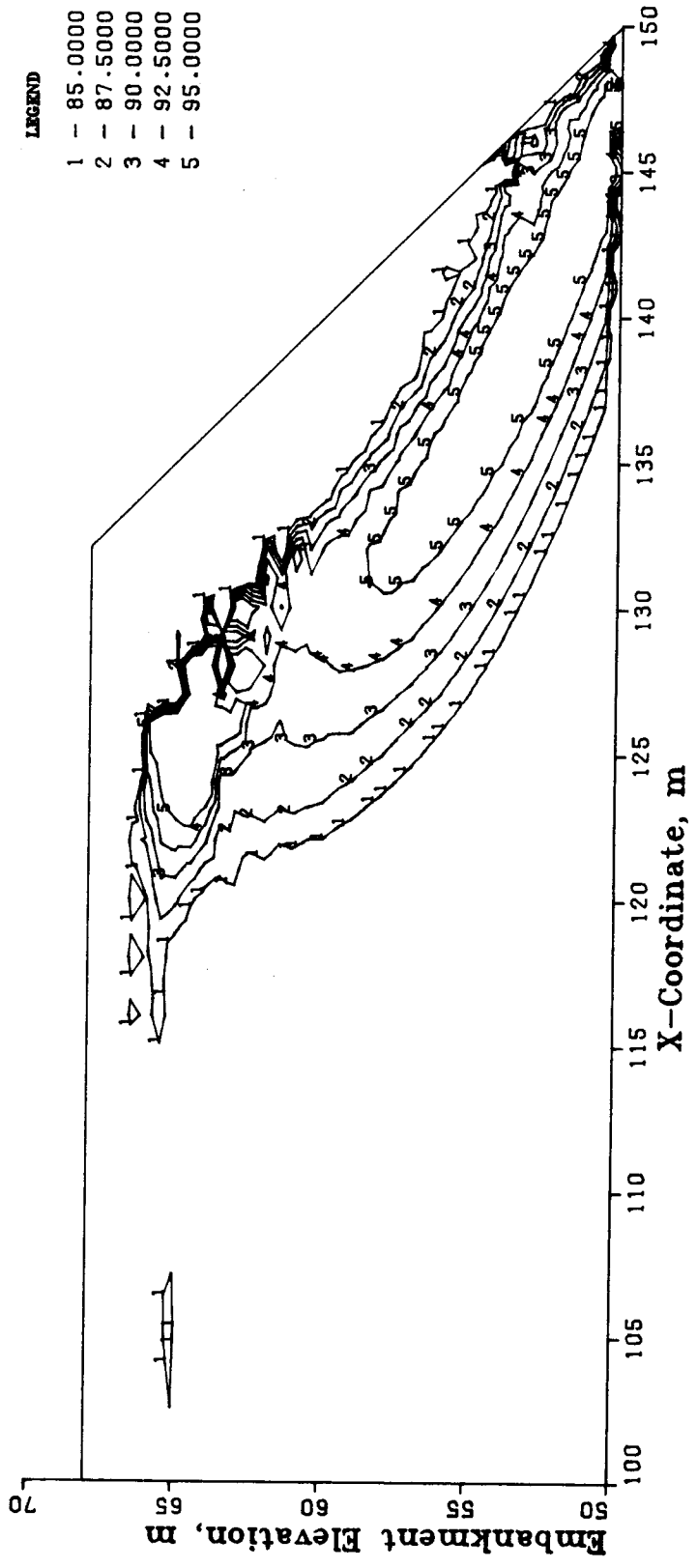


Figure 4.6 Mobilized Soil Strength (%) in Nonreinforced Embankment, H = 18 m

consequently, as the embankment deforms laterally to the right, the horizontal fixity at this boundary will induce tensile stresses in the regions illustrated in Figure 4.7. The magnitude of the tensile stresses in these zones is small compared to the compressive stresses in the slope portion of the embankment and thus, do not greatly affect the overall embankment behaviour.

**4.4.2 Strains**

The angular distortion occurring within the soil mass can be evaluated by examining the maximum shearing strains. Figure 4.8 illustrates the maximum shearing strains within the nonreinforced embankment at the end of construction. A maximum shear strain of greater than 20% was reached in the toe region of the slope. Similar to the mobilized strength contours, the contours of  $\gamma_{max}$  also indicate the formation of a "yield" band which follows a circular arc shape.

The horizontal strains,  $\epsilon_x$ , in the embankment slope are illustrated in Figure 4.9. A maximum horizontal strain of 4.5% was reached at a point below the embankment crest and approximately midheight in the slope. Examination of the  $\epsilon_x$  contours for embankment heights of 5 m, 10 m and 15 m (see Appendix C), reveals that the maximum value occurs in the same location for all the embankment heights.

The vertical strains,  $\epsilon_y$ , developed at the end of construction are illustrated in Figure 4.10. A maximum  $\epsilon_y$  of

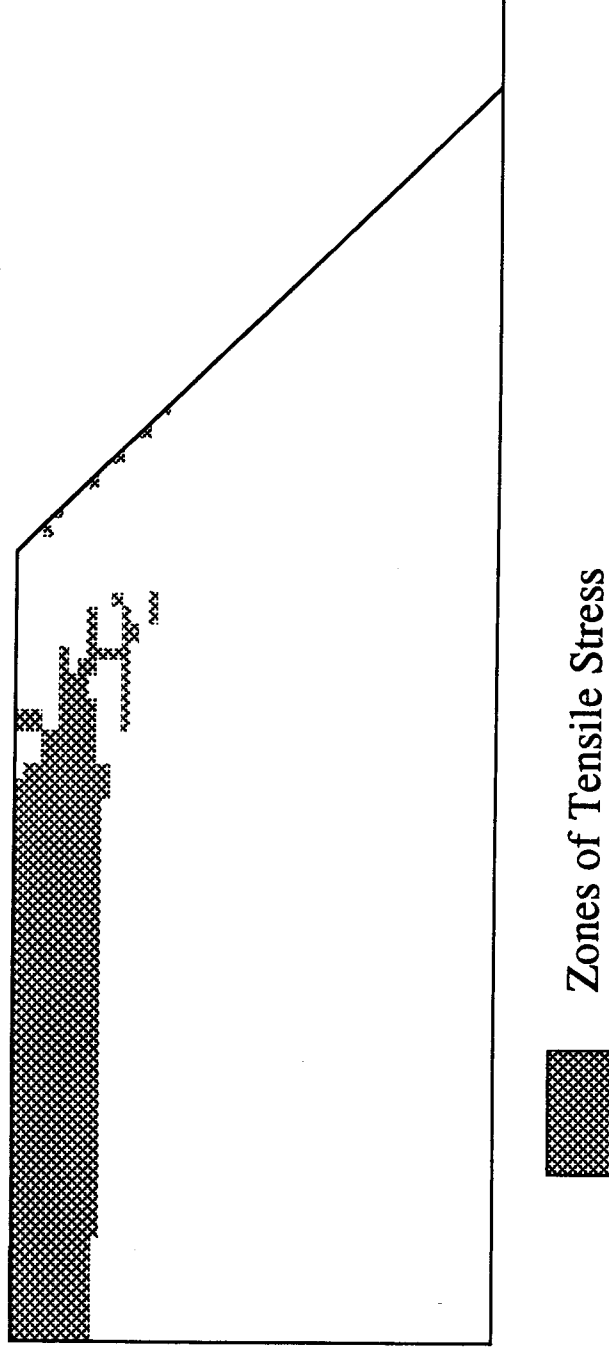


Figure 4.7 Tensile Stress Zones in Nonreinforced Embankment,  $H = 18$  m

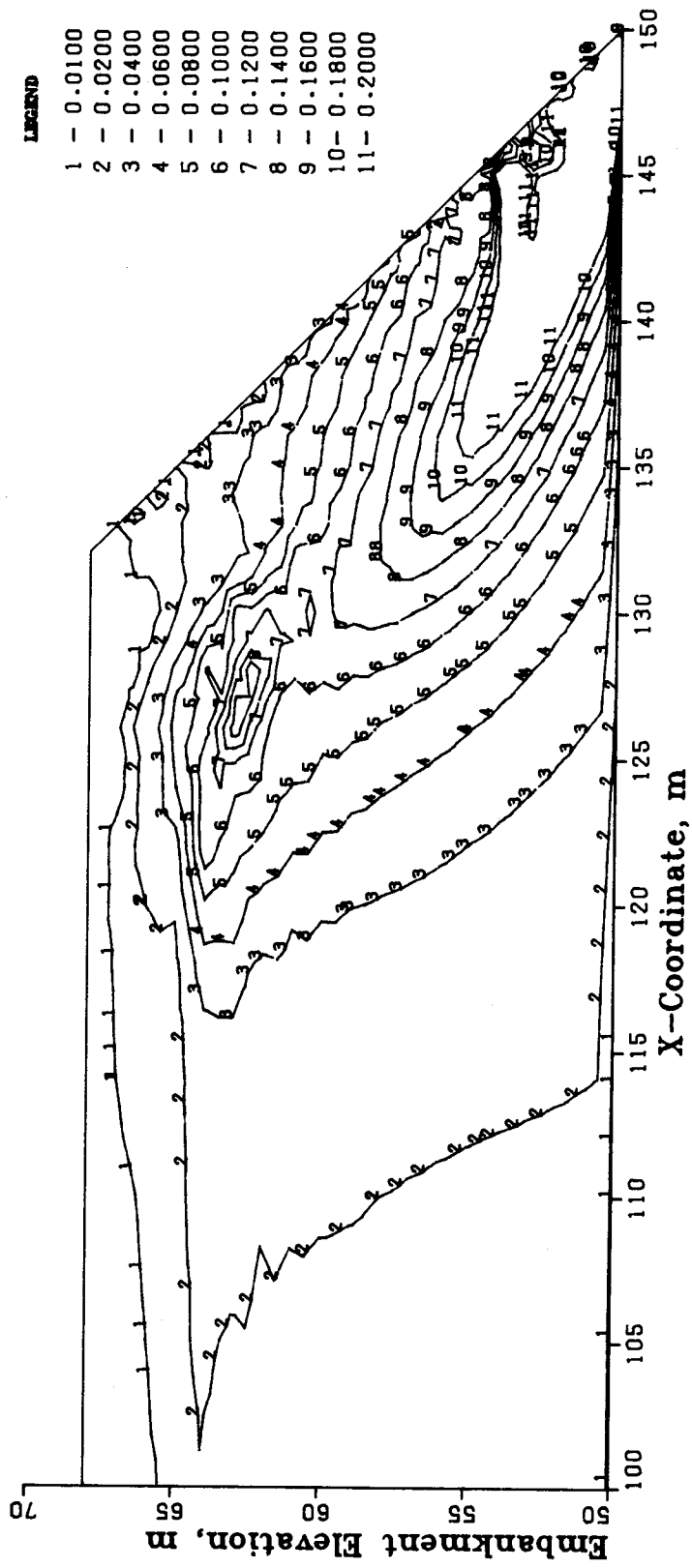


Figure 4.8 Maximum Shear Strains,  $\gamma_{max}$ , in Nonreinforced Embankment,  $H = 18$  m

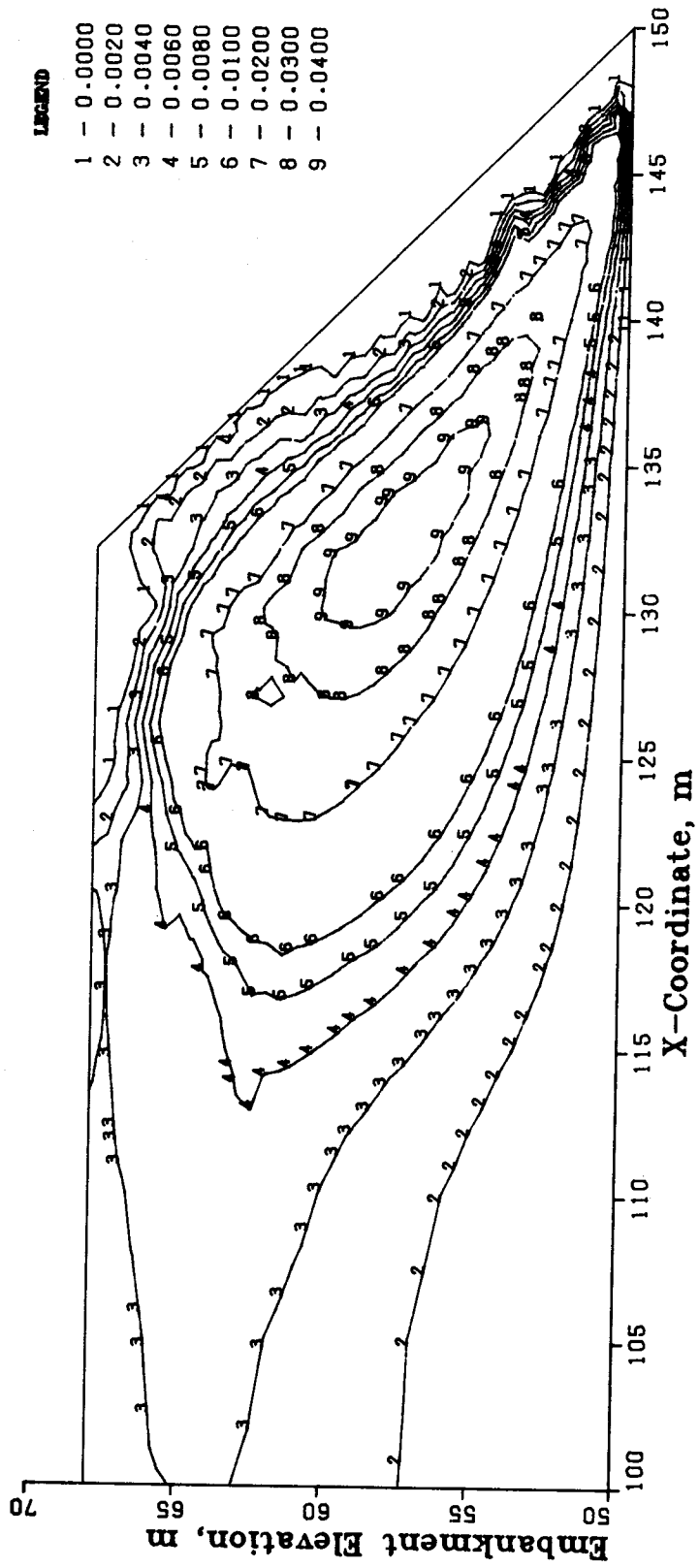


Figure 4.9 Horizontal Strain,  $\epsilon_x$ , in Nonreinforced Embankment,  $H = 18$  m



8.2% was realized in the nonreinforced embankment. The  $\epsilon_y$  contours for embankment heights of 5 m, 10 m and 15 m (see Appendix C) and for 18 m show that the contour of maximum vertical strain develops below the slope crest but moves up in the slope as the slope height increases.

Several investigators (Ingold (1982), McGown et al. (1978), Jones (1984)) have shown that in order to obtain maximum tensile resistance from planar reinforcement, their orientation within a soil mass should follow the orientation or direction of the maximum tensile strains. The magnitude and orientation of the maximum tensile strains,  $\epsilon_3$ , for the nonreinforced embankment are illustrated in Figure 4.11. It is clear that in the toe region of the slope, a significant rotation of the tensile strain axis occurs. Note also that the magnitude of  $\epsilon_3$  is a maximum in the toe region of the slope and remains relatively large within the zone of the slope where  $\epsilon_x$  and  $\epsilon_y$  attain their peak value.

#### 4.4.3 Deformations

By examining the velocity field within the embankment, the internal deformation pattern of the soil mass can be studied. A velocity field is created by plotting displacement arrows from the initial position of a point within the embankment to its final displaced position. The velocity field for the nonreinforced embankment at the end of construction is illustrated in Figure 4.12. This figure clearly shows the presence of a circular displacement

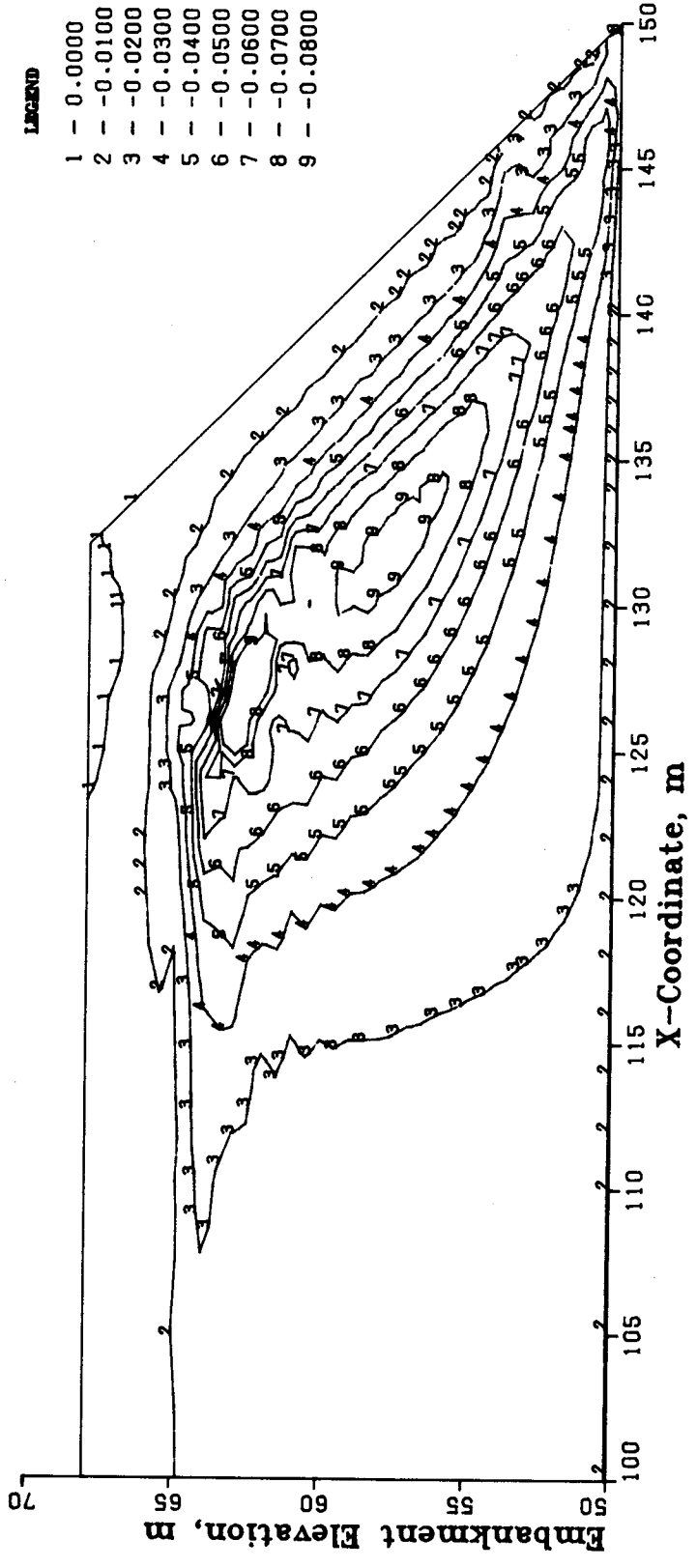


Figure 4.10 Vertical Strain,  $\epsilon_y$ , in Nonreinforced Embankment, H = 18 m

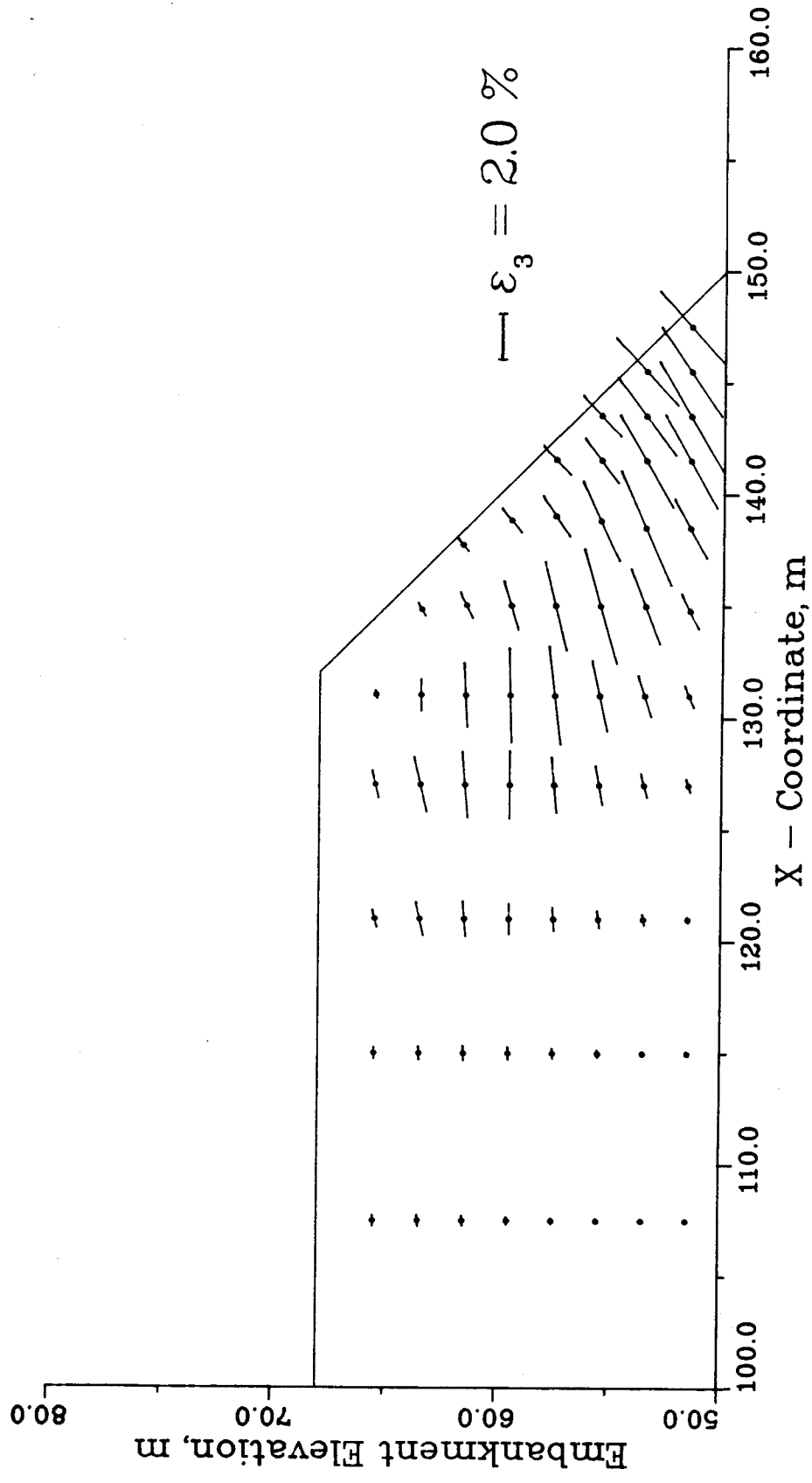


Figure 4.11 Principal Tensile Strains,  $\epsilon_3$ , in Nonreinforced Embankment, H = 18 m

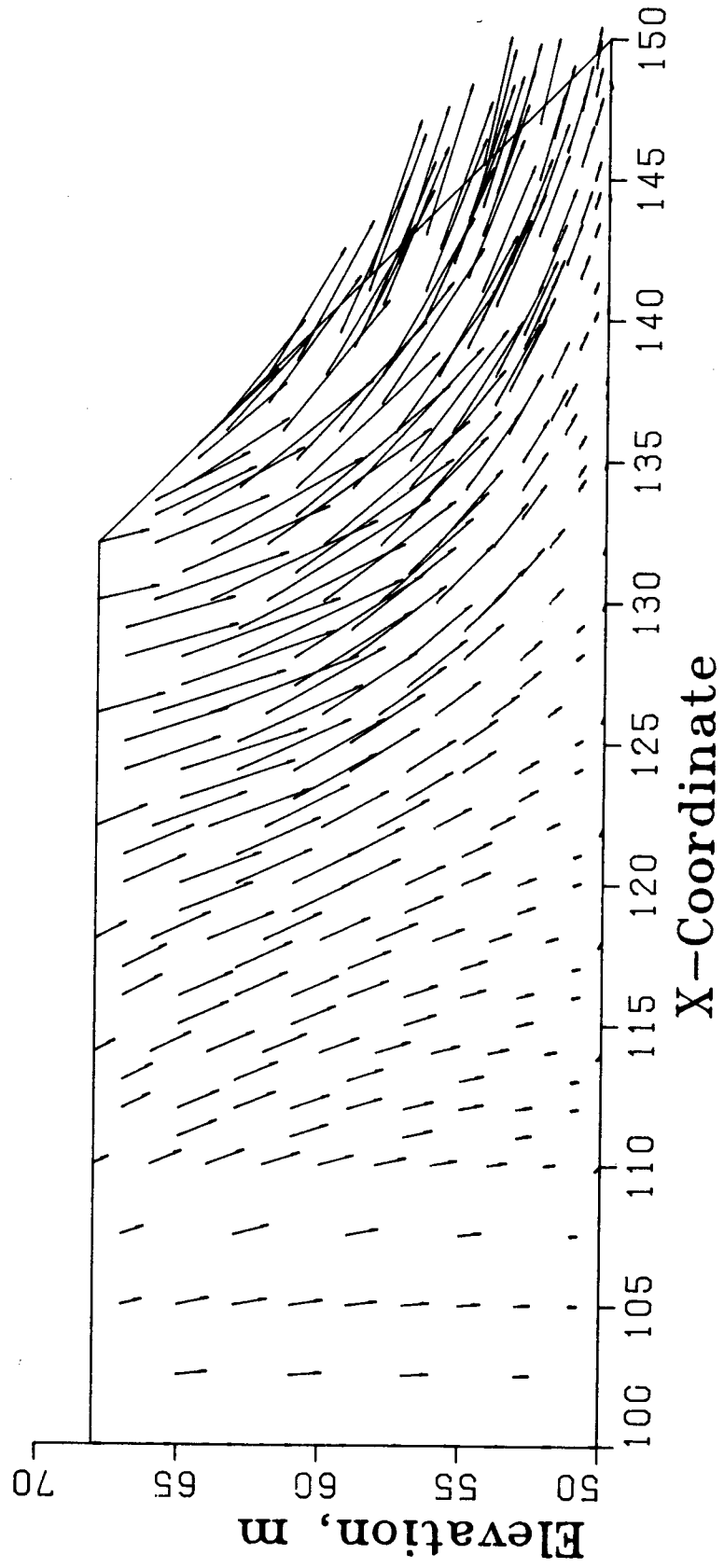


Figure 4.12 Velocity Field for Nonreinforced Embankment,  $H = 18$  m, (Scale: 1 cm = .5 m)

pattern establishing increased confidence in the observations of the development of a circular shaped failure surface. A maximum horizontal outward displacement of 55.4 cm occurred on the slope face at an elevation of 58 m or 8 m above the foundation. The displacement pattern for an embankment height of 5 m shows very little movement within the slope. The movements begin to increase at a height of 10 m and at 15 m are beginning to show the circular displacement pattern that is clearly visible in Figure 4.12.

#### **4.5 Reinforced Slope Analysis Results**

This section presents the results from an incremental, total stress, nonlinear finite element analysis of a reinforced embankment. Each load step of the embankment construction involved the placement of one layer of reinforcement and a 1 m lift of soil. The following results present the stresses, strains, deformations and reinforcement loads for the final embankment height of 18 m. The results for embankment heights of 5 m, 10 m and 15 m are presented in Appendix D.

##### **4.5.1 Stresses**

Applying the same definition for mobilized soil strength used in the nonreinforced embankment case (see Equation 4.1), Figure 4.13 illustrates the degree of soil strength mobilized in the reinforced embankment at the end of construction. A relatively small zone of soil in the toe

region of the slope has mobilized 92.5% of its strength. A circular shaped "yield" band appears to be developing but is not as readily apparent as it was in the nonreinforced slope.

The distribution of tensile stresses throughout the reinforced embankment are shown in Figure 4.14. The major cause of the tensile stresses is due to the phenomena described in section 4.4.1; the lateral displacements of the embankment are restricted by the left boundary constraint resulting in the development of tensile stresses within the soil mass.

#### 4.5.2 Strains

The maximum shearing strain,  $\gamma_{\max}$ , developed within the reinforced embankment was 18%. The distribution of  $\gamma_{\max}$  within the embankment is illustrated in Figure 4.15. As was the case in the nonreinforced slope, the largest shearing strain or angular distortion is concentrated in the toe region of the slope.

Figure 4.16 shows the distribution of horizontal strains within the reinforced embankment at the end of construction. A maximum  $\epsilon_x$  of 2.2% occurred below the crest and approximately midheight of the embankment.

The vertical strain,  $\epsilon_y$ , achieved a maximum value of 5.3% in approximately the same location as the maximum  $\epsilon_x$  value. Figure 4.17 illustrates the vertical strain contours

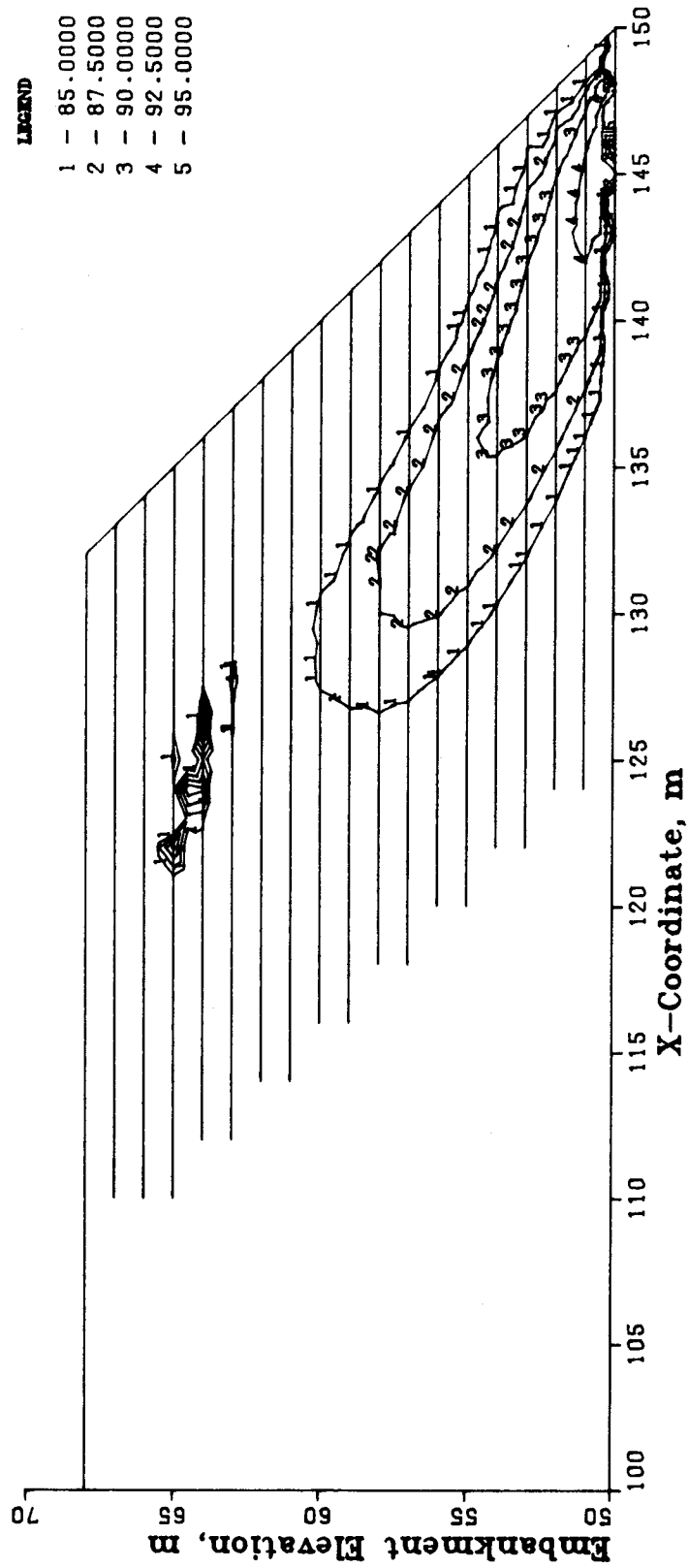


Figure 4.13 Mobilized Soil Strength (%) in Reinforced Embankment, H = 18 m

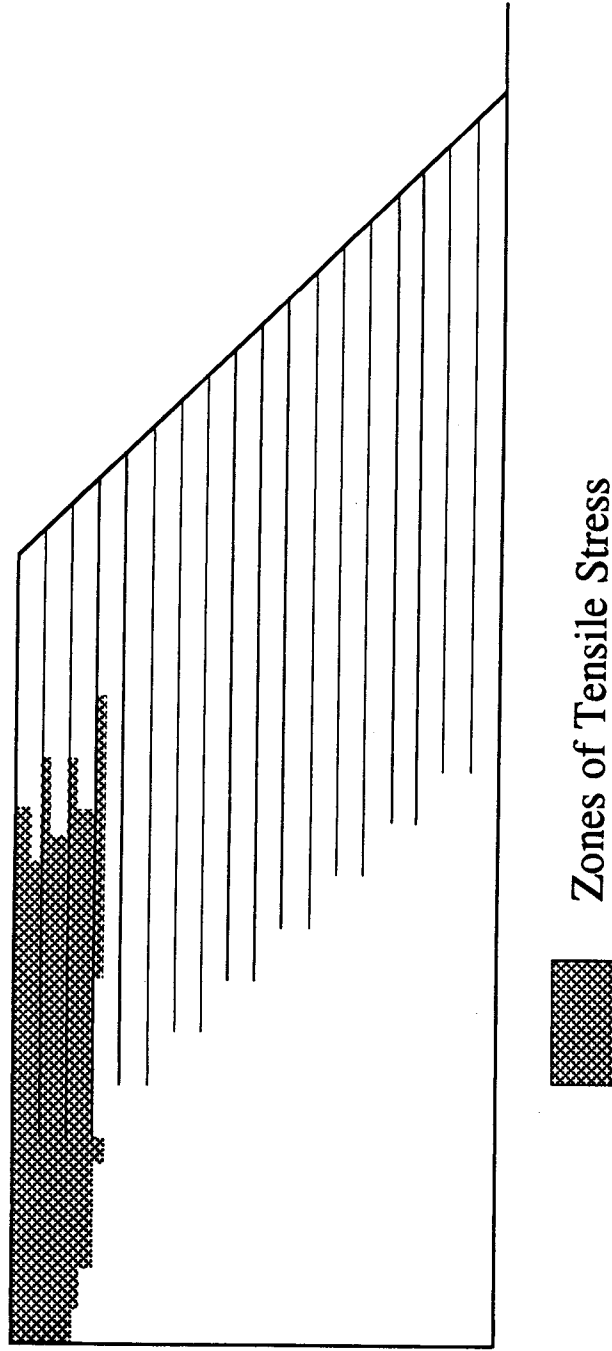


Figure 4.14 Tensile Stress Zones in Reinforced Embankment,  $H = 18 \text{ m}$



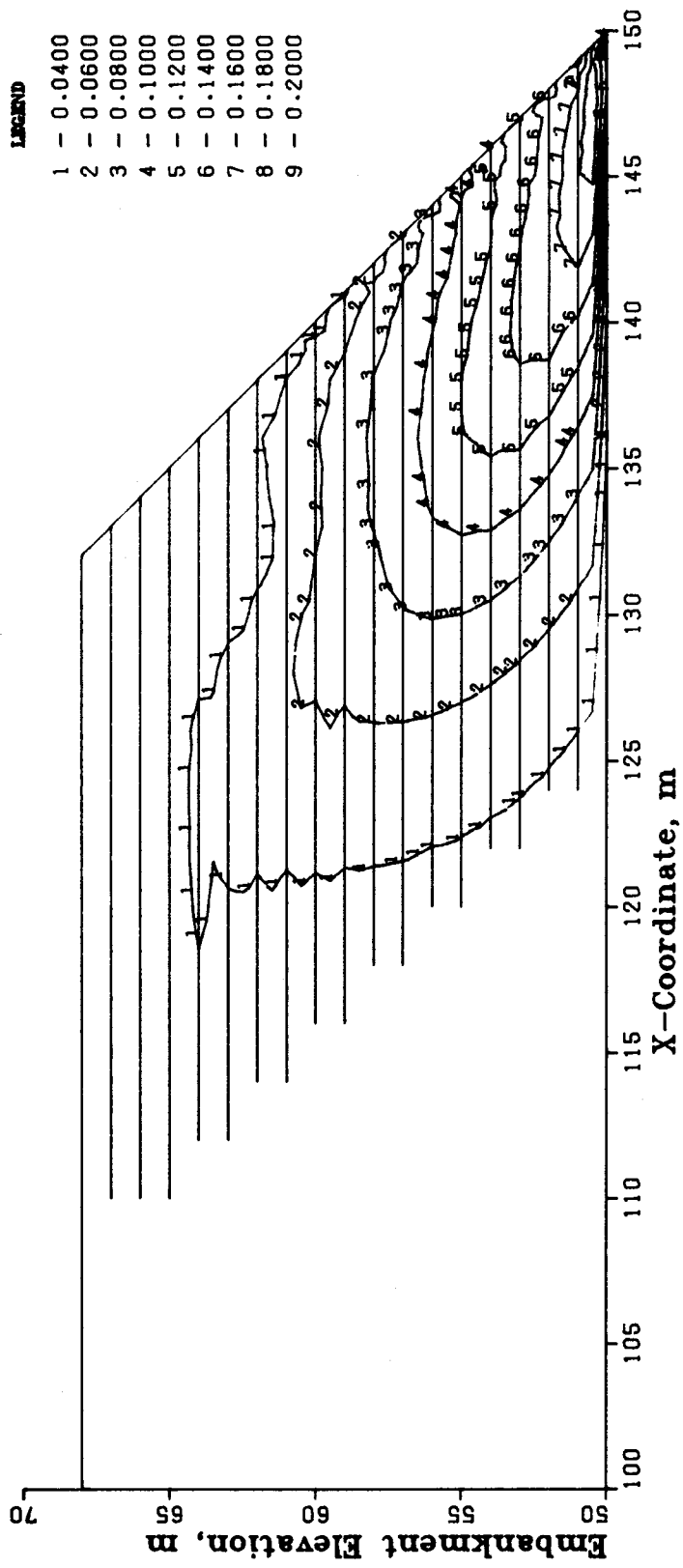


Figure 4.15 Maximum Shear Strain,  $\gamma_{max}$ , in Reinforced Embankment,  $H = 18$  m

for the reinforced embankment. As for the nonreinforced slope, the maximum  $\epsilon_x$  contour remained below the slope crest and midheight in the slope for all the slope heights while the maximum  $\epsilon_y$  contour moved upward in the slope immediately below the slope crest.

As discussed in Section 4.4.2, the orientation and magnitude of the maximum tensile strains,  $\epsilon_3$ , is an important consideration in the design of reinforced soil structures. For the reinforced embankment at a height of 18 m, Figure 4.18 illustrates the magnitude and orientation of  $\epsilon_3$ . It is clear that a significant rotation of the  $\epsilon_3$  axis still occurs in the toe region of the slope irregardless of the presence of the reinforcement.

#### 4.5.3 Deformation

The velocity field for the reinforced embankment at the end of construction is illustrated in Figure 4.19. The development of a circular displacement pattern is observed but not to the degree the pattern was discernible in the velocity field of the nonreinforced slope. A maximum horizontal displacement of 36.5 cm was reached at a location on the slope surface 8 m above the foundation. The velocity field for a slope height of 5 m illustrated in Figure D.13 indicates very little movement within the reinforced slope. An increase in the slope displacements is clearly visible in the velocity fields for the slope heights of 10 m and 15 m shown in Figures D.14 and D.15, respectively.

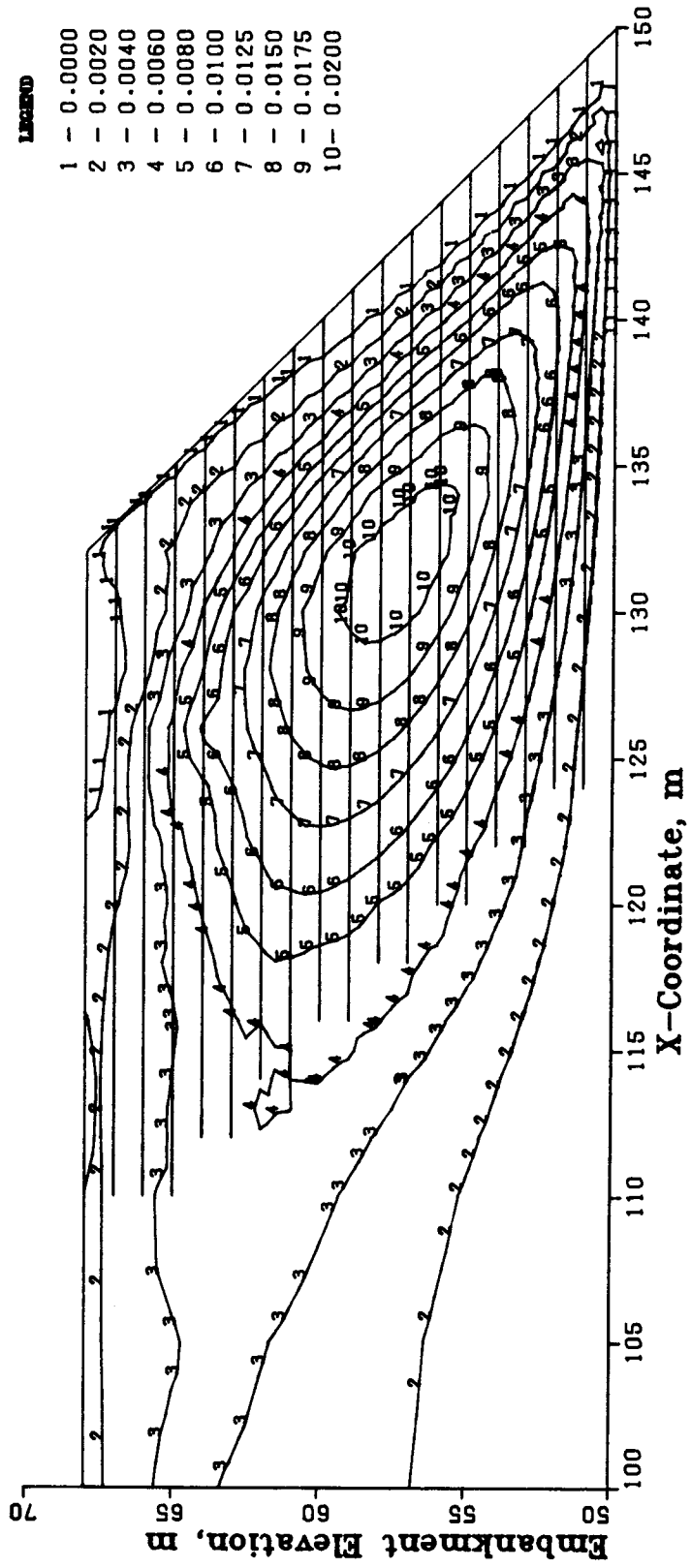


Figure 4.16 Horizontal Strain,  $\epsilon_x$ , in Reinforced Embankment,  $H = 18$  m

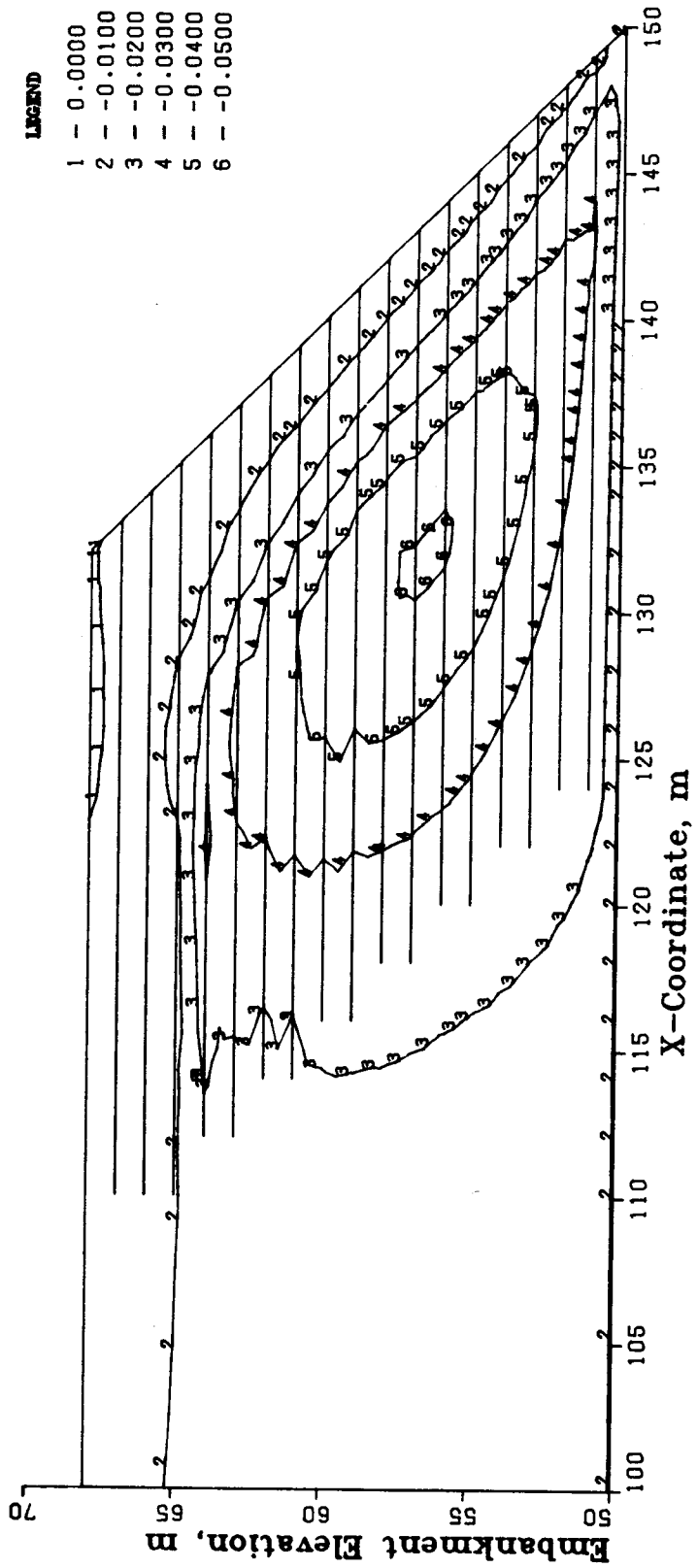


Figure 4.17 Vertical Strain,  $\epsilon_y$ , in Reinforced Embankment,  $H = 18$  m

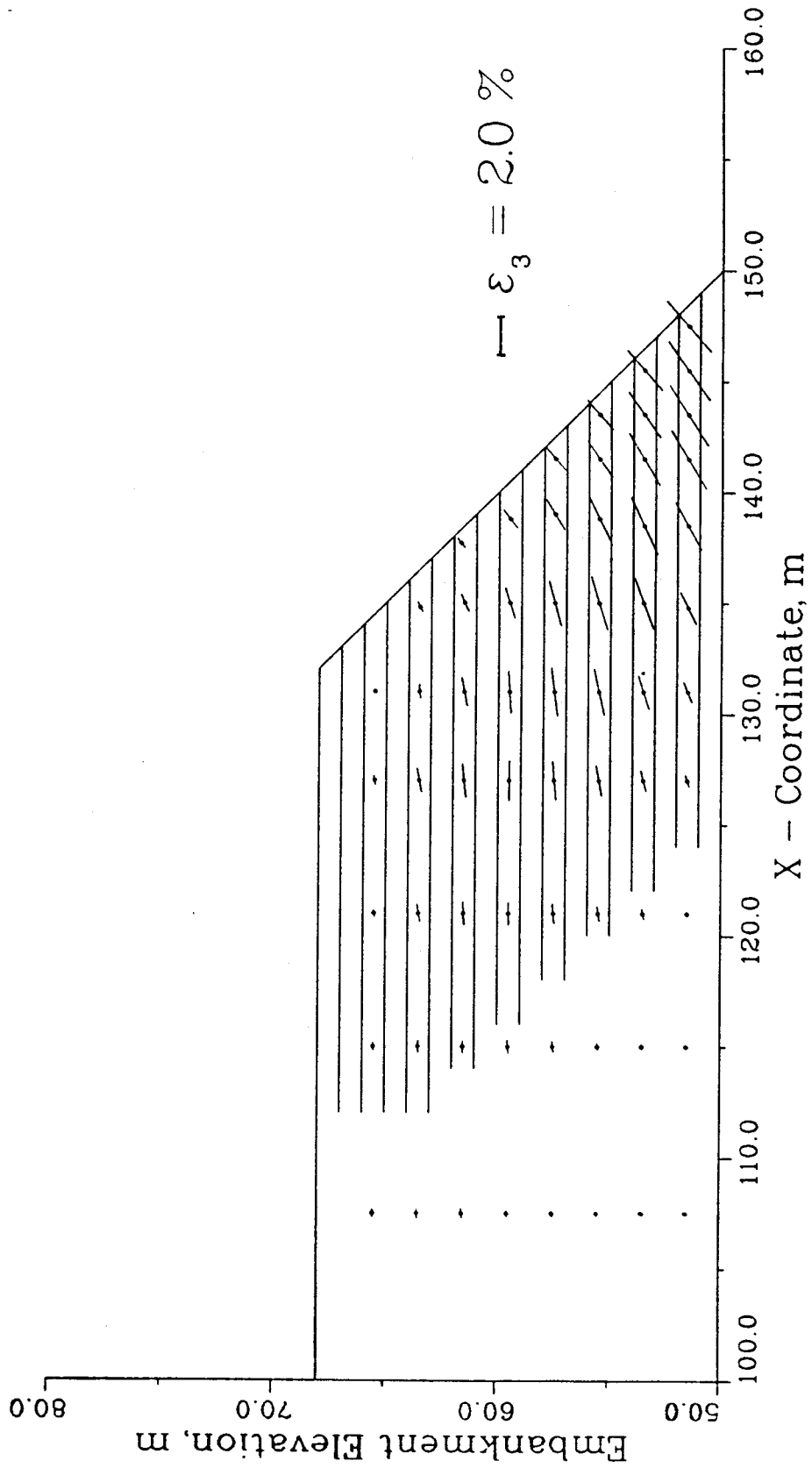


Figure 4.18 Principal Tensile Strains,  $\epsilon_3$ , in Reinforced Embankment, H = 18 m

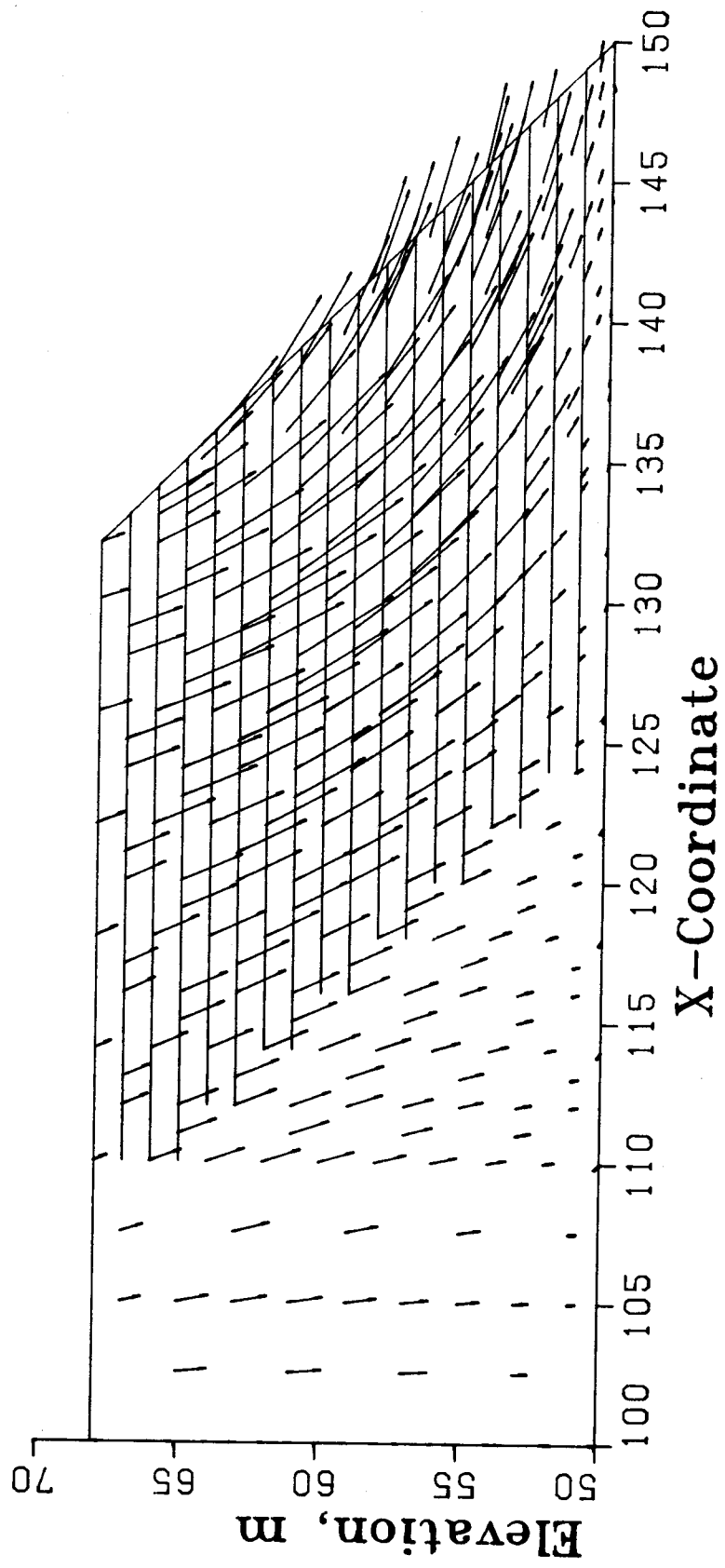


Figure 4.19 Velocity Field for Reinforced Embankment,  $H = 18$  m, (Scale: 1 cm = .5 m)

#### 4.5.4 Reinforcement Loads

As a result of the incremental analysis of the reinforced embankment, the loads in each layer of reinforcement are computed for each step of the embankment construction. Figure 4.20 illustrates the load distribution in the reinforcement layer 4 m above the foundation for embankment heights of 5 m, 10 m, 15 m and 18 m. The load distributions for the remainder of the reinforcement layers are presented in Appendix E.

Figure 4.20 shows the smooth mobilized load distribution along the reinforcement length. The development of load at the left end of the reinforcement is due to the restriction of zero relative displacement between the soil and the reinforcement; the displacements of reinforcement element nodes are compatible with the displacements of adjacent soil elements. Another important trend highlighted in Figure 4.20 is the zone of zero reinforcement load at the face of the embankment. Due to its negligible compressional stiffness, the reinforcement can not resist load in the compressive zones within the soil mass.

In order to handle the "no-compression" condition for the reinforcement, an allowable compressive load tolerance is assigned to the reinforcement. If the compressive load generated within the reinforcement due to soil compression exceeds the tolerance, the excess load is "removed" from the reinforcement, the reinforcement load is set to the

tolerance load level and the excess load is reapplied to the finite element system as an unbalanced load. This procedure is repeated until the soil resists the compressive loads and equilibrium is achieved. In this way, the reinforcement offers no resistance to compressive deformations within the soil mass. This procedure is similar to Zienkiewicz's stress transfer approach for handling "no-tension" analyses for soil or rock (Zienkiewicz et al. 1968). The reinforcement compression load tolerance for the present analyses was set to  $-0.001$  kN/m, where the negative sign denotes compression.

In studying the reinforcement load distributions, two important relationships have been discovered. The nomenclature shown in Figure 4.21 will be used to describe these relationships. Firstly, a unique correlation exists between  $h_i/H$ , which represents the level of the reinforcement compared to the embankment height, and  $T_i/T_{max}$ , which represents any reinforcement load compared to the maximum reinforcement load for a particular embankment height. Figure 4.22 illustrates the relationship between  $h_i/H$  and  $T_i/T_{max}$  for embankment heights of 5 m, 10 m, 15 m and 18 m. This figure clearly shows that regardless of the height of the embankment, the relationship describing the distribution of peak reinforcement loads within the slope remains unchanged.

It is important to realize that the shape of the curve in Figure 4.22 is unique to the reinforced slope



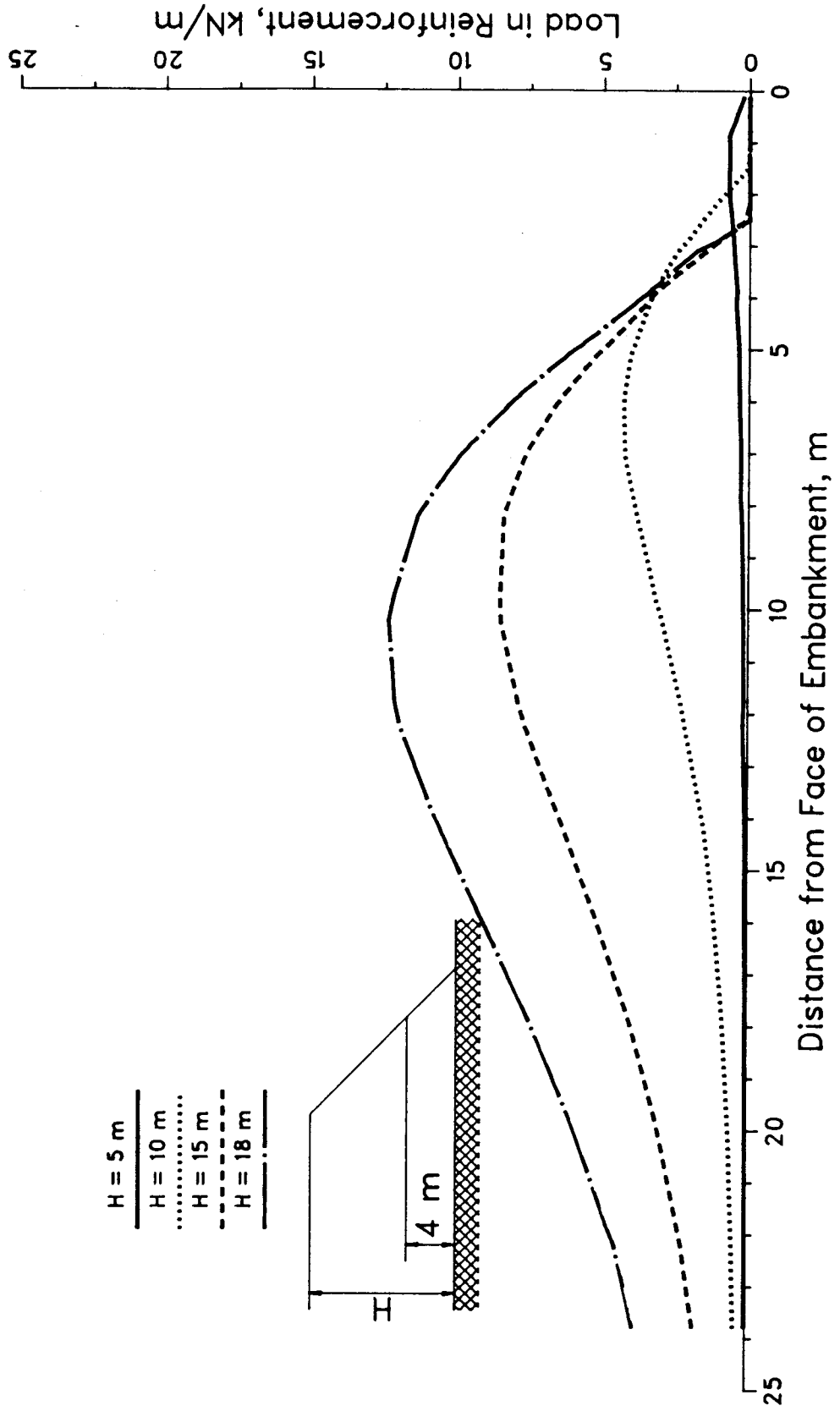
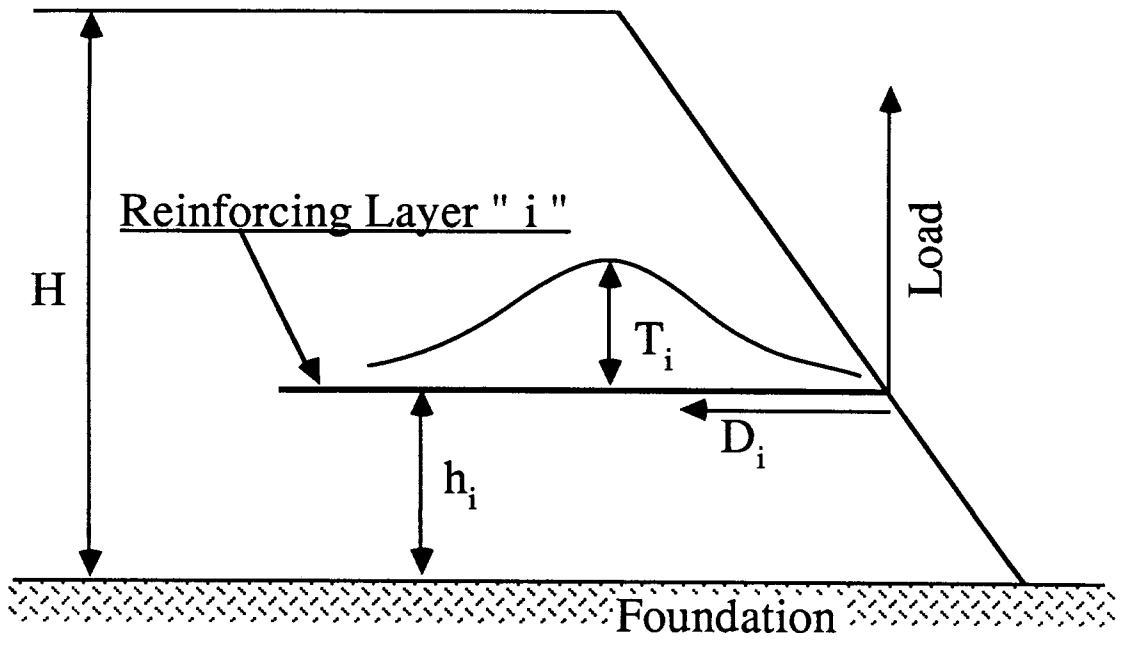


Figure 4.20 Mobilized Loads Along Reinforcement Layer Located 4 m Above the Foundation



- $T_i$  = the maximum load in the  $i^{th}$  Reinforcing Layer
- $T_{max}$  = the largest value of  $T_i$  within the Embankment
- $H$  = height of the Embankment
- $h_i$  = height of  $i^{th}$  Reinforcing Layer above the Foundation
- $D_i$  = distance along Reinforcing Layer from Face of Embankment

Figure 4.21 Parameters used in Defining the Relationship Between  $h_i/H$  and  $T_i/T_{max}$

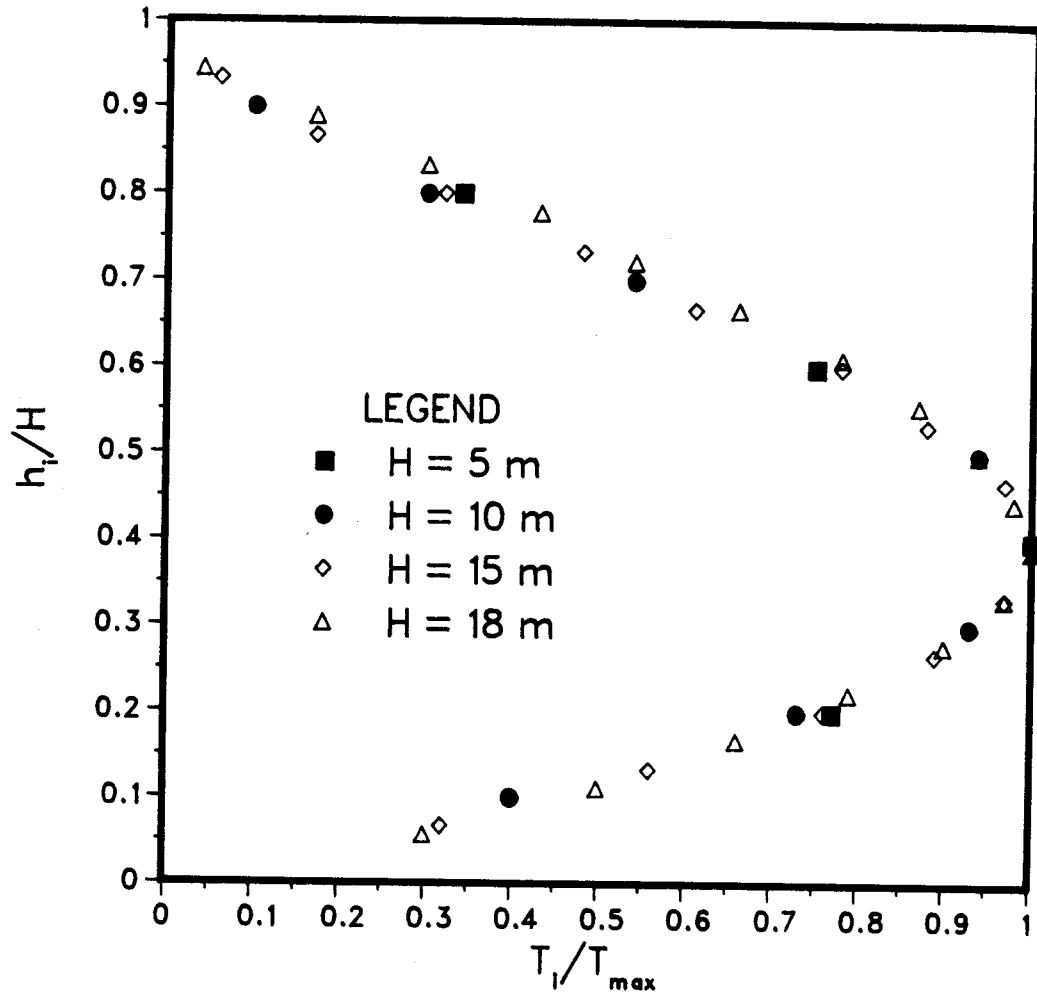


Figure 4.22 Relationship Between the Level of the Reinforcing Layer Within the Embankment and the Mobilized Load in the Reinforcement

configuration analyzed in this study. The form of the relationship between  $h_i/H$  and  $T_i/T_{max}$  will likely depend upon the relative stiffness between the foundation and the embankment, spacing of the reinforcement, stress-strain behaviour of the embankment soil, slope angle of the embankment and the degree of soil-reinforcement interaction.

The second relationship concerns the location and magnitude of the maximum reinforcement load along a reinforcement layer. By nondimensionalizing the maximum load position,  $D_i$ , with the reinforcement's elevation within the embankment,  $h_i$ , a unique relationship can be shown to exist between  $D_i/h_i$  and  $T_i/T_{max}$ . Figure 4.23 illustrates the correlation between  $D_i/h_i$  and  $T_i/T_{max}$ . This figure demonstrates that the position of the maximum loads within reinforcement layers do not depend on the height of the embankment but rather on the position or level of the reinforcement within the embankment.

The relationships illustrated in Figures 4.22 and 4.23 provide sufficient information to enable the determination of the location and magnitude of the maximum loads in each reinforcing layer. By setting  $T_{max}$  equal to the design tensile strength of the reinforcement, the loads in each reinforcing layer at its intersection with a circular slip surface can be determined. Once the ratio  $T_i/T_{max}$  is determined, the location or position of  $T_i$  along each reinforcing layer can be found using Figure 4.23. This

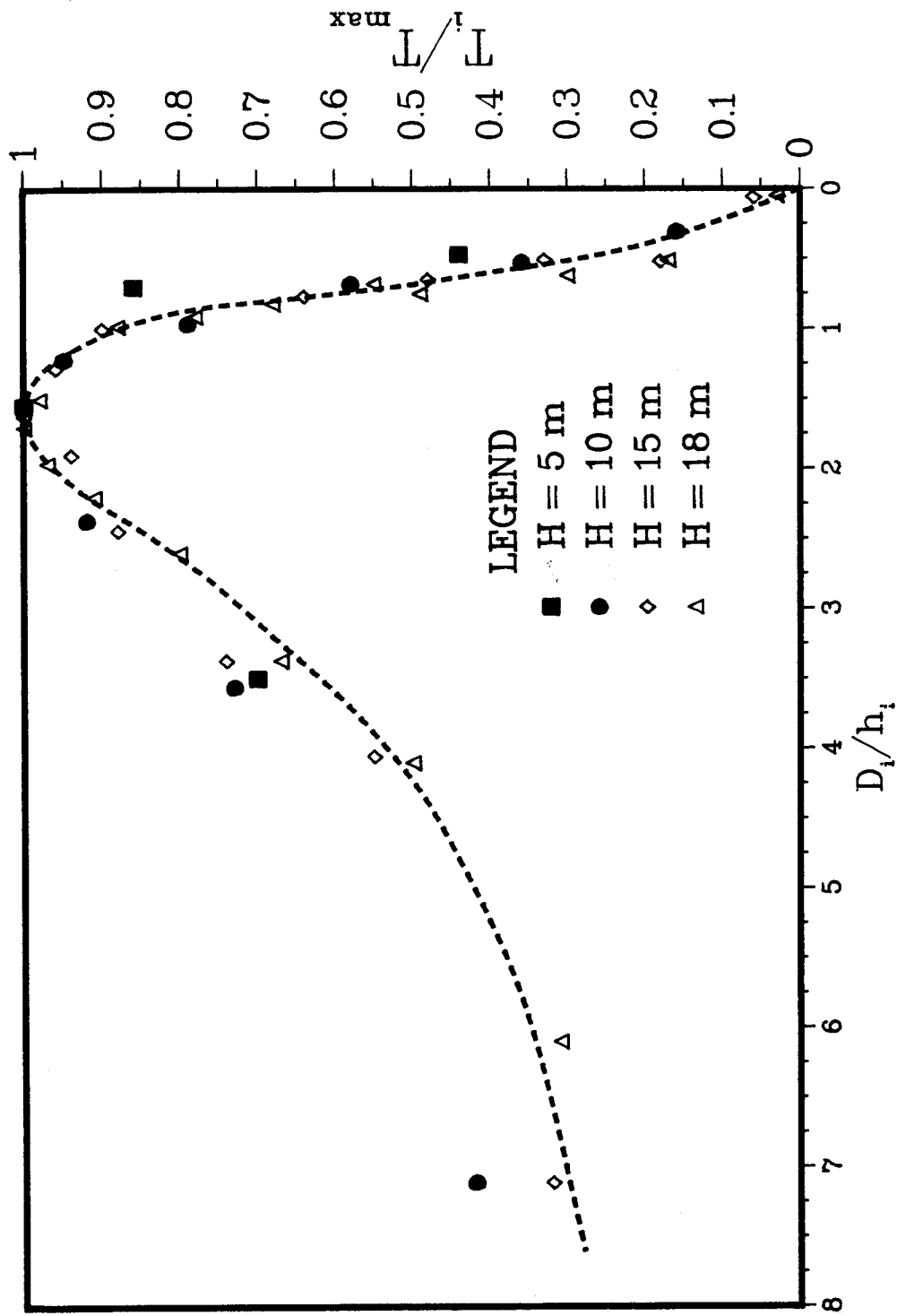


Figure 4.23 Relationship Between the Maximum Load and its Location Relative of the Face of the Embankment for any Reinforcing Layer

provides the pertinent information required to perform a stability analysis or to assess the embedment length of each reinforcing layer. Unfortunately, the curves in Figures 4.22 and 4.23 are valid only for the reinforced slope configuration analyzed in this study. If general forms of these relationships were developed they would provide a very powerful and useful reinforced slope design tool.

#### **4.6 Discussion on the Influence of the Soil-Reinforcement Interface**

In the complex system of reinforced soil, the soil-reinforcement interface plays an important role in determining the behaviour of a reinforced soil structure. It is through the soil-reinforcement interface that soil strains are influenced by the tensile resistance of the reinforcement. Inadequate interfacial strength results in poor performance of a reinforced soil system. A comprehensive analysis of a reinforced soil structure, then, should include the behaviour of the soil-reinforcement interface in the analysis.

Inclusion of the soil-reinforcement interface in a finite element analysis requires the implementation of a special interface element designed to model the relative displacement behaviour between the soil and the reinforcement. Appendix B presents the formulation of an interface element suitable for modelling the behaviour of a soil-reinforcement interface. The interface element uses the

hyperbolic elastic model to represent the nonlinear shear stress-relative displacement behaviour between soil and reinforcement. The hyperbolic model was chosen based on the direct shear interface test results from a comprehensive study on the behaviour of cohesive soil-geosynthetic interfaces conducted by Bobey (1988). Figure 4.24 illustrates the shear stress - relative displacement behaviour between Tensar SR2 and the clayey silty soil used in the present analyses. The formulation for an interface element was provided in Appendix B in order to form a framework for this discussion of soil-reinforcement interface effects. The interface element was not incorporated into SAFE for use in the present research since it would represent a substantial increase in the complexity of the finite element analysis and would be beyond the scope of this thesis. The prohibitive cost in performing a finite element analysis of a reinforced slope with interface elements was also a leading factor in deciding not to use the interface elements. It will be shown subsequently, that, for the reinforced slope configuration studied in the present research, the interface element was not required in order to adequately analyze the reinforced slope.

In the analysis of the reinforced slope presented in section 4.5, no interface elements were provided to allow relative movements between the soil and the reinforcement elements. The question arises then, about what influence would the inclusion of interface elements or more

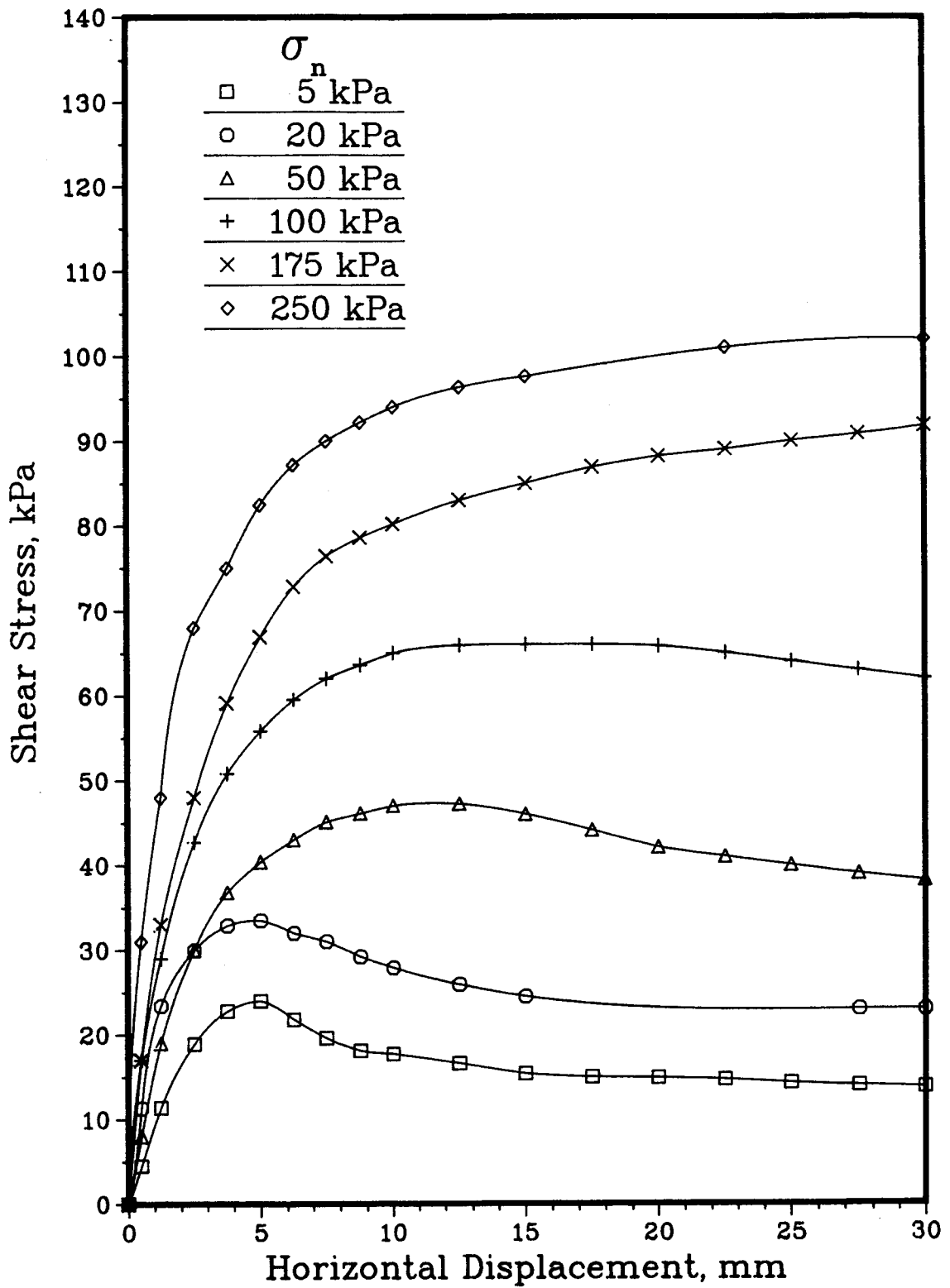


Figure 4.24 Shear Stress - Displacement Behaviour of Soil-Reinforcement Interface (modified from Bobey, 1988)



specifically, the possibility for relative displacement between the soil and the reinforcement, have on the behaviour of the reinforced slope. It is clear the influence of the interface will depend greatly on the behaviour of the interface itself. From Bobey (1988), it was found that the ratio between the direct shear strength of the interface and the direct shear strength of the soil for Tensar SR2 was 0.8 over a normal stress range up to 250 kPa. Using this ratio for the present analysis, the strength of the soil-reinforcement interface can be expressed as:

$$\tau_f = 0.8 (33.0 + \sigma_n \tan(17^\circ)) \text{ kPa} \quad [4.2]$$

A second factor controlling the influence of the interface will be the amount of strength mobilized at the soil-reinforcement interface. If the interface must mobilize 100% of its strength then failure will be occurring along the interface while mobilizing less than 100% of its strength indicates a stable interface condition.

In performing a number of finite element analyses on geotextile reinforced embankments constructed on weak foundations, Rowe and Soderman (1985) provided an interface element to allow for slip between the soil and geotextile. They modelled the interface shear stress-relative displacement behaviour using a rigid-perfectly plastic model. They assumed that at "each point on the interface, the displacement of the soil and the geotextile were

compatible until the shear stress reached the shear strength defined by a Mohr-Coulomb criterion of the interface". In terms of the analysis presented in Section 4.5, the same condition of compatible displacements is inherent in the analysis but no check was made on the mobilized interface strength. Assuming the maximum shear stress that any interface element will develop can be determined from the shear stress,  $\tau_{xy}$ , occurring in the soil mass immediately adjacent to the interface, then it is possible to examine the magnitude of the mobilized interface strengths for the reinforced slope analysis. Figures 4.25 and 4.26 illustrate the distribution of  $\tau_{xy}$  and  $\sigma_y$ , respectively, within the reinforced soil for an embankment height of 18 m. The vertical stress  $\sigma_y$ , is used to obtain the normal stress acting along the interface.

Figure 4.25 shows that a maximum mobilized interfacial shear stress,  $\tau_{mob}$ , of 55 kPa occurs along the lowest reinforcing layer. A normal stress at this point of 250 kPa is obtained from Figure 4.26. Using the relationship for the interface strength given in Equation 4.2 and  $\sigma_n = 250$  kPa, the interfacial shear strength at failure,  $\tau_f$ , is equal to 88 kPa. Comparing this to the mobilized shear stress,  $\tau_{mob}$ , of 55 kPa reveals that only 62% of the interface strength has been mobilized at the maximum  $\tau_{xy}$  location for an embankment height of 18 m.

### X-Y Shear Stress Contours (kPa) Reinforced Embankment

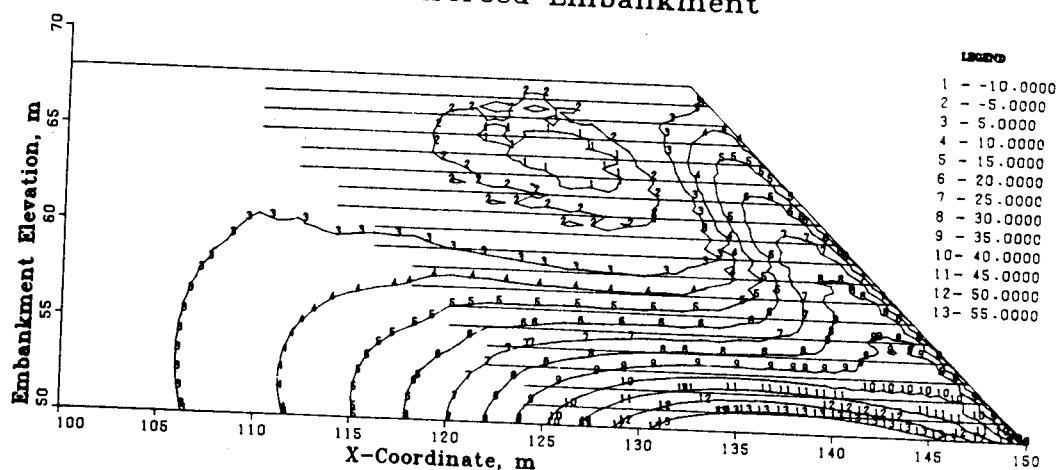


Figure 4.25 Shear Stress,  $\tau_{xy}$  (kPa), Developed in Reinforced Embankment, H = 18 m

### Vertical Stress Contours (kPa) Reinforced Embankment

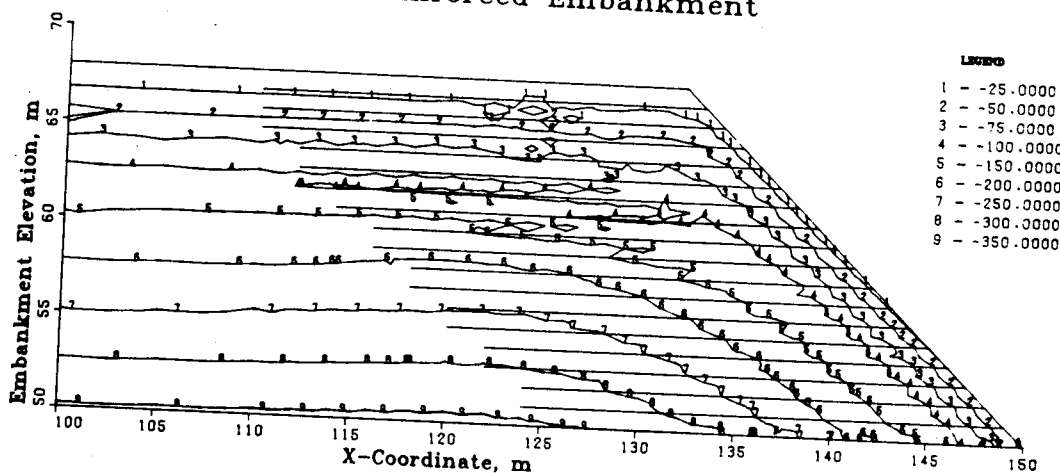


Figure 4.26 Vertical Stress,  $\sigma_y$  (kPa), Developed in Reinforced Embankment, H = 18 m

Based on the low mobilization of strength required along the soil-reinforcement interfaces, it is assumed that no significant relative movement between the soil and the reinforcement takes place. It is realized, however, that the interface may still represent a potential sliding surface if the reinforced slope approaches a state of incipient failure. As the slope approaches failure, the interface at high soil shear stress locations may exert a strong influence on the slope's behaviour. For the present reinforced slope, however, the strength mobilized along the interface is low indicating its influence on the slope behaviour will be minimal. Hence, the reinforced slope analysis presented in section 4.5 is assumed to adequately model the reinforced embankment to a height of 18 m without the inclusion of interface elements in the analysis.

#### **4.7 Comparison of the Nonreinforced and Reinforced Slope Behavior**

A comparison between the behaviour of the nonreinforced slope and reinforced slope serves to illustrate the beneficial effects provided by the presence of reinforcement within the soil slope. The following sections provide an evaluation of these ameliorations in terms of soil stresses, strains and embankment deformations.

#### 4.7.1 Stresses

The modification of the stress field within the embankment due to the reinforcement can be examined by illustrating the difference in the mobilized soil strengths between the two cases. The mobilized strength was defined as:

$$\% \text{ Strength Mobilized} = \frac{(\sigma_1 - \sigma_3)_{\text{mobilized}}}{(\sigma_1 - \sigma_3)_{\text{failure}}} \times 100 \quad [4.3]$$

Figure 4.27 shows the zones within the 18 m embankment where greater than 90% of the soil strength has been mobilized. It is clear from this figure that a significant reduction in the mobilized soil strength occurs due to the presence of the reinforcement.

Equation 4.3 indicates that both the major and minor principal stresses govern the magnitude of the mobilized strength. For the shaded regions of Figure 4.27, the major principal stress,  $\sigma_1$ , was found to effectively remain unchanged between the nonreinforced and reinforced slope analyses. The minor principal stress,  $\sigma_3$ , however maintained a much larger value in the reinforced slope. Therefore, in reducing the mobilized soil strength, the reinforcement's horizontal stiffness has allowed the soil to sustain a higher confining stress. By maintaining a higher confining stress, the mobilized deviatoric stress is decreased.

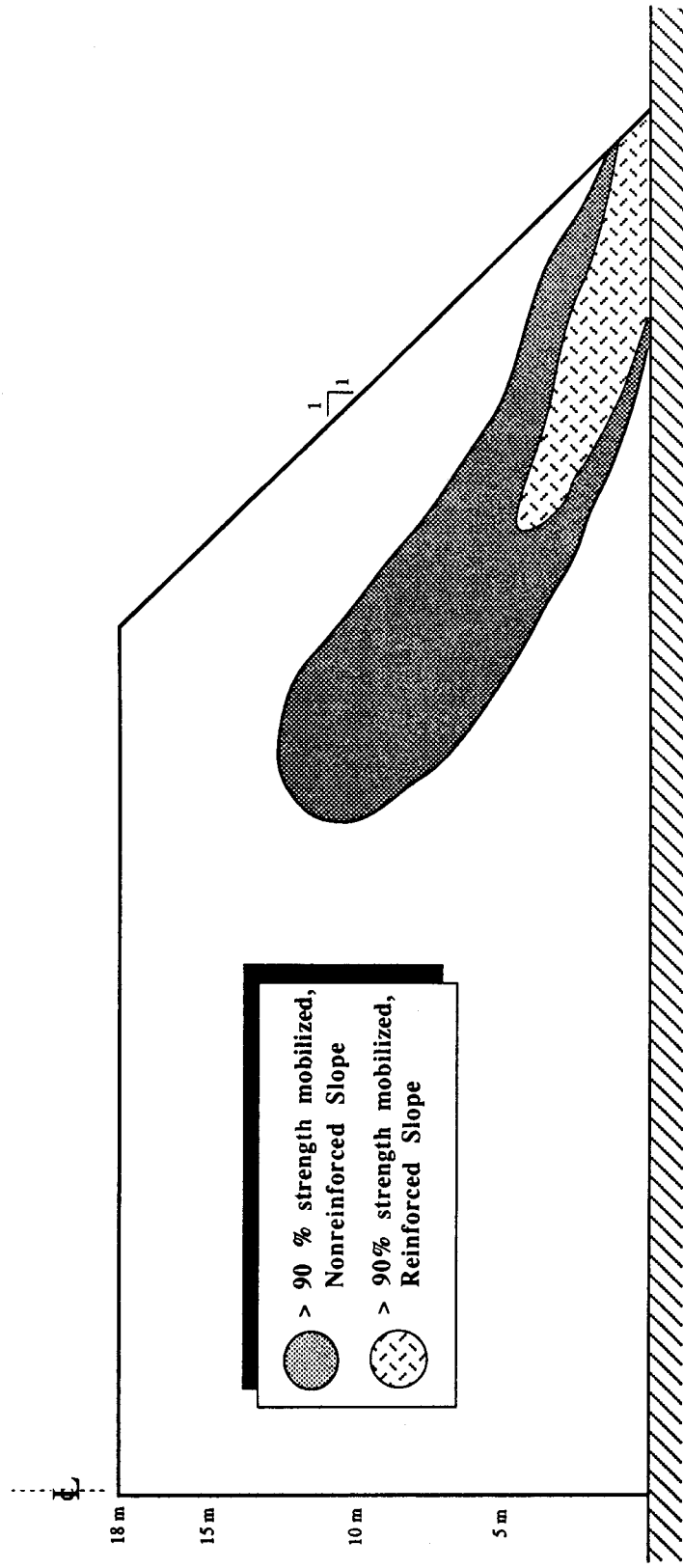


Figure 4.27 Comparison of Mobilized Soil Strengths in Nonreinforced and Reinforced Embankments,  $H = 18 \text{ m}$

109

Consequently, the soil strength is increased in comparison with the nonreinforced slope which results in the substantial difference in mobilized soil strengths illustrated in Figure 4.27. Another advantage of the reinforcement is that by allowing the soil to maintain higher confining stresses, it also provides improvement in the compaction characteristics of the fill near the slope edges.

The reinforcement also reduces the amount and magnitude of the tensile stresses within the embankment. Comparison of Figures 4.7 and 4.14 indicate the reduction in tensile stresses between the nonreinforced and reinforced slopes. Of importance is the elimination of the tensile stresses that occur at the face of the slope. It is apparent in Figure 4.7 that tensile stresses are occurring at the face of the slope. The presence of the reinforcement near the slope face provides an increased horizontal stiffness thereby eliminating the development of tensile stress in this region.

#### **4.7.2 Strains**

The improvement in the angular distortion or shearing strains within the embankment provided by the reinforcement is illustrated in Figure 4.28. This figure shows the zones in the nonreinforced and reinforced slope where the maximum shearing strain has exceeded 10%. By providing a horizontal tensile stiffness within the soil mass, the reinforcement

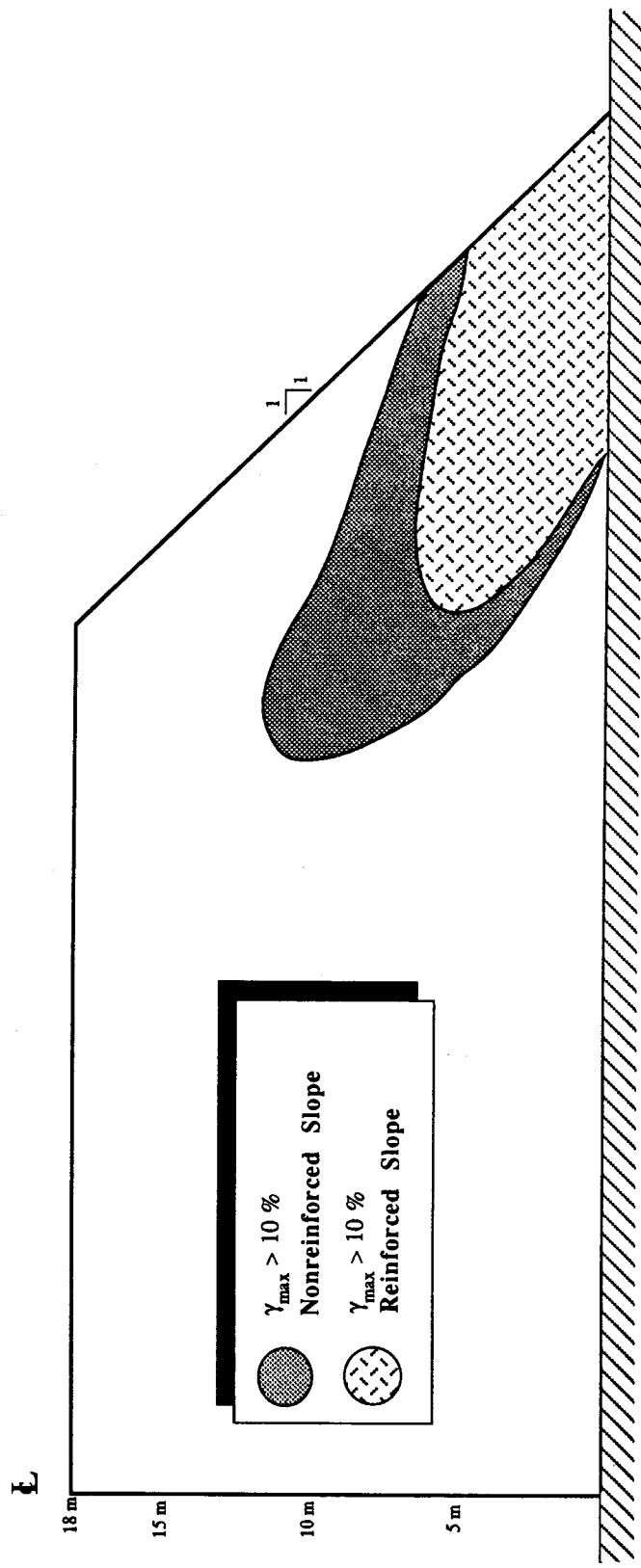


Figure 4.28 Comparison of Maximum Shear Strains in Nonreinforced and Reinforced Embankments,  $H = 18$  m



has reduced the areal extent of  $\gamma_{\max} > 10\%$  by approximately 40% over the nonreinforced slope.

Figure 4.29 illustrates the comparison in horizontal strains between the nonreinforced and reinforced slope. The shaded zones indicate areas of  $\epsilon_x > 2\%$ . It is clear that the horizontal stiffness provided by the reinforcement has significantly reduced  $\epsilon_x$  within the slope. The peak value of  $\epsilon_x$  for the nonreinforced slope of 4.4% has been reduced to 2.1% within the reinforced slope. This represents a 52% reduction in  $\epsilon_x$  due to the reinforcement. The influence of the reinforcement on the vertical strains within the embankment is illustrated in Figure 4.30. The shaded zones represent the areas where the vertical strain,  $\epsilon_y$ , exceeds 4%. Figure 4.30 clearly shows that the presence of the reinforcement reduces  $\epsilon_y$  although not to the same degree as the reduction in  $\epsilon_x$ . The peak vertical strain of 8.2% in the nonreinforced slope has been reduced to 5.0% in the reinforced slope representing a 39% reduction in  $\epsilon_y$ .

For a level within the embankment 7 m above the foundation, Figure 4.31 shows the difference in the distribution of  $\epsilon_x$  for both the nonreinforced and reinforced slope. This figure shows that the reinforcement does not significantly affect the location of the peak horizontal strain but it clearly illustrates the substantial reduction in  $\epsilon_x$  provided by the reinforcement.

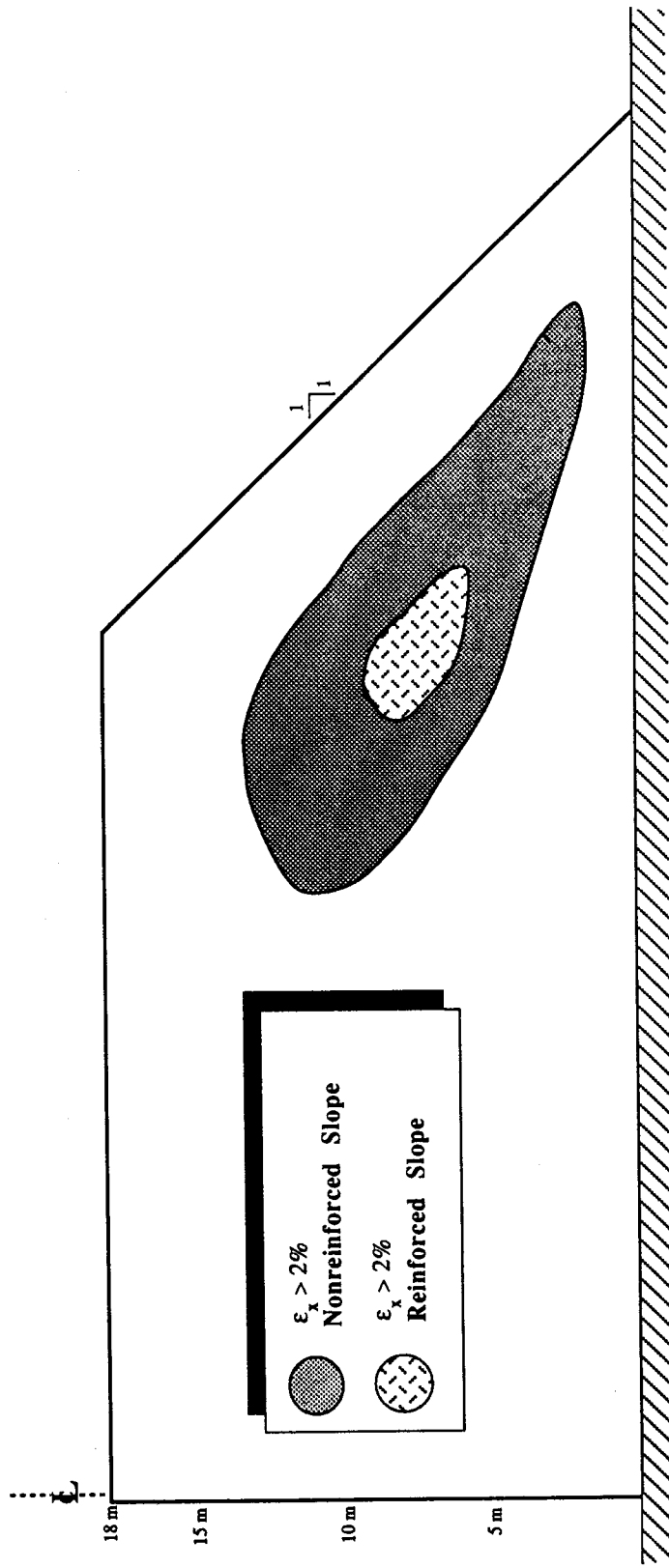


Figure 4.29 Comparison of Horizontal Strains in Nonreinforced and Reinforced Embankments,

H = 18 m

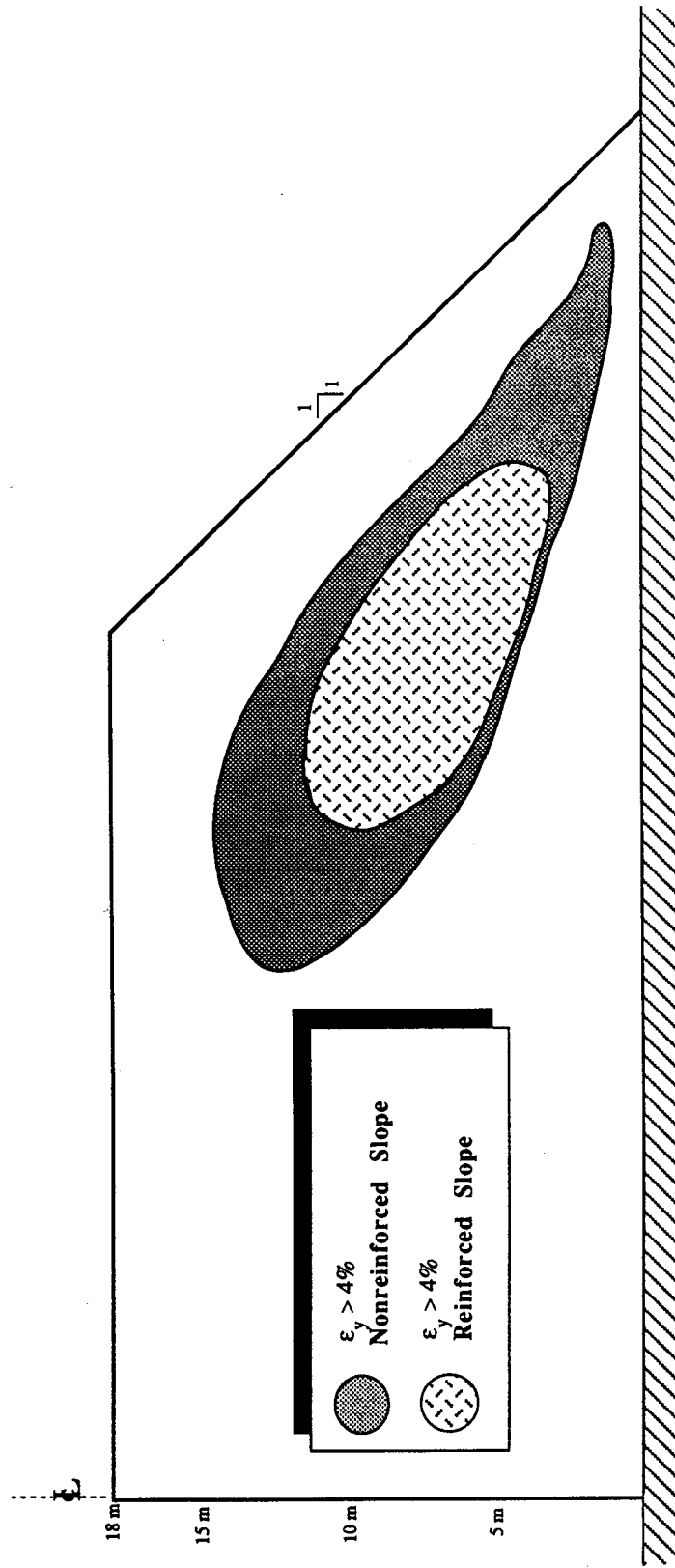


Figure 4.30 Comparison of Vertical Strains in Nonreinforced and Reinforced Embankments, H

= 18 m

For the same embankment level of 7 m as Figure 4.31, Figure 4.32 illustrates the difference in the distribution of  $\epsilon_y$  resulting from the presence of the reinforcement within the slope. In the same manner as  $\epsilon_x$ , the reinforcement does not significantly affect the location of the maximum value of  $\epsilon_y$ , but the figure clearly shows the reduction in  $\epsilon_y$  due to the reinforcement. The reduction in  $\epsilon_y$  is due to a "Poisson's Effect" whereby the reinforcement has added a horizontal stiffness to the soil, reducing  $\epsilon_x$  and consequently reducing  $\epsilon_y$  in order to satisfy the "Poisson's" ratio effect for the overall slope. It is likely the reinforcement will have no effect on the consolidation settlements of the fill or the foundation.

A basic premise in the theory of reinforced soil, first presented by McGown et al. (1978), states that "inclusions must be placed along the directions of principal tensile strain and in the zones of maximum tensile strain in the soil alone, under the same operational conditions". Ingold (1982) and Jones (1984) both concur with this premise. In the present analysis, the maximum tensile strains and their corresponding directions were illustrated in Figures 4.11 and 4.18 for the nonreinforced and reinforced slopes, respectively. Figure 4.33 illustrates the maximum tensile strains in a magnified section of the embankment slope for both cases. It is clear from this figure that the reinforcement has produced a significant reduction in the maximum tensile strains but no appreciable change in

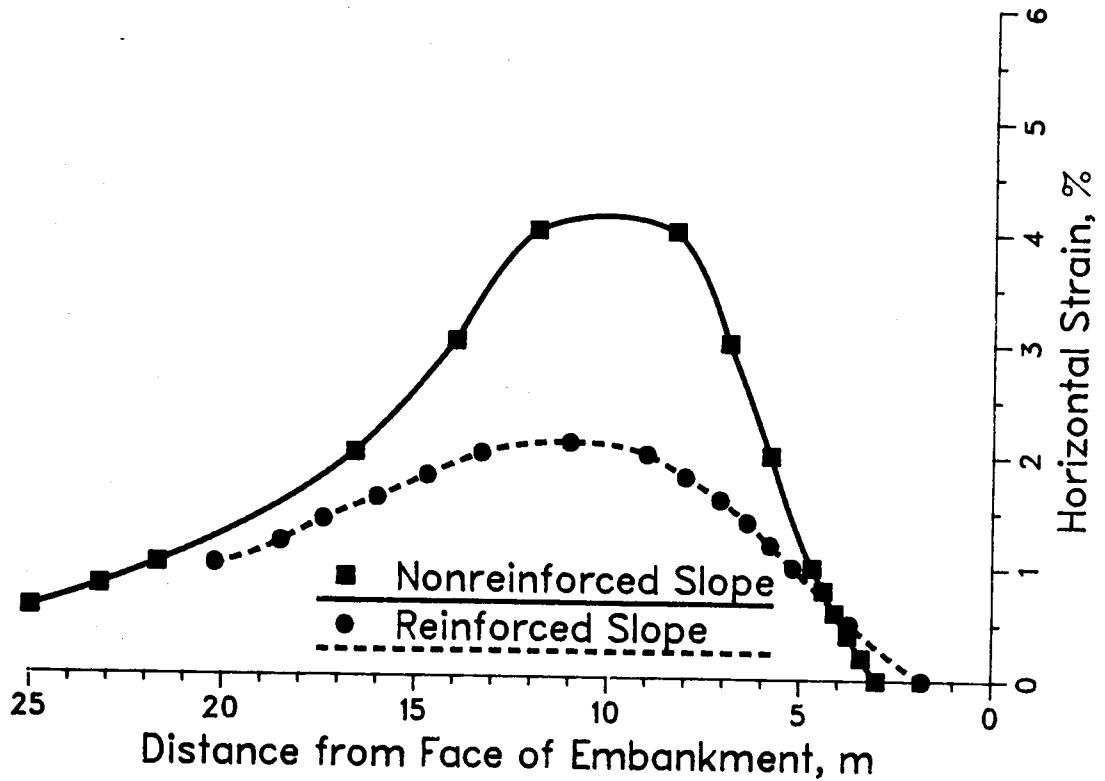


Figure 4.31 Reduction in  $\epsilon_x$  due to Reinforcement,  $H = 18$  m

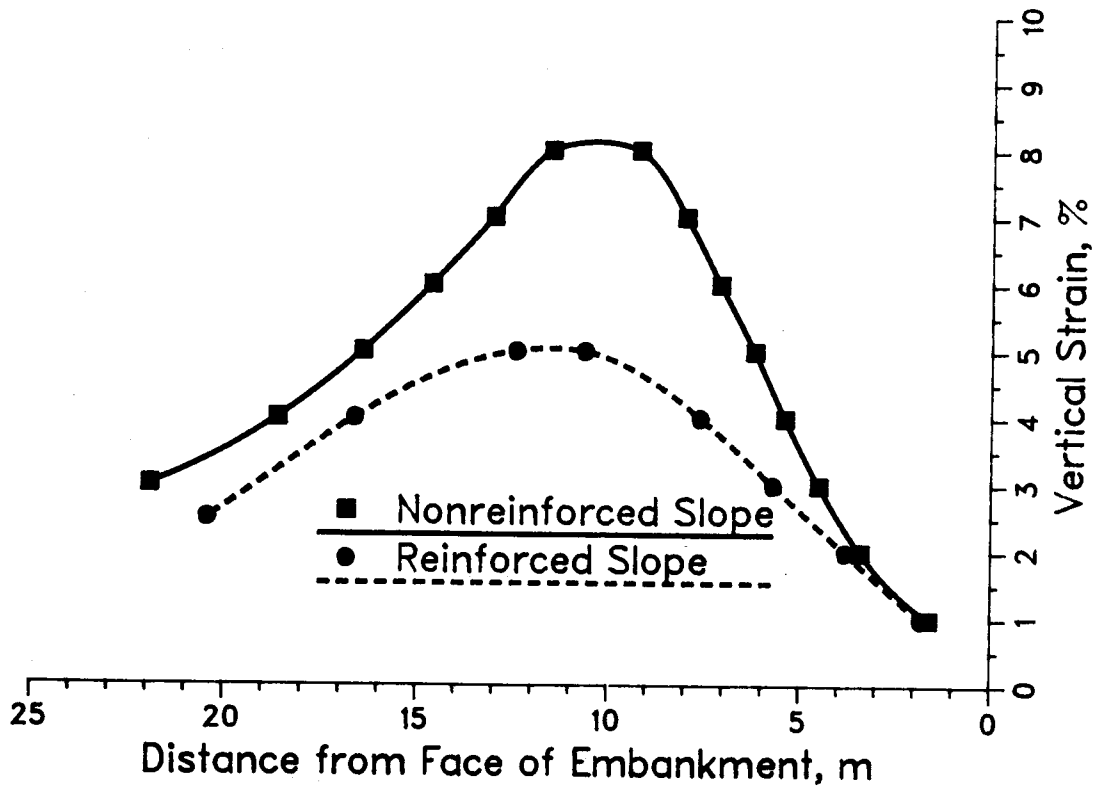


Figure 4.32 Reduction in  $\epsilon_y$  due to Reinforcement,  $H = 18$  m

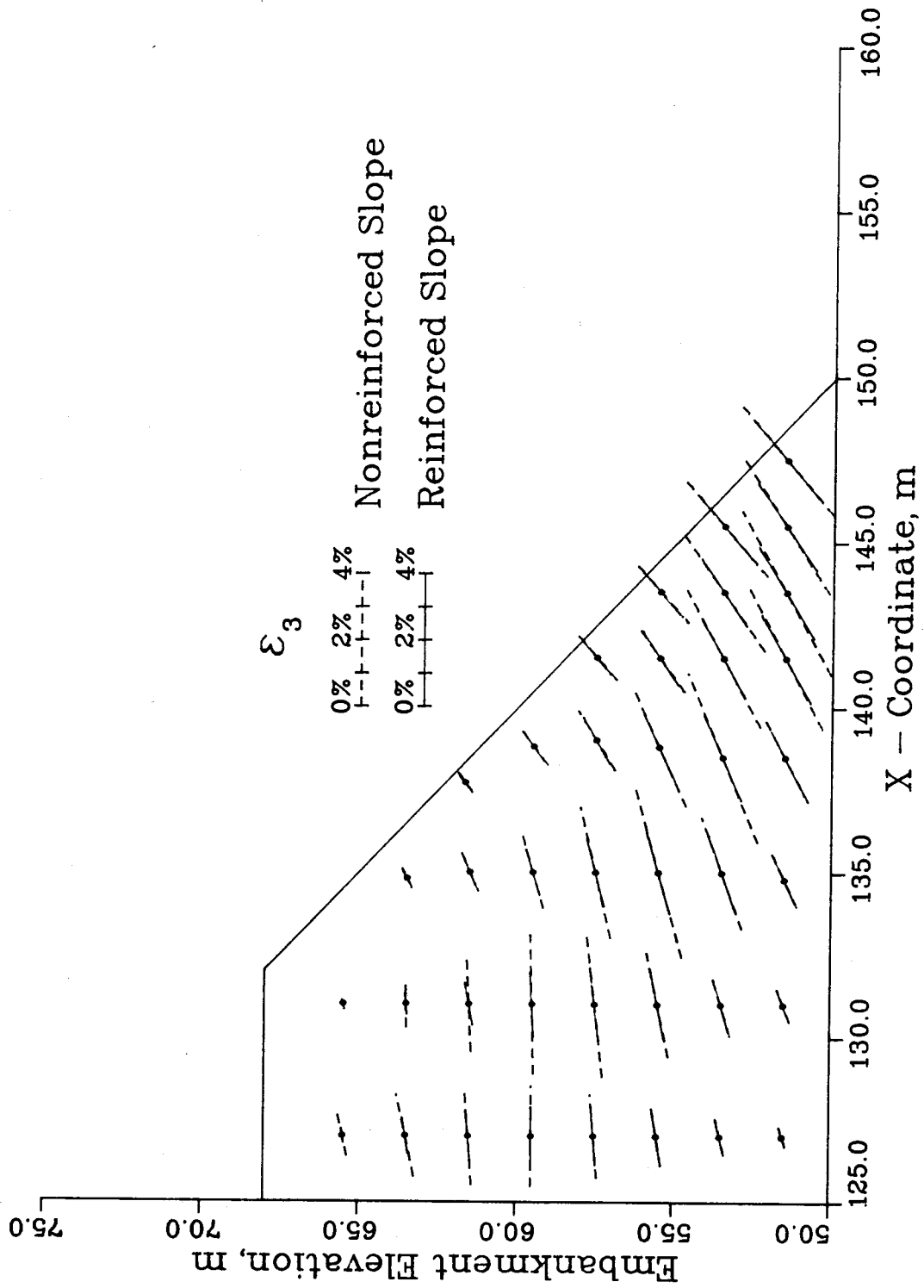


Figure 4.33 Comparison of Tensile Strains,  $\epsilon_3$ , in Nonreinforced and Reinforced Embankments, H = 18 m

rotation of the strain axes in comparison with the nonreinforced slope. This is in conflict with Jones (1985) who speculates that the presence of the reinforcement will cause reorientation of the principal strain axes. It should be noted that in the present analysis, the reinforced embankment is not at incipient failure and some reorientation of the principal strain axes may occur near failure.

#### **4.7.3 Deformations**

Considering the influence the reinforcement has on the strain field within the embankment, it is expected a concurrent result should be found for the embankment deformations. Figure 4.34 illustrates the difference in the deformed shape between the nonreinforced and reinforced embankment. In the same manner as the strains, the vertical displacement of the reinforced embankment is reduced and the maximum horizontal nonreinforced slope deflection of 55.4 cm is reduced to 36.5 cm in the reinforced slope. This represents a 34% reduction in the outward deflection of the slope face which can be attributed to the presence of the reinforcement within the soil mass.

#### **4.8 Summary and Conclusions**

A nonlinear, total stress finite element analysis was conducted in order to study the comparative short term, end-of-construction behaviour of a nonreinforced and

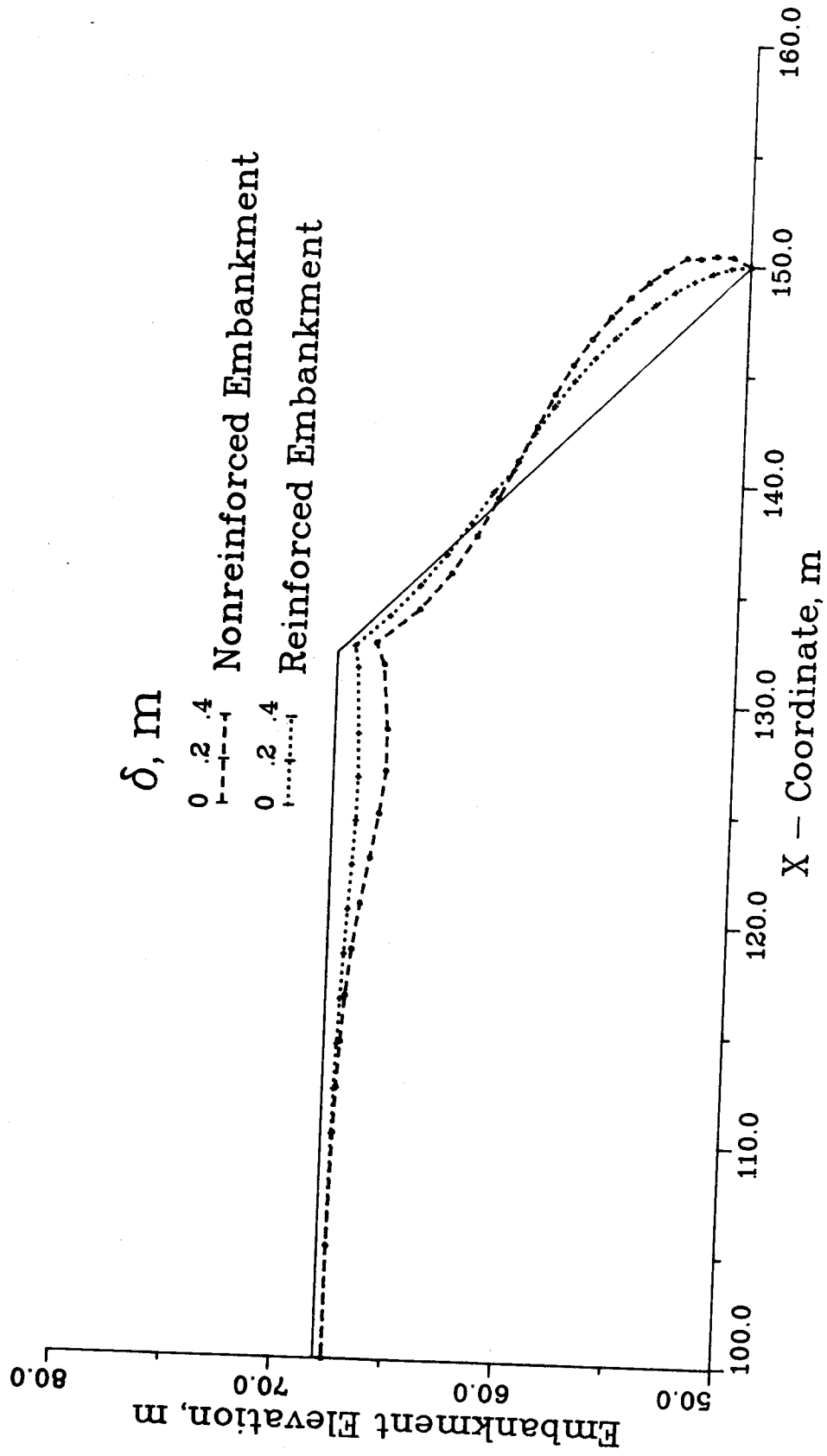


Figure 4.34 Comparison Between Nonreinforced and Reinforced Embankment Deformations, H = 18 m



reinforced embankment. A maximum embankment height of 18 m having 1:1 side slopes was built incrementally in lifts of 1 m on a rigid foundation. The reinforcement layers were evenly spaced at 1 m intervals.

The analysis of the nonreinforced slope showed that for an embankment height of 18 m, the slope was approaching failure conditions. A definite band of soil within the slope had mobilized greater than 95% of its strength. The slope face underwent a relatively large lateral displacement of 55.4 cm. Significant horizontal and vertical strains of 8.4% and 5.2%, respectively, developed within the slope. The analysis of the reinforced slope indicated the same stress, strain and deformational patterns as the nonreinforced slope but, in general, were of a smaller magnitude. The presence of the reinforcement within the slope resulted in 52% and 39% reductions in  $\epsilon_x$  and  $\epsilon_y$ , respectively. The lateral deflection of the slope was reduced to 36.2 cm from 55.4 cm. The zone of soil within the slope where 95% of the soil strength had been exceeded was reduced substantially in comparison to the nonreinforced slope indicating a much more stable embankment.

The development of load within the reinforcement layers was obtained from the analysis of the reinforced embankment. The maximum load occurring in the reinforcing layers was found to vary according to the position or level of the reinforcing layer within the slope. The maximum load

occurred in the reinforcement layer placed at a height above the foundation of  $0.4H$  where  $H$  is the height of the embankment. At an embankment height of 18 m, the maximum load at this reinforcement level was 15.5 kN/m. The analysis also revealed a unique relationship between the dimensionless parameter  $h_i/H$  and  $T_i/T_{max}$  where  $h_i$  refers to a reinforcement's distance above the foundation,  $H$  is the embankment height,  $T_i$  is the maximum load in any reinforcement layer and  $T_{max}$  is the maximum reinforcement load developed for an embankment height  $H$ . The position of the maximum load within a reinforcement layer,  $D_i$ , also depends on  $h_i$ . A plot of  $D_i/h_i$  against  $T_i/T_{max}$  yields a unique relationship regardless of the height of the embankment.

The consequence of these unique relationships, found to exist for a reinforced slope constructed on a rigid foundation, is the possibility of designing an embankment using the actual working load distribution in the reinforcement. This should be qualified by stating that these unique relationships may not be similar or apparent for embankment configurations different than the case analyzed in the present study.

In examining the difference between the nonreinforced and reinforced embankment, the contribution of the reinforcement to the overall improvement of the slope performance was significant. Reductions in soil stresses, shearing strains, horizontal and vertical strains and

displacements could be attributed to the presence of reinforcement within the slope.

## 5. LIMIT EQUILIBRIUM ANALYSIS OF A REINFORCED SOIL SLOPE

### 5.1 Introduction

This chapter presents the results of a total stress limit equilibrium analysis conducted in order to assess the short term, end of construction stability of a steep (1:1) reinforced cohesive soil slope using Bishop's Modified Method (BMM). No consideration has been given to an assessment of the long term stability of the reinforced slope which would demand an effective stress analysis.

As a clarification of terminology, the slope stability analysis developed by Bishop (1955) where interslice forces are assumed to act horizontally and horizontal force equilibrium is ignored, will be referred to as Bishop's Simplified Method (BSM). The limit equilibrium method resulting from the incorporation of reinforcement forces into BSM will be termed Bishop's Modified Method (BMM).

### 5.2 Bishops Modified Method

Bishop's Modified Method (BMM) is a reinforced soil limit equilibrium method developed by incorporating the effects of the reinforcement into Bishop's Simplified Method (BSM) of analysis. BSM is based on the method of slices and is restricted to analyzing slip surfaces of circular shape. Vertical equilibrium for each slice and overall moment equilibrium are satisfied by BSM. Figure 5.1 illustrates the comparison between BSM and other more rigorous limit

equilibrium methods which satisfy all the conditions of equilibrium. Although BSM neglects horizontal equilibrium, the method has been found to be an accurate method of analysis for circular slip surfaces which gives virtually the same factor of safety as methods which satisfy all conditions of equilibrium (Duncan and Wright, 1980).

The factor of safety used in BSM is defined as that factor by which the shear strength parameters may be reduced in order to bring the soil mass into a state of limiting equilibrium along a given slip surface. For a nonreinforced slope, the factor of safety is expressed as:

$$F_0 = \frac{\text{Shear Strength}}{\text{Shear Stress}} = \frac{\sum \left\{ \frac{(c' b + W(1-r_u) \tan \phi') \sec \alpha}{\left(1 + \frac{\tan \alpha \tan \phi'}{F}\right)} \right\}}{\sum (W \sin \alpha)} \quad [5.1]$$

A complete derivation of this equation was presented by Bishop (1955). Figure 5.2 illustrates the forces acting on a typical slice.

Currently, the incorporation of reinforcement forces into a limit equilibrium slope stability analysis has been accomplished in one of two ways. The reinforcement force can be included as a "free body" force acting at some inclination to the failure surface and contributing to force and moment equilibrium or the reinforcement force can be assumed to increase the shear strength of the soil. The

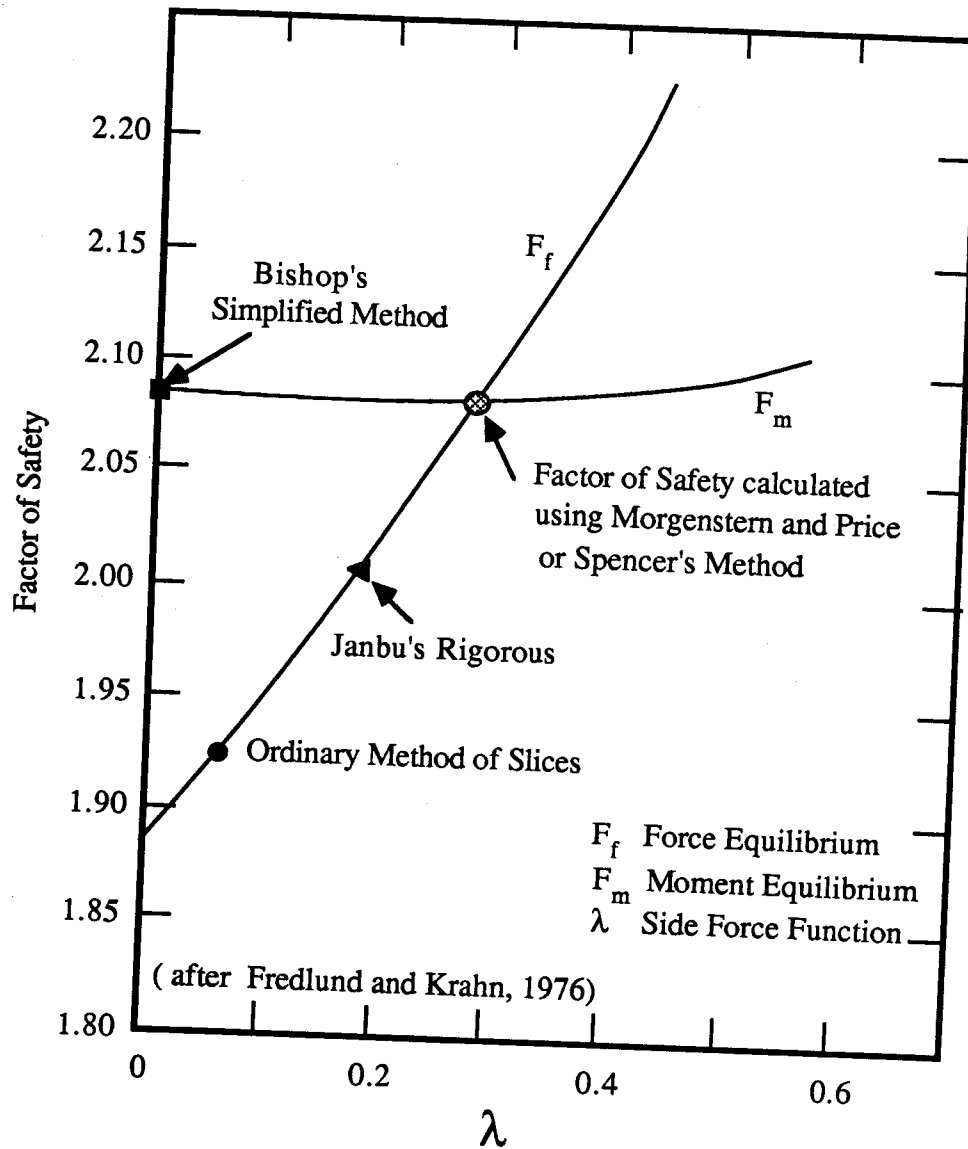
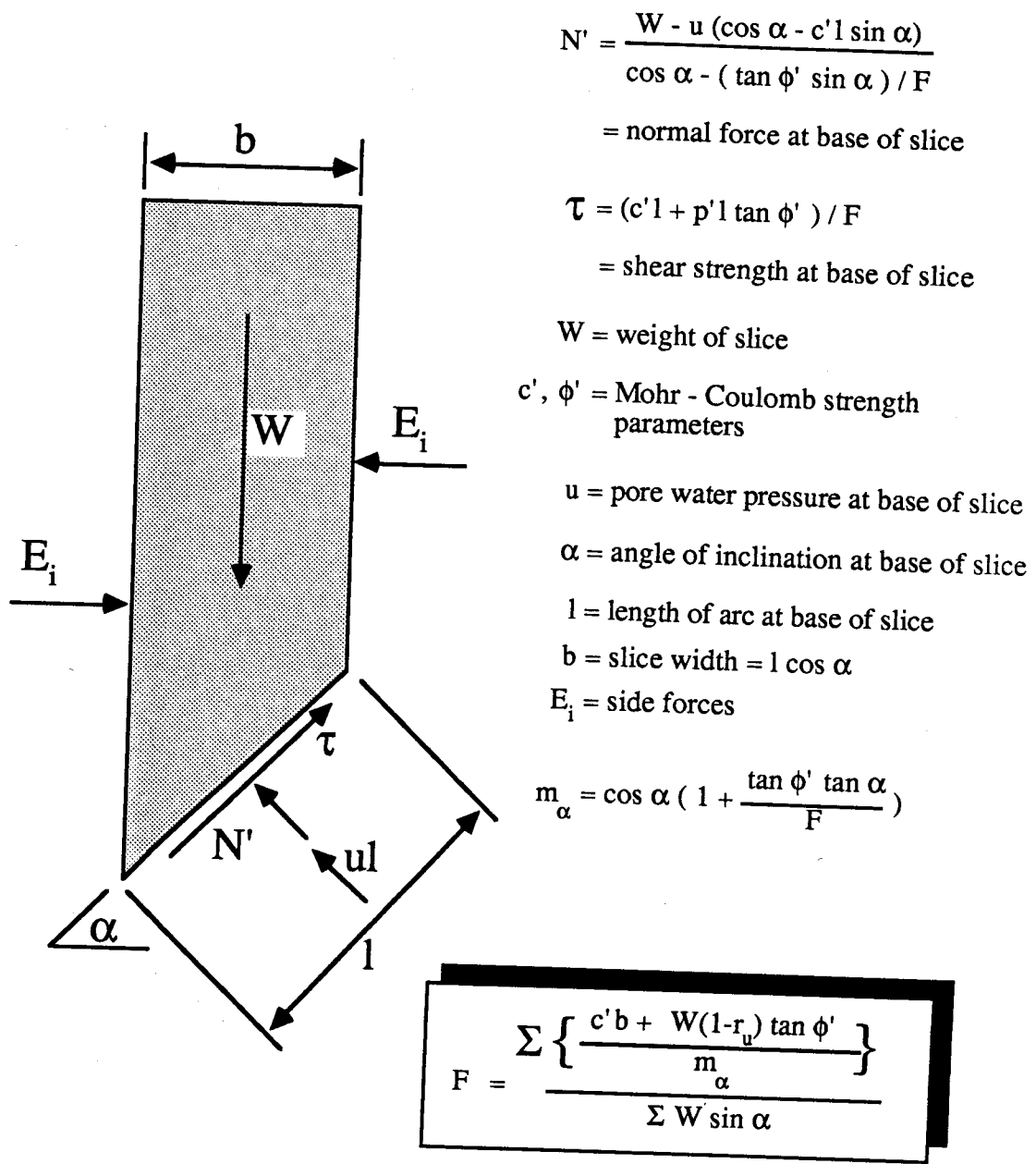


Figure 5.1 Comparison of Bishop's Simplified Method with other Limit Equilibrium Methods (modified from Fredlund and Krahn, 1976)



**Note:** For a total stress analysis,  $r_u = 0.0$  and  $c'$  and  $\phi'$  become  $c$  and  $\phi$ .

Figure 5.2 Slice Forces used in Bishop's Simplified Method

reinforcement force components parallel to the failure surface provide an additional "cohesive" component to the soil strength while the normal force increases the frictional component of the soil shear strength.

### 5.2.1 Reinforcement Acting as a Free Body Force

The Bishop's Modified Method used in the present research includes the reinforcement force as a free body force. The reinforcement force can be specified as acting horizontally or tangentially to the failure surface. Figure 5.3 and 5.4 illustrates these two cases. These two cases can be assumed to represent the upper and lower bounds of reinforcement orientation. For relatively stiff reinforcement or small embankment deformations, a horizontal orientation is likely the most appropriate reinforcement force orientation assumption. However, if the flexural rigidity of the reinforcement is negligible, very little deformation of the slope may be required to orient the reinforcement tangentially along the failure surface.

It is assumed that the reinforcement provides an additional resisting moment in order to increase the factor of safety of the slope. The reinforcement force is also assumed not to reduce the soil disturbing moment,  $M_0$ , since the force mobilized within the reinforcement depends upon the deformation of the soil (Low and Duncan, 1985). The factor of safety of a reinforced slope,  $F_R$ , is defined as:



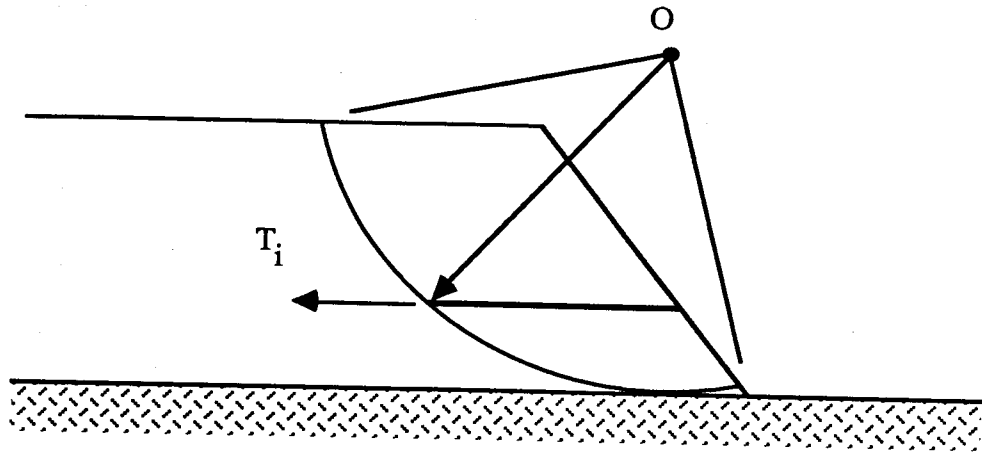


Figure 5.3 Horizontal Reinforcement Force Orientation

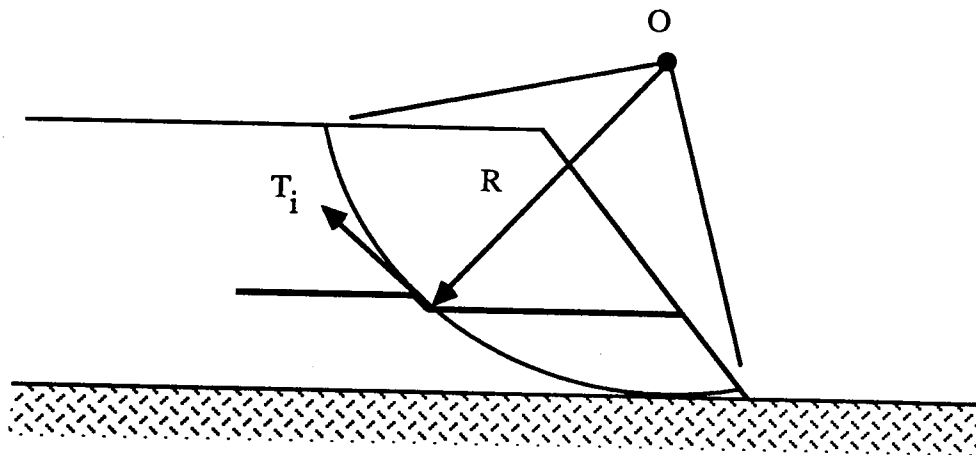


Figure 5.4 Tangential Reinforcement Force Orientation

$$F_R = \frac{M_{ST} + M_R}{M_O} \quad [5.2]$$

The total resisting moment provided by a horizontal force orientation,  $M_{Rh}$ , is defined as:

$$M_{Rh} = \sum_{i=1}^n T_i (R - h_i) \quad [5.3]$$

The total resisting moment provided by a tangential force orientation,  $M_{Rt}$ , is defined as:

$$M_{Rt} = R \sum_{i=1}^n T_i \quad [5.4]$$

It is clear that for a horizontal force assumption, the level of a reinforcing layer within a slope,  $h_i$ , will affect the magnitude of its resisting moment whereas for a tangential force, the resisting moment depends only upon the radius,  $R$ , of a slip surface.

**5.2.2 Reinforcement Acting to Increase the Soil Shear Strength**

It was previously stated that the reinforcement can be included in a limit equilibrium method as either a free body force or assuming it increases the soil's shear strength. In order to appreciate the differences between these two assumptions, a comparison of BMM with an equivalent limit equilibrium method is presented. Schmertmann et al. (1987)

have developed TENSLO1, a limit equilibrium method based on BSM which incorporates the reinforcement force assuming it increases the soil's shear strength. Figure 5.5 illustrates the reinforcement force orientation assumed by Schmertmann et al. (1987). The definition for the factor of safety is identical to Equation 5.2 but the expression for  $M_R$ , the reinforcement resisting moment, is substantially different.  $M_R$  is defined as:

$$M_R = R \sum_{i=1}^n T_i (\cos (.75\alpha_i) + \sin (.75\alpha_i) \tan \phi) \quad [5.5]$$

where  $\alpha_i$  = slope of failure surface at intersection  
with reinforcing layer  $i$   
 $= \cos^{-1} \left( 1 - \frac{h_i}{R} \right)$

In contrast to assuming either a horizontal or tangential orientation of the reinforcement force at the slip surface, Schmertmann et al. have assumed that the reinforcement force will form an angle,  $.25a$ , to the horizontal; where  $a$  is the slope of the failure surface at its intersection with the reinforcement. Although the equations for the resisting moments provided by the reinforcement are different in Equations 5.3 to 5.5, a dimensionless parameter,  $M_{Ri}/T_i R$ , can be extracted from each equation. This parameter represents the magnitude of the resisting moment provided by any reinforcement layer "i" assuming a reinforcement design load  $T_i$  and a circular slip surface of radius  $R$ . Employing the geometry in Figure 5.6, Equation's 5.3 to 5.5 can be rewritten as:

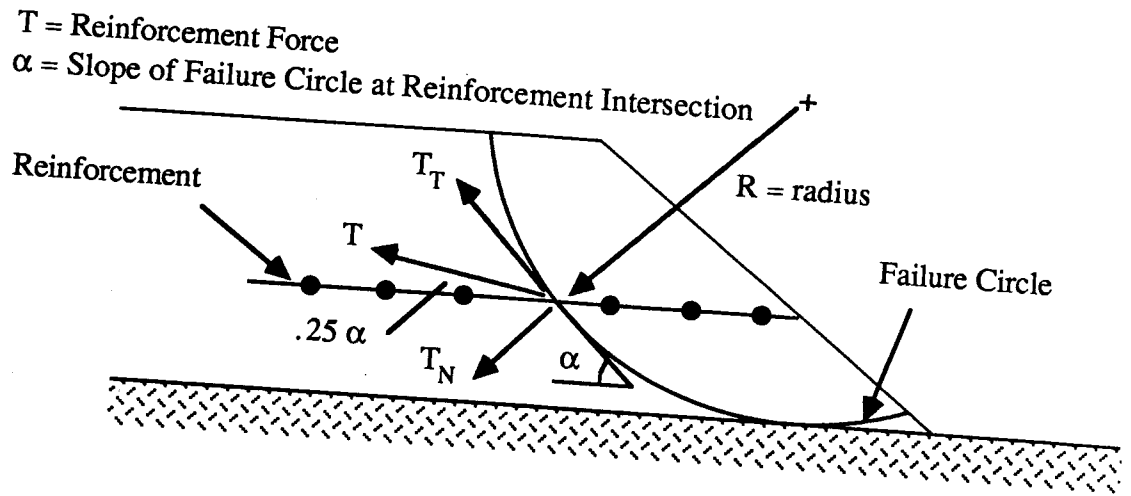


Figure 5.5 Reinforcement Force Orientation assumed by Schmertmann et al. (1987)

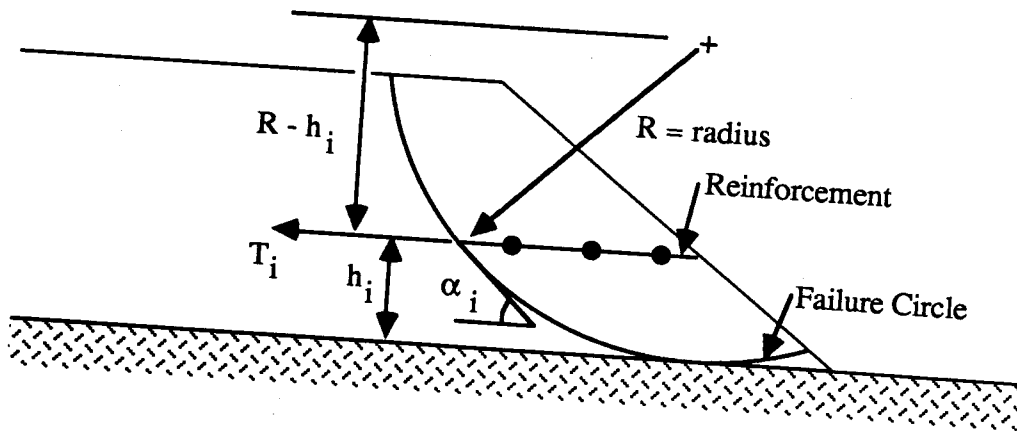


Figure 5.6 Geometry for Comparing Reinforcement Force Assumptions

$$\frac{M_{Ri}}{T_i R} = \left(1 - \frac{h_i}{R}\right), \text{ horizontal force orientation} \quad [5.6]$$

$$\frac{M_{Ri}}{T_i R} = 1.0, \text{ tangential force orientation} \quad [5.7]$$

$$\frac{M_{Ri}}{T_i R} = \cos(.75\alpha_i) + \sin(.75\alpha_i) \tan \phi, \text{ increase in soil soil strength} \quad [5.8]$$

Figure 5.7 illustrates the relationships described by Equations 5.6 to 5.8. The curves in Figure 5.7 clearly indicate that substantially different reinforcement resisting moments are obtained depending on which assumption is employed in the analysis. It is evident that the horizontal force orientation provides the lowest and hence, most conservative value of the reinforcement resisting moment.

It was mentioned previously that the horizontal and tangential orientation represent the upper and lower bound to possible reinforcement orientations and while this is true, it is clear they may not represent upper and lower bounds on the magnitude of the resisting moment provided by the reinforcement. Figure 5.7 shows that a substantially higher resisting moment can be obtained by assuming the reinforcement increases the soil strength rather than assuming either a horizontal or tangential reinforcement orientation. For noncohesive soils in particular, Schmertmann et al.'s value of  $M_{Ri}/T_i R$  can be 100% higher than the horizontal force value and 30% greater than the

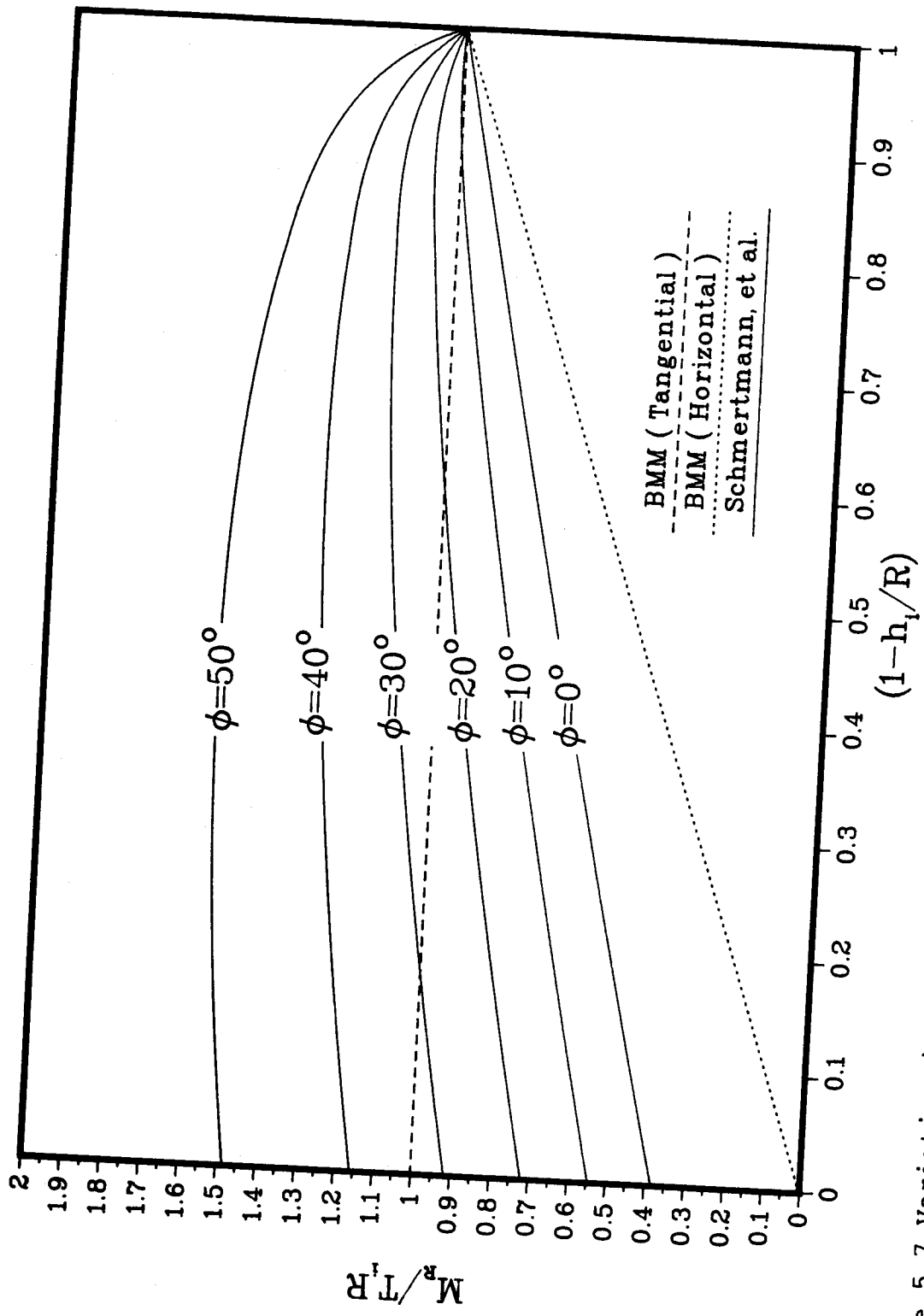


Figure 5.7 Variation in the Reinforcement Resisting Moment for Different Force Orientation Assumptions

tangential force value. Figure 5.7 serves to illustrate the significant differences that exist between the two methods presently used for incorporating the reinforcement force into limit equilibrium methods of analysis. The determination of which method is more appropriate is a subject of debate and is beyond the scope of this thesis.

For the present research, the free body reinforcement force approach will be used in Bishop's Modified Method. The free body approach allows for easy comparisons to be made with the finite element analysis results and the computer program obtained for performing the limit equilibrium analyses is based on the free body force approach.

### **5.3 Limit Equilibrium Analysis of a Reinforced Slope**

#### **5.3.1 Introduction**

A total stress, limit equilibrium analysis of the short term, end-of-construction stability of a reinforced slope was conducted using Bishop's Modified Method. STABGM, a computer program for the slope stability analysis of reinforced embankments and slopes, was obtained in order to conduct the analyses (Duncan et al. 1985). This program utilizes the Ordinary Method of Slices (OMS) as well as Bishop's Modified Method (BMM). The factor of safety of the reinforced embankment was computed at each 1 m height assuming both horizontal and tangential reinforcement force orientations. The following sections present the results of

the limit equilibrium stability analyses.

### 5.3.2 Reinforced Embankment Geometry

The geometry of the reinforced slope used for the limit equilibrium stability analyses is identical to the slope configuration used in the finite element analysis. The reinforced slope configuration is illustrated in Figure 5.8. The reinforced cohesive soil slope is constructed on a rigid foundation to a maximum height of 18 m. An embankment height of 18 m for a nonreinforced slope indicated its factor of safety against failure to be 1.11. The reinforcement layers are uniformly spaced at 1 m intervals with lengths ranging from 21 m to 25 m. A vertical spacing of 1 m was selected in order to generalize the reinforcement pattern and to eliminate the effects of nonuniform spacing.

An integral part of the design of a reinforced slope is the selection of appropriate embedment lengths for each reinforcing layer. Adequate embedment is required so each reinforcing layer can fully develop its design load without pulling out of the soil. The program STABGM does not include the effects of embedment length in the limit equilibrium analysis and as such, no consideration has been given to an effective design of the reinforcement embedment lengths. It is assumed adequate embedment length has been provided for each layer of reinforcement. An investigation on the effects of embedment length on the behaviour of reinforced slopes is beyond the scope of this thesis and will not be dealt with



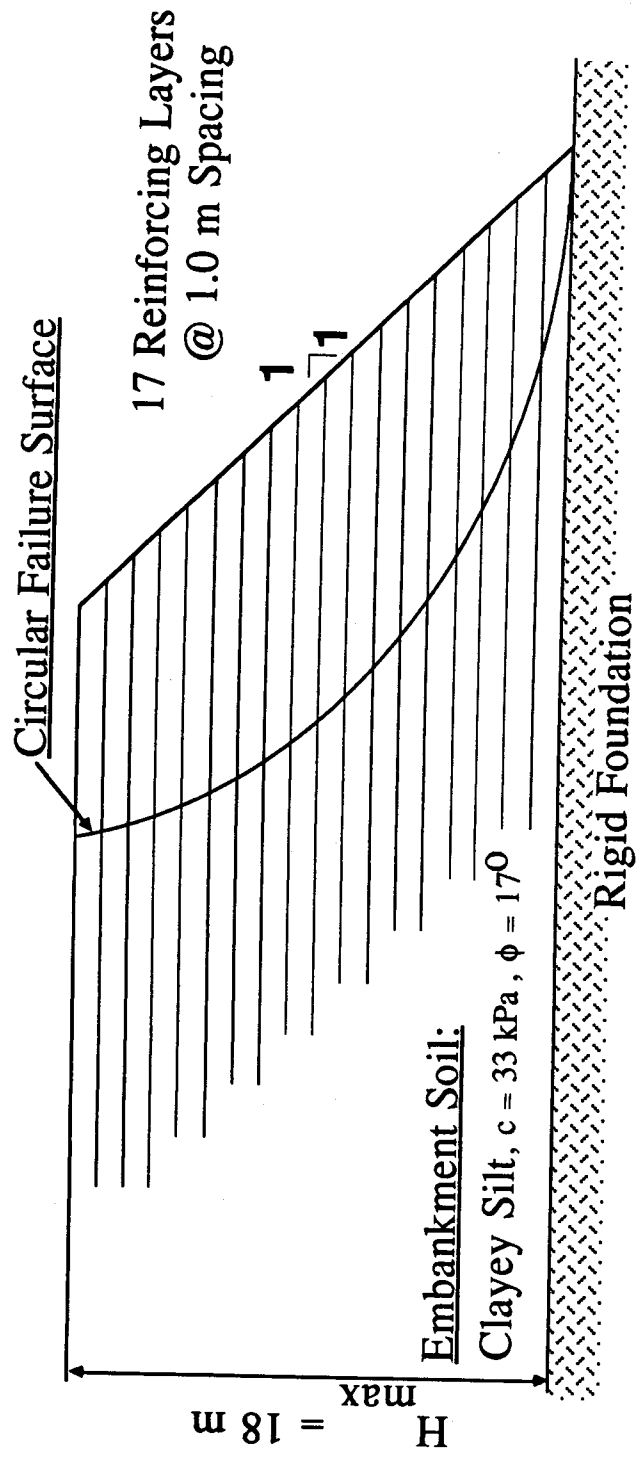


Figure 5.8 Reinforced Slope Geometry

in any detail.

### 5.3.3 Soil and Reinforcement Characteristics

The cohesive soil type selected for the analysis is presently being utilized in the construction of the Devon Geogrid Test Fill (Scott et al. 1986). The cohesive soil is a low to medium plastic clayey silt. An extensive soil testing program was initiated as part of the test fill project. The isotropically consolidated undrained triaxial compression test results from this testing program will be used in the limit equilibrium analysis. Details of the testing program and the soil test results can be found in Hofmann (1988). A discussion on the total stress, CIU stress-strain characteristics of the soil has been presented in Chapter 4. Figure 5.9 illustrates the hyperbolic stress-strain curves that were derived in Chapter 4 to model the soils behaviour. Figure 5.10 illustrates the total stress failure envelope for this soil type, defined by a cohesion intercept of 33 kPa and a friction angle of  $17^\circ$ .

These soil strengths represent ultimate soil strength parameters and have not been selected in order to ensure soil-reinforcement strain compatibility. Figure 5.11 illustrates the reinforcement load-strain model used in the finite element analysis. It is clear that the reinforcement fails at a strain value of 18% while the ultimate strength of the soil is reached at a strain of approximately 9%. Present design practice advocates that limit equilibrium

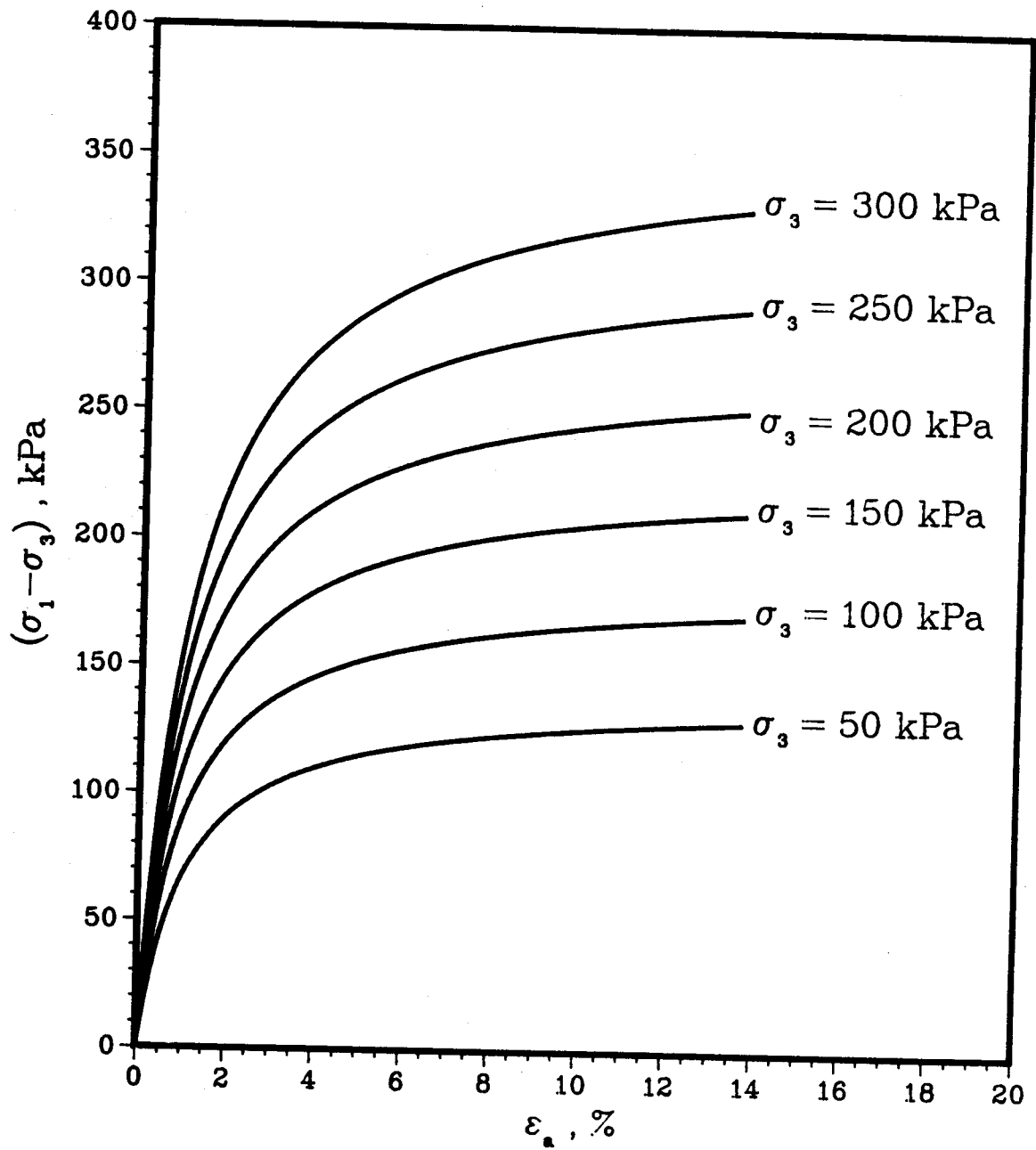


Figure 5.9 Hyperbolic Stress Strain Curves of Embankment Soil

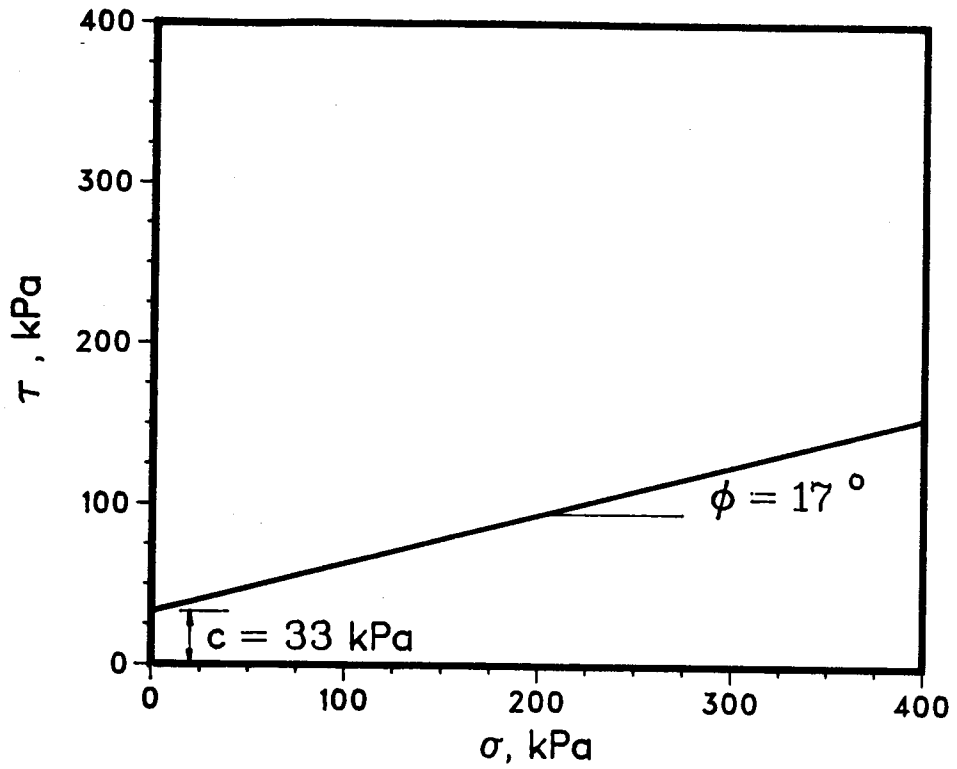


Figure 5.10 Total Stress, Mohr-Coulomb Failure Envelope for Soil

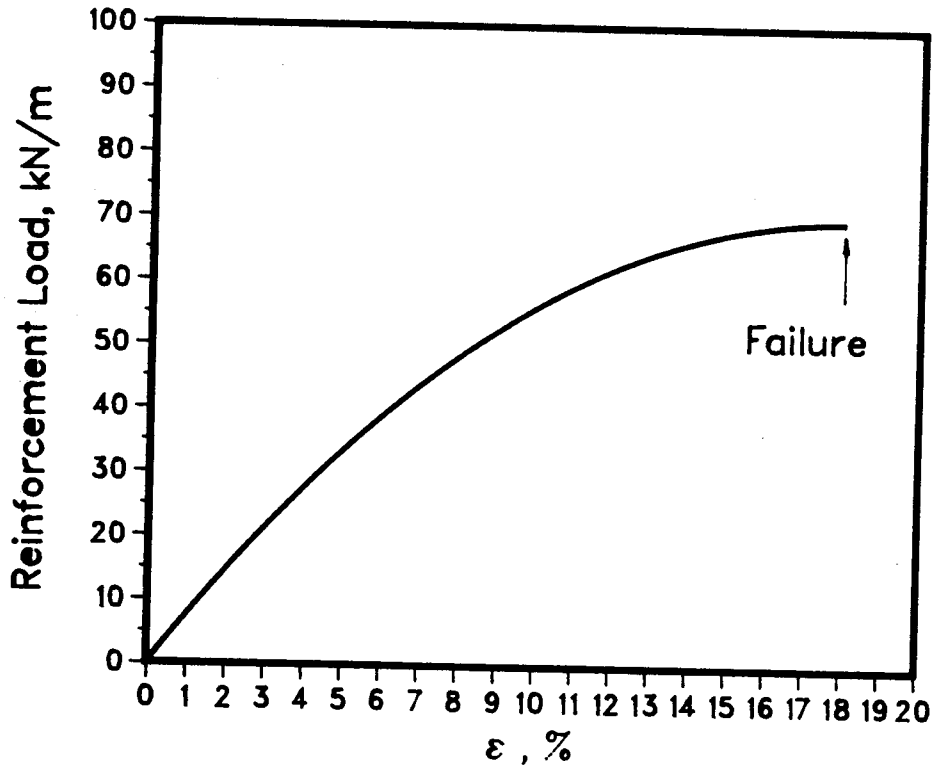


Figure 5.11 Load-Strain Relationship of Reinforcement

analyses be carried out using peak soil shear strengths and an allowable reinforcement tensile load selected at strain values compatible with the peak soil strength strain. If the soil is brittle or exhibits strain-softening behaviour, it is recommended that the constant volume or large strain strength of the soil be utilized in the limit equilibrium analysis.

The present analysis uses the peak soil strengths in the limit equilibrium analyses but no attempt is made to select a "design load" for the reinforcement. The selection of an appropriate reinforcement design load for use in limit equilibrium analyses is difficult and depends on a great many factors. The selection of the design load will depend on:

- 1) polymer type used in manufacturing the geosynthetic reinforcement
- 2) tensile test method used in determining the tensile behaviour of the geosynthetic
- 3) strain compatibility between the reinforcement and the soil
- 4) soil - reinforcement interaction
- 5) time (creep, stress relaxation and deterioration)
- 6) temperature and construction damage

Excellent discussions on the selection of allowable/design loads for polymeric reinforcement can be found in Bonaparte et al. (1986), Koerner and Hausmann (1987) and Jewell (1985).

### 5.3.4 Limit Equilibrium Analysis Results

Limit equilibrium analyses were conducted for each 1 m height of embankment. For each embankment level, the factor of safety was computed for each of the following cases:

- 1) nonreinforced slope
- 2) reinforced slope,  $T_i = 50$  kN/m  
horizontal force orientation
- 3) reinforced slope,  $T_i = 100$  kN/m  
horizontal force orientation
- 4) reinforced slope,  $T_i = 50$  kN/m  
tangential force orientation
- 5) reinforced slope,  $T_i = 100$  kN/m  
tangential force orientation

The reinforcement design loads were varied in order to examine their effect on the factor of safety of the reinforced slope. The results from the limit equilibrium analysis are listed in Table 5.1. The x and y coordinates of the centers of each critical slip surface are also included in Table 5.1. For both horizontal and tangential force orientation assumptions, Figure 5.12 presents the variation in the factor of safety with increasing reinforcement design loads for various embankment heights. Expectedly, the factor of safety of the slope increases as the design load is increased.

Two important trends emerge from the curves illustrated in Figure 5.12. The first trend shows that the rate at which

Table 5.1 Limit Equilibrium Analysis Results

Embnk. Ht. (m)	Load (kN/m)	HORIZONTAL			TANGENTIAL		
		X	Y	F.S. *	X	Y	F.S. *
2	0	99.5	497	5.65	n/a	n/a	n/a
	50	99.5	497	6.88	99.5	496.5	7.41
	100	99.5	497	8.1	99.5	496	9.07
3	0	99.5	495.5	3.97	n/a	n/a	n/a
	50	99	496	5.07	99.5	494	5.56
	100	99	496.5	6.1	99	494	7.03
4	0	99.5	493.5	3.13	n/a	n/a	n/a
	50	99	494.5	4.06	99	493	4.48
	100	98.5	496	4.9	99	491.5	5.72
5	0	99.5	492	2.62	n/a	n/a	n/a
	50	98.5	493.5	3.42	99	490.5	3.78
	100	98	495	4.13	99	489	4.85
6	0	99	491.5	2.28	n/a	n/a	n/a
	50	98.5	492	2.98	99	489	3.31
	100	98	494	3.61	98.5	487.5	4.24
7	0	99	490	2.04	n/a	n/a	n/a
	50	98.5	490.5	2.66	98.5	488	2.95
	100	97.5	493	3.21	98.5	485.5	3.78
8	0	99	488.5	1.85	n/a	n/a	n/a
	50	98	490	2.41	98.5	486	2.68
	100	97	492	2.91	98.5	484	3.43
9	0	99	487.5	1.71	n/a	n/a	n/a
	50	98	488.5	2.22	98.5	484.5	2.47
	100	97	491	2.67	98.5	481.5	3.15
10	0	99	486	1.59	n/a	n/a	n/a
	50	98	487	2.06	98.5	482.5	2.29
	100	96.5	490	2.48	98	480.5	2.92
11	0	99	485	1.49	n/a	n/a	n/a
	50	97.5	486.5	1.9	98.5	481	2.15
	100	96.5	489	2.32	98.5	478	2.73
12	0	99.5	482.5	1.41	n/a	n/a	n/a
	50	97.5	486	1.82	98.5	479.5	2.02
	100	96.5	488	2.18	98	476.5	2.57
13	0	99.5	481.5	1.35	n/a	n/a	n/a
	50	97.5	484	1.73	98.5	478	1.92
	100	96	487	2.07	98	475.5	2.43
14	0	99.5	480	1.29	n/a	n/a	n/a
	50	97.5	482.5	1.65	98.5	476.5	1.83
	100	96.5	486	1.97	98	473.5	2.31
15	0	99.5	479	1.24	n/a	n/a	n/a
	50	97	482	1.58	98.5	475	1.75
	100	95.5	485	1.88	97.5	473	2.2
16	0	100	476.5	1.19	n/a	n/a	n/a
	50	97.5	480	1.52	98.5	473.5	1.68
	100	95.5	484	1.8	98	470	2.11
17	0	100	475.5	1.15	n/a	n/a	n/a
	50	97.5	478.5	1.46	99	471.5	1.62
	100	95.5	483	1.73	98	468.5	2.03
18	0	100	474.5	1.11	n/a	n/a	n/a
	50	97.5	476.5	1.41	98.5	470.5	1.56
	100	95	482	1.67	98	466.5	1.95

\* F.S. stands for " Factor of Safety"

X - Horizontal Axis Coordinate ( X=100 is the Toe of the Embankment)  
 Y - Vertical Axis Coordinate ( Y=500 is Elevation of the Foundation)

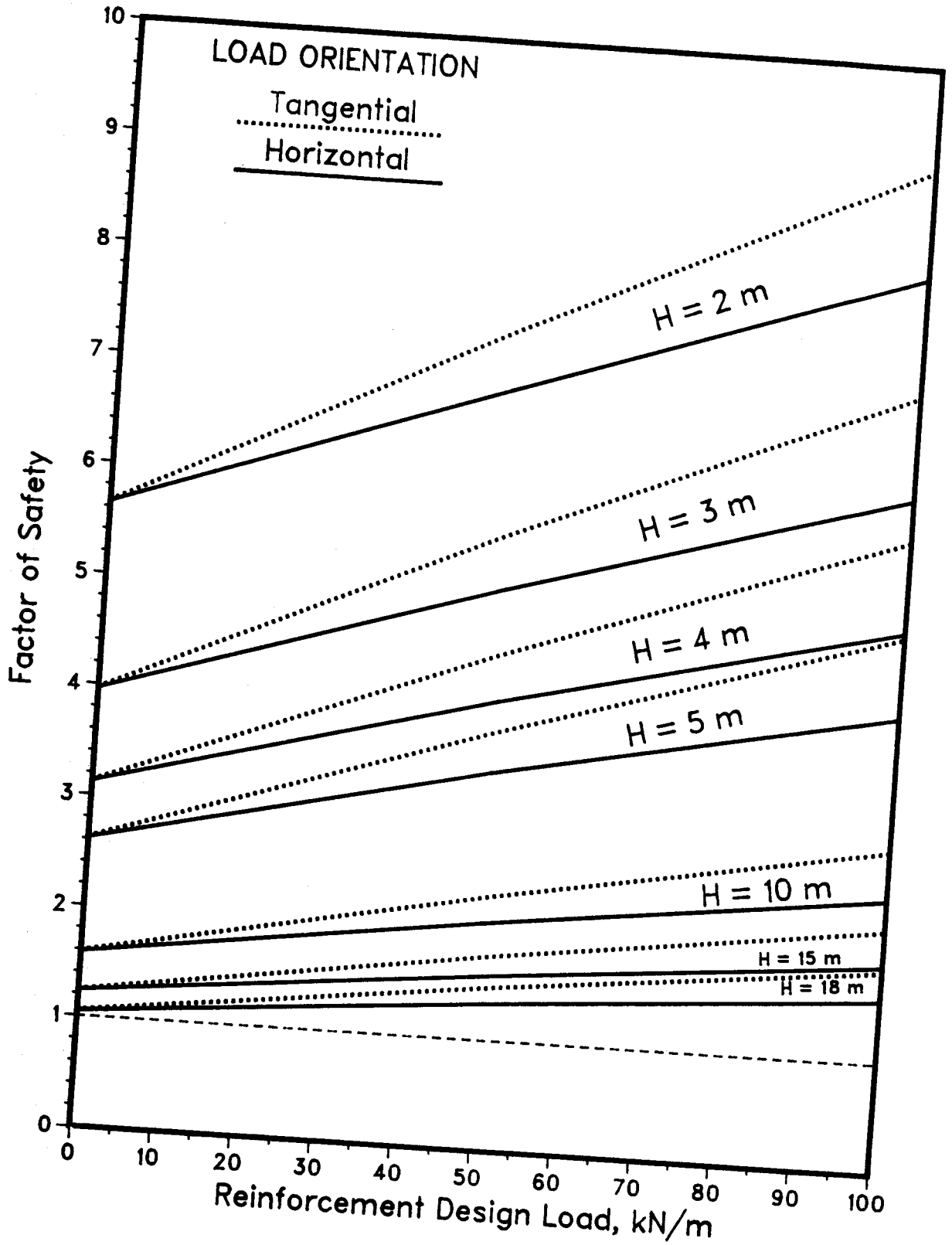


Figure 5.12 Limit Equilibrium Results



the reinforced slope factor of safety,  $F_r$ , increases depends not only on the reinforcement design load but on the factor of safety of the nonreinforced slope,  $F_o$ . This means that for any given reinforcement design load, the contribution provided by the reinforcement in increasing the slope safety factor will decrease as the nonreinforced slope safety factor,  $F_o$ , decreases. Figure 5.13 illustrates the relationship between  $F_o$  and the additional factor of safety provided by the reinforcement,  $\Delta F_r$ , for both the horizontal and tangential reinforcement force orientation assumptions.  $\Delta F_r$  has been normalized by the reinforcement design load,  $T_i$ , in order to generalize the relationship between  $F_o$  and  $\Delta F_r$ . The curves in Figure 5.13 simply show that for any reinforcement design load,  $T_i$ , any additional safety factor that will be provided by the reinforcement will decrease as the factor of safety of the nonreinforced slope decreases. Low and Duncan (1985) also found that the effects of the reinforcement on the slope safety factor decreased as the nonreinforced slope safety factor decreased.

The second observable trend in Figure 5.12 concerns  $\Delta F_{th}$ , the difference between the safety factors calculated for horizontal and tangential reinforcement force orientations. In the same manner as  $\Delta F_r$ ,  $\Delta F_{th}$  decreases with a decrease in the nonreinforced slope safety factor,  $F_o$ , for any particular reinforcement design load. Figure 5.14 illustrates the relationship between  $F_o$  and  $\Delta F_{th}/T_i$  and again,  $\Delta F_{th}$  is normalized to  $T_i$  in order to generalize the

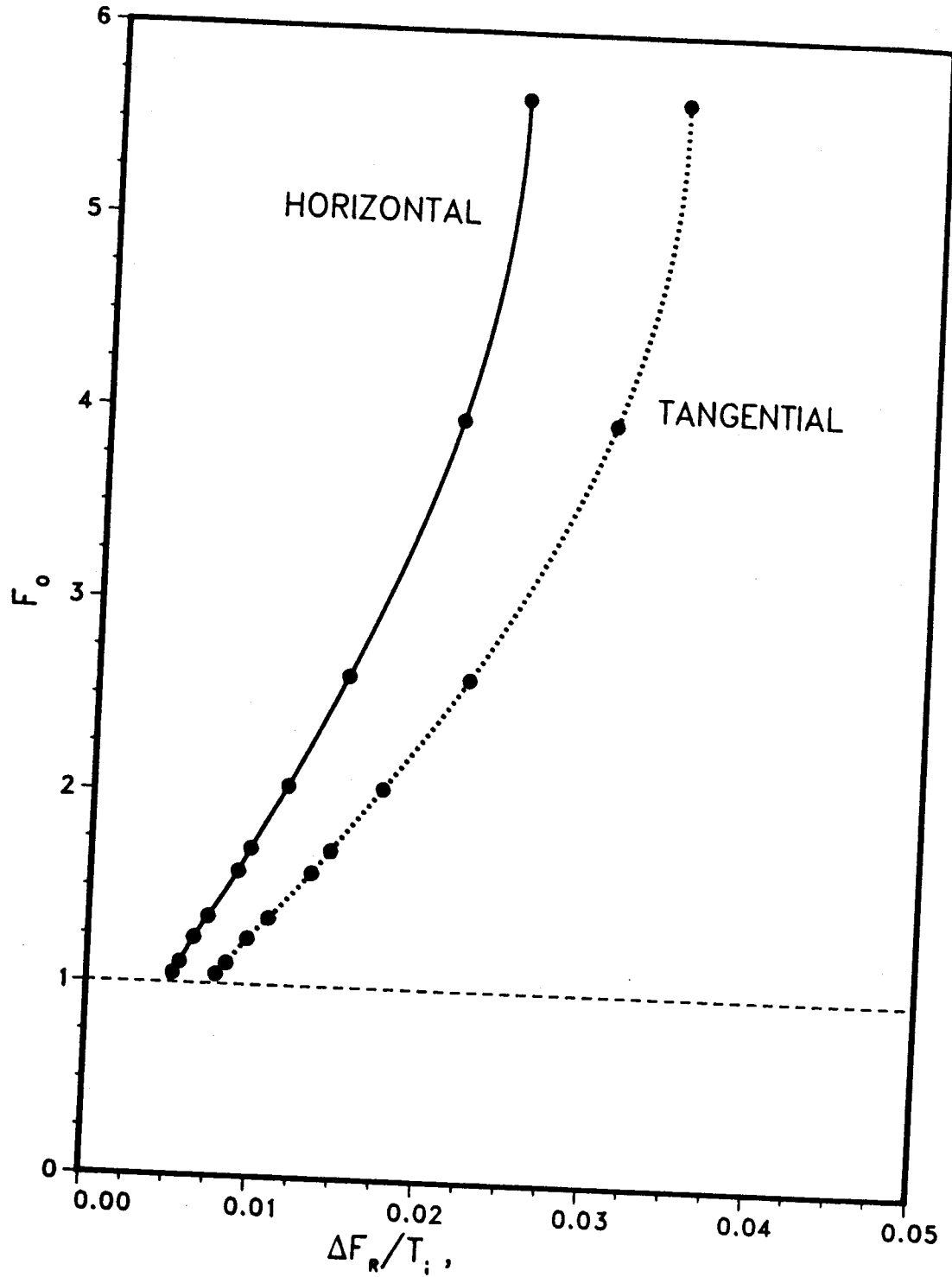


Figure 5.13 Effect of  $F_o$  on the Additional Factor of Safety Provided by the Reinforcement

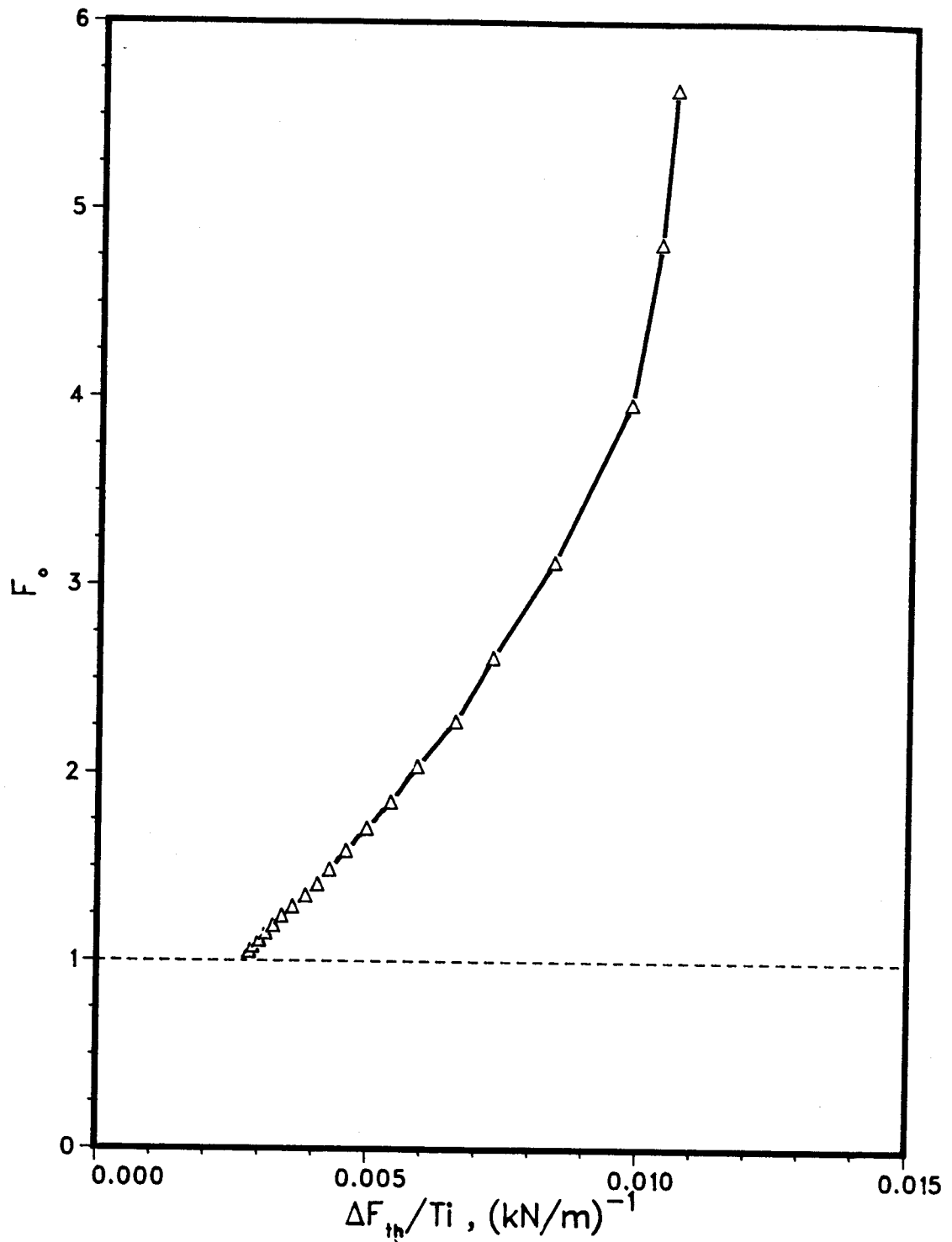


Figure 5.14 Effect of the Nonreinforced Slope Safety Factor,  $F_o$ , on the Difference Between Safety Factors Computed for Horizontal and Tangential Reinforcement Force Orientations,  $\Delta F_{th}$

relationship. The curve in Figure 5.14 serves to illustrate that in reinforcing a slope which has a relatively low factor of safety, both the horizontal and tangential force orientation assumptions will yield approximately the same reinforced slope safety factor.

### 5.3.5 Location of Critical Slip Surfaces

Using tangential or horizontal force orientations will yield different locations for the critical slip surface. Figures 5.15 to 5.18 present the critical slip surface locations predicted by BMM for embankment heights of 5 m, 10 m, 15 m and 18 m, respectively, for a reinforcement design load of 50 kN/m. In all cases, the tangential force assumption results in deeper critical slip surfaces and as indicated in Table 5.1, larger factors of safety than for a horizontal force orientation.

The reason a tangential force orientation results in deeper failure surfaces is due to the difference in the resisting moment definition between horizontal and tangential force assumptions. For any given slip surface, the resisting moment provided by horizontal forces,  $M_{Rh}$ , will always be smaller than the resisting moment provided by the tangential forces,  $M_{Rt}$ . This is shown in the form of Equation's 5.6 and 5.7. In terms of critical slip surfaces, then, a horizontal force assumption, which provides smaller resisting moments, will "find" a critical slip surface sooner than tangential force assumptions. This effect can

Tangential Force Orientation  
Nonreinforced Slope  
.....  
Horizontal Force Orientation  
-----

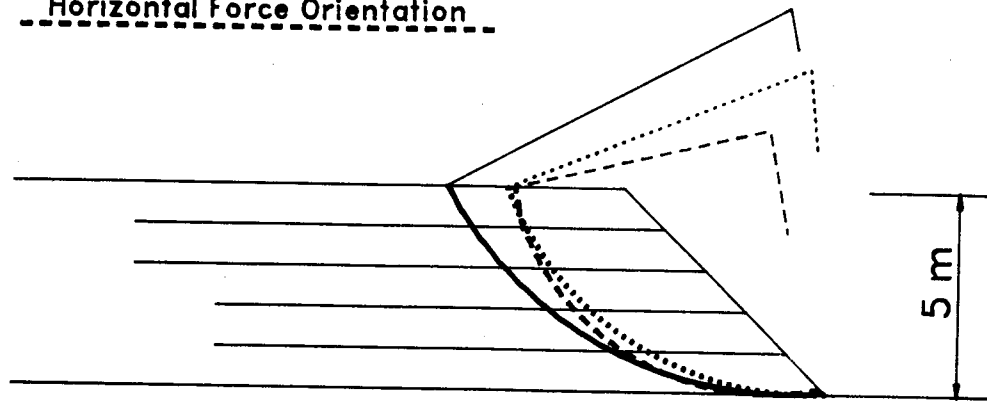


Figure 5.15 Critical Slip Surfaces for  $H = 5$  m

Tangential Force Orientation  
Nonreinforced Slope  
.....  
Horizontal Force Orientation  
-----

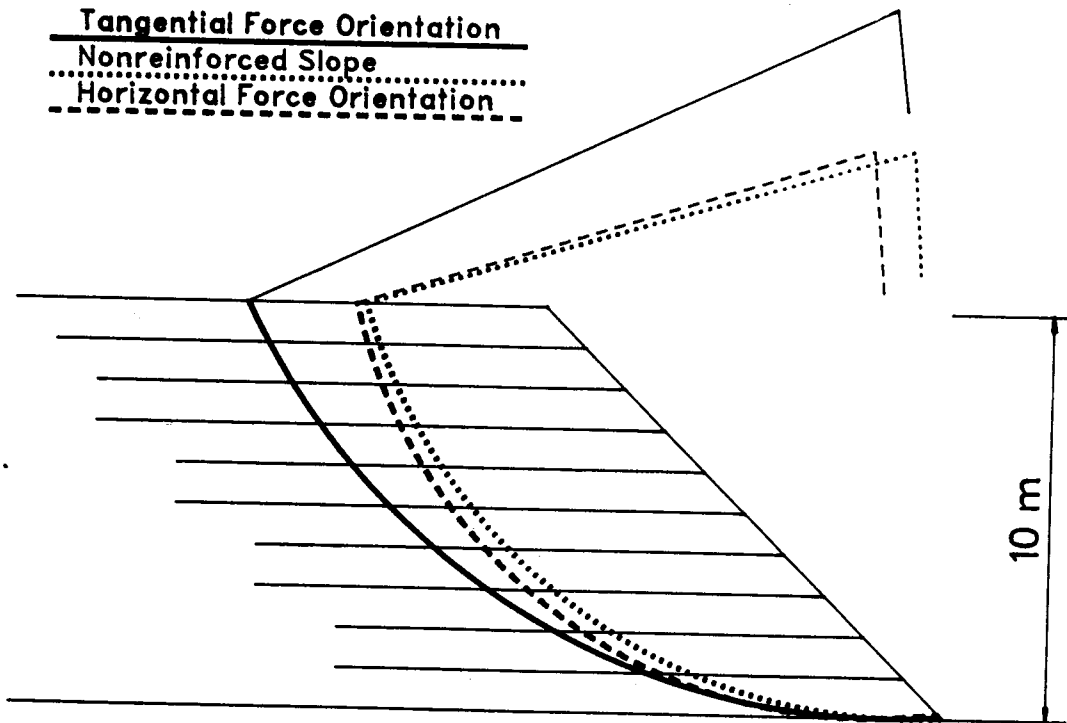


Figure 5.16 Critical Slip Surfaces for  $H = 10$  m

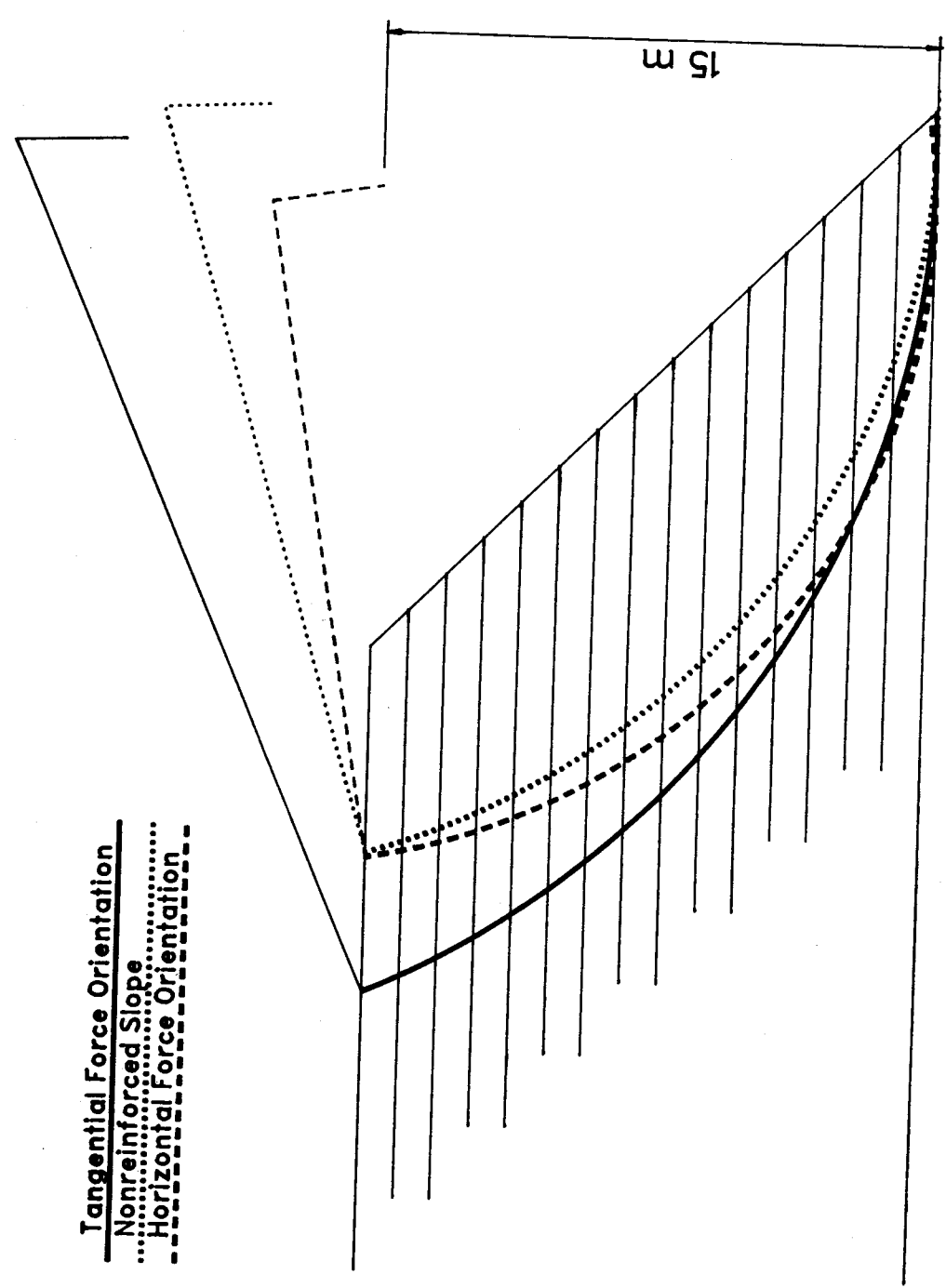


Figure 5.17 Critical Slip Surfaces for H = 15 m

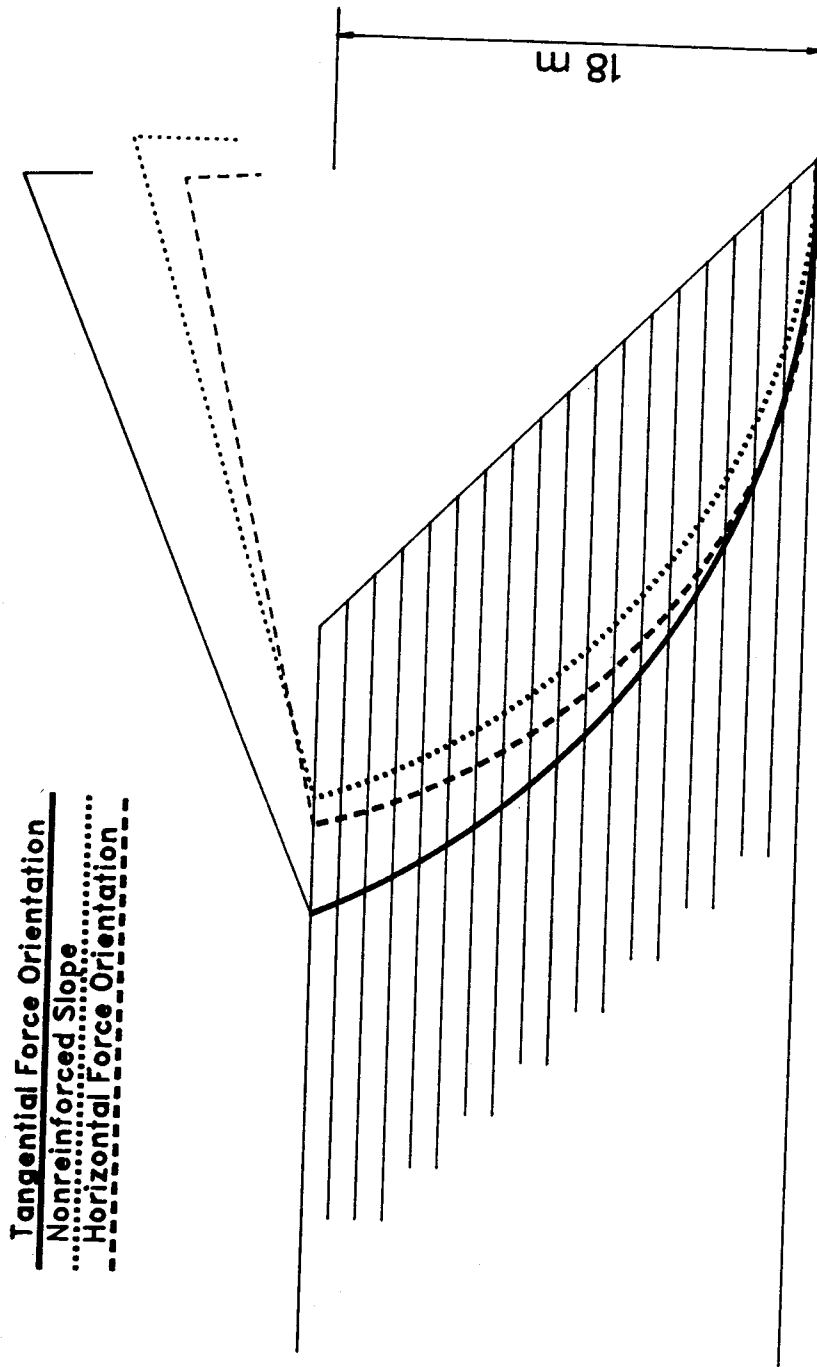


Figure 5.18 Critical Slip Surfaces for  $H = 18$  m

also be interpreted by stating that as the resisting moment provided by the reinforcement increases, the deeper the critical surface will be in the embankment. Leschinsky and Volk (1986) also found that the critical failure surface progressed deeper into the slope as the reinforcement strength increased.

The difference in the location of the critical slip surfaces predicted using a horizontal or tangential force orientation can also be examined using the locations of the critical slip surface centers. Figure 5.19 illustrates the direction of movement of the slip surface centers as a function of the design reinforcement load,  $T_i$ , for embankment heights of 5 m, 10 m, 15 m and 18 m. With reference to the nonreinforced slip surface centers, a horizontal force assumption causes a decrease in the slip surface radius and a tangential force assumption causes an increase in the slip surface radius. Both assumptions result in movement of the slip surface centers towards the crest of the slope. Even more important, is that for any embankment height  $H$ , increasing the design strength  $T_i$  of the reinforcement causes the critical slip surface radius to decrease for horizontal force assumptions and increase for tangential force assumptions. This trend is important to realize since the design of the reinforcement embedment length will depend upon the position of the critical slip surface. So not only does the assumption of horizontal or tangential forces affect the magnitude of the



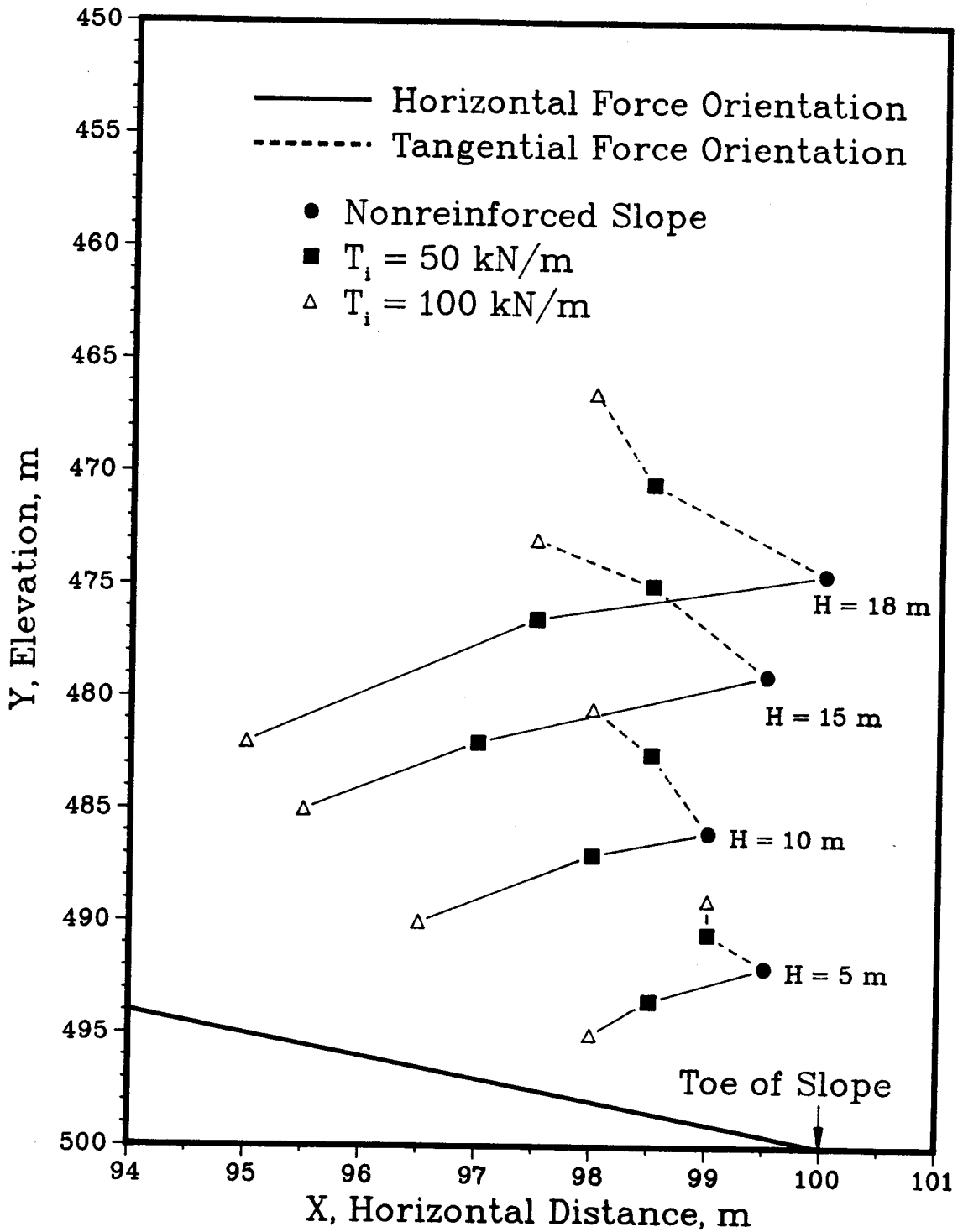


Figure 5.19 Location of Critical Slip Surface Centers

reinforcement's resisting moment, but different locations of the critical slip surface and different lengths of reinforcement are predicted.

#### 5.4 Summary and Conclusions

A limit equilibrium analysis of a steep reinforced cohesive soil slope has been conducted. Bishop's Modified Method of slope stability analysis, which incorporates the effects of reinforcement as free body forces, was used for the stability calculations. The results of the analysis have yielded the following conclusions:

- 1) A significant difference in the reinforcement resisting moment may exist between assuming the reinforcement force increases soil strength and assuming the reinforcement force acts as a "free body" force.
- 2) Factor's of safety calculated assuming horizontal reinforcement force orientations are more conservative than when assuming tangential reinforcement force orientations.
- 3) The effect of reinforcement on the factor of safety becomes less significant as the nonreinforced slope factor of safety becomes smaller.
- 4) The magnitude of the reinforcement contribution in stabilizing slopes is dependent on the factor of safety of the nonreinforced slope.
- 5) The location of the critical slip surfaces

determined by BMM will differ depending on the reinforcement force orientation assumption.

- 6) For any increasing reinforcement design strength, a horizontal force orientation results in a reduction of the critical slip surface radius and a tangential force orientation results in an increase of the critical slip surface radius. These changes in the position of the shear surface result in changes in the required length of the reinforcement layers.

## 6. COMPARISON BETWEEN THE LIMIT EQUILIBRIUM AND FINITE ELEMENT ANALYSES

### 6.1 Introduction

The intent of this chapter is to compare the results of the limit equilibrium and the finite element analyses of both the nonreinforced and reinforced soil slope. The calculated factors of safety of the slopes will serve as the means of comparison. The safety factors for the nonreinforced slope are first compared in order to gain confidence in the methods of analysis and the procedure for calculating a factor of safety from the results of the finite element analysis. The safety factors for the reinforced slope,  $F_{r1}$  and  $F_r$ , calculated using the results from the limit equilibrium and the finite element analyses, respectively, are then compared in order to examine the two methods of analysis.

A comparison between the two safety factors,  $F_{r1}$  and  $F_{r2}$ , computed using Bishop's Modified Method (BMM), is presented in order to study the effects of conventional load assumptions on the factor of safety. The effects of the reinforcement on the reinforced slope behaviour are examined through comparisons of the nonreinforced and reinforced slope safety factors. It was shown in Chapter 4 that the reinforcement alters the state of stress within the slope. In this chapter it will be shown that this change in stress is also reflected in the factor of safety of the reinforced

slope. A comparison between  $F_{fe}$ , the finite element safety factor for the nonreinforced slope, and  $F_{ro}$ , the finite element safety factor computed using only the soil stresses in the reinforced slope, reveals the degree to which the reinforcement effects the state of stress within the reinforced slope soil mass.

Given the multitude of definitions for a "factor of safety", the following section defines the safety factors used in the present research as well as a discussion on the calculation of these safety factors using both the limit equilibrium and the finite element results.

## 6.2 Definition of Safety Factors used in the Comparisons

In the present research, the comparison of the limit equilibrium and finite element analyses will be based on factors of safety. Unfortunately, in geotechnical practice the precise meaning of the factor of safety is difficult to establish and is found to depend on the method of analysis (limit equilibrium or stress-deformation) and experience. Fundamentally, however, the factor of safety of a nonreinforced soil slope can be defined as:

$$F_O = \frac{s}{\tau} \quad [6.1]$$

where  $F_O$  = Factor of Safety

$s$  = soil shear strength

$\tau$  = shear stress

The difficulty in defining  $F_O$  arises from the evaluation of

s and  $\tau$ .

Presently, the factor of safety of a slope is commonly defined as that factor by which the soil shear strength can be reduced in order to bring the slope into a state of limiting equilibrium along a given slip surface. In terms of Equation 6.1,  $F_0$  is set to unity, which defines a state of limiting equilibrium, and a factor of safety is applied to the shear strength parameters,  $c$  and  $\phi$ , used in defining  $s$ . The factor of safety calculated by BMM is based on this definition of the factor of safety. It should be noted that this definition implies that the factor of safety is constant over the length of the slip surface.

#### **6.2.1 Finite Element Safety Factors: Nonreinforced Slope**

The factors of safety determined from the finite element results of the nonreinforced slope analysis are also based on Equation 6.1. A finite element analysis yields the normal and shear stress distributions along any slip surface within a slope. The factor of safety from the finite element analysis may be specified in terms of stress equilibrium at a point, a "local factor of safety", or stress equilibrium of the entire slip surface, an "overall factor of safety". In order to be as consistent as possible with the safety factor definition used in BMM, an overall factor of safety will be computed from the finite element results.

Applying the safety factor to the strength parameters and assuming it is constant along a slip surface, the soil shear strength,  $s$ , is evaluated from the finite element results using:

$$s = \int_L \left( \frac{c}{F_{fe}} + \sigma_n \frac{\tan \phi}{F_{fe}} \right) dL \quad [6.2]$$

The shear stress,  $\tau$ , along a slip surface is evaluated using:

$$\tau = \int_L (\tau_{mob}) dL \quad [6.3]$$

Since the factor of safety is assumed to be constant along the slip surface, it can be extracted from the integral expression in Equation 6.2. Setting  $F_o=1$  in Equation 6.1 and substituting Equation 6.2 for  $s$  and Equation 6.3 for  $\tau$  into Equation 6.1, the factor of safety of the nonreinforced slope determined from the finite element analysis,  $F_{fe}$ , is defined as:

$$F_{fe} = \frac{\int_L (c + \sigma_n \tan \phi) dL}{\int_L (\tau_{mob}) dL} \quad [6.4]$$

For both the nonreinforced and reinforced slope comparisons, only the critical slip surfaces determined by BMM are used. No attempt has been made to determine the location of a critical slip surface from the finite element

results. The determination of the normal and shear stress distributions along a slip surface from the results of the finite element analysis are explained in Appendix F.

### 6.2.2 Finite Element Safety Factors: Reinforced Slope

Calculation of the nonreinforced slope safety factor from the limit equilibrium or finite element analysis results now becomes straightforward.  $F_{1e}$  is evaluated using Equation 6.1 and the method of slices while  $F_{fe}$  is evaluated using Equation 6.4 and the stress distributions along the slip surface. The calculation of the reinforced slope safety factor, however, is not as straightforward. For BMM it was assumed the reinforcement provided a "free body" force in stabilizing the slope and consequently, the factor of safety was defined as:

$$F_{r2} = \frac{M_{ST} + M_R}{M_O} \quad [6.5]$$

The theory and application of Equation 6.5, within the context of BMM, is fully discussed in Chapter 5.

In order to be consistent in the safety factor definitions used in the limit equilibrium and finite element methods, the reinforcement force will also be assumed to provide a "free body" force in the finite element analysis but  $M_{ST}$  and  $M_O$  are now defined as:

$$M_{ST} = R \int_L (c + \sigma_n \tan \phi) dL \quad [6.6]$$



$$M_O = R \int_L (\tau_{mob}) dL. \quad [6.7]$$

Therefore, the definition of the reinforced slope safety factor determined from the finite element results becomes:

$$F_R = \frac{R \int_L (c + \sigma_n \tan \phi) dL + M_R}{R \int_L (\tau_{mob}) dL} \quad [6.8]$$

The integral expressions in Equation 6.8 are evaluated in the same manner as for the nonreinforced slope case (see Appendix F) but the determination of  $M_R$  still demands an assessment of the mobilized force within the reinforcement and whether the force acts horizontally, tangentially or at some other orientation with respect to the slip surface.

Figure 6.1 illustrates the deformed shape of several reinforcing layers within the reinforced slope for a height of 18 m. The critical slip surface predicted by BMM assuming a horizontal force orientation is also shown in Figure 6.1. Given the small angular rotation of the reinforcement at its intersection with the slip surface (note the deformation scale in Figure 6.1), it is assumed the horizontal force assumption represents the best force orientation assumption. Consequently, the resistance moment provided by the reinforcement in the finite element analysis calculations,  $M_R$ , will be determined by:

$$M_{Rh} = \sum_{i=1}^n T_i (R - h_i) \quad [6.9]$$

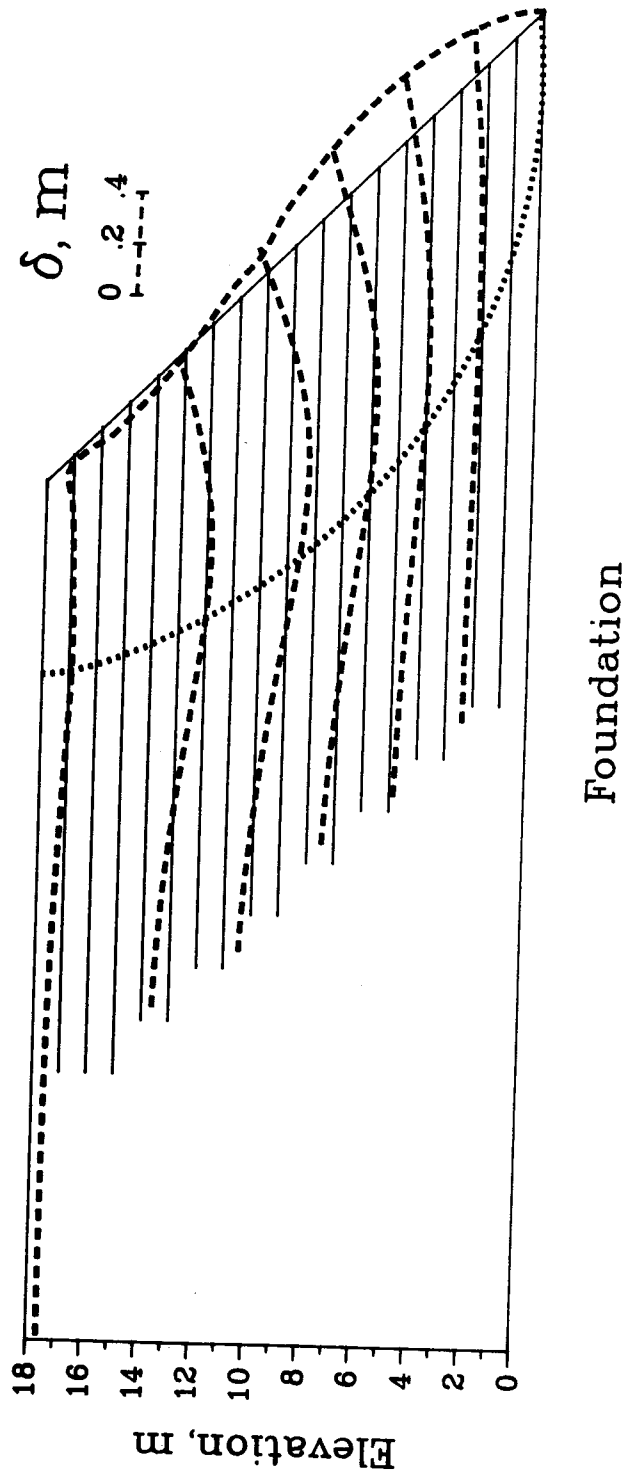


Figure 6.1 Deformed Shape of Reinforcement within the Reinforced Embankment,  $H = 18$  m

The magnitude of the reinforcement forces,  $T_i$ , are still required in order to determine  $F_r$ . It should be noted that the value of  $M_{Rh}$  must reflect the potential resisting moment that the reinforcement is capable of providing. The potential strength of the reinforcement is latent within the reinforced slope and so to determine the factor of safety of the slope, the potential reinforcement resistance moment must be calculated. The finite element analysis yields the working loads in each reinforcing layer and hence, the working resistance moment provided by the reinforcement. The results of the finite element analysis presented in Chapter 4, however, revealed that a unique relationship exists between  $h_i/H$  and  $T_i/T_{max}$ . This relationship is illustrated in Figure 6.2.

As a design philosophy, it can be stated that once the load in any reinforcing layer equals the design tensile strength of the reinforcement, the potential resistance moment that can be provided by all the reinforcement in the slope has been reached. Using the curve in Figure 6.2 and selecting  $T_{max}$  as the design tensile strength of the reinforcement, the loads in each reinforcing layer,  $T_i$ , can be determined. Using these potential values of  $T_i$ , the potential resistance moment,  $M_{Rh}$ , can be computed and used in Equation 6.8 to calculate the factor of safety of the reinforced slope.

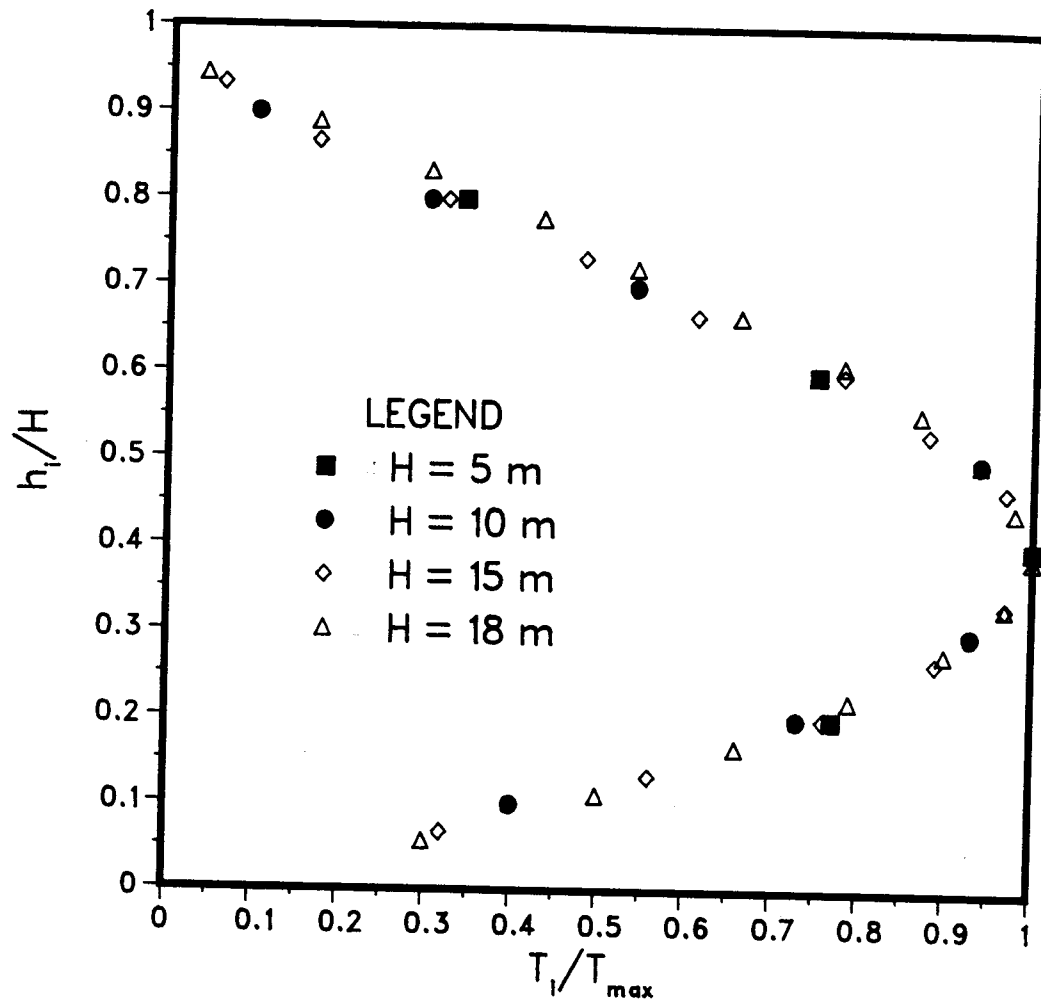


Figure 6.2 Relationship Between the Level of Reinforcing Layer Within the Embankment and the Mobilized Load in the Reinforcement

### 6.2.3 Partial Factor of Safety

It is also possible to examine the factors of safety with respect to the soil and to the reinforcement separately. Low and Duncan (1985), in their analysis of the behaviour of reinforced embankments constructed on weak foundations, provided a methodology for determining the partial factor of safety of the soil and the reinforcement. At any embankment height  $H$ , the condition of static equilibrium requires that the mobilized soil and reinforcement moments,  $M_{sm}$  and  $M_{rm}$  respectively, sum to a moment which exactly balances the disturbing or overturning moment,  $M_o$ . In the calculation of the overall reinforced slope factor of safety, the maximum possible restoring moment that can be provided by the soil and the reinforcement,  $M_{ST}$  and  $M_{Rh}$  respectively, can be determined. Using the results from the finite element analysis:

$$M_{rm} = \sum_{i=1}^n T_{mob}(R - h_i) \quad [6.10]$$

$$M_o = R \int_L (\tau_{mob}) dL \quad [6.11]$$

From the conditions of static equilibrium which must exist along a possible slip surface:

$$M_{sm} = M_o - M_{rm} \quad [6.12]$$

Now, the factor of safety with respect to the soil alone,  $F_{rs}$ , can be defined as:

$$F_{rs} = \frac{M_{ST}}{M_{sm}} \quad [6.13]$$

and the factor of safety with respect to the reinforcement alone,  $F_{rr}$ , can be defined as:

$$F_{rr} = \frac{M_{Rh}}{M_{rm}} \quad [6.14]$$

By comparing the factors of safety computed from the limit equilibrium and finite element results, some understanding of the reliability and accuracy of BMM for analyzing the stability of a multilayer reinforced soil slope can be obtained. In order to establish confidence in the comparison of safety factors computed using the two analytical methods, the safety factors determined for the nonreinforced slope will be compared first. Subsequently, an examination of the reinforced slope safety factors will be conducted in order to identify the suitability and limitations of BMM for analyzing reinforced soil slopes.

### 6.3 Comparison of the Nonreinforced Embankment Analyses

The factors of safety for the nonreinforced slope are listed in Table 6.1. The results in Table 6.1 indicate that for an embankment height of 18 m, the limit equilibrium method generates a factor of safety,  $F_{le}$ , equal to 1.11

Table 6.1 Factors of Safety of Nonreinforced and Reinforced Slope

Embankment Height (m)	NONREINFORCED SLOPE		REINFORCED SLOPE			
	$F_{le}$ LEM <sup>1</sup>	$F_{fe}$ FEM <sup>2</sup>	$F_{ro}$ FEM	$F_r$ FEM	$F_{r1}^3$ LEM	$F_{r2}^4$ LEM
5	2.62	2.78	2.78	3.12	2.95	3.01
10	1.59	1.67	1.78	1.96	1.77	1.82
15	1.24	1.30	1.43	1.55	1.36	1.41
18	1.11	1.16	1.24	1.35	1.23	1.26

1. LEM = Limit Equilibrium Method
2. FEM = Finite Element Method
3.  $F_{r1}$  calculated assuming potential reinforcement load distribution from finite element analysis
4.  $F_{r2}$  calculated assuming a constant reinforcement load of 26 kN/m

while  $F_{fe}$ , the factor of safety from the finite element analysis, is equal to 1.16. A difference of only 4.5% between these computed safety factors indicates very good agreement. The safety factors for the lower embankment heights show the same close agreement. The finite element method, however, consistently shows a slightly higher factor of safety than the limit equilibrium method. This trend is likely due to the greater accuracy with which the finite element method calculates the stresses along a slip surface. BMM, through the method of slices, provides only an approximation to the state of stress along a slip surface, albeit for most cases the approximation is very close to the stresses predicted by the finite element method. Wright et al. (1973) and Chen and Chameau (1982) also found that BMM and the finite element method gave close agreement between the computed safety factors with the finite element method consistently yielding slightly higher values. Thus it appears the finite element method and the limit equilibrium method provide comparable safety factors and the power of the finite element method does not offer any improvement over BMM in analyzing the factor of safety of nonreinforced slopes.

The close agreement between  $F_{le}$  and  $F_{fe}$  is also illustrated in Figure 6.3. Both curves lie close to one another and show rapid decreases in the factor of safety as the embankment height increases. The curves indicate that the factor of safety will equal one for an embankment height



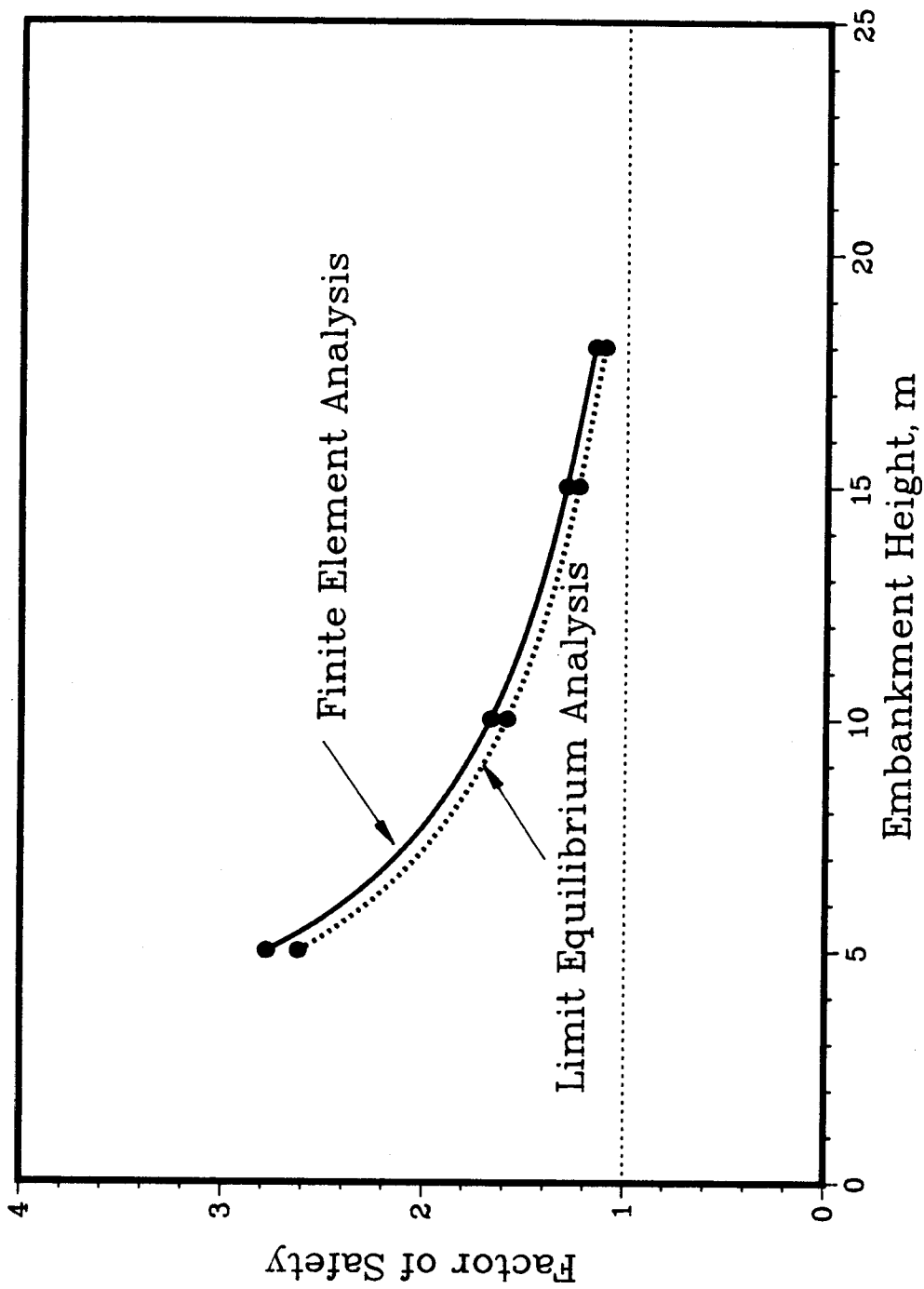


Figure 6.3 Variation in Nonreinforced Embankment Safety Factors Computed from the Limit Equilibrium and Finite Element Analyses

of approximately 23 m.

Given the close agreement between  $F_{1e}$  and  $F_{fe}$ , it can be concluded that the method used in calculating the factor of safety from the finite element results is consistent with the safety factor determined from the limit equilibrium results. This provides confidence in comparing the safety factors from the reinforced embankment analyses.

#### 6.4 Comparison of the Reinforced Embankment Analyses

Besides  $F_{1e}$  and  $F_{fe}$ , four additional safety factors,  $F_o$ ,  $F_r$ ,  $F_{r1}$  and  $F_{r2}$  will also be involved in comparing the reinforced slope analyses. Table 6.1 lists the values of  $F_o$ ,  $F_r$ ,  $F_{r1}$  and  $F_{r2}$  for embankment heights of 5 m, 10 m, 15 m and 18 m. Comparisons between  $F_r$ , the overall safety factor of the reinforced slope calculated using the results from the finite element analysis, and  $F_{r1}$ , the reinforced slope safety factor determined using BMM, are used to show the agreement between the two methods of analysis. Comparison between the two limit equilibrium safety factors for the reinforced slope,  $F_{r1}$  and  $F_{r2}$ , provides insight into the effects of selecting constant working strengths in each layer of reinforcement. The nonreinforced slope safety factors,  $F_{fe}$  and  $F_{1e}$ , and the reinforced slope safety factors,  $F_{r1}$  and  $F_{r2}$ , are compared in order to examine the increase in the factor of safety due to the reinforcement. An evaluation of the degree to which the reinforcement alters the state of stress within the soil mass is presented

through a comparison of  $F_{fe}$  and  $F_{ro}$ .

#### 6.4.1 Reinforced Slope Safety Factors

The factors of safety determined from the finite element and the limit equilibrium analyses of the reinforced slope,  $F_r$  and  $F_{r1}$ , respectively, show satisfactory agreement. Figure 6.4 illustrates the variation of these two safety factors as a function of embankment height. As for the nonreinforced slope case, the finite element safety factor,  $F_r$ , is slightly larger than the limit equilibrium safety factor,  $F_{r1}$ . The magnitude of the difference, however, is larger for the reinforced slope case.

The method of including the reinforcement in the safety factor determination is identical for both the limit equilibrium and the finite element calculations. The value of  $F_{r1}$  is computed using the load distribution within the reinforcement obtained in the finite element analysis. Since the magnitude of the reinforcement resistance moment is the same in both safety factor calculations, the difference in safety factors clearly illustrated in Figure 6.4 is a result of a difference in the state of stress within the soil mass of the reinforced slope. The limit equilibrium method ignores any soil-reinforcement interaction effect and includes the reinforcement in the form of a free body force only. The finite element method, on the other hand, does include soil-reinforcement interaction effect. By incorporating the change in the state of stress within the

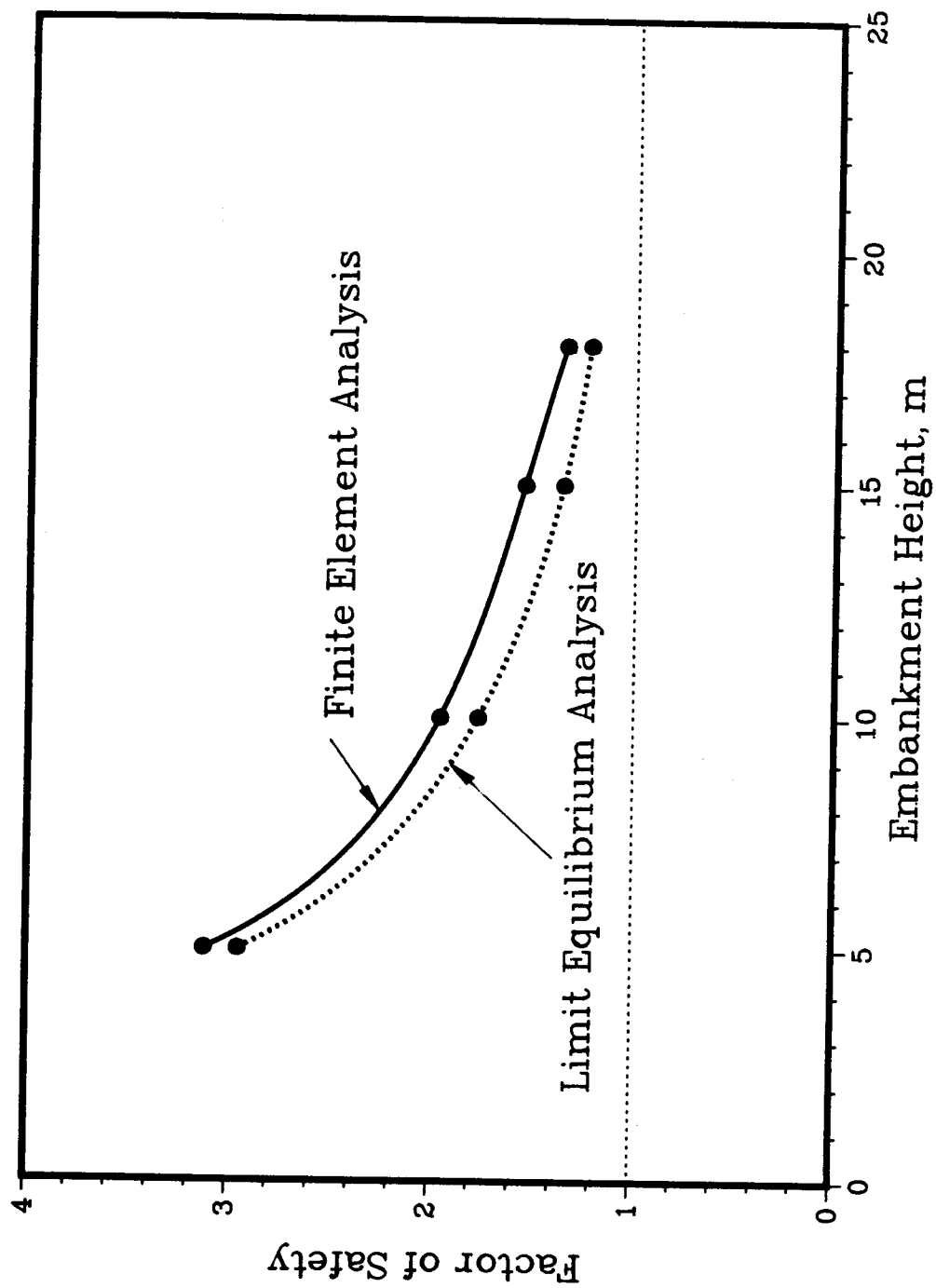


Figure 6.4 Variation in the Reinforced Embankment Safety Factors Computed From the Limit Equilibrium and the Finite Element Analyses

soil, the finite element analysis shows that a smaller soil strength is required to maintain equilibrium within the slope because of the presence of the reinforcement. This in turn leads to an increase in the overall factor of safety of the reinforced soil slope.

#### 6.4.2 Limit Equilibrium Safety Factors

In order to examine the effects of assuming a constant load in every reinforcing layer on the factor of safety of the reinforced slope, the limit equilibrium safety factor,  $F_{r1}$ , which assumes a load distribution obtained from the finite element analysis and a limit equilibrium safety factor,  $F_{r1}$ , calculated assuming a constant load in each reinforcing layer, are compared. The potential reinforcement load distribution determined from the finite element analysis was used in calculating  $F_{r1}$ . The reinforcement load distributions are illustrated in Figures 6.5 to 6.8 for embankment heights of 5 m, 10 m, 15 m and 18 m respectively.

In general, however, the finite element method is not used for reinforced slope design and consequently the reinforcement load distribution will not be known *a priori*. Some assumption regarding the loads which will develop in the reinforcing layers is required. If it is assumed the factor of safety is constant along a possible slip surface, then for a condition of limiting equilibrium, the same loads will develop in each reinforcing layer. By restricting the magnitude of the load in any reinforcing layer to its

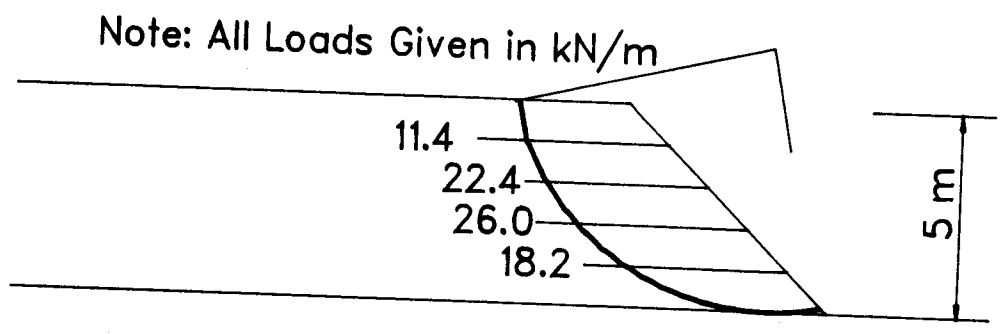


Figure 6.5 Potential Reinforcement Load Distribution for a Slope Height of 5 m

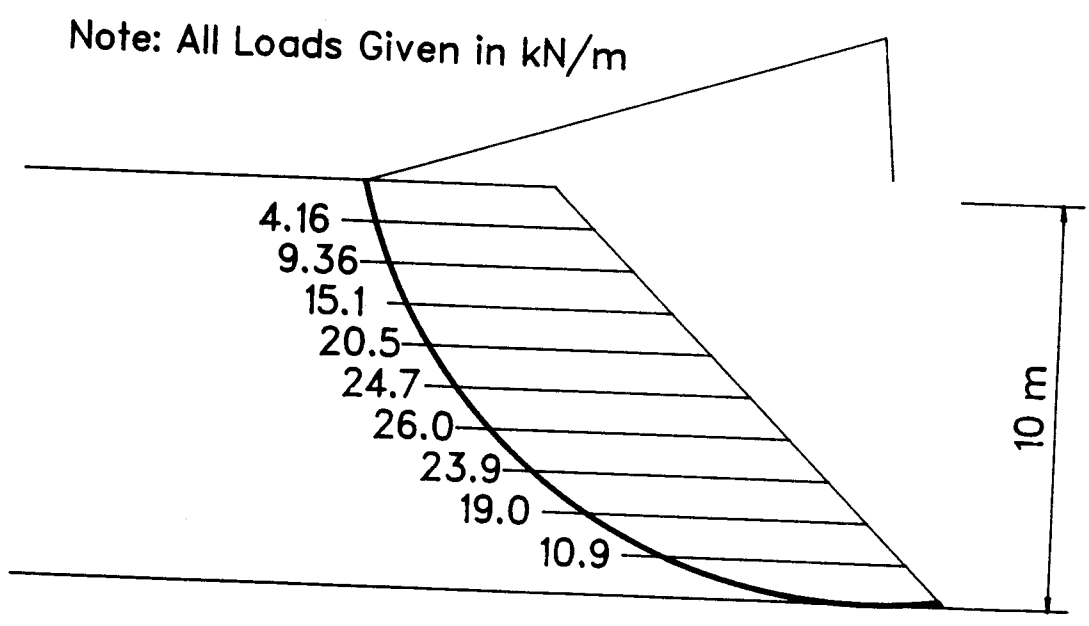


Figure 6.6 Potential Reinforcement Load Distribution for a Slope Height of 10 m

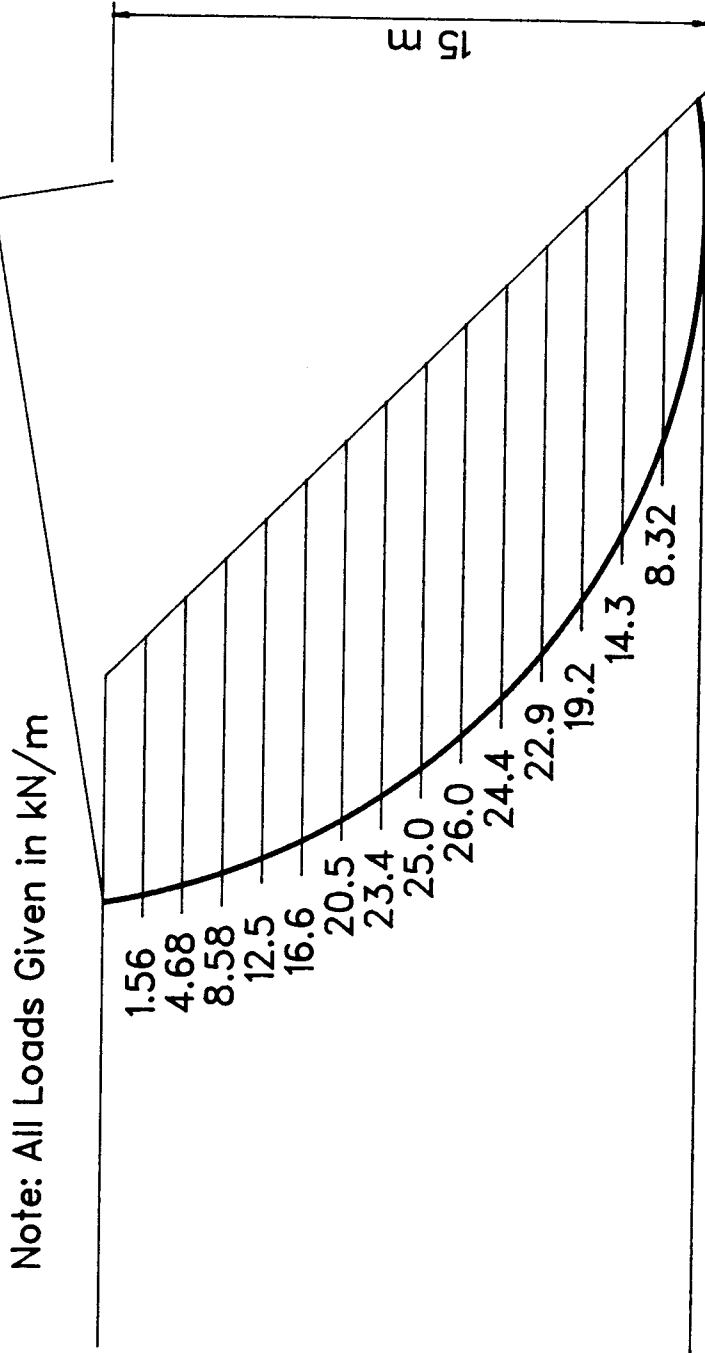


Figure 6.7 Potential Reinforcement Load Distribution for a Slope Height of 15 m

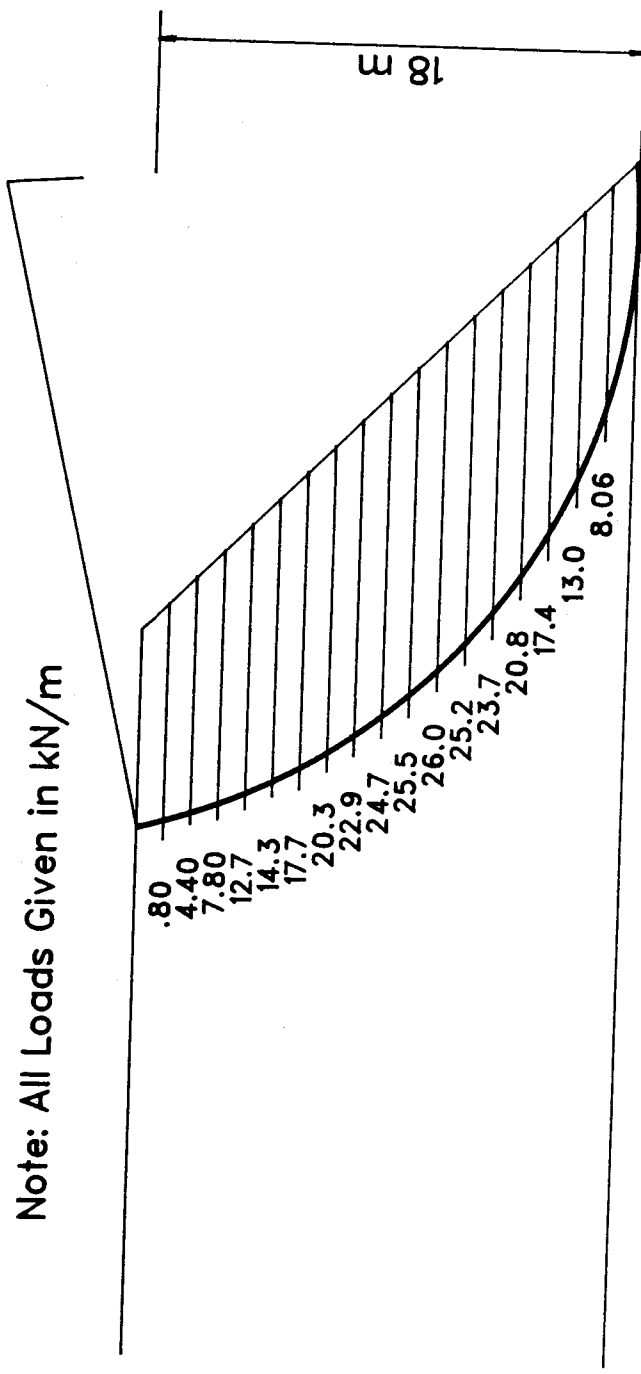


Figure 6.8 Potential Reinforcement Load Distribution for a Slope Height of 18 m



allowable tensile strength, the reinforced slope can be designed using BMM. Using these assumptions and selecting an allowable tensile strength of 26 kN/m for the reinforcement, the values of  $F_{r2}$  have been calculated. Figure 6.9 illustrates a constant reinforcement load distribution for an embankment height of 18 m.

Figure 6.10 illustrates the variation in  $F_{r1}$  and  $F_{r2}$  as a function of embankment height. Although two different reinforcement load distributions are used, the values of  $F_{r1}$  and  $F_{r2}$  are almost identical with the values of  $F_{r2}$  slightly larger than  $F_{r1}$ . Since a larger reinforcement resistance moment,  $M_{Rh}$ , results from assuming a constant load in each reinforcing layer rather than a load distribution derived from the curve in Figure 6.2, it is expected  $F_{r2}$  will be larger than  $F_{r1}$ . The magnitude of this difference, however, is small. The values of  $F_{r2}$  are only approximately 3% larger than  $F_{r1}$  indicating that for the reinforced slope geometry analyzed, a constant design load assumption does not significantly affect the safety factor computed by BMM. The reason for the insensitivity of the safety factor to the magnitude of  $M_{Rh}$  can be explored using the safety factor equation:

$$F_r = \frac{M_{ST} + M_{Rh}}{M_O} = F_O + \Delta F_r \quad [6.15]$$

$$\text{where } F_O = \frac{M_{ST}}{M_O}$$

$$\Delta F_r = \frac{M_{Rh}}{M_O}$$

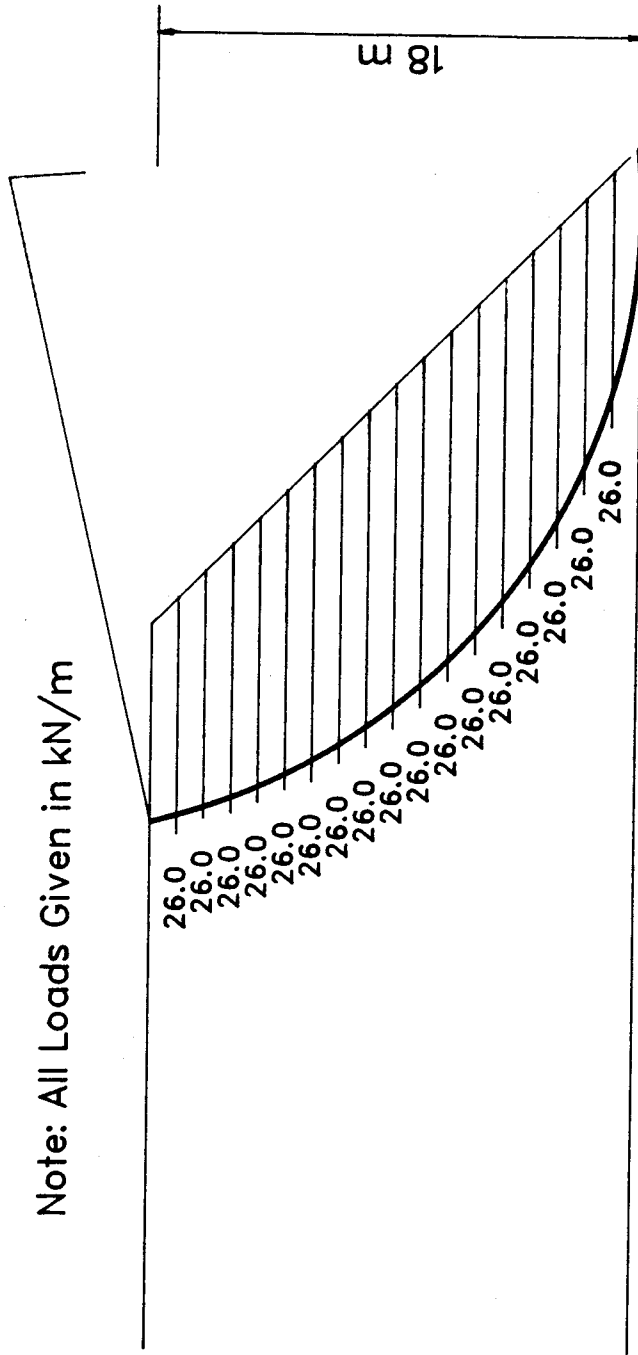


Figure 6.9 Constant Reinforcement Load Distribution for a Slope Height of 18 m

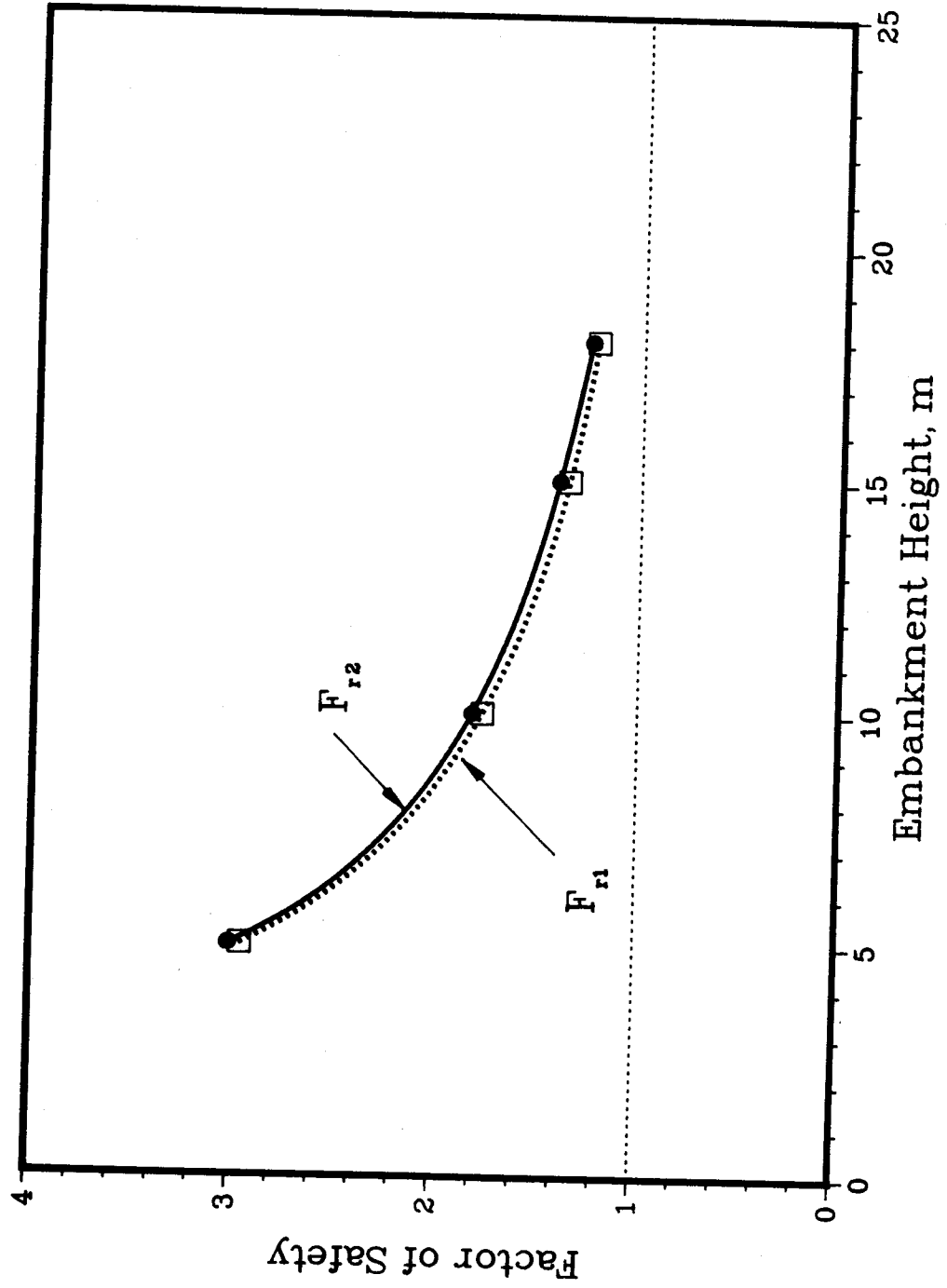


Figure 6.10 Variation in Limit Equilibrium Safety Factors,  $F_{r1}$  and  $F_{r2}$

It can be seen that if the value of  $M_{Rh}$  is small compared to the magnitude of  $M_o$ , changes in the value of  $M_{Rh}$  may have little effect on  $F_r$ . It should be noted that this will only be true if  $M_{ST}$  and  $M_o$  are of the same order of magnitude.

From the finite element results for the 15 m high reinforced slope:  $M_{ST} = 31957$  kNm and  $M_o = 22306$  kNm. It is clear these two values are of the same order of magnitude. For the potential load distribution determined using the curve in Figure 6.2,  $M_{Rh} = 2603$  kNm and for a constant load distribution,  $M_{Rh} = 3822$  kNm. These two values of  $M_{Rh}$  are one order of magnitude less than  $M_o$  and when Equation 6.16 is evaluated, the contribution of  $\Delta F_r$  becomes small relative to  $F_o$ . In terms of the difference between  $F_{r1}$  and  $F_{r2}$ , the difference between the two values of  $M_{Rh}$  presented above in relation to the magnitude of  $M_o$  indicates the reason only a 3% discrepancy exists between  $F_{r1}$  and  $F_{r2}$ .

#### **6.4.3 Improvement in Factor of Safety Due to Reinforcement**

In assessing the improvement in the slope factor of safety provided by the reinforcement, comparisons between  $F_{fe}$  and  $F_r$  and between  $F_{1e}$  and  $F_{r1}$  can be made.  $F_{fe}$  and  $F_r$  are calculated using the results from the finite element analysis and  $F_{1e}$  and  $F_{r1}$  are calculated using BMM. Figure 6.11 illustrates the comparison between  $F_{fe}$  and  $F_r$ . Figure 6.12 illustrates the variation in  $F_{1e}$  and  $F_{r1}$ . These two curves show the relative increase in the factor of safety of the nonreinforced slope resulting from the placement of

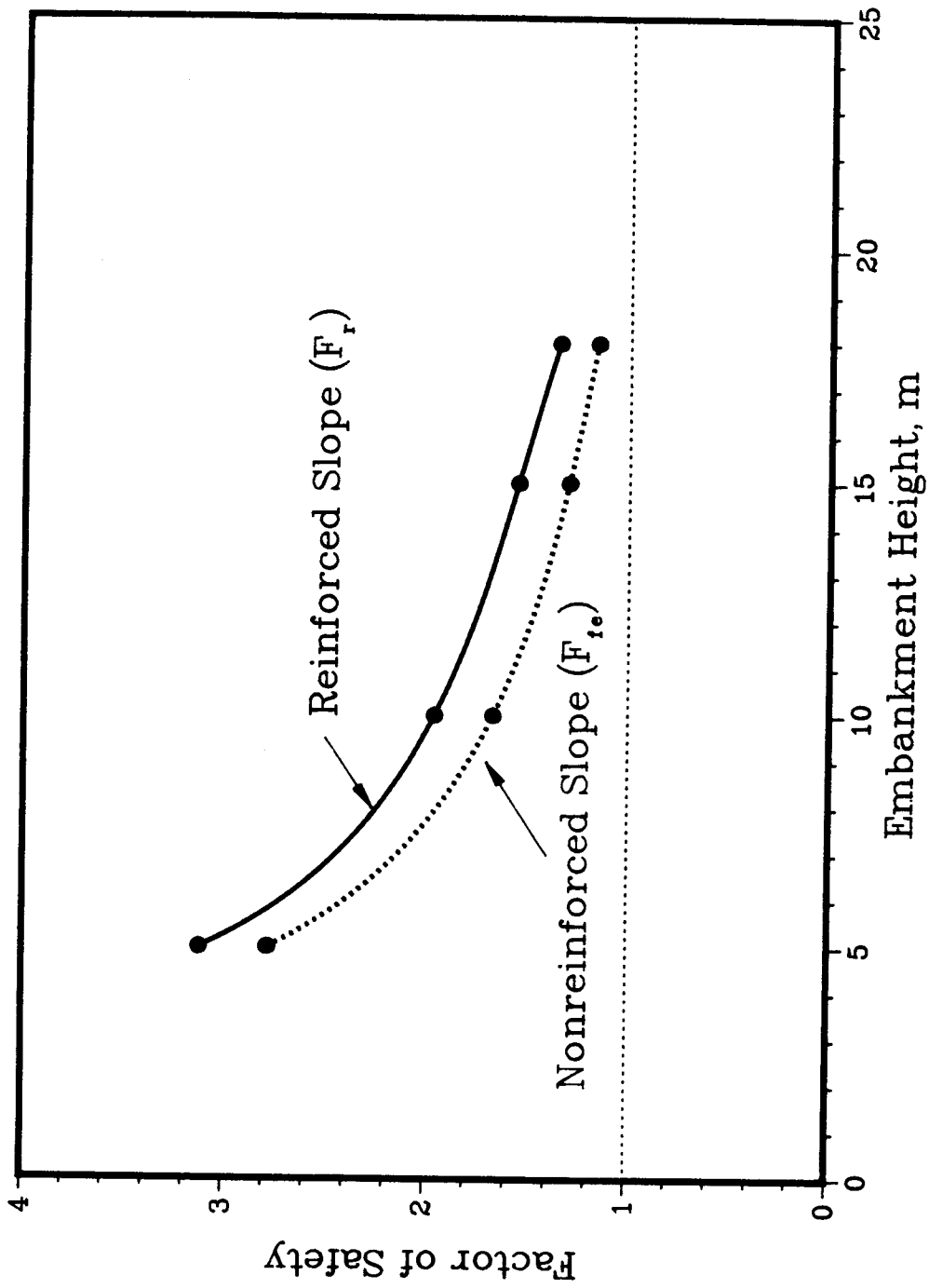


Figure 6.11 Variation in the Nonreinforced and Reinforced Slope Safety Factors,  $F_{re}$  and  $F_r$ , Calculated Using the Finite Element Analysis Results

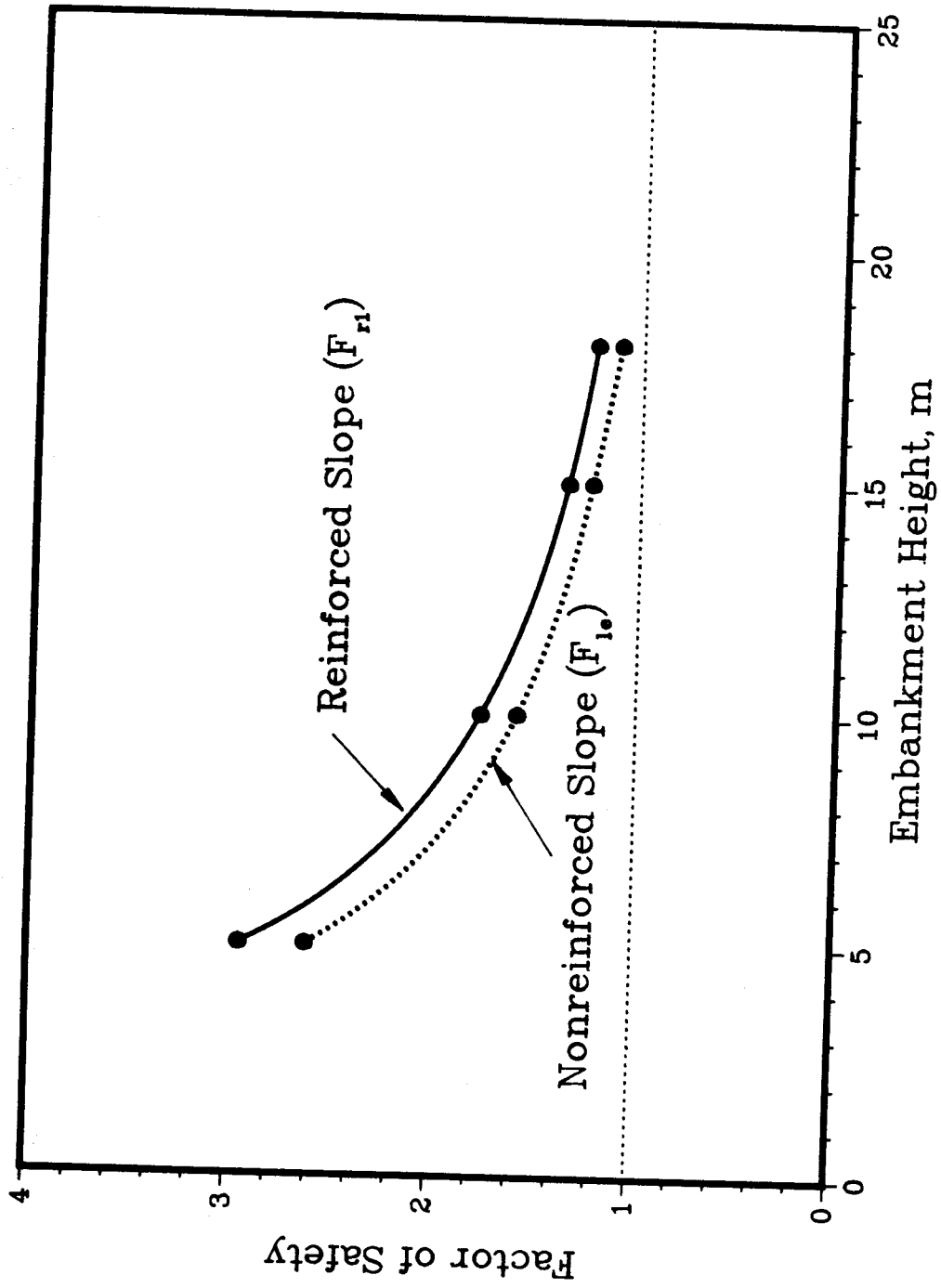


Figure 6.12 Variation in the Nonreinforced and Reinforced Slope Safety Factors,  $F_{1e}$  and  $F_{r1}$ , Calculated Using the Limit Equilibrium Analysis Results

reinforcing layers within the slope. A larger increase in the factor of safety is predicted by the finite element analysis than by the limit equilibrium analysis. The reason the finite element method provides larger safety factor increases is due to the soil-reinforcement interaction effect on the stress field within the soil mass. The increase shown for the limit equilibrium method is due only to the resistance moment provided by the "free body" reinforcement force. No change in the soil stress is accommodated for in the limit equilibrium method.

In order to examine the relative improvements in the factor of safety predicted by the limit equilibrium and the finite element methods, an improvement ratio defined as:

$$I_R = \frac{\left( \text{Factor of Safety of Reinforced Slope} \right) - \left( \text{Factor of Safety of Nonreinforced Slope} \right)}{\left( \text{Factor of Safety of Nonreinforced Slope} \right)} \quad [6.16]$$

can be utilized. Figure 6.13 illustrates the variation in the improvement ratio for the finite element and limit equilibrium methods as a function of embankment height. Although curves have been drawn in Figure 6.13, the limited amount of data points do not allow for any conclusions on the relationship between  $I_R$  and  $H$ . The curves were drawn to highlight the differences in  $I_R$  that exist between the finite element and limit equilibrium methods. In interpreting the curves in Figure 6.13, it is noted that the method of including the reinforcement forces and the

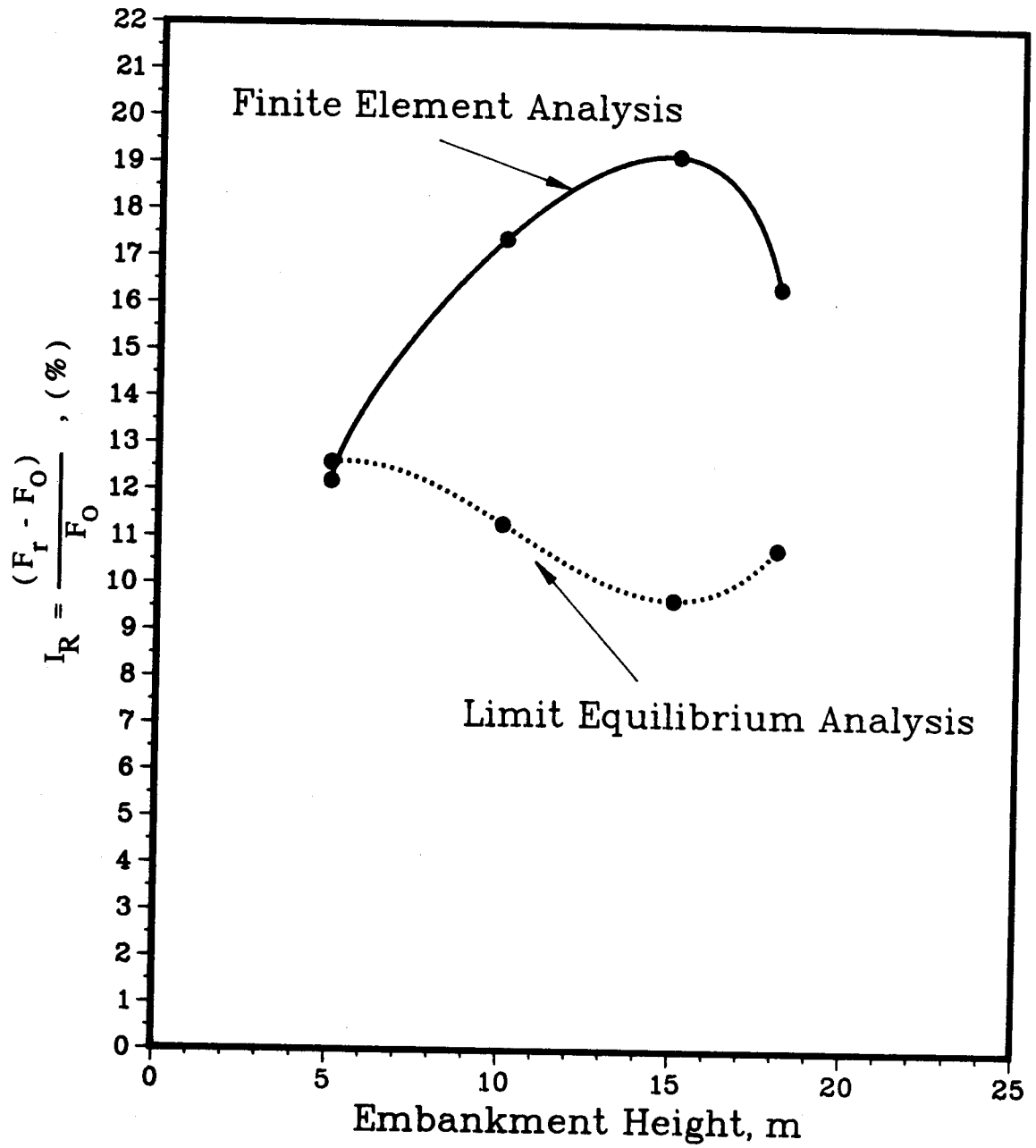


Figure 6.13 Variation in the Improvement Ratio for the Reinforced Slope



183

magnitude of the resistance moments provided by the reinforcement are identical in the two methods of analysis. The difference in the improvement ratios of the two methods, then, is a function only of the change in the state of stress within the soil mass of the reinforced slope. On average, an additional 7% increase in the improvement ratio is due solely to the modification of the stresses within the soil mass of the reinforced soil slope.

#### 6.4.4 State of Stress Within the Soil of the Reinforced Slope

The effects of the soil-reinforcement interaction on the state of stress within the soil mass of a reinforced soil slope can be examined by comparing the values of  $F_{fe}$  and  $F_{ro}$ .  $F_{ro}$  represents the contribution of the soil shear strength to the overall factor of safety of the reinforced slope,  $F_r$ . In terms of Equation 6.8,  $M_r$  is set to zero in order to calculate  $F_{ro}$ . The values of  $F_{ro}$  for embankment heights of 5 m, 10 m, 15 m and 18 m are listed in Table 6.1. Figure 6.14 illustrates the variation in  $F_{fe}$  and  $F_{ro}$  with embankment height.

For an embankment height of 5 m,  $F_{fe}$  and  $F_{ro}$  are equal indicating that the state of stress within the soil has not been altered by the presence of the reinforcement. This result supports the hypothesis of Low and Duncan (1985) that the enhanced safety of a reinforced embankment may not be noticeable at working conditions if the mobilized force in

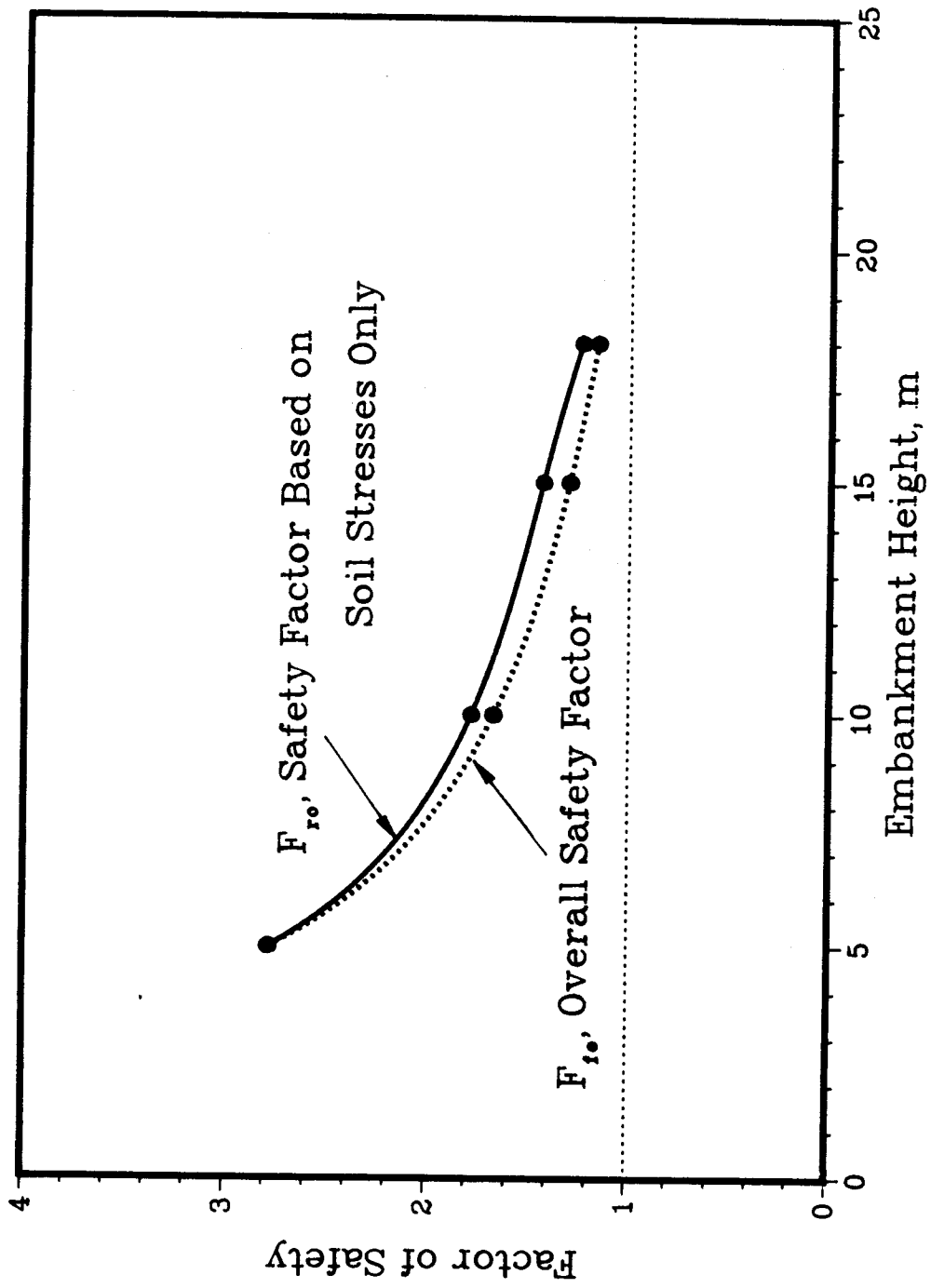


Figure 6.14 Variation in the Nonreinforced Slope Safety Factor,  $F_{fe}$ , and  $F_{ro}$

the reinforcement is small. A reinforced embankment not close to failure might exhibit almost the same behaviour as its nonreinforced counterpart. However, the potential strength of the reinforcement still provides an additional margin of safety which is reflected in the value of  $F_r$ .

As the embankment height increases, the value of  $F_{ro}$  becomes larger than  $F_{fe}$  indicating that the reinforcement is affecting the state of stress within the soil mass. Assuming the magnitude of the disturbing forces are unaffected by the presence of the reinforcement (Low and Duncan, 1985), the divergence between  $F_{fe}$  and  $F_{ro}$  can be explained as an increase in the available soil shear strength. As discussed in Chapter 4, the reinforcement permits the reinforced soil to sustain a higher confining stress than its nonreinforced counterpart. The higher confining stress leads to an increase in the available soil shear strength which is reflected in the difference between  $F_{fe}$  and  $F_{ro}$ .

In terms of the overall factor of safety of the reinforced slope,  $F_r$ , the favorable change in the state of stress of the soil mass accounts for a large portion of the safety factor increase from  $F_{fe}$  to  $F_r$ . Using the improvement ratio approach, Figure 6.15 illustrates the percent improvement in the slope factor of safety  $F_r$ , over that of the nonreinforced slope,  $F_{fe}$ . The contribution to the increase in the factor of safety provided by the change in the state of stress within the soil is also shown in Figure

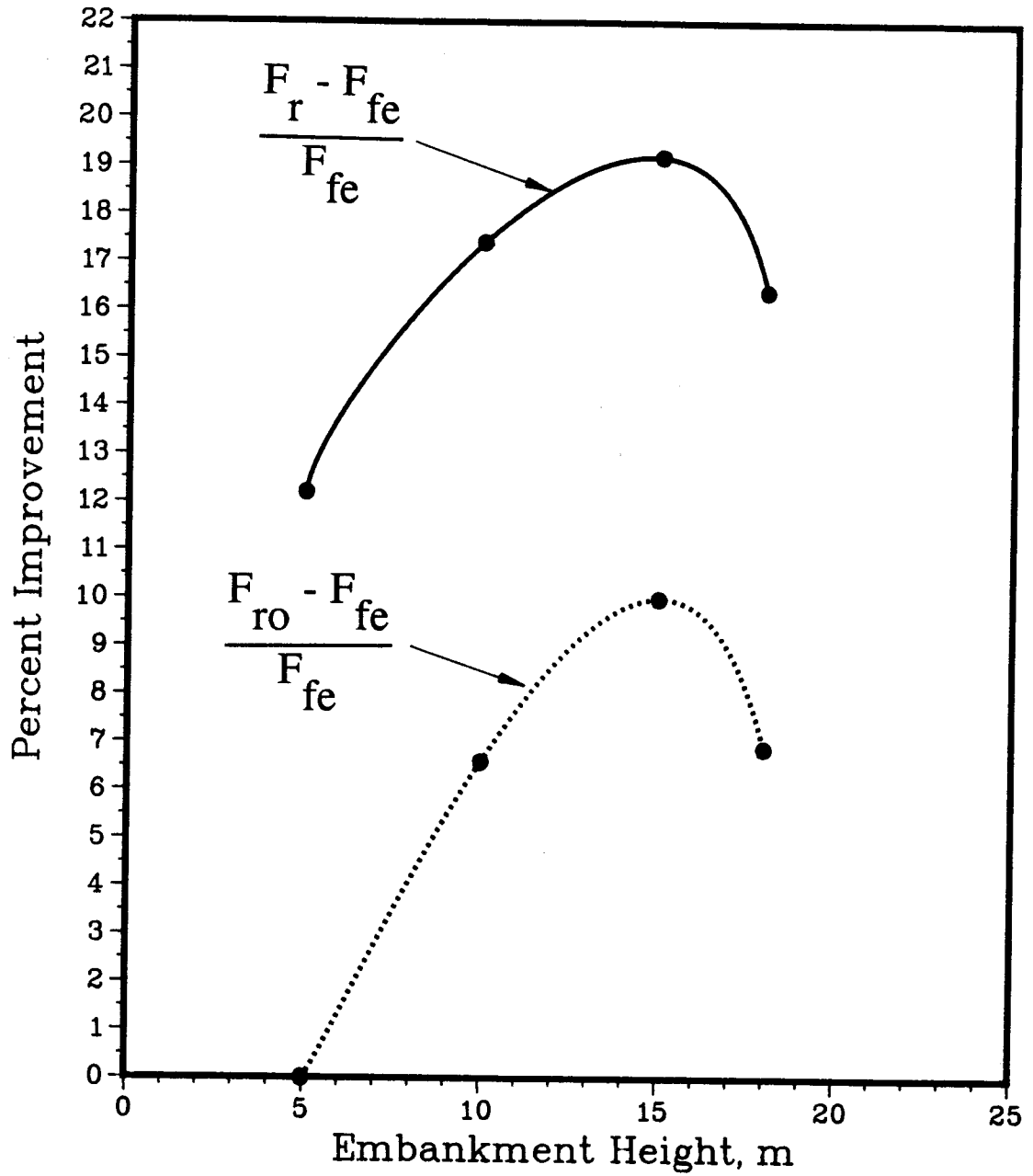


Figure 6.15 Relative Improvement in the Safety Factor due to a Modification of the Soil Stresses by the Reinforcement

6.15. It is clear that the increase from  $F_{fe}$  to  $F_{ro}$  resulting from the modification of the soil stresses constitutes a significant portion of the increase from  $F_{fe}$  to  $F_r$ . For an embankment height of 15 m, 9% of a total safety factor improvement of 18% was due to the reinforcement modifying the soil stresses by allowing the soil to maintain higher confining stresses within the soil mass.

The change in the stress state within the reinforced soil mass becomes an important issue with respect to BMM which neglects any interaction between the reinforcement and the soil. It is apparent that by neglecting this interaction, a significant factor influencing the stability of a reinforced soil mass is being omitted from the limit equilibrium calculations. It should be emphasized, however, that by disregarding the soil-reinforcement interaction, as it relates to the state of stress in the reinforced soil mass, BMM will yield conservative values for the factor of safety of a reinforced slope. The degree of conservatism will depend on reinforcement stiffness, the amount and spacing of the reinforcement within the slope, the stress-strain behaviour of the soil and whether the reinforced slope is near failure.

## **6.5 Partial Factors of Safety of the Soil and Reinforcement**

This section is intended only to present and discuss the partial factors of safety of the soil and reinforcement within the context of the present research. No

recommendations on the selection of partial safety factors or their use within an analysis will be given.

An alternate method of employing safety factors in the design of reinforced slopes is to apply partial factors of safety to each design parameter. Partial load factors can be applied to the soil weight, surcharge loads, seepage forces and other load effects. Partial resistance factors can be applied to the soil shear strength and reinforcement tensile force (Bonaparte et al. 1986). Unfortunately, while partial safety factors can be used to consider the uncertainty in some design parameters, its use in slope stability analyses is more complex than using an overall factor of safety and has not been verified through comparisons with case histories.

Bonaparte et al. (1986) provide recommendations for incorporating an overall factor of safety into reinforced soil design analyses. They suggest that no additional factor of safety should be applied to the reinforcement tensile design strength and for the evaluation of slope stability, the overall slope safety factor should be applied to the soil shear strength. The authors point out, however, that because the soil and the reinforcement exhibit markedly different stress-strain behaviour, the definition of an overall factor of safety may become meaningless. The reinforcement and the soil may possess different factors of safety at different stages during the construction of a

reinforced slope embankment.

From the finite element analyses, Table 6.2 lists the safety factors  $F_{rs}$  and  $F_{rr}$ , for the soil and reinforcement alone, respectively. Also included in Table 6.2 is the overall factor of safety of the reinforced slope,  $F_r$ . The variation of these safety factors with embankment height is illustrated in Figure 6.16.

Figure 6.16 clearly shows the dramatic difference between the soil and reinforcement safety factors,  $F_{rs}$  and  $F_{rr}$ . As discussed previously, the magnitude of the mobilized reinforcement loads is small at low embankment heights. Consequently, the reinforcement is mobilizing very little of its potential strength which results in a very high partial factor of safety,  $F_{rr}$ . As the embankment height increases, the reinforcement begins to mobilize a greater portion of its potential strength and the value of  $F_{rr}$  decreases significantly. At an embankment height of 18 m, the curve defining the variation in  $F_{rr}$  appears to become asymptotic to the curve defining the overall factor of safety,  $F_r$ . Whether  $F_{rr}$  remains above  $F_r$  or falls below  $F_r$  cannot be determined from the present analyses. Finite element analyses for embankment heights, both nonreinforced and reinforced, greater than 18 m would be required.

The variation in the soil safety factor,  $F_{rs}$ , serves to illustrate, again, the redistribution of soil stresses within the slope due to the presence of the reinforcement.

Table 6.2 Partial Factors of Safety for the Soil and Reinforcement

Embankment Height (m)	$M_O^*$	$M_{Tm}^*$	$M_{sm}^*$	$M_{ST}^*$	$M_{Rh}^*$	$F_{IS}$	$F_{IR}$	$F_I$
5	1170	20	1150	3251	402	2.83	19.7	3.12
10	7879	221	7658	14049	1384	1.83	6.27	1.96
15	22306	1115	21191	31957	2603	1.51	2.33	1.55
18	43163	3075	40088	53543	4855	1.34	1.58	1.35

\* Moments are given in units of kN m



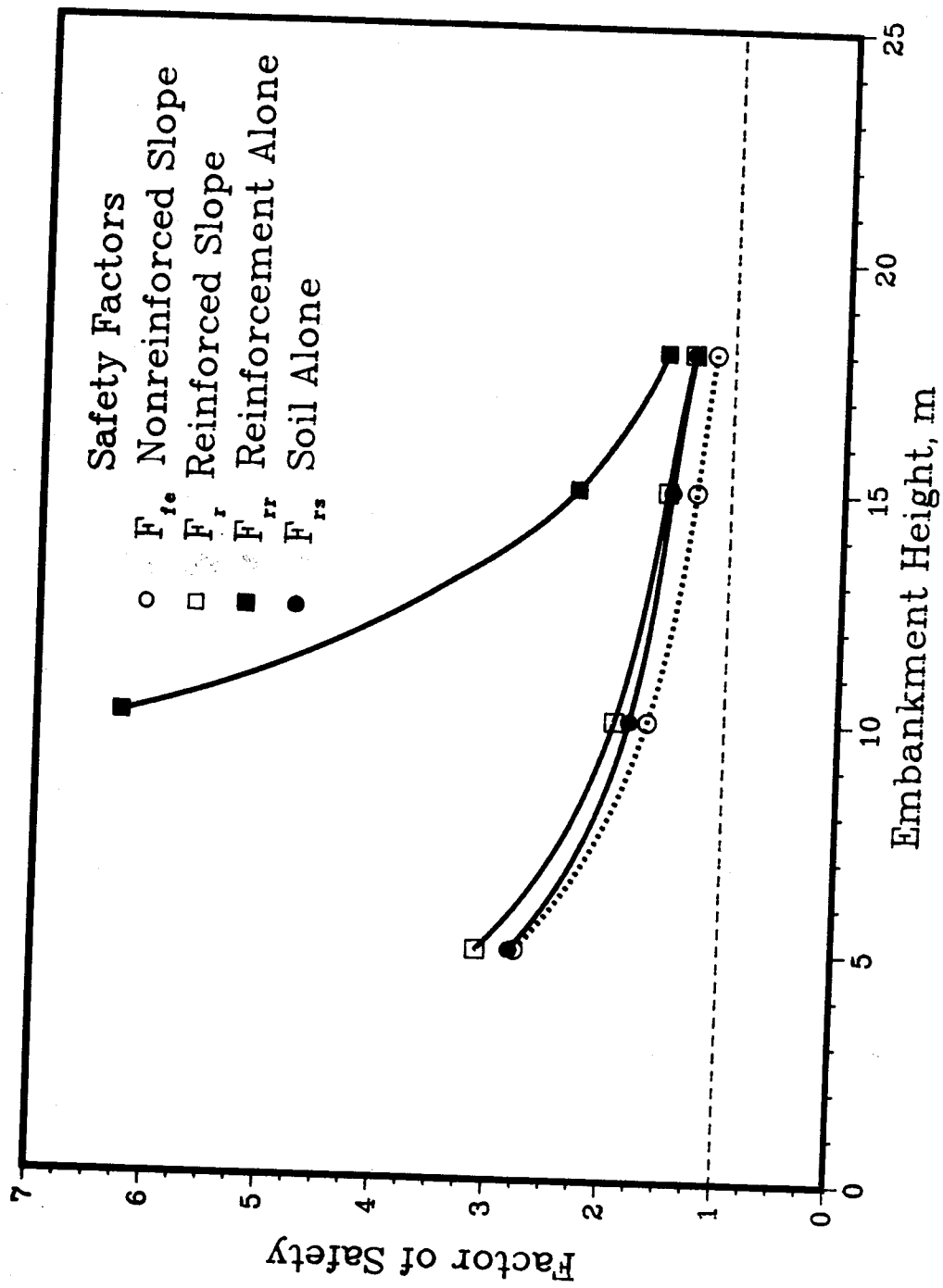


Figure 6.16 Variation in the Partial Factors of Safety for the Soil and Reinforcement

At a low embankment height,  $F_{rs}$  has a value very close to the overall factor of safety of the nonreinforced slope,  $F_{fe}$ . As the embankment height increases, however,  $F_{rs}$  remains larger than  $F_{fe}$  indicating that the stress field present within the soil mass of the nonreinforced slope is being changed by the reinforcement. The comparison between  $F_{fe}$  and  $F_{ro}$ , which is essentially the same as the comparison between  $F_{fe}$  and  $F_{rs}$ , showed the same relationship.

### 6.6 Verification of Circular Slip Surface Assumption

In the present study, BMM, which assumes circular slip surfaces, was used in examining the stability of a reinforced embankment. Confidence in using BMM for analyzing reinforced soil slopes can be enhanced if it can be shown that the shape of a potential slip surface passing through the reinforcing layers is indeed circular. At a condition of limiting equilibrium along any slip surface, it is reasonable to assume that the largest displacements in the embankment are occurring along this slip surface. If reinforcing layers are placed across this slip surface, the position of the maximum loads in the reinforcing layers will coincide with its intersection with the slip surface. Using these assumptions, the use of circular slip surfaces within BMM can be evaluated using the finite element analysis results which provide the load distributions in each layer of reinforcement. The reinforcement load distributions determined in the finite element analyses are given in

Appendix E. If a circular slip surface is valid, then the position of the maximum loads in the reinforcing layers should correspond with the location of the critical slip surfaces predicted by BMM.

Figures 6.17 to 6.20 illustrate the locations of the critical slip surfaces predicted by BMM and the maximum mobilized force in each reinforcing layer for embankment heights of 5 m, 10 m, 15 m and 18 m, respectively. For embankment heights of 5 m and 10 m, the circular failure surfaces do not agree well with the position of maximum reinforcement tension. The corresponding factor of safety,  $F_r$ , for these two embankment heights of 5 m and 10 m are 3.12 and 1.96, respectively. These high factors of safety indicate a very stable embankment slope. It has also been shown that at these embankment heights, the presence of the reinforcement is not significantly affecting the performance of the slope, hence the resulting poor agreement between the position of the maximum reinforcement loads and the circular slip surface.

Figure 6.19 reveals that at  $H = 15$  m, where  $F_r$  drops to 1.55 and the reinforcement begins to mobilize greater loads and play an increasing role in the stability of the slope, the correspondence between the position of the maximum reinforcement loads and the location of the critical slip surface predicted by BMM for a horizontal force orientation assumption improve. More important is the tendency for the

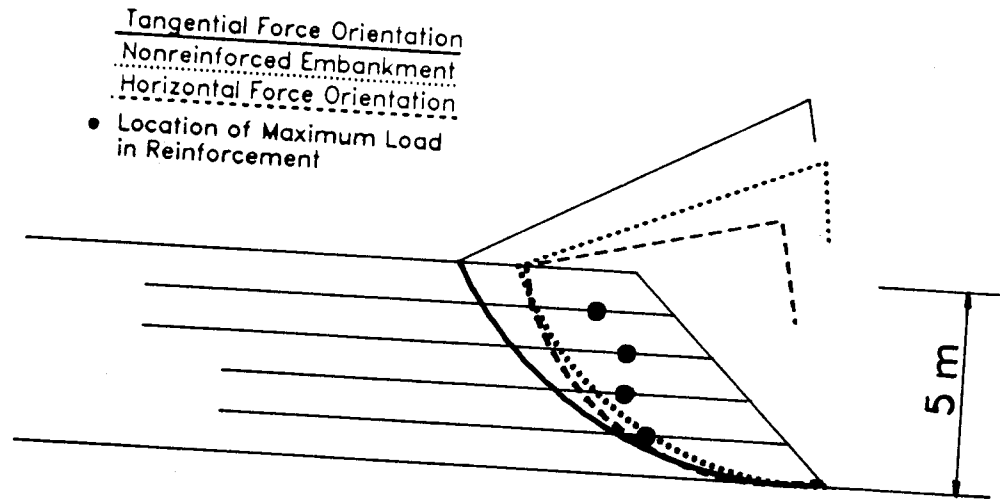


Figure 6.17 Comparison Between the Position of the Maximum Reinforcement Loads and Critical Slip Surfaces,  $H = 5$  m

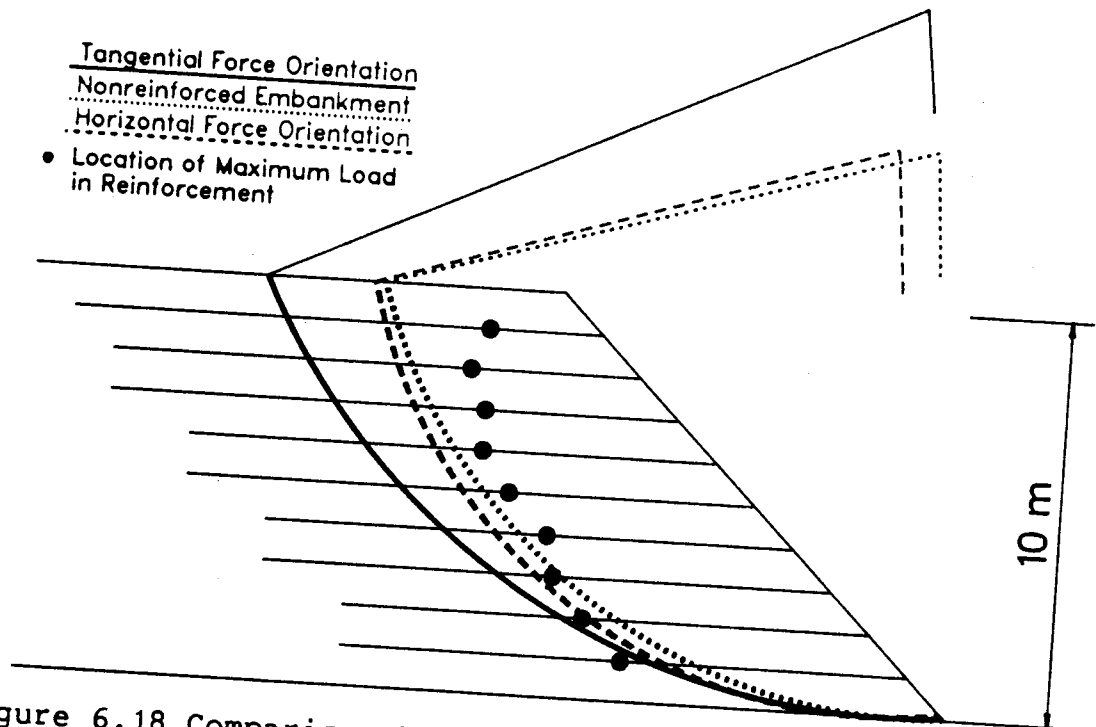
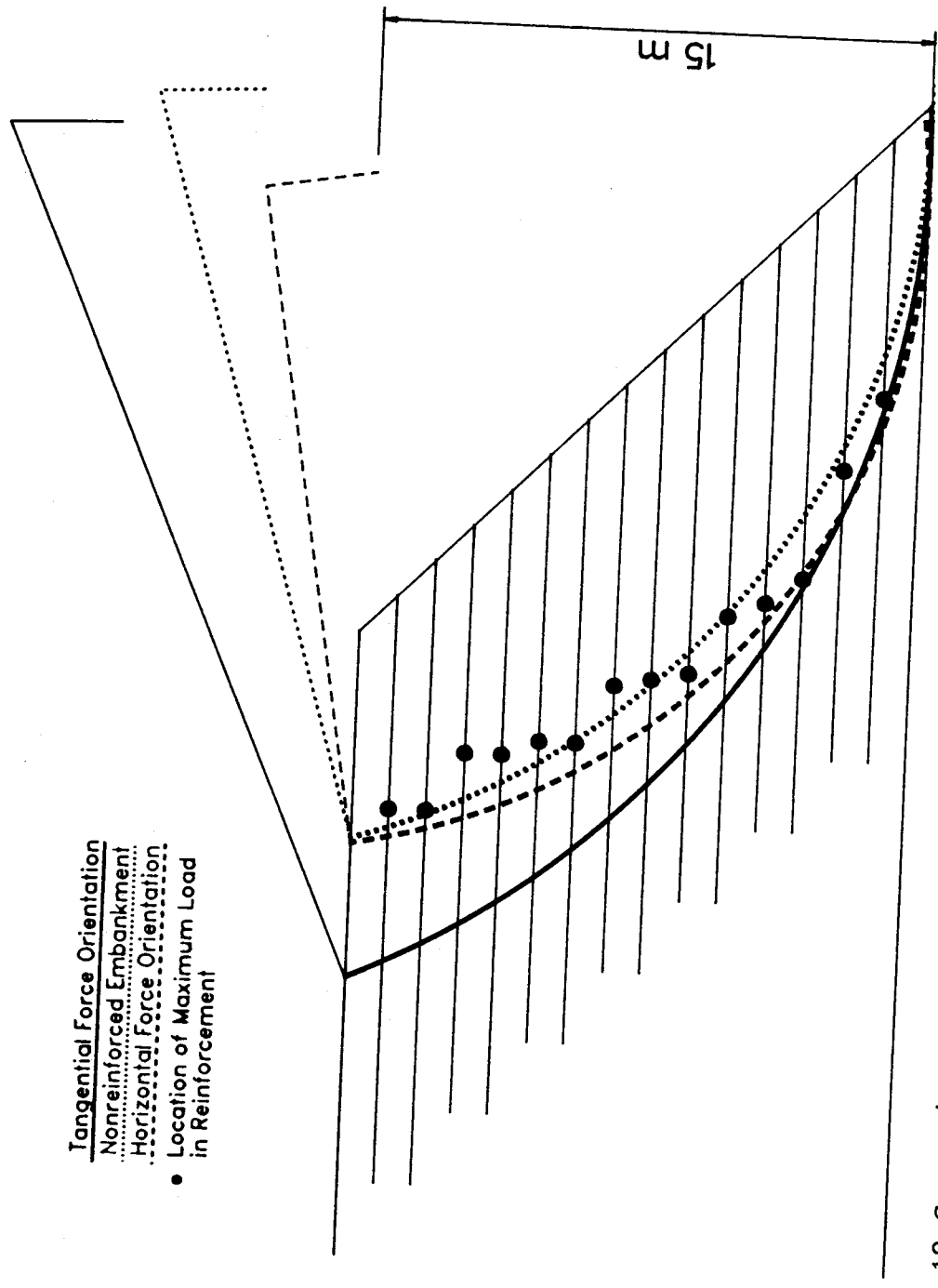


Figure 6.18 Comparison Between the Position of the Maximum Reinforcement Loads and Critical Slip Surfaces,  $H = 10$  m



- Tangential Force Orientation
- ..... Nonreinforced Embankment
- ..... Horizontal Force Orientation
- Location of Maximum Load in Reinforcement

Figure 6.19 Comparison Between the Position of the Maximum Reinforcement Loads and Critical Slip Surfaces,  $H = 15$  m

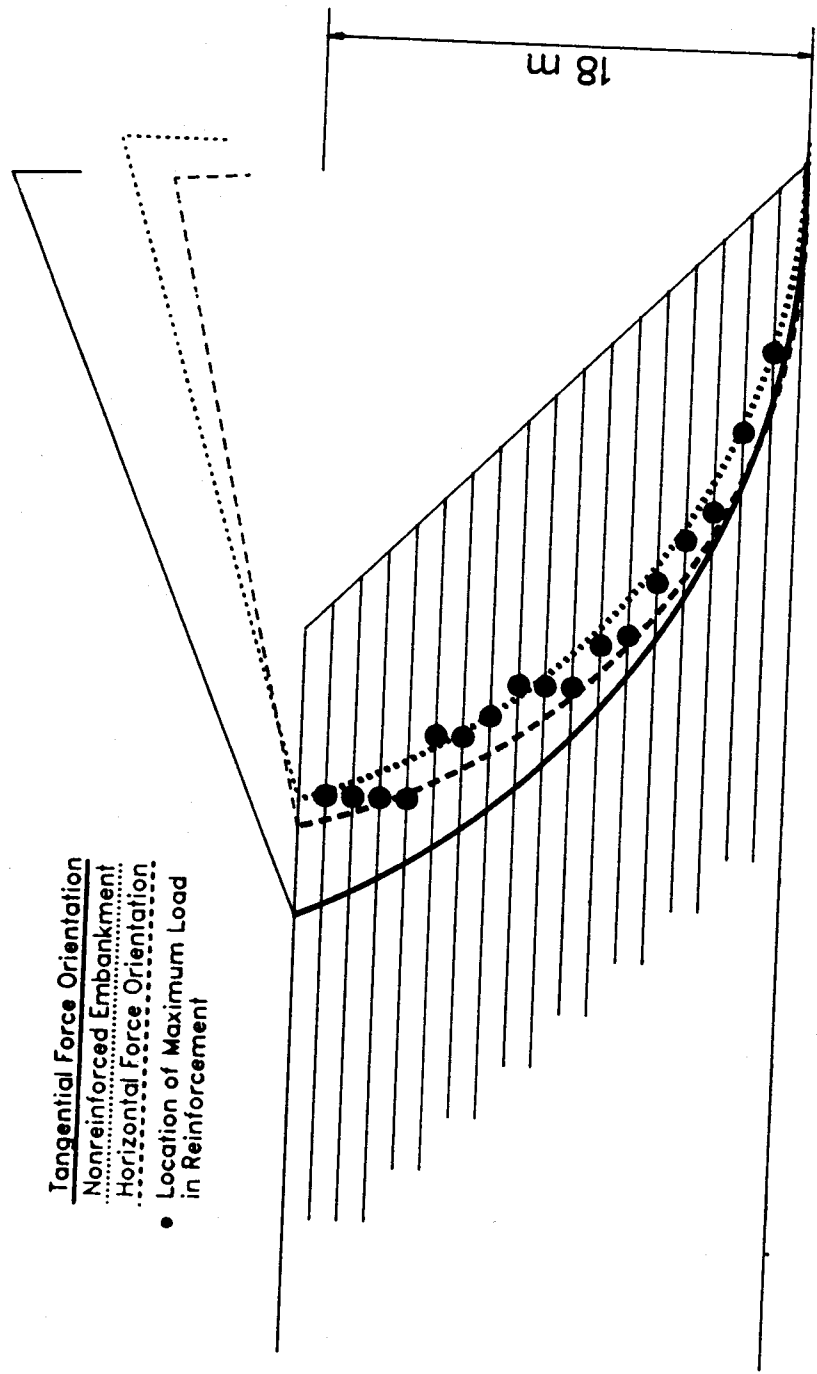


Figure 6.20 Comparison Between the Position of the Maximum Reinforcement Loads and Critical Slip Surfaces, H = 18 m

157  
points of maximum reinforcement load in forming a circular arc pattern which strongly indicates the presence of circular failure surfaces.

Figure 6.20 provides the strongest evidence that the potential slip surface within the reinforced slope is circular in shape. At  $H = 18$  m, the critical slip surface for a horizontal force assumption lies very close to the points of maximum load in each reinforcing layer. Although the exact shape of the failure surface at failure or  $F_r=1$  is not clear since the embankment was not taken to failure in the finite element analysis, these figures do provide supporting evidence for the use of circular shaped failure surfaces in the limit equilibrium analysis of a multilayer reinforced slope.

## 6.7 Summary and Conclusions

Using the results from the finite element analysis of the reinforced slope as a basis for comparison, the factors of safety of both the nonreinforced and reinforced slope, the partial factors of safety of the soil and the reinforcement and the shape and location of the slip surface have been discussed. Within the context of the reinforced slope analyzed in the present research, BMM has been found to provide reasonable yet conservative safety factors for a reinforced slope constructed on a rigid foundation. From the comparison between BMM and the finite element method (FEM), the following conclusions were made:

- 1) The factor of safety of a nonreinforced slope determined using BMM and the FEM showed close agreement with the FEM providing slightly higher safety factors.
- 2) The presence of the reinforcement exhibits very little influence on the behaviour of a reinforced embankment having a high overall factor of safety.
- 3) When sufficient deformations occur within the reinforced slope, the reinforcement significantly alters the state of stress within the soil mass resulting in an increase in the available shear strength of the soil. The increase in soil shear strength results in an increase in the overall factor of safety of the reinforced slope.
- 4) The points of maximum load in each reinforcing layer follow closely the shape of a circular slip surface. This provides evidence for the selection of circular slip surfaces in a limit equilibrium analysis rather than wedge type slip surfaces.
- 5) An examination of the partial factors of safety of the soil and reinforcement showed a substantial difference in their magnitude as the reinforced embankment was constructed. At low embankment heights, the reinforcement safety factor was very high and the soil safety factor was close to the safety factor of the nonreinforced slope. Near the maximum embankment height, the reinforcement safety



factor decreased significantly and converged on the safety factor of the soil which equalled the overall factor of safety of the reinforced embankment.

- 6) For a reinforced soil slope with uniformly spaced reinforcement, the conventional assumption of a constant load within each reinforcing layer for use in a limit equilibrium analysis will provide satisfactory values for the slope safety factor.

## 7. CONCLUSIONS AND RECOMMENDATIONS

### 7.1 General

The research documented in this thesis investigated the stability of a reinforced soil slope by comparing factors of safety computed from limit equilibrium and from finite element analyses. Partial factors of safety for soil and for reinforcement were discussed. The shape of possible slip surfaces within the reinforced soil slope were also examined. Comparisons between the nonreinforced slope and reinforced slope analyses were provided in order to examine the role played by the reinforcement in increasing the factor of safety of the slope. The finite element analysis of the nonreinforced and reinforced slope provided the opportunity to examine the stresses and strains within the slopes and evaluate the reinforcement's influence on the stress-deformational behaviour of the slope.

Only one specific reinforced slope geometry has been analyzed in the present research. No attempt has been made to generalize the results of the analyses to include other slope geometries or soil and reinforcement materials. The behaviour of a reinforced soil slope is very complex and factors such as foundation stiffness, embankment soil stiffness, reinforcement strength, reinforcement spacing and slope inclination will influence its behaviour. It is noted, then, that the following conclusions are only strictly valid for the reinforced slope case analyzed in this study. The

conclusions may be valid for other reinforced slope configurations but further analyses would be required to confirm the generality of the conclusions.

## **7.2 Conclusions**

### **7.2.1 Nonreinforced Slope Factors of Safety**

The factors of safety computed from the limit equilibrium and finite element analyses of the nonreinforced slope showed excellent agreement. The safety factor calculated using the results from the finite element analysis consistently gave slightly higher values than the limit equilibrium analysis safety factor. The good agreement between the factors of safety calculated using the two methods of analysis provides confidence that the limit equilibrium and the finite element methods are consistent in their assessment of the factor of safety of the nonreinforced slope.

### **7.2.2 Reinforced Slope Factors of Safety**

The factors of safety for the reinforced slope determined from the limit equilibrium and finite element method of analysis compare favourably with the finite element method consistently giving the larger safety factor of the two methods. The difference in the safety factors of the two methods, however, is greater than the difference found for the nonreinforced slope case. The reason for the

larger difference lies in the fact that the finite element analysis showed that due to the horizontal stiffness provided by the reinforcement, the soil maintained a higher confining stress. The higher confining stress increases the soil strength which consequently increases the factor of safety of the reinforced soil slope. The limit equilibrium method, Bishop's Modified Method (BMM), neglects this stress modification effect and only includes the reinforcement force as a free body force. As a result, BMM calculates lower factors of safety for the reinforced slope than the finite element method. By ignoring the change in the state of stress, BMM calculates a conservative factor of safety for the reinforced soil slope.

The factors of safety determined from BMM using two different load distribution cases within the reinforcement were found to be of approximately the same magnitude. The loads determined from the finite element analysis and the conventional assumption of a constant load in each reinforcing layer equal to the reinforcements' design strength resulted in factors of safety differing by only 3%. It is concluded, then, that for reinforced slopes with uniformly spaced reinforcement, the conventional constant load distribution will provide satisfactory values for the slope factor of safety.

The modification of the state of stress within the soil mass of the reinforced soil slope was found to be a major

component in increasing the factor of safety above that of the nonreinforced slope. The magnitude of the increase is a function of slope height since the effect of reinforcement is small at low embankment heights where small soil strains occur.

### **7.2.3 Shape of Slip Surfaces Within the Reinforced Slope**

It has been shown that the choice of circular slip surfaces as a failure mechanism within reinforced soil slopes is reasonable. The load distribution in each reinforcing layer show that the points of maximum load in each layer of reinforcement follow a circular arc pattern within the slope and correspond very closely with the shape and location of the critical slip surfaces predicted by BMM.

### **7.2.4 Partial Safety Factor of Soil and Reinforcement**

The finite element analysis results have afforded the opportunity to examine the factor of safety of the soil and reinforcement independent from the overall factor of safety of the slope. At low embankment heights, where relatively small reinforcement loads are mobilized, the reinforcement safety factor is very large. As the embankment height is increased, the reinforcement safety factor decreases dramatically, approaching the value of the overall slope factor of safety.

The partial factor of safety of the soil follows the same trend but does not exhibit a dramatic decrease in the

factor of safety. At low embankment heights the soil safety factor lies closer to the factor of safety of the nonreinforced slope than to the reinforced slope overall factor of safety. As the embankment height increases, the soil safety factor approaches the overall factor of safety for the reinforced slope which is due to the modification in the soil stresses resulting from the presence of the reinforcement within the slope.

#### 7.2.5 Load Distribution in Reinforcement

The finite element analysis of the reinforced slope revealed several interesting trends concerning the magnitude and distribution of loads within the reinforcement. The first important discovery was that the maximum reinforcement load did not occur in the lowest reinforcing layer. The maximum load was found to occur at  $0.4H$ , where  $H$  is the height of the slope. The value of  $0.4H$  is only strictly valid for the reinforced soil slope geometry studied for this research and will likely vary depending on the relative stiffness between the foundation and the embankment, spacing of the reinforcement, stress-strain behaviour of the embankment soil, slope inclination and the degree of soil-reinforcement interaction.

A unique relationship was found to exist between the position of a reinforcing layer within the slope and the load mobilized in the reinforcing layer. Figure 7.1 illustrates the relationship between  $h_i/H$  and  $T_i/T_{max}$ . A

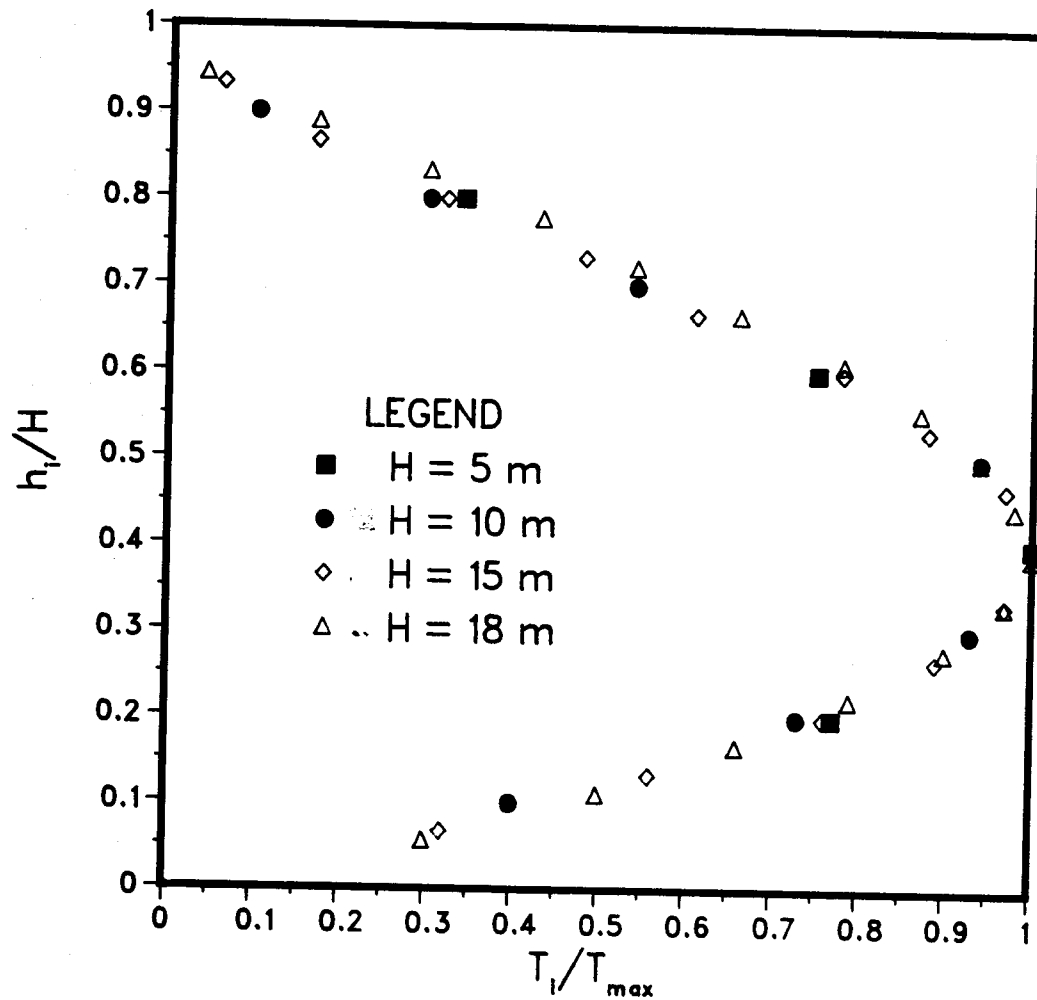


Figure 7.1 Relationship Between the Level of the Reinforcing Layer within the Embankment and the Mobilized Load in the Reinforcement

second relationship was found between the location and magnitude of the maximum load in each reinforcing layer and the position of the reinforcing layer within the slope. Figure 7.2 illustrates the form of the relationship between  $D_i/h_i$  and  $T_i/T_{max}$ .

#### 7.2.6 Stress-Deformation Behaviour

The major contribution provided by the reinforcement in improving the behaviour of a soil slope is the additional horizontal stiffness it provides within the soil mass allowing the soil to maintain a larger confining stress than the soil in the nonreinforced slope. Through increased confining stresses on the soil within the reinforced slope, the soil strength required to maintain equilibrium was reduced. The horizontal stiffness provided by the reinforcement led to significant reductions in horizontal strains and deformations and moderate reductions in vertical strains and deformations. The principal tensile strains within the reinforced slope were reduced substantially but no reorientation of the principal tensile strain axes resulted due to the presence of the reinforcement. The reinforcement, by providing additional stiffness at the face of the slope, eliminated the presence of tensile stresses within the soil at the face of the slope.



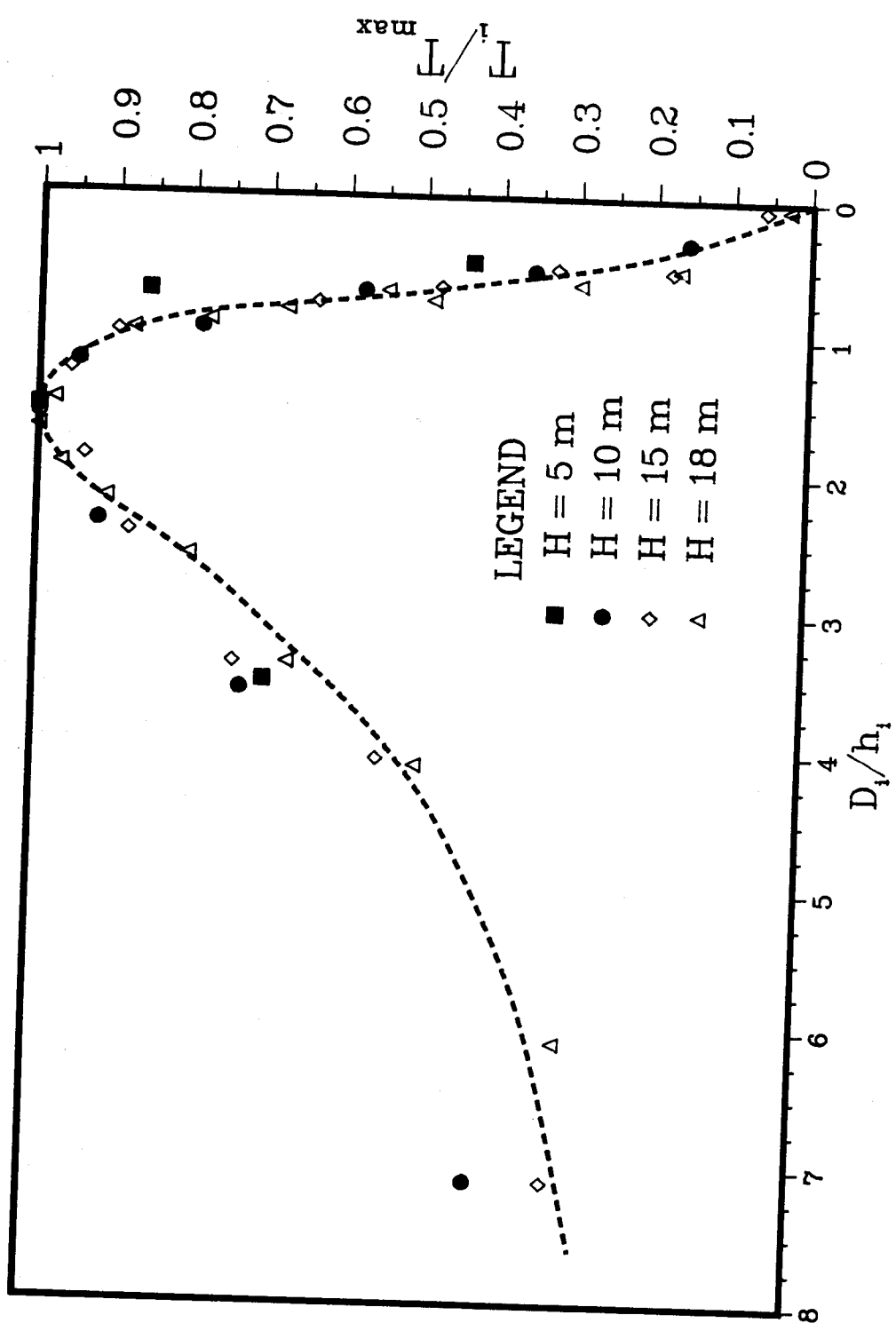


Figure 7.2 Relationship Between the Maximum Load and its Location Relative to the Face of the Embankment for any Reinforcing Layer

### 7.3 Recommendations for Future Research

During the progress of the present research, it became very clear that the factors influencing the behaviour of a reinforced soil slope are numerous and complex; the reinforcement spacing, the extensibility of the reinforcement, the relative stiffness between the foundation and the embankment soil, the slope inclination, the soil-reinforcement interfacial characteristics and the pullout resistance of the reinforcement being some of the major factors. As well, the present research was concerned only with the total stress, short term stability of a reinforced slope and as such, the effect of pore pressures (i.e. effective stresses) on the behaviour of a reinforced soil slope was not considered. Given the aforementioned factors and the conclusions reached from this research, the following are recommendations for future research on the behaviour of reinforced soil slopes:

1. Further analytical studies should be done employing relatively weak soils. The greatest advantage in using geosynthetics as reinforcement within slopes will be achieved when it can be shown that very economic and effective reinforced soil slopes can be constructed using reinforcement in conjunction with weak soils.
2. The modes of failure possible within a reinforced soil slope should be examined. An elasto-plastic finite element analysis of a reinforced soil slope

analyzed in this research. These safety factors should then be compared to the finite element results to ascertain whether a better correspondence between the factors of safety is obtained.

## REFERENCES

- Al-Hussaini, M.M. and Johnson, L.D. 1978. Numerical Analysis of a Reinforced Earth Wall. Proc. Symposium on Earth Reinforcement, ASCE, Pittsburgh, Penn., pp. 98-126.
- Al-Yassin, Z. 1979. Analysis and Design of Reinforced Earth Walls. Ph.D. thesis, University of California, Davis, 173 p.
- Al-Yassin, Z. and Hermann, L.R. 1979. Finite Element Analysis of Reinforced Earth Walls. Int. Conf. on Soil Reinforcement: Reinforced Earth and other Techniques, Vol. 1, Paris, pp. 3-9.
- Andrawes, K.Z., McGown, A., Mashhour, M.M. and Wilson-Fahmy, R.F. 1980. Tension Resistant Inclusions in Soils. ASCE JGED, GT12, Vol. 106, pp. 1313-1326.
- Andrawes, K.Z., McGown, A., and Murray, R.T. 1986. The Load-Strain-Time-Temperature Behaviour of Geotextiles and Geogrids. Proc. 3rd Int. Conf. on Geotextiles, Vienna, Austria, pp. 707-712.
- Andrawes, K.Z., McGown, A., Wilson-Fahmy, R.F. and Mashhour, M.M. 1982. The Finite Element Method of Analysis Applied to Soil-Geotextile Systems. Proc. 2nd Int. Conf. on Geotextiles, Vol. 2, Las Vegas, pp. 695-700.
- Bathe, K.J. 1982. Finite Element Procedures in Engineering Analysis. Prentice Hall, New Jersey, 735 p.
- Beech, J.F. 1987. Importance of Stress-Strain Relationships in Reinforced Soil System Design. Geosynthetics Conference '87, Vol. 1, New Orleans, pp. 133-144.
- Bishop, A.W. 1955. The Use of the Slip Circle in the Stability Analysis of Slopes. Géotechnique, Vol. 5, No. 1, pp. 7-17.
- Bobey, L. 1988. Soil-Geogrid Interfacial Shear Strength. M.Sc. thesis, University of Alberta, 195 p.
- Bonaparte, R., Holtz, R.D. and Giroud, J.P. 1986. Soil Reinforcement Design Using Geotextiles and Geogrids. Proc. Symp. on Geotextile Testing and the Design Engineer, ASTM STP 952, Los Angeles, California, pp. 69-116.

- Boutrup, E. and Holtz, R.D. 1983. Analysis of Embankments on Soft Ground Reinforced with Geotextiles. VIII European Conf. Soil Mech. and Found. Eng., Helsinki, Finland, pp. 469-472.
- Brown, B.S. and Poulos, H.G. 1984. Analysis of Full Scale Experimental Reinforced Embankments. Proc. 4th Australia-New Zealand Conf. on Geomechanics, Vol. 1, Perth, Australia, pp. 183-187.
- Chan, D. 1986. Finite Element Analysis of Strain Softening Material. Ph.D. thesis, University of Alberta, 345 p.
- Chang, J.C. and Forsyth, R.A. 1977a. Finite Element Analysis of Reinforced Earth Wall. ASCE JGED, GT7, Vol. 103, pp. 711-724.
- Chang, J.C., Hannon, J.B. and Forsyth, R.A. 1977b. Pull Resistance and Interaction of Earthwork Reinforcement and Soil. Transportation Research Record, No. 640, pp. 1-7.
- Chen, R.H. and Chameau, J.-L. 1982. Three Dimensional Limit Equilibrium Analysis of Slopes. Géotechnique, Vol. 32, No. 1, pp. 31-40.
- Chowdhury, R.N. 1978. Slope Analysis. Developments in Geotechnical Engineering, Vol. 22, Elsevier, Amsterdam, 423 p.
- Cook, R.D. 1981. Concepts and Applications of Finite Element Analysis. John Wiley & Sons, New York, 537 p.
- Desai, C.S., Zaman, M.M., Lightner, J.G. and Siriwardene, H.J. 1984. Thin-Layer Element for Interfaces and Joints. Int. J. Num. Analy. Methods in Geomechanics, Vol. 8, pp. 19-43.
- Duncan, J.M. and Chang, C.Y. 1970. Nonlinear Analysis of Stress and Strain in Soils. ASCE JSMPD, SM5, Vol. 96, pp. 1629-1653.
- Duncan, J.M., Byrne, P., Wong, K.S. and Mabry, P. 1980. Strength, Stress-Strain and Bulk Modulus Parameters for Finite Element Analysis of Stresses and Movements in Soil Masses. Report No. UCB/GT/80-01, University of California, Berkeley.
- Duncan, J.M., Low, B.K. and Schaefer, V.R. 1985. STABGM: A Computer Program for Slope Stability Analysis of Reinforced Embankments and Slopes. Virginia Polytechnic Institute and State University, Blacksburg, 28 p.

- Duncan, J.M. and Wright, S.G. 1980. The Accuracy of Limit Equilibrium Methods of Slope Stability Analysis. Engineering Geology, Vol. 16, pp. 5-17.
- Fowler, J. 1982. Theoretical Design Considerations for Fabric-Reinforced Embankments. Proc. 2nd Int. Conf. on Geotextiles, Vol. 2, Las Vegas, pp 665-670.
- Fredlund, D.G. and Krahn, J. 1976. Comparison of Slope Stability Methods of Analysis. Canadian Geotechnical Journal, Vol. 14, pp. 429-439.
- Ghaboussi, J., Wilson, E.L. and Isenberg, J. 1973. Finite Element for Rock Joints and Interfaces. ASCE JSMFD, SM10, Vol. 99, pp. 833-848.
- Goodman, R.E. 1977. Analysis in Jointed Rocks, in Finite Elements in Geomechanics, G. Gudehus (ed.), John Wiley & Sons, New York, 573 p.
- Heuze, F.E. and Barbour, T.G. 1982. New Models for Rock Joints and Interfaces. ASCE JGED, GT5, Vol. 108, pp. 757-776.
- Hofmann, B.A. 1988. Personal Communication of M.Sc. Thesis in Progress.
- Ingold, T.S. 1980. Reinforced Clay. Ph.D. thesis, University of Surrey, 252 p.
- Ingold, T.S. 1982. An Analytical Study of Geotextile Reinforced Embankments. Proc. 2nd Int. Conf. on Geotextiles, Vol. 2, Las Vegas, pp. 683-688.
- Ingold, T.S. and Miller, K.S. 1986. Short, Intermediate and Long Term Stability of Geotextile Reinforced Embankments over Soft Clays. Proceedng, 3rd Int. Conf. on Geotextiles, Vienna, Austria, Vol. 3. pp. 337-342.
- Janbu, N. 1963. Soil Compressibility as Determined by Oedometer and Triaxial Tests. European Conf. Soil Mech. Foun. Eng., Wissbaden, Germany, Vol. 1, pp. 19-25.
- Jewell, R.A. 1982. A Limit Equilibrium Design Method for Reinforced Embankments on Soft Foundations. Proc. 2nd Int. Conf. on Geotextiles, Las Vegas, pp. 671-676.
- Jewell, R.A. 1985. Material Properties for the Design of Geotextile Reinforced Slopes. Geotextiles and Geomembranes, Vol. 2, No. 2, pp. 83-109.

- Jewell, R.A. 1980. **Some Effects of Reinforcement on the Mechanical Behaviour of Soils**. Ph.D. thesis, Cambridge University, Cambridge, 117 p.
- Jewell, R.A., Milligan, G.W.E., Sarsby, R.W. and DuBois, D. 1984. **Interaction Between Soil and Geogrids**. Symposium on Polymer Grid Reinforcement in Civil Engineering, London, Paper #1.3, 13 p.
- Jones, C.J.F.P. 1984. **Earth Reinforcement and Soil Structures**. Butterworths, London, 183 p.
- Katona, M.G. 1983. **A Simple Contact-Friction Interface Element with Applications to Buried Culverts**. Int. J. Num. Anal. Methods in Geomechanics, Vol. 7, pp. 371-384.
- Koerner, R.M. and Hausmann, M.R. 1987. **Strength Requirements of Geosynthetics for Soil Reinforcement**. Geotechnical Fabrics Report, Vol. 5, No. 1, pp. 18-26.
- Kulhawy, F.H. 1977. **Embankments and Excavations**, in **Numerical Methods in Geotechnical Engineering**. Desai, C.S. and Christian, J.T. (ed.), McGraw-Hill Inc., 783 p.
- Leshchinsky, D. and Volk, J.C. 1986. **Stability of Geotextile Retained Earth Railroad Embankments**. Geotextiles and Geomembranes, Vol. 3, No. 2 and 3, pp. 105-128.
- Lightner, J.G., III 1981. **A Mixed Finite Element Procedure for Soil-Structure Interaction Including Construction Sequences**. Ph.D. thesis, Virginia Polytechnic Institute and State University, 235 p.
- Low, B.K. and Duncan, J.M. 1985. **Analysis of the Behaviour of Reinforced Embankments on Weak Foundations**. Report No. VPI/CE-GT-85-11, Virginia Polytechnic Institute, Blacksburg, VA, 274 p.
- McGown, A. and Andrawes, K.Z. 1977. **The Influence of NonWoven Fabric Inclusions on the Stress Strain Behaviour of a Soil Mass**. Int. Conf. Use of Fabrics in Geotechnics, Vol. 1, pp. 161-166.
- McGown, A. and Andrawes, K.Z. and Al-Hasani, M.M. 1978. **Effect of Inclusion Properties on the Behaviour of Sand**. Géotechnique, Vol. 28, No. 3, pp. 327-346.
- McGown, A., Andrawes, K.Z., Mashhour, M.M. and Myles, B. 1981. **Strain Behaviour of Soil-Fabric Model Embankments**. Proc. 10th ICSMFE, Stockholm, pp.739-744.

- Mitchell, J.K. 1987. Reinforcement for Earthwork Construction and Ground Stabilization. VIII CPMSIF-PCSMFE, Cartagena, Columbia, pp. 349-380.
- Mowafy, Y.M.M. 1986. Analysis of Grid Reinforced Earth Structures. Ph.D. thesis, Carleton University, Ottawa, 384 p.
- Murray, R.T. 1982. Fabric Reinforcement of Embankments and Cuttings. Proc. 2nd Int. Conf. on Geotextiles, Vol. 3, Las Vegas, pp. 707-713.
- Richards, E.A. and Scott, J.D. 1985. Soil Geotextile Friction Properties. 2nd Canadian Symp. on Geotextiles and Geomembranes, Edmonton, pp. 13-24.
- Rowe, R.K. 1984. Reinforced Embankments: Analysis and Design. ASCE JGED, Vol. 110, No. 2, pp. 231-246.
- Rowe, R.K., MacLean, M.D. and Soderman, K.L. 1983. Analysis of a Geotextile Reinforced Embankment on Peat. Canadian Geotechnical Journal, Vol. 21, pp. 563-576.
- Rowe, R.K. and Soderman, K.L. 1985. An Approximate Method for Estimating the Stability of Geotextile Reinforced Embankments. Canadian Geotechnical Journal, Vol. 22, pp. 392-398.
- Rowe, R.K. and Soderman, K.L. 1985. Geotextile Reinforcement of Embankments on Peat. Geotextiles and Geomembranes, Vol. 2, pp.277-298.
- Schmertmann, G.R., Chouery-Curtis, V.E., Johnson, R.D. and Bonaparte, R. 1987. Design Charts for Geogrid Reinforced Soil Slopes. Geosynthetics Conference '87, New Orleans, pp. 108-120.
- Schneider, H.R. and Holtz, R.D. 1986. Design of Slopes with Geotextiles and Geogrid. Geotextiles and Geomembranes, Vol. 3, pp. 29-51.
- Scott, J.D., Segó, D.C., Richards, E.A, Hofmann, B.A. and Burch, E.R. 1987. Design of Devon Geogrid Test Fill. Geosynthetics Conference '87, New Orleans, Vol. 1, pp. 157-168.
- SCRC (Study Centre for Road Construction) 1979. Stability of Slopes Constructed with Polyester Reinforcing Fabric. Report of Investigation at Almere in 1979, The Netherlands, 24 p.



210

**Symposium on Polymer Grid Reinforcement in Civil  
Engineering. March 22-23, 1984, London, England.**

Vidal, H. 1969. The Principle of Reinforced Earth. Highway  
Research Record No. 282, pp. 1-16.

Wright, S.G., Kulhawy, F.H. and Duncan, J.M. 1973. Accuracy  
of Limit Equilibrium Slope Stability Analyses. ASCE  
JSMFD, SM10, Vol. 99, pp. 783-791.

Zeevaert, A.E. 1980. **Finite Element Formulation for the  
Analysis of Interfaces, Nonlinear and Large  
Displacement Problems in Geotechnical Engineering.**  
Ph.D. thesis, Georgia Institute of Technology,  
Georgia, 265 p.

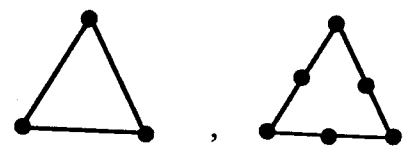
Zienkiewicz, O.C., Valliappan, S. and King, I.P. 1968.  
Stress Analysis of Rock as a "No Tension" Material.  
Géotechnique, Vol. 18, pp. 56-66.

## APPENDIX A: General Description of SAFE

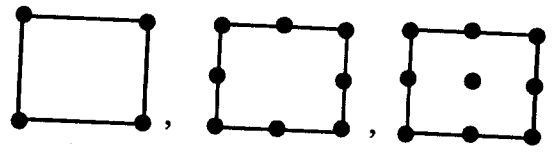
SAFE (Soil Analysis by Finite Elements) is a general purpose finite element program developed at the University of Alberta (Chan, 1986). The initial development of the program focused on analyzing the post peak deformation of strain softening soil but the program is capable of performing two and three dimensional plane stress and plane strain analyses as well as axisymmetric analyses. An analysis can be performed using a total or effective stress formulation for fully undrained or drained conditions. For the present study, the modifications to SAFE included the implementation of a two dimensional bar element specifically suited to modelling the behaviour of geosynthetic reinforcing materials and the implementation of an interface element for modelling the soil-reinforcement interaction. The program SAFE was selected for this study for two reasons; 1) the program was intentionally written in a manner which facilitates the simple implementation of additional elements and constitutive models and 2) the developer of the program is an assistant professor at the University of Alberta which allowed for expeditious answers to questions about SAFE. The following section briefly outlines the capabilities of SAFE.

SAFE was developed using a small strain, small deformation displacement formulation. The element types available in the program are illustrated in Figure A.1. Linear elastic, hyperbolic elastic and several plasticity

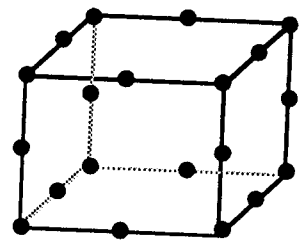
Triangular Elements :



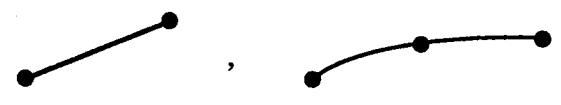
Rectangular Elements :



3 Dimensional Brick Elements :



Reinforcement Elements:



Interface Elements :



Figure A.1 Types of Elements Available in SAFE

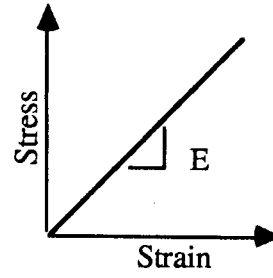
models including strain softening models, are available within SAFE. The linear elastic and hyperbolic elastic models are utilized in the present investigation on reinforced soils. Figure A.2 illustrates some the available soil models. Some standard features implemented within SAFE include;

- 1) Prescribed concentrated point force or distributed pressure boundary conditions.
- 2) Prescribed displacement boundary conditions.
- 3) Changing material properties at any stage of the analysis.
- 4) Choice of 2x2 or 3x3 integration schemes as well as independent 1,2 or 3 point integration schemes for reinforcing elements
- 5) Element birth and death option

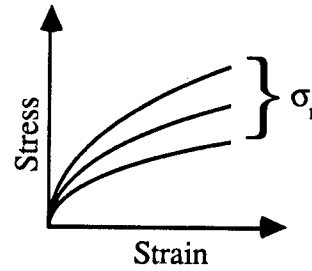
In order to ensure an efficient and effective nonlinear analysis procedure, several analysis techniques have been incorporated into SAFE. These include;

- 1) Program restart capability at any stage in the analysis. By storing the converged results at the end of every iteration and/or load step, the stress and strain state is available for restarting the analysis.
- 2) A Newton-Rhapson or Modified Newton-Rhapson iterative scheme for the solution of nonlinear finite element equations. Figures A.3 graphically illustrates the iteration process. A detailed

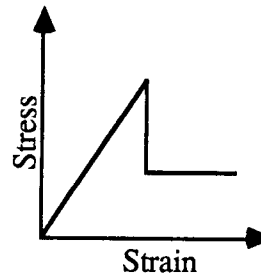
Elastic



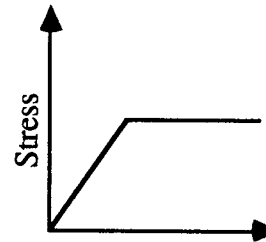
Hyperbolic Elastic



Elastic - Brittle Plastic:



Elastic - Perfectly Plastic



Elastic - Hyperbolic Softening

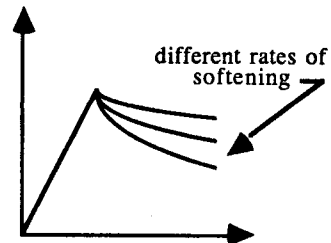


Figure A.2 Material Models Available in SAFE

explanation of these two iterative schemes can be found in Bathe (1982).

- 3) Load increment subdivision provision which allows the total applied load in any time step to be subdivided into smaller load steps which are applied incrementally until the total load is applied. This option is invaluable for problems exhibiting a high degree of nonlinearity or where "failure" is imminent.
- 4) Three methods have been provided for the calculation of stress within the elements.
  - i) Euler forward integration scheme
  - ii) Improved Euler scheme
  - iii) Runge-Kutta scheme

A complete description of these methods, as implemented in SAFE, can be found in Chan (1986).

To aid in the synthesis of the finite element results, several post-processing programs have been developed. These programs include;

- 1) Finite element mesh and deformed mesh plotting
- 2) Stress and strain contour plotting
- 3) Displacement arrow plotting
- 4) Reinforcement load distribution plotting
- 5) Interface shear stress and normal stress plotting

The preceding brief description of the finite element program SAFE was intended only to elucidate the programs' capabilities. Chan (1986) presents the details of the

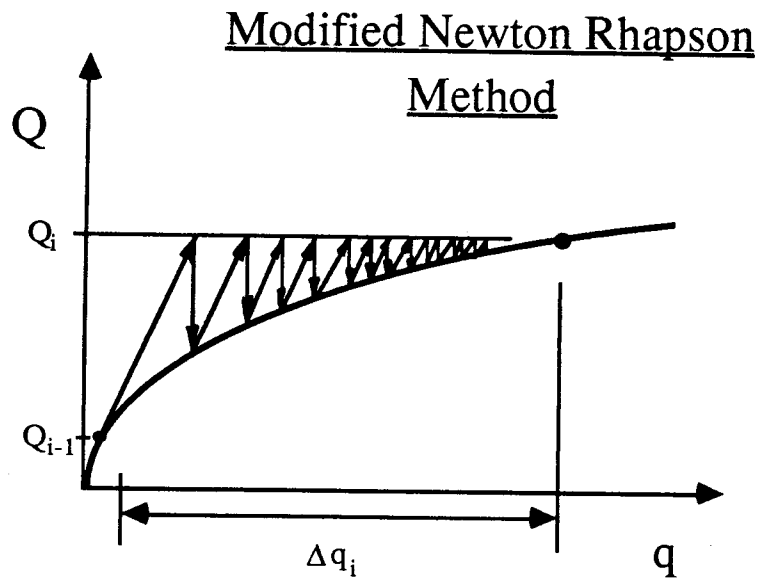
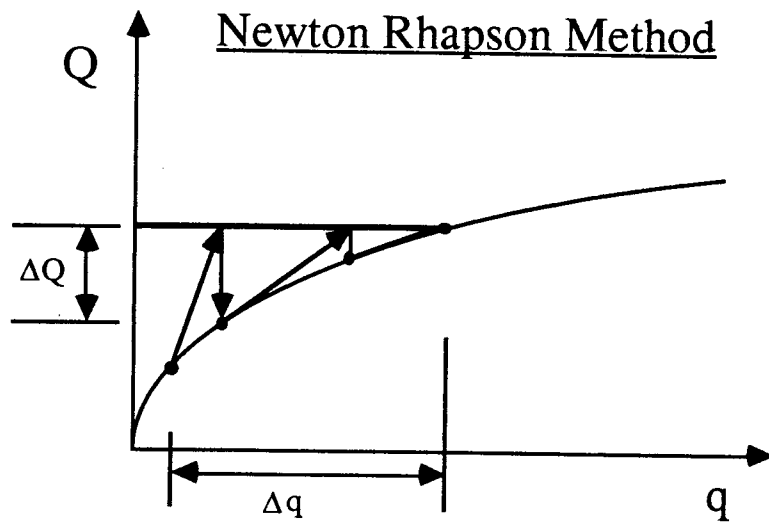


Figure A.3 Solution Schemes used in SAFE

program development and explains the solution strategies and analysis techniques incorporated within SAFE.



## APPENDIX B: Finite Element Formulation for an Interface Element

### B.1 Introduction

A two dimensional interface element has been implemented in SAFE in order to model the soil-reinforcement interaction. The importance of including the behaviour of the soil-reinforcement interface in the analysis of reinforced soil structures has been recognized by many researchers including Richards and Scott (1985), Bonaparte et al. (1986) and Jewell et al. (1984). The behaviour of the interface will likely control the amount and rate of load transfer from the soil to the reinforcement and influence the stability of a reinforced soil structure.

The interface element is a variable node (4 or 6) isoparametric element formulated using a displacement formulation assuming small strains and small deformations. The relative displacements between adjacent nodes represent the elements independent degrees of freedom. The formulation of this element follows previous work on interface elements performed by Heuze and Barbour (1982), Katona (1983) and Ghaboussi et al. (1973). The following sections present the details of the element formulation and the constitutive models used to represent the soil-reinforcement interaction.

## B.2 Interface Element Formulation

The interface element developed for this study was formulated using a conventional displacement formulation. The configuration of the interface element is shown in Figure B.1. Figure B.2 illustrates the element's role in the finite element analysis of reinforced soil.

The stiffness matrix developed using a displacement formulation employing the principle of virtual displacements (Bathe, 1982) has the form:

$$[K] = \int_V [B]^T [C] [B] dV \quad [B.1]$$

Assuming plane strain conditions and a constant interface thickness,  $t$ , the volume integral of Equation B.1 can be reduced to an integration along the length of the interface element. The constitutive relationship for the interface element is derived using shear stress-displacement test results from a direct shear test. The generality of the constitutive relationship is lost, however, when displacement is utilized as a model parameter. Scale effects, such as test apparatus dimensions, will influence the shape and form of the shear stress displacement results. In order to achieve the generality required in the constitutive relationship, a dimensionless parameter is formed by dividing the displacement by the interface thickness,  $t$ . But since the interface thickness is assumed to be constant,  $1/t$  can be extracted from the constitutive

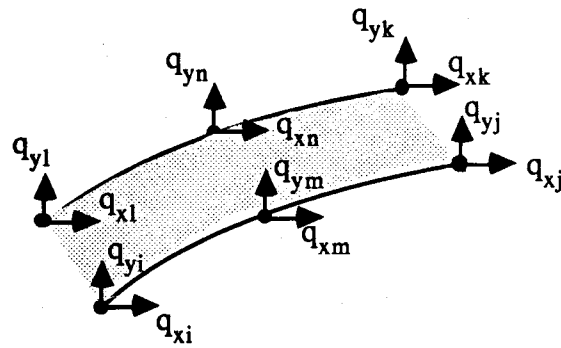


Figure B.1 Interface Element Degrees of Freedom

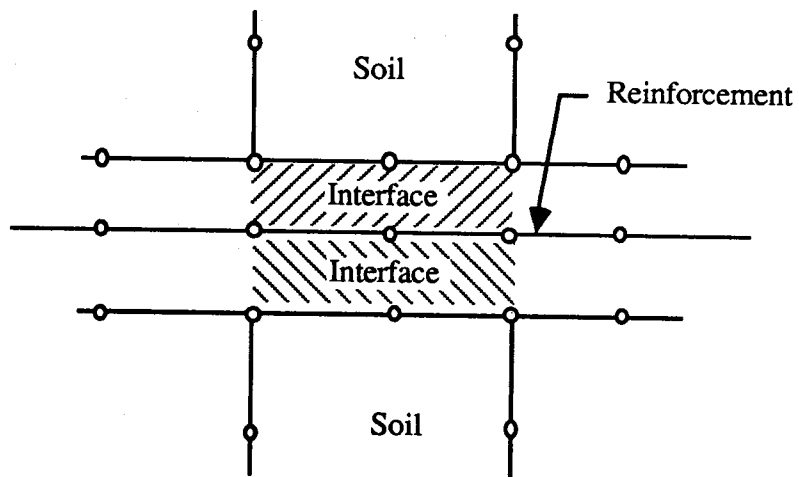


Figure B.2 Role of Interface Element in Finite Element Mesh Assemblage

equations. The stiffness matrix equation will then become:

$$[K] = \int_1^l [B]^T [C] [B] dl \quad [B.2]$$

$$\text{where } [C] = \begin{bmatrix} k_s & 0 \\ 0 & k_n \end{bmatrix}$$

$k_s$  = shear stiffness

$k_n$  = normal stiffness

The shear stiffness is defined as the slope of a shear stress displacement curve. The normal stiffness is arbitrarily selected in order to prevent the interpenetration of adjacent nodes.

The interface contact surface is described by a set of midplane nodes;  $i, j$  and  $k$ , located between adjacent nodal pairs. The independent degrees of freedom for the interface element are defined as the relative displacements at each midplane node. The relative displacements,  $\Delta u_r$  and  $\Delta v_r$ , at each midplane node are obtained from the difference in displacements at each adjacent nodal pair. The relative displacements at any point along the element are obtained by interpolating  $\Delta u_r$  and  $\Delta v_r$ .

The relative displacements anywhere along the element are expressed as:

$$\begin{Bmatrix} \Delta u_r \\ \Delta v_r \end{Bmatrix} = \begin{bmatrix} N_1 & 0 & N_2 & 0 & N_3 & 0 \\ 0 & N_1 & 0 & N_2 & 0 & N_3 \end{bmatrix} \begin{Bmatrix} \Delta u_{r_i} \\ \Delta v_{r_i} \\ \Delta u_{r_j} \\ \Delta v_{r_j} \\ \Delta u_{r_k} \\ \Delta v_{r_k} \end{Bmatrix} \quad [\text{B.3}]$$

The same interpolation function is used to define the geometry of the interface element:

$$\begin{Bmatrix} x \\ y \end{Bmatrix} = \begin{bmatrix} N_1 & 0 & N_2 & 0 & N_3 & 0 \\ 0 & N_1 & 0 & N_2 & 0 & N_3 \end{bmatrix} \begin{Bmatrix} x_i \\ y_i \\ x_j \\ y_j \\ x_k \\ y_k \end{Bmatrix} \quad [\text{B.4}]$$

The relative displacements at each midplane node are related to the adjacent nodal displacements. Using the upper surface as a datum, the relative displacements are defined as:

$$\begin{aligned} \Delta u_{r_i} &= u_4 - u_1 & \Delta u_{r_j} &= u_3 - u_2 & \Delta u_{r_k} &= u_6 - u_5 \\ \Delta v_{r_i} &= v_4 - v_1 & \Delta v_{r_j} &= v_3 - v_2 & \Delta v_{r_k} &= v_6 - v_5 \end{aligned}$$

Substituting these relationships into Equation B.3, the expression for the relative displacements becomes:

$$\begin{Bmatrix} \Delta u_r \\ \Delta v_r \end{Bmatrix} = [N^*] \begin{Bmatrix} u_1 \\ v_1 \\ u_2 \\ \vdots \\ u_6 \\ v_6 \end{Bmatrix} \quad [\text{B.5}]$$

$$\text{where } [N^*] = \begin{bmatrix} -N_1 & 0 & -N_2 & 0 & N_2 & 0 & N_1 & 0 & -N_3 & 0 & N_3 & 0 \\ 0 & -N_1 & 0 & -N_2 & 0 & N_2 & 0 & N_1 & 0 & -N_3 & 0 & N_3 \end{bmatrix}$$

In terms of the local coordinate system,  $r$ , the relative displacement at any position along the element can now be defined with respect to the local nodal displacements of the adjacent nodal pairs. A transformation from the local to global coordinate system is performed on [B] in order to define the global stiffness matrix [K]. Figure B.3 illustrates the geometry involved in transforming the local nodal displacements,  $u$  and  $v$ , into the global displacements,  $q_x$  and  $q_y$ . The transformation from  $q_x$  and  $q_y$  to  $u$  and  $v$  and ultimately to  $\Delta u_r$  and  $\Delta v_r$ , must be completed at each node separately. For any node  $i$ , the transformation equations have the following form:

$$u_i = \frac{dx/dr}{dl/dr} q_{xi} + \frac{dy/dr}{dl/dr} q_{yi} \quad [\text{B.6}]$$

$$v_i = \frac{dx/dr}{dl/dr} q_{yi} - \frac{dy/dr}{dl/dr} q_{xi} \quad [\text{B.7}]$$

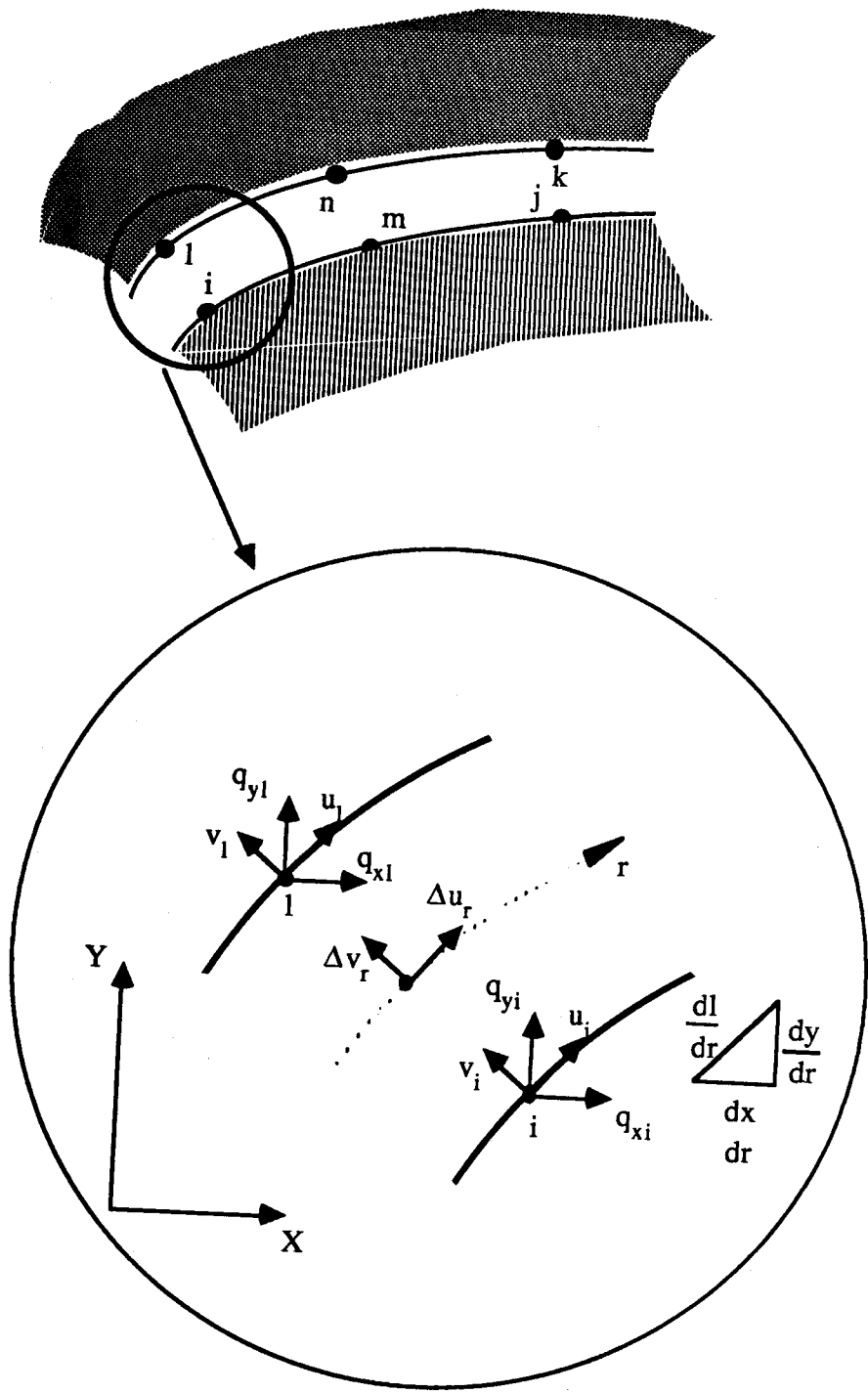


Figure B.3 Coordinate Transformation Geometry for Interface Element

Combining these equations to include all the nodes in the element yields the coordinate transformation equation:

$$\begin{Bmatrix} u \\ v \end{Bmatrix} = [T^*] \begin{Bmatrix} q_x \\ q_y \end{Bmatrix} \quad [B.8]$$

where

$$[T^*] = \begin{bmatrix} [L]_{r=-1} & & & & & \\ & [L]_{r=1} & & \text{zero's} & & \\ & & [L]_{r=1} & & & \\ & & & [L]_{r=-1} & & \\ \text{zero's} & & & & [L]_{r=0} & \\ & & & & & [L]_{r=0} \end{bmatrix}$$

$$[L]_{r=-1} = \frac{1}{dl/dr} \begin{bmatrix} dx/dr & dy/dr \\ -dy/dr & dx/dr \end{bmatrix} \text{ evaluated @ } r=-1$$

$$dx/dr = \frac{d[N]}{dr} \{x_i\}$$

$$dy/dr = \frac{d[N]}{dr} \{y_i\}$$

$$dl/dr = \sqrt{(dx/dr)^2 + (dy/dr)^2}$$

$$\frac{d[N]}{dr} = \langle (r-0.5) (r+0.5) (-2r) \rangle$$



The final expression defining the relative displacement in the element in terms of the global nodal displacements is:

$$\begin{Bmatrix} \Delta u_r \\ \Delta v_r \end{Bmatrix} = [B] \begin{Bmatrix} q_{x1} \\ q_{y1} \\ q_{x2} \\ q_{y2} \\ \vdots \\ q_{x6} \\ q_{y6} \end{Bmatrix} \quad [B.9]$$

$$\text{where } [B] = [N^*][T^*]$$

Substituting [B] into Equation B.2 results in:

$$[K] = \int_{-1}^{+1} M^{-1} [T^*]^T [N^*]^T [C] [N^*] [T^*] dr \quad [B.10]$$

Direct integration of the stiffness matrix expression is very difficult due to the complexity of the matrix expression in terms of the local coordinate system,  $r$ . Consequently, a Gauss-Legendre numerical integration scheme (Bathe, 1982) is employed to evaluate the stiffness matrix. The stiffness matrix expression in terms of numerical integration is:

$$[K] = \sum_{i=1}^n w_i M(r_i)^{-1} [T^*]^T [N^*(r_i)]^T [C] [N^*(r_i)] [T^*] \quad [B.11]$$

where  $w_i$  = gaussian weighting factors

$r_i$  = gaussian sampling point

A complete discussion outlining the practical considerations of performing numerical integration can be found in Bathe

(1982).

The traction force vector,  $\{P\}$ , as derived from the displacement formulation has the form:

$$\{P\} = \int_V [B]^T \{\sigma\} dV \quad [B.12]$$

As for the stiffness matrix, the volume integral can be reduced to an integration along the element length:

$$\therefore \{P\} = \int_l [B]^T \{\sigma\} dl \quad [B.13]$$

But  $dl = \frac{dl}{dr} dr$

So,

$$\{P\} = \int_{-1}^{+1} [B]^T \{\sigma\} M^{-1} dr \quad [B.14]$$

where  $\{\sigma\} = \left\{ \begin{matrix} \tau \\ \sigma_n \end{matrix} \right\}$

Using the same numerical integration scheme used in evaluating the stiffness matrix, the load vector expression becomes:

$$\{P\} = \sum_{i=1}^n w_i [T^*]^T [N^*(r_i)]^T \left\{ \begin{matrix} \tau(r_i) \\ \sigma_n(r_i) \end{matrix} \right\} \quad [B.15]$$

### B.3 Interface Element Constitutive Models

Modelling the interaction between two dissimilar materials using the finite element method is an area of active research. The characteristics of an interface and their corresponding effects on the interfacial behaviour are very difficult to analyze. In general, the interface behaviour is defined in terms of a shear stress - deformation relationship coupled with a suitable failure criterion. This relationship is usually determined using a direct shear apparatus but a pullout test may also be utilized.

In this research, the soil-reinforcement interface element constitutive models are based on shear stress-displacement curves developed from interfacial direct shear tests (Bobey, 1988). A Mohr-Coulomb failure criterion is utilized in each model. The dilatancy effect during shear is neglected. The following sections describe each model in detail.

#### B.3.1 Linear Elastic Model

The shear stress - displacement behaviour in the linear elastic model is illustrated in Figure B.4. The shear modulus,  $G$ , remains constant until a failure condition is reached along the interface. The failure condition is defined using the Mohr-Coulomb relationship:

$$\tau_f = a + \sigma_n \tan \delta$$

[B.16]

Figure B.4 illustrates the Mohr-Coulomb failure envelope. In the finite element analysis, the shear stress at each integration point is checked with the failure criterion. If failure is reached, a constant shear stress equal to  $\tau_f$  is applied and maintained at the integration point throughout the remainder of the analysis.

In general, the soil-reinforcement interaction measured from a direct shear test displays marked nonlinearity (Bobey, 1988). For this reason, the use of the linear elastic model is limited to initial finite element studies only.

### B.3.2 Hyperbolic Model with Linear Failure Envelope

The use of the hyperbolic equation in curve fitting applications is a common practice in geotechnique (Duncan and Chang, 1970). This interface model was developed by defining the shear stress-displacement behaviour using the hyperbolic equation. The resulting hyperbolic relationship has the form:

$$\tau = \frac{\Delta u}{\frac{1}{G_i} + \frac{\Delta u}{\tau_{ult}}} \quad [B.17]$$

where  $\tau$  = shear stress  
 $\Delta u$  = shear displacement  
 $\tau_{ult}$  = ultimate shear stress  
 $G_i$  = initial shear modulus

The hyperbolic relationship is illustrated in Figure B.5.

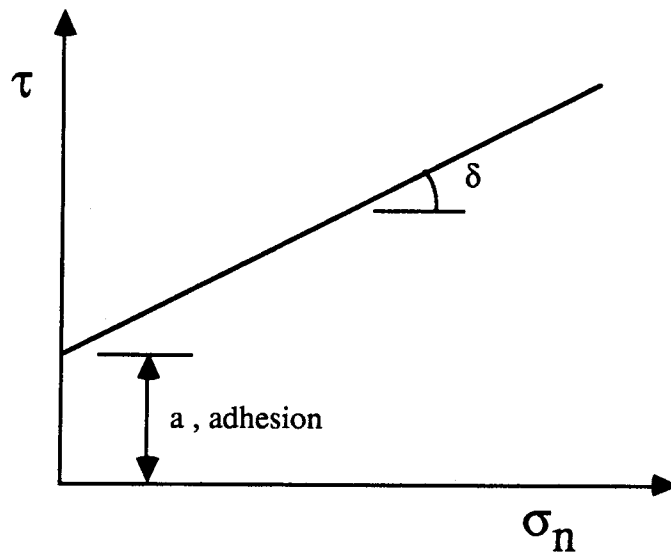
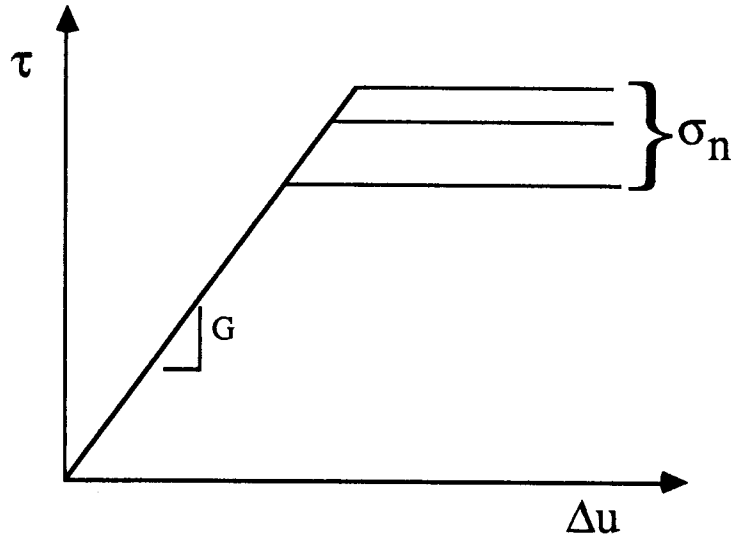


Figure B.4 Linear Elastic  $\tau$ - $\Delta u$  Model for Interface Element

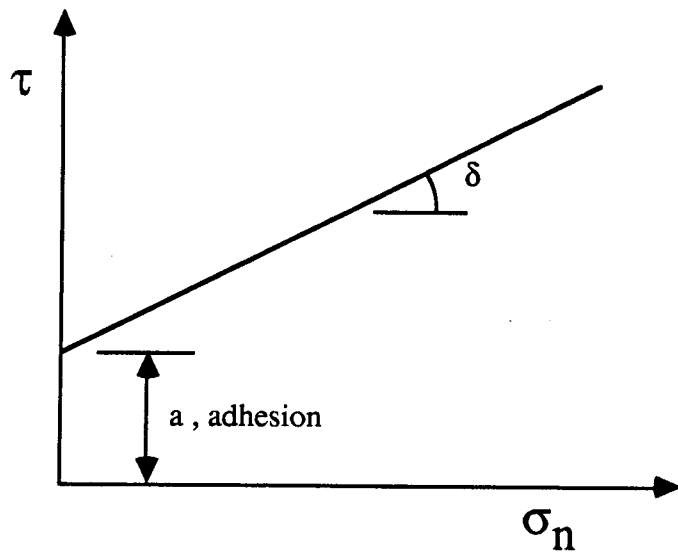
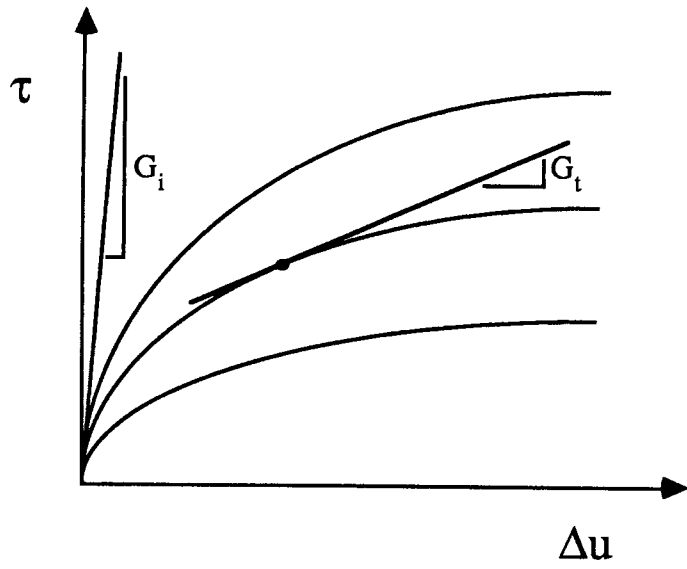


Figure B.5 Hyperbolic Elastic  $\tau$ - $\Delta u$  Model for Interface Element

The instantaneous shear modulus,  $G_t$ , is defined by differentiating Equation B.17 with respect to  $\Delta u$ :

$$G_t = \frac{\partial \tau}{\partial \Delta u} = G_i \left( 1 - \frac{(R_f \tau)}{\tau_f} \right)^2 \quad [\text{B.18}]$$

The failure envelope is defined using the conventional Mohr-Coulomb relationship:

$$\tau_f = a + \sigma_n \tan \delta \quad [\text{B.19}]$$

and the initial shear modulus, which increases with increasing normal pressure, is defined using Janbu's (1963) concept (originally developed for the elastic modulus of soil):

$$G_i = K_i p_a \left( \frac{\sigma_n}{p_a} \right)^n \quad [\text{B.20}]$$

Substituting Equation's B.19 and B.20 into Equation B.18 gives the final form of the hyperbolic relationship:

$$\tau_f = c + \frac{\sigma_n}{\frac{1}{K_{MC_i}} + \frac{\sigma_n}{\tau_p}} \quad [\text{B.21}]$$

Any unloading-reloading behaviour is accounted for by introducing an elastic unloading shear modulus in the same manner in which Duncan and Chang (1970) utilize an elastic

unloading stress - strain modulus. This will likely only be a crude approximation of the true unloading behaviour since a large amount of hysteresis will likely occur due to the undulating nature of the shear surface caused by the geogrid structure. No test results on the unload-reload response of a soil-reinforcement interface could be found in the literature.

### **B.3.3 Hyperbolic Model with Curved Failure Envelope**

This model adopts an identical approach as the previous model in characterizing the shear stress - displacement behaviour of the soil-reinforcement interface. The behaviour is modelled using the hyperbolic equation (see Equation B.17) and the instantaneous shear modulus as defined in Equation B.21. A curved failure envelope, however, is implemented in this model. Interfacial direct shear test results by Bobey (1988) indicated a marked curvature in the failure envelope for tests on clay soils. Without debating the rationale or validity of the curved failure envelope, a curved failure envelope was incorporated into this interface model.



A hyperbolic equation was also employed for the curve fitting of this nonlinear failure envelope. The hyperbolic expression defining the relationship between the shear stress at failure and the normal pressure has the form:

$$G_t = K p_a \left( \frac{\sigma_n}{p_a} \right)^n \left( 1 - \frac{R_f \tau}{(a + \sigma_n \tan \phi)} \right)^2 \quad [B.22]$$

This hyperbolic relationship is illustrated in Figure B.6. Substituting Equation B.22 into Equation B.18, the final form of the hyperbolic equation for this model is:

$$\tau = \frac{\Delta u_r}{\frac{1}{K p_a \left( \frac{\sigma_n}{p_a} \right)^n} + \frac{R_f \Delta u_r}{\left[ c_a + \frac{\sigma_n}{\left\{ \frac{1}{K_{MC_i}} + \frac{\sigma_n}{\tau_p} \right\}} \right]}} \quad [B.23]$$

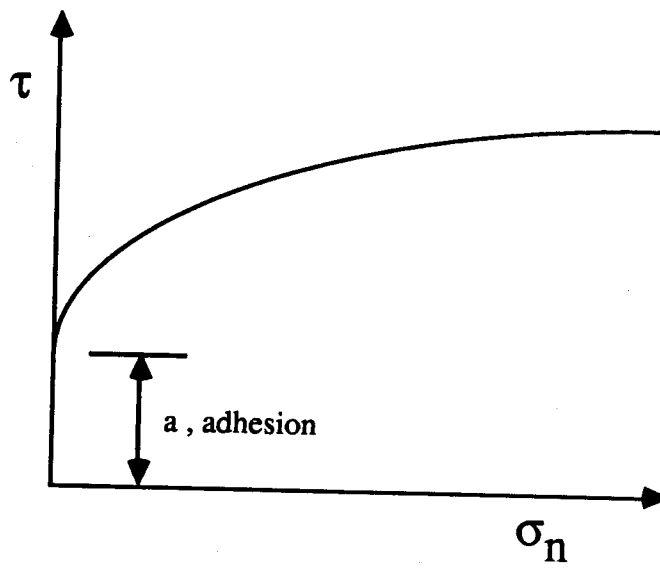
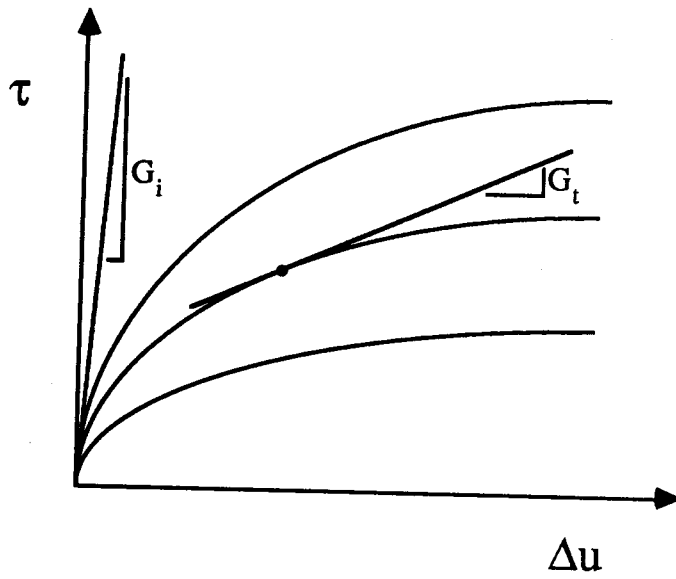


Figure B.6 Hyperbolic Model with Curved Failure Envelope

## APPENDIX C: Nonreinforced Embankment Finite Element Results

The mobilized strength, maximum shear strains, horizontal strain, vertical strain and velocity field results from the finite element analysis of the nonreinforced slope are illustrated on the following pages for embankment heights of 5 m, 10 m and 15 m.

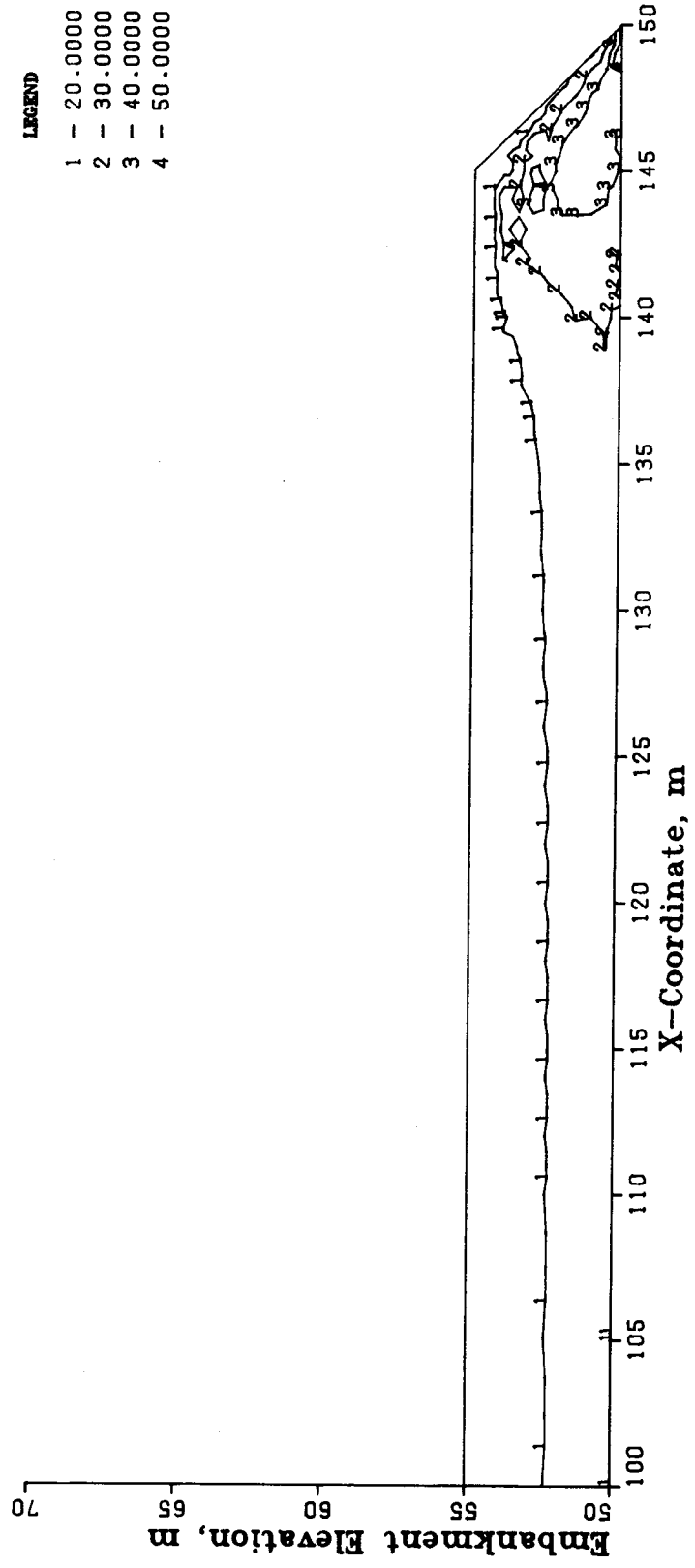


Figure C.1 Mobilized Soil Strength (%), H = 5 m

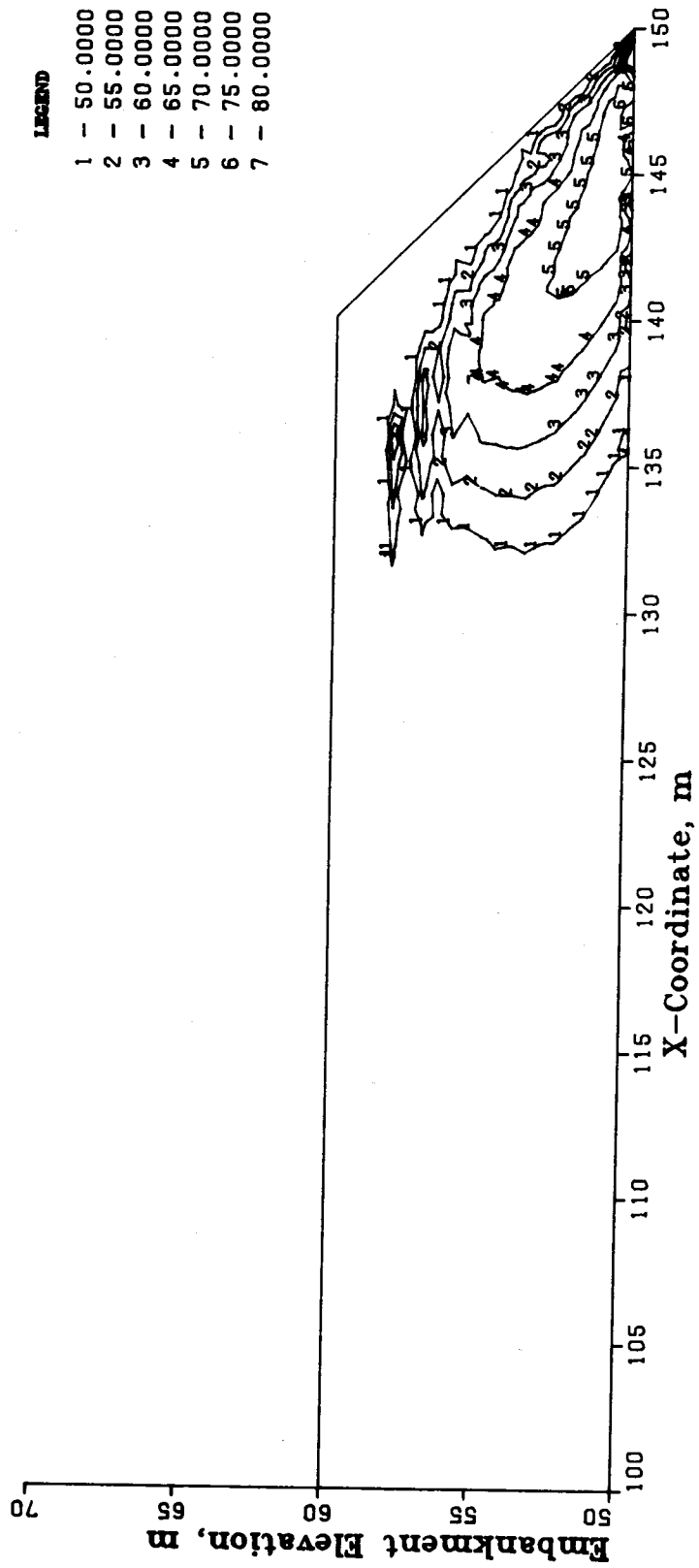


Figure C.2 Mobilized Soil Strength (%), H = 10 m

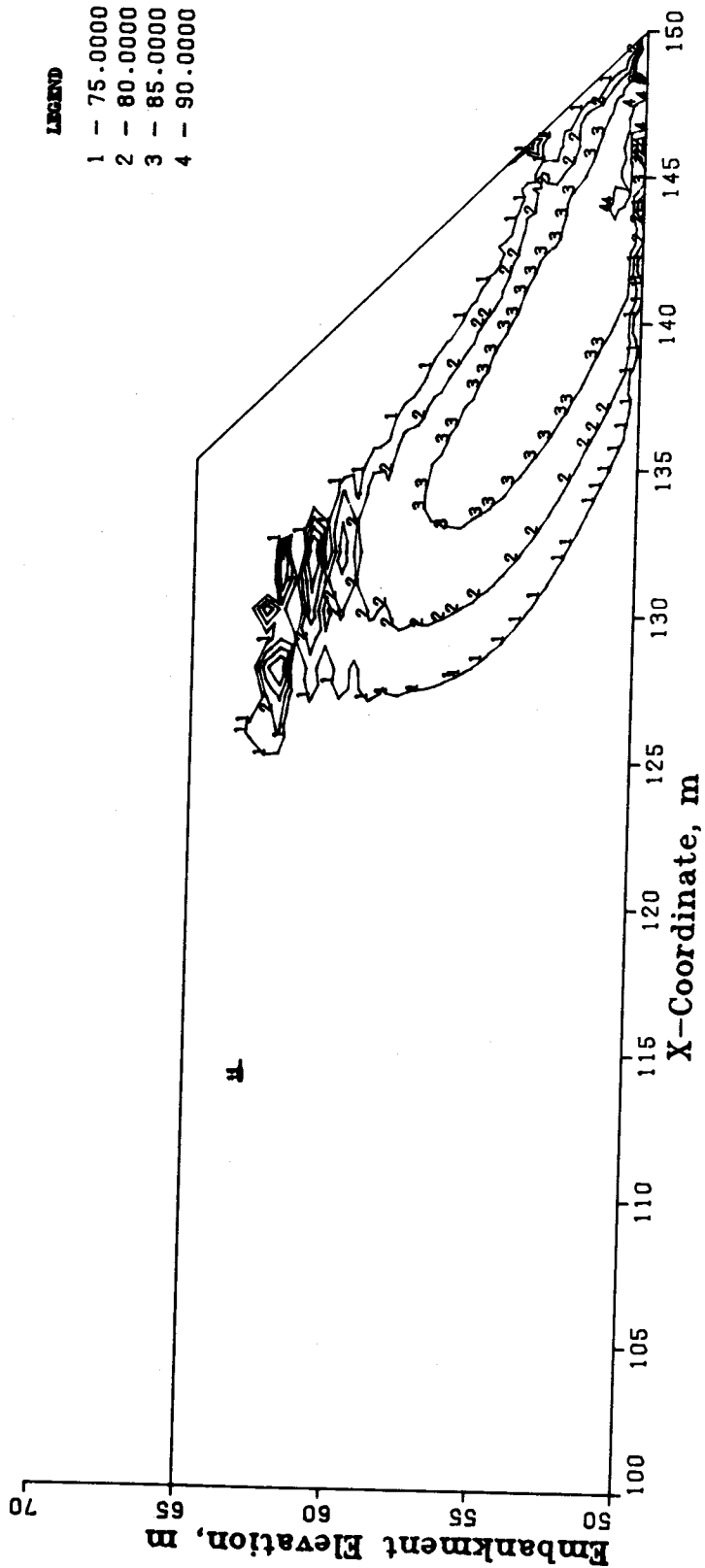


Figure C.3 Mobilized Soil Strength (%), H = 15 m

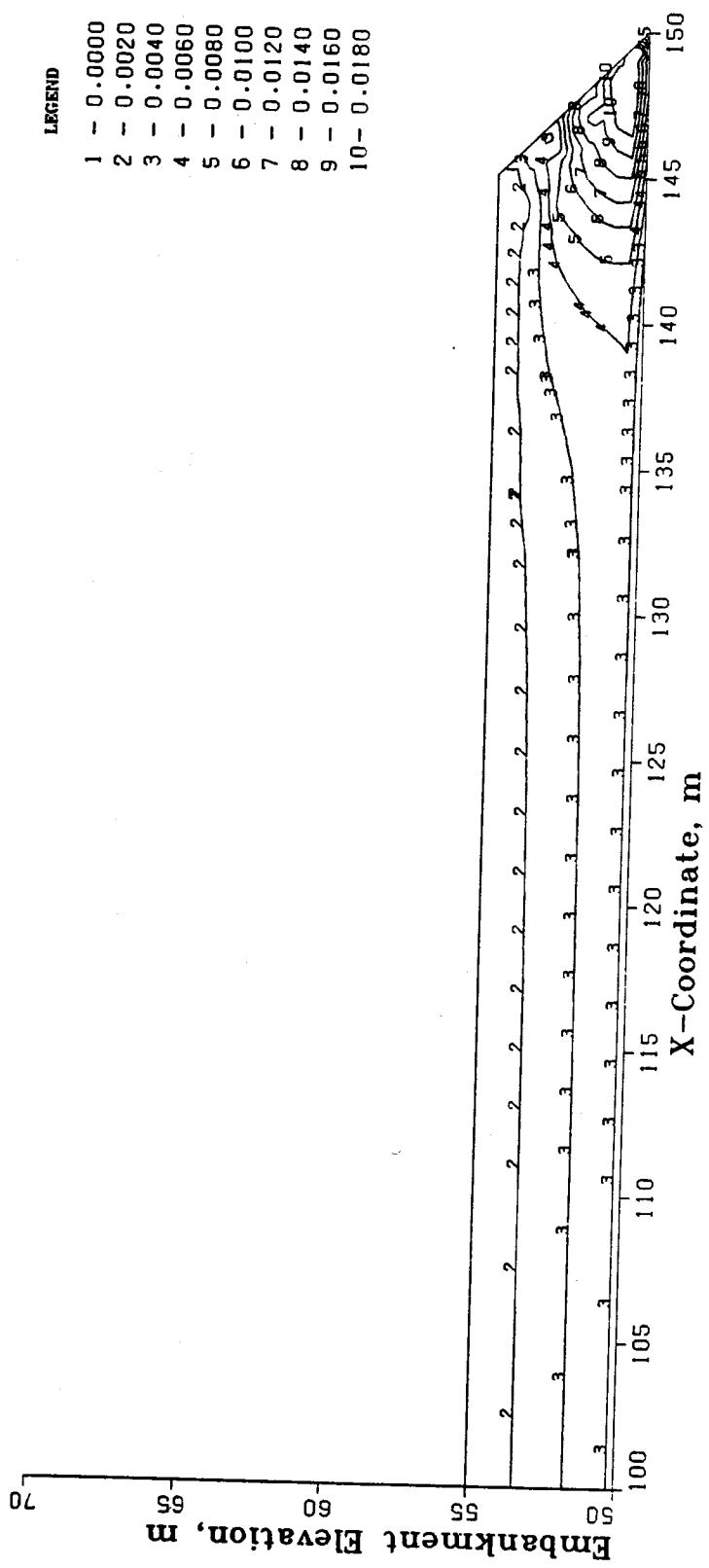


Figure C.4 Maximum Shear Strains, H = 5 m

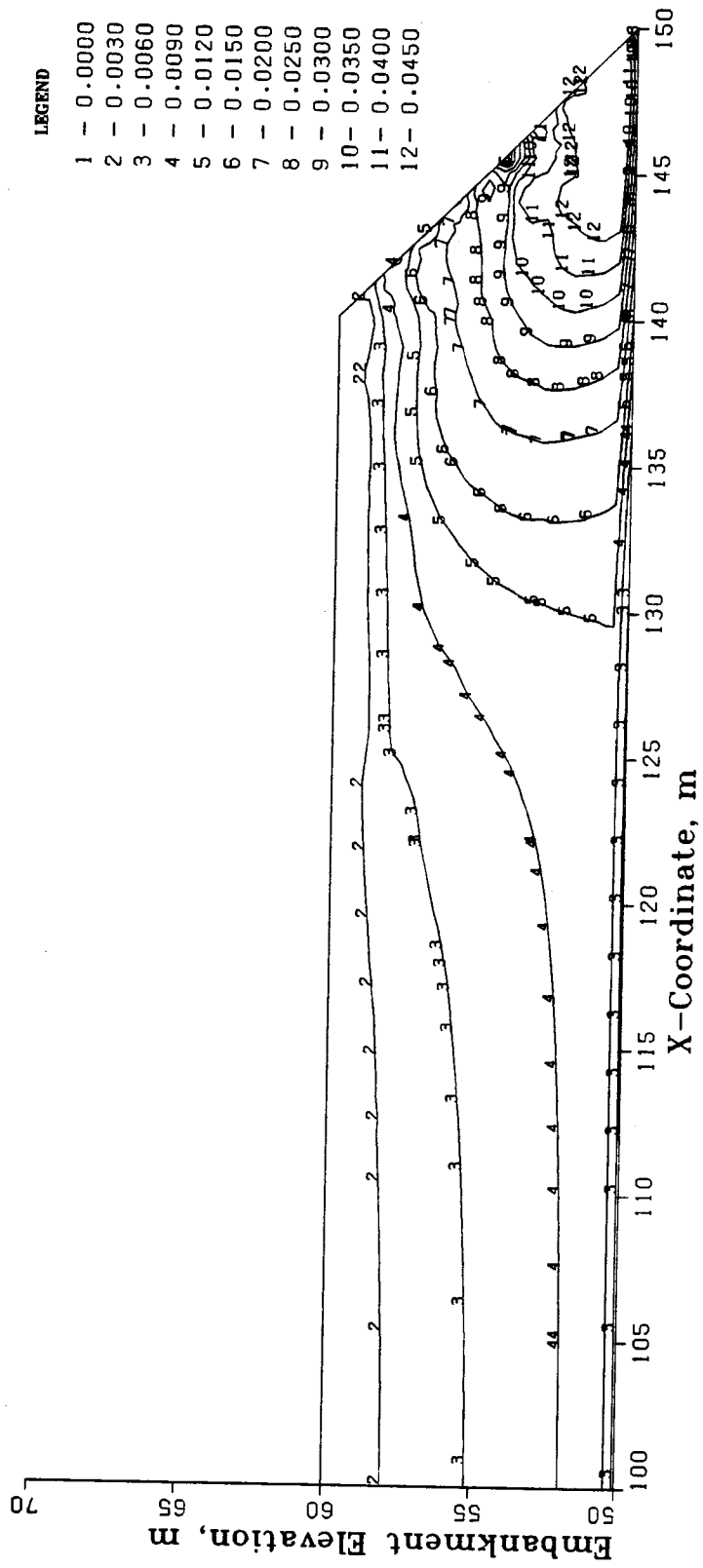


Figure C.5 Maximum Shear Strains, H = 10 m



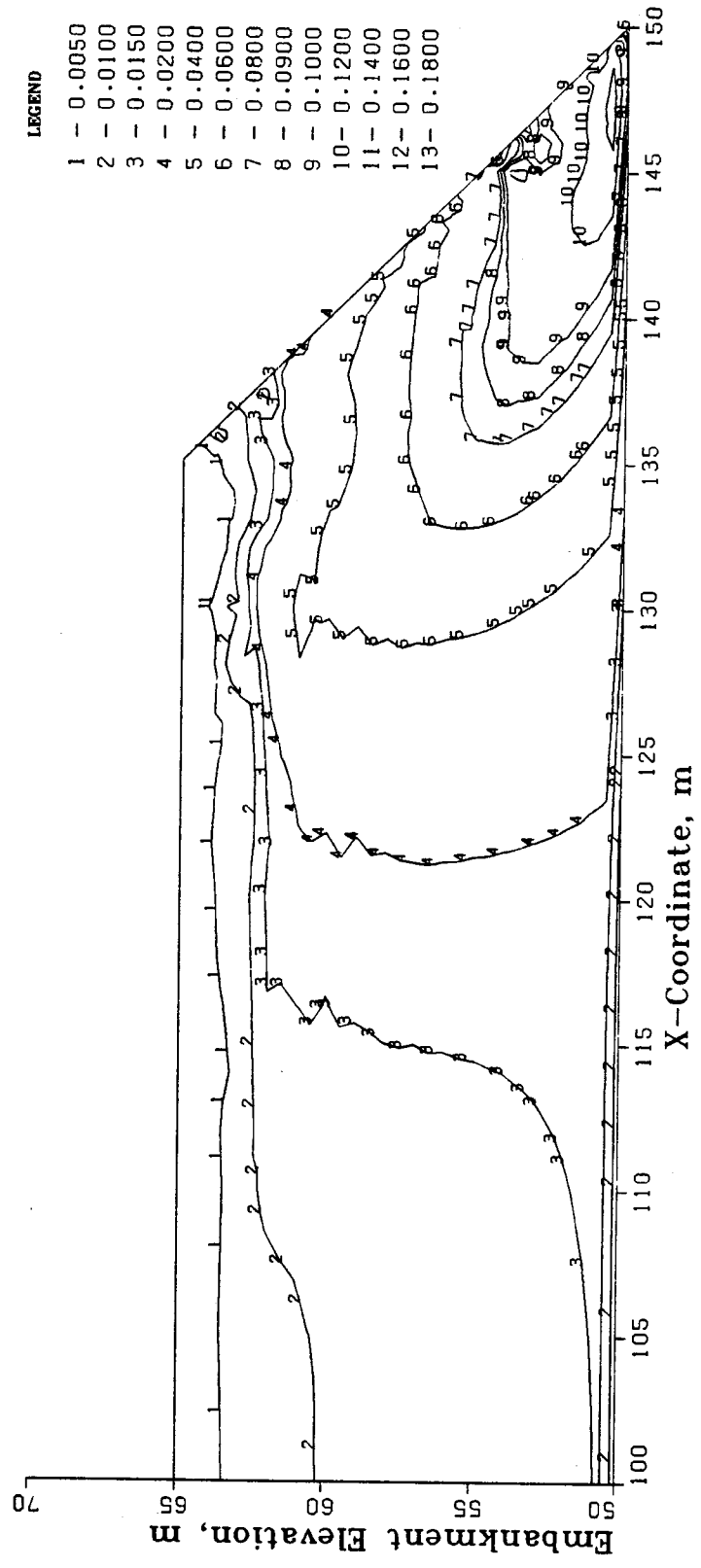


Figure C.6 Maximum Shear Strains, H = 15 m

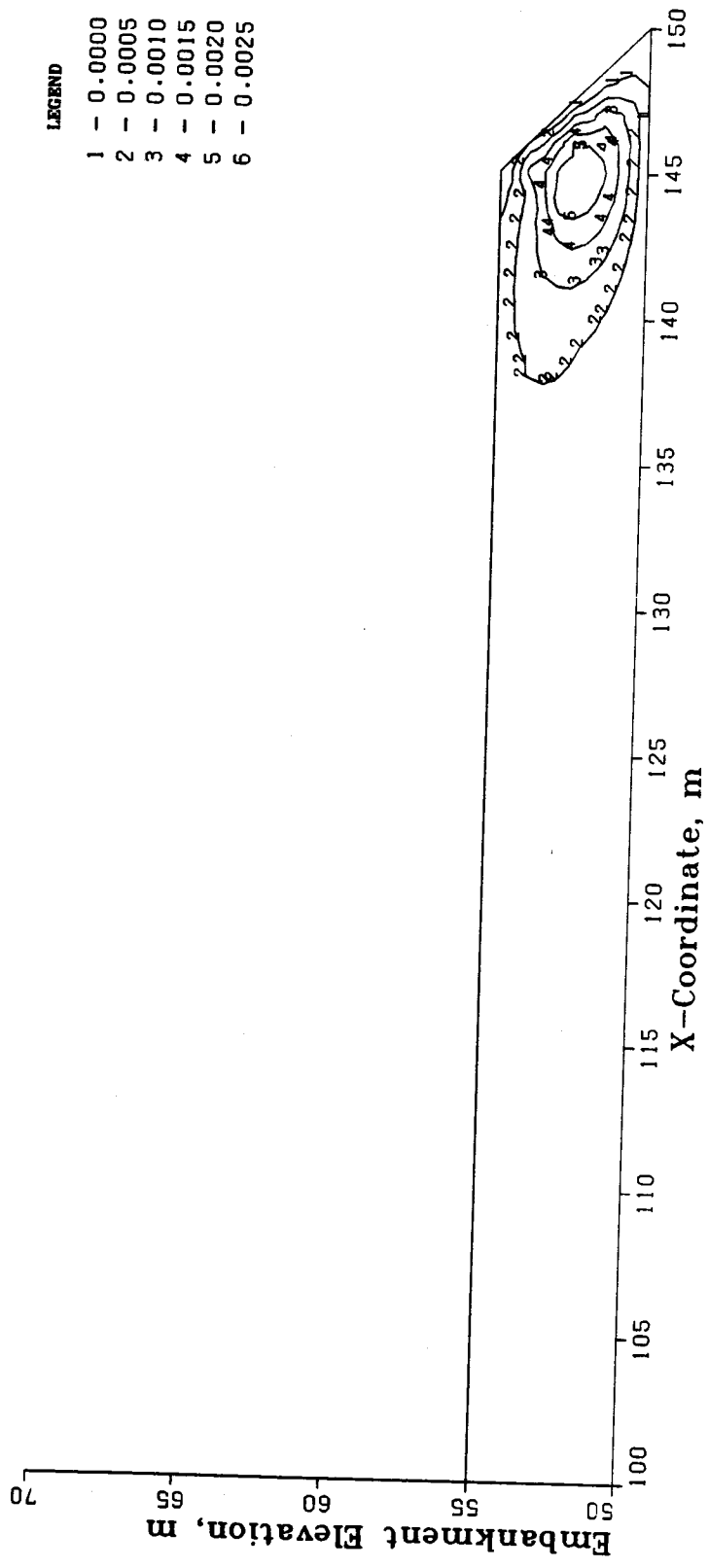


Figure C.7 Horizontal Strains, H = 5 m

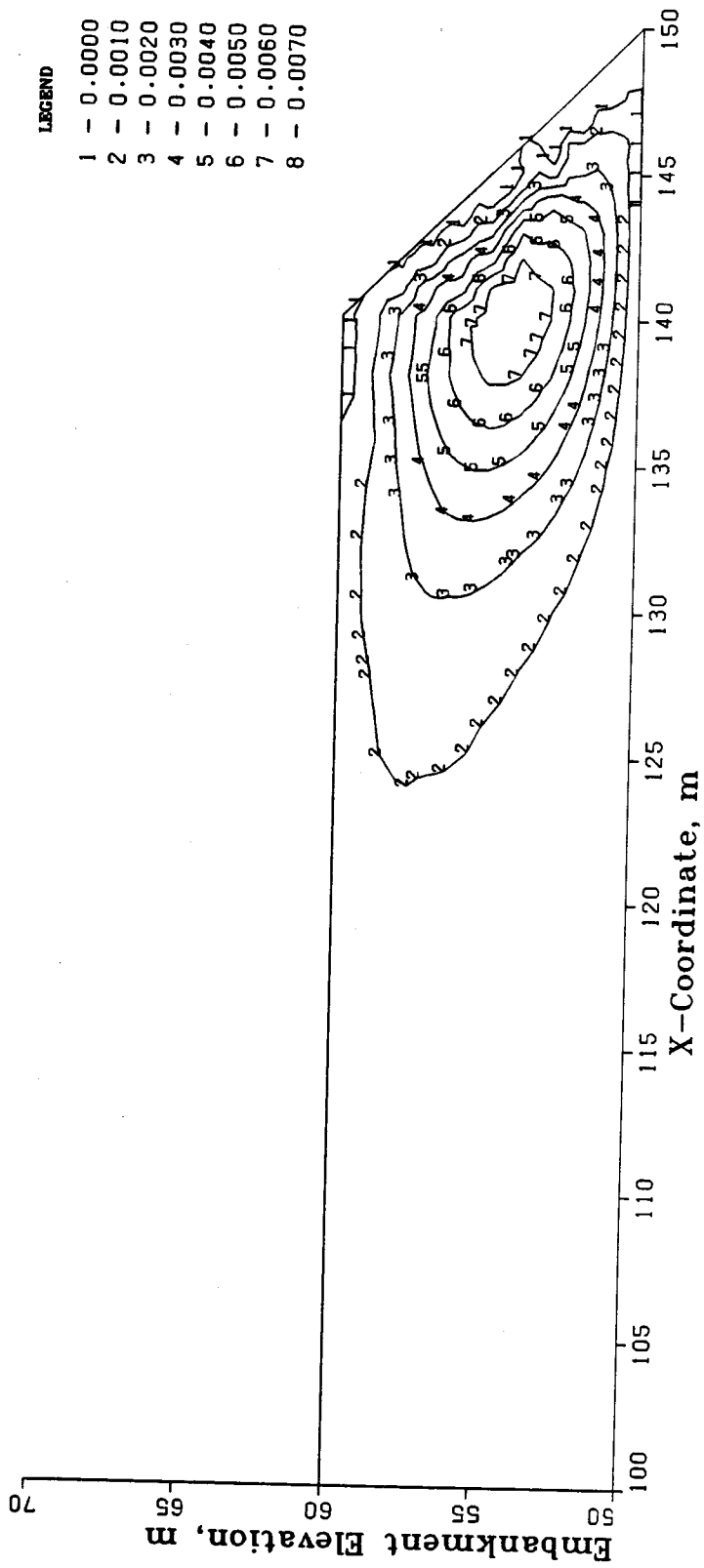


Figure C.8 Horizontal Strains, H = 10 m

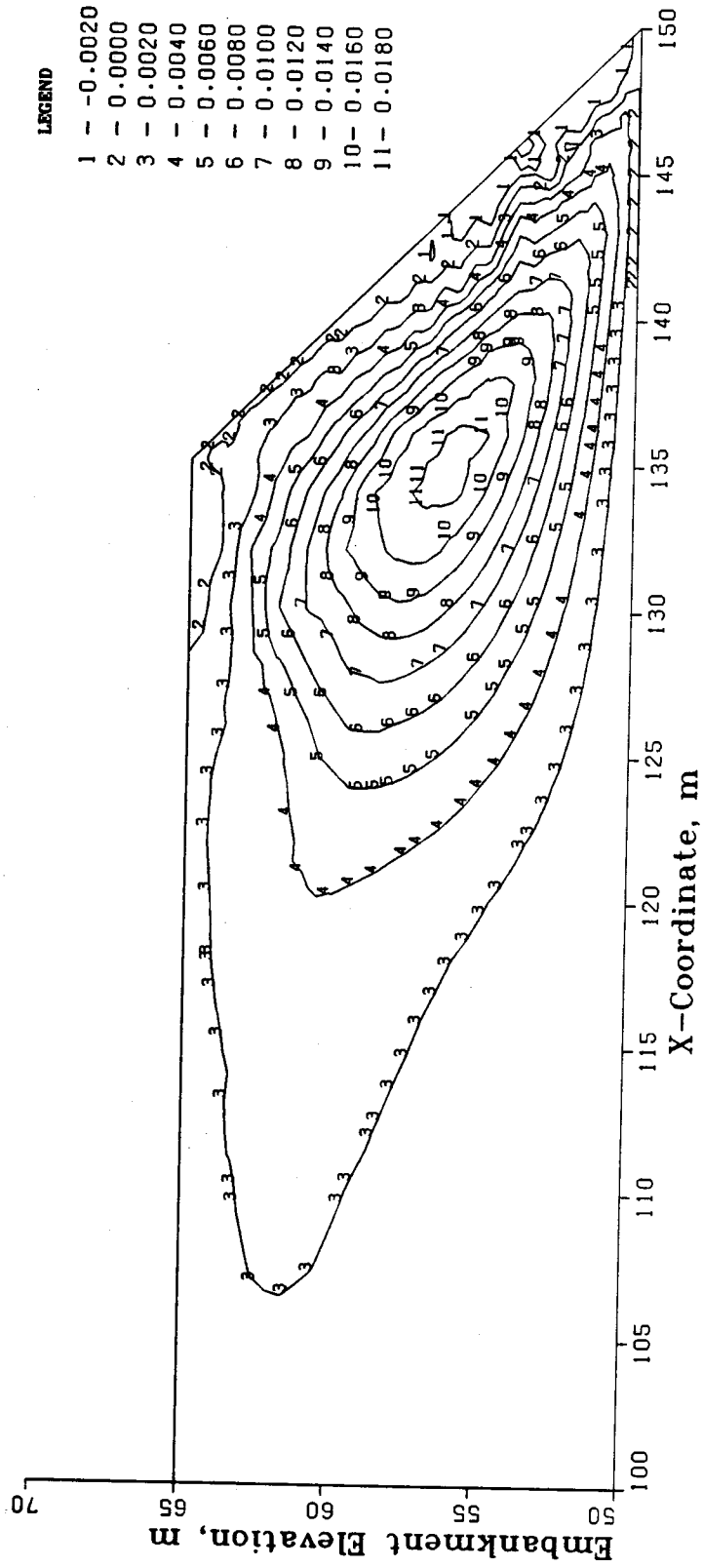


Figure C.9 Horizontal Strains, H = 15 m

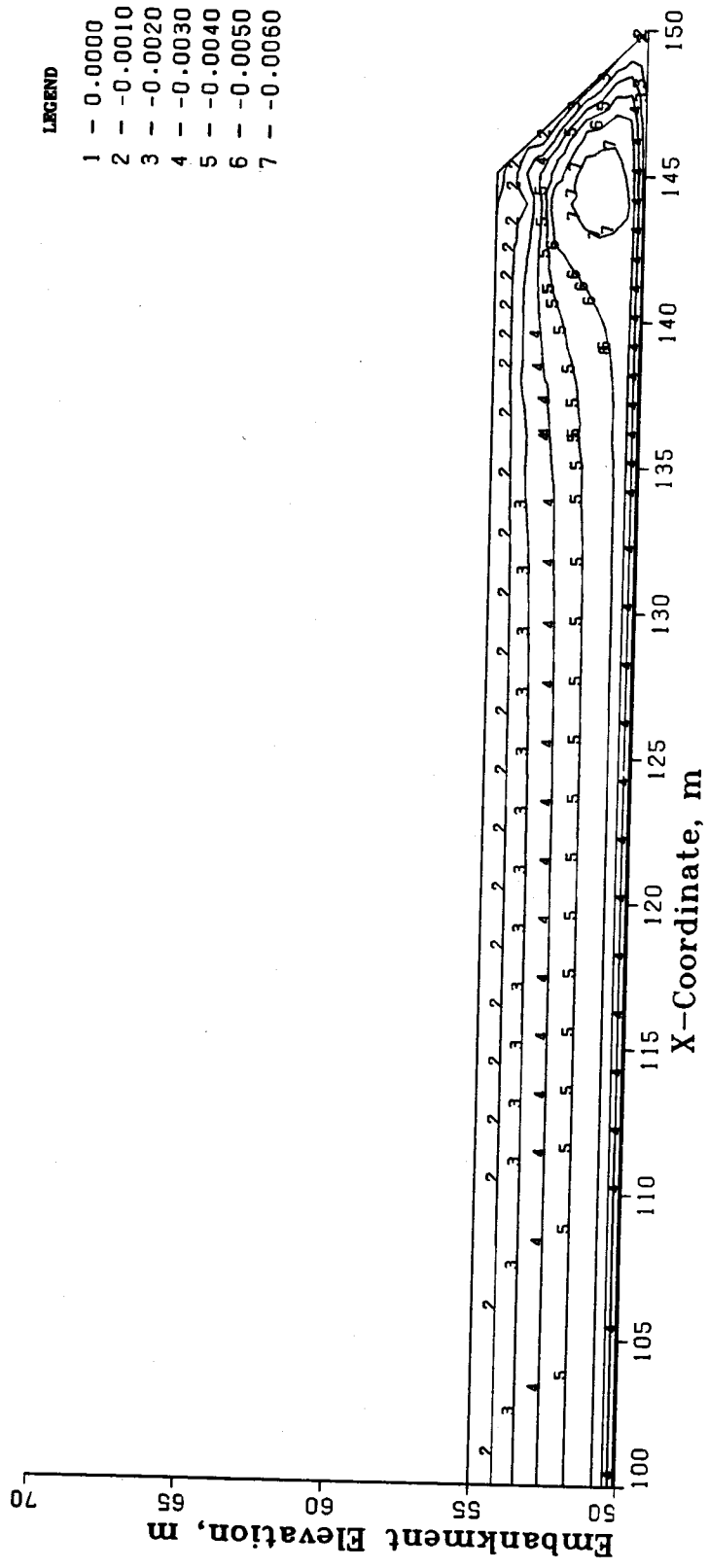


Figure C.10 Vertical Strains, H = 5 m

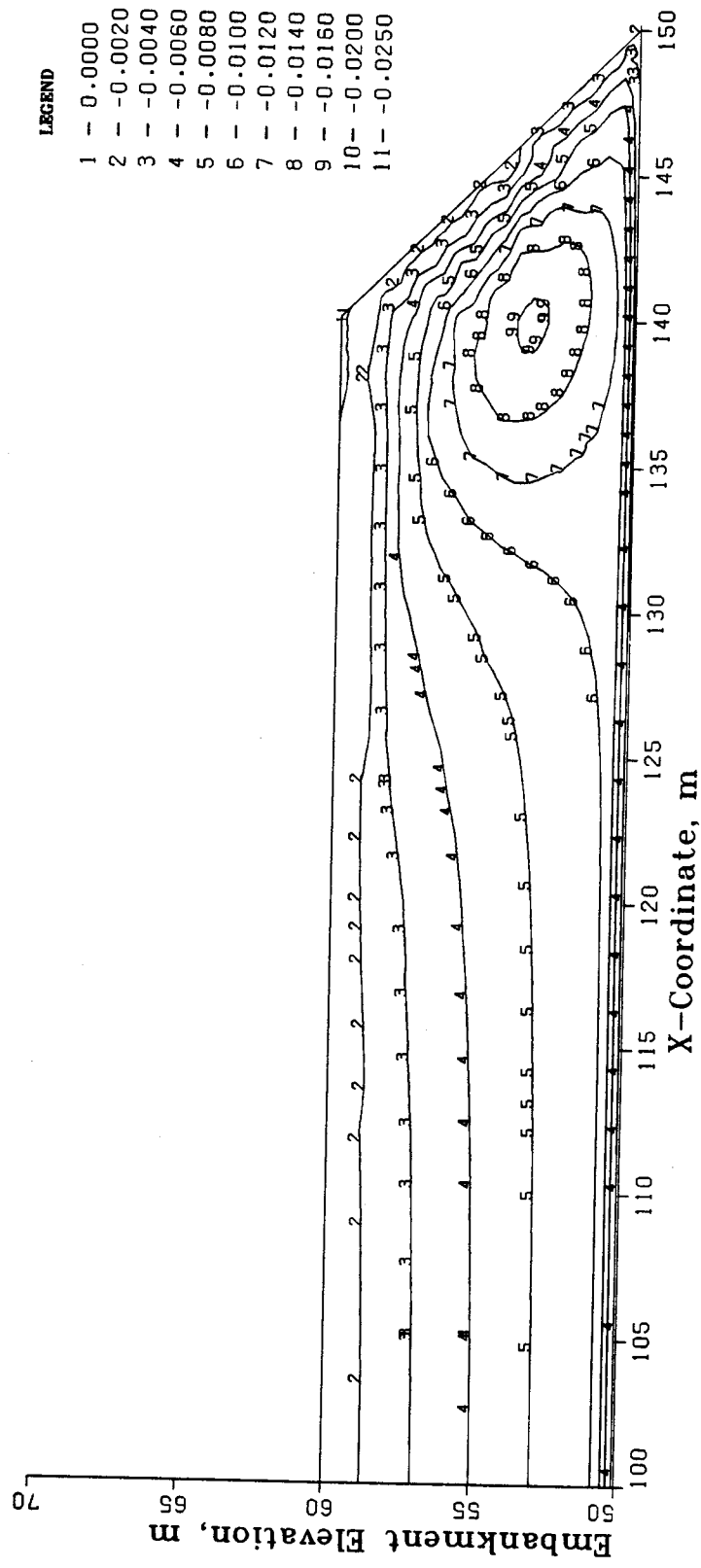


Figure C.11 Vertical Strains, H = 10 m

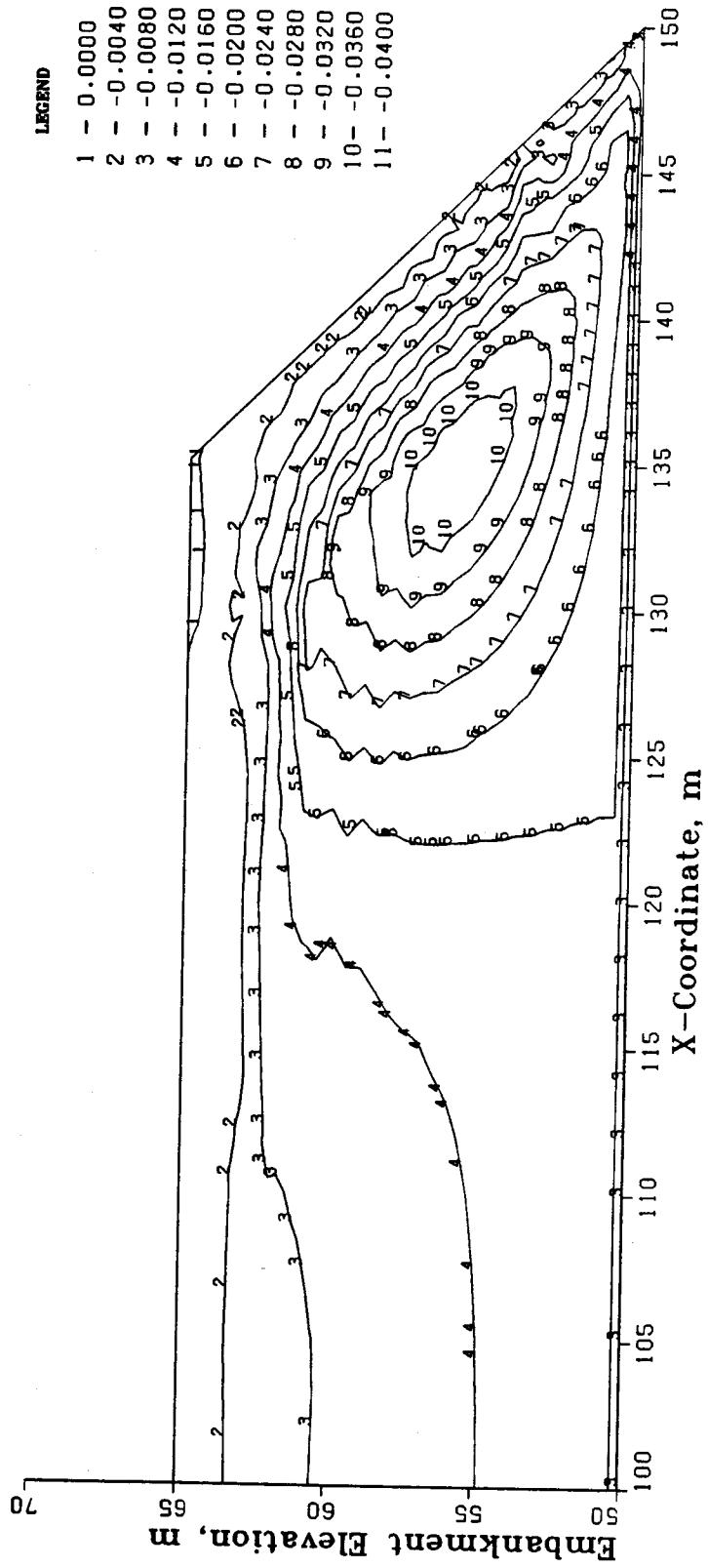


Figure C.12 Vertical Strains, H = 15 m

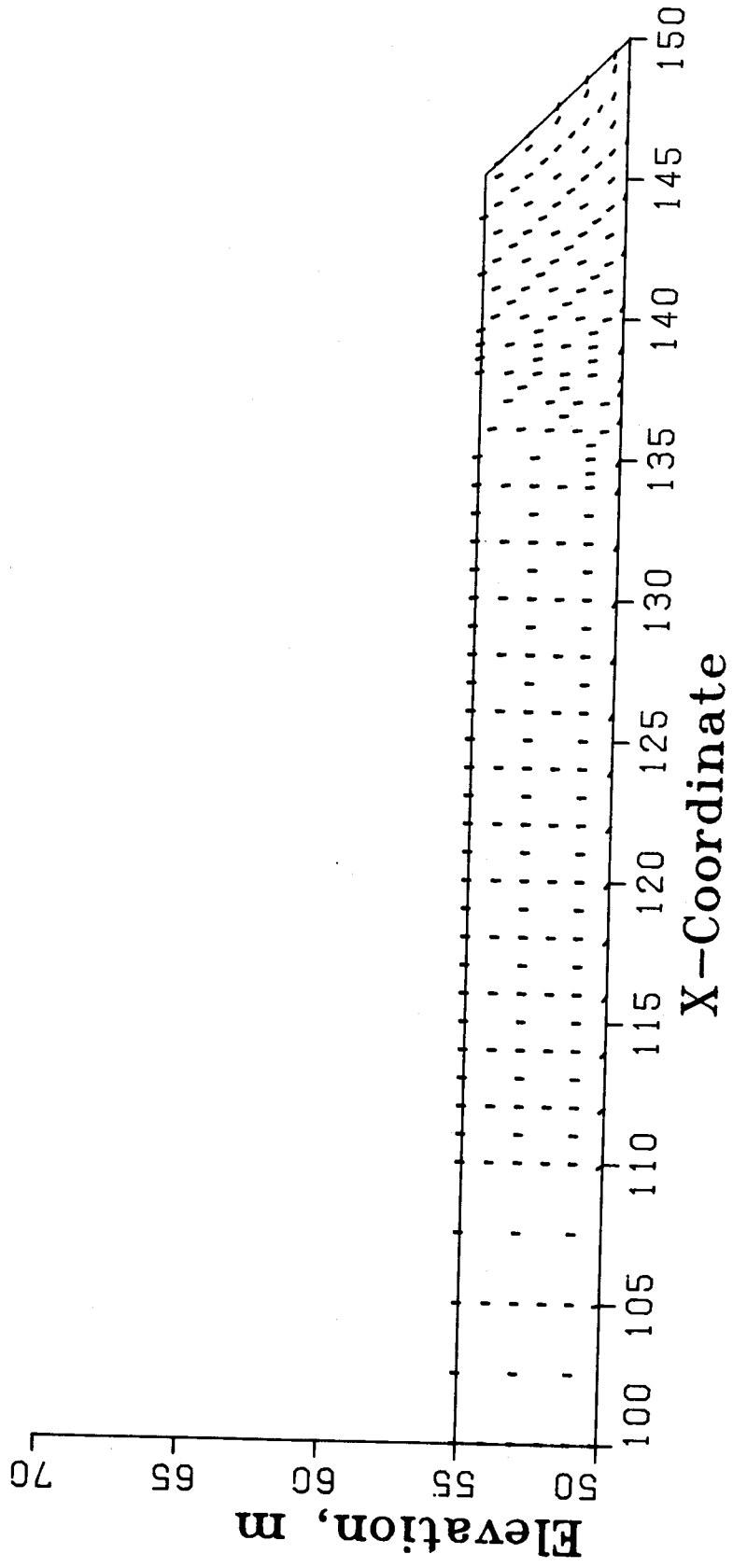


Figure C.13 Velocity Field,  $H = 5$  m, (Scale: 1 cm = .5 m)



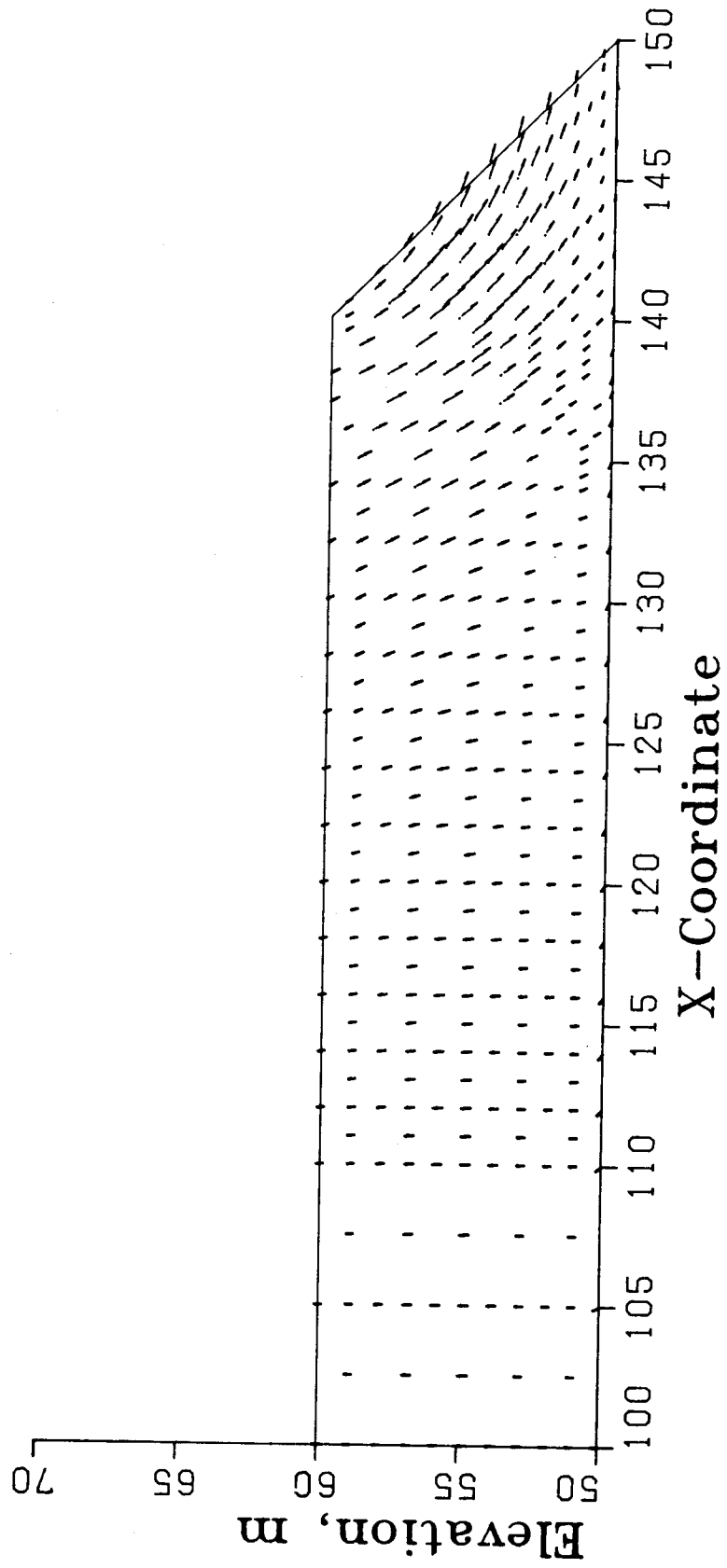


Figure C.14 Velocity Field,  $H = 10$  m, (Scale: 1 cm = .5 m)

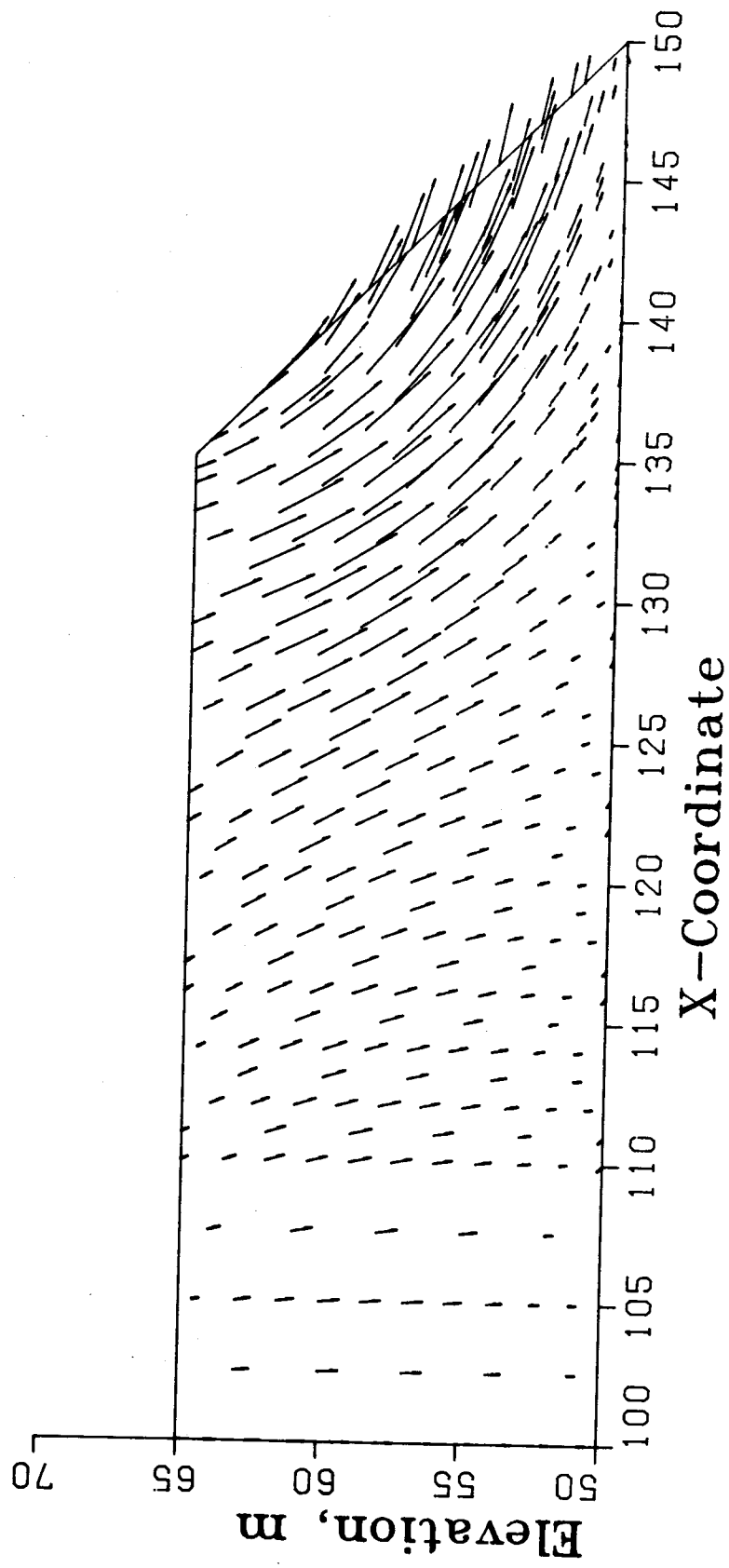


Figure C.15 Velocity Field,  $H = 15$  m, (Scale: 1 cm = .5 m)

## APPENDIX D: Embankment Finite Element Results

The mobilized strength, maximum shear strains, horizontal strain, vertical strain and velocity field results from the finite element analysis of the reinforced slope are illustrated on the following pages for embankment heights of 5 m, 10 m and 15 m.

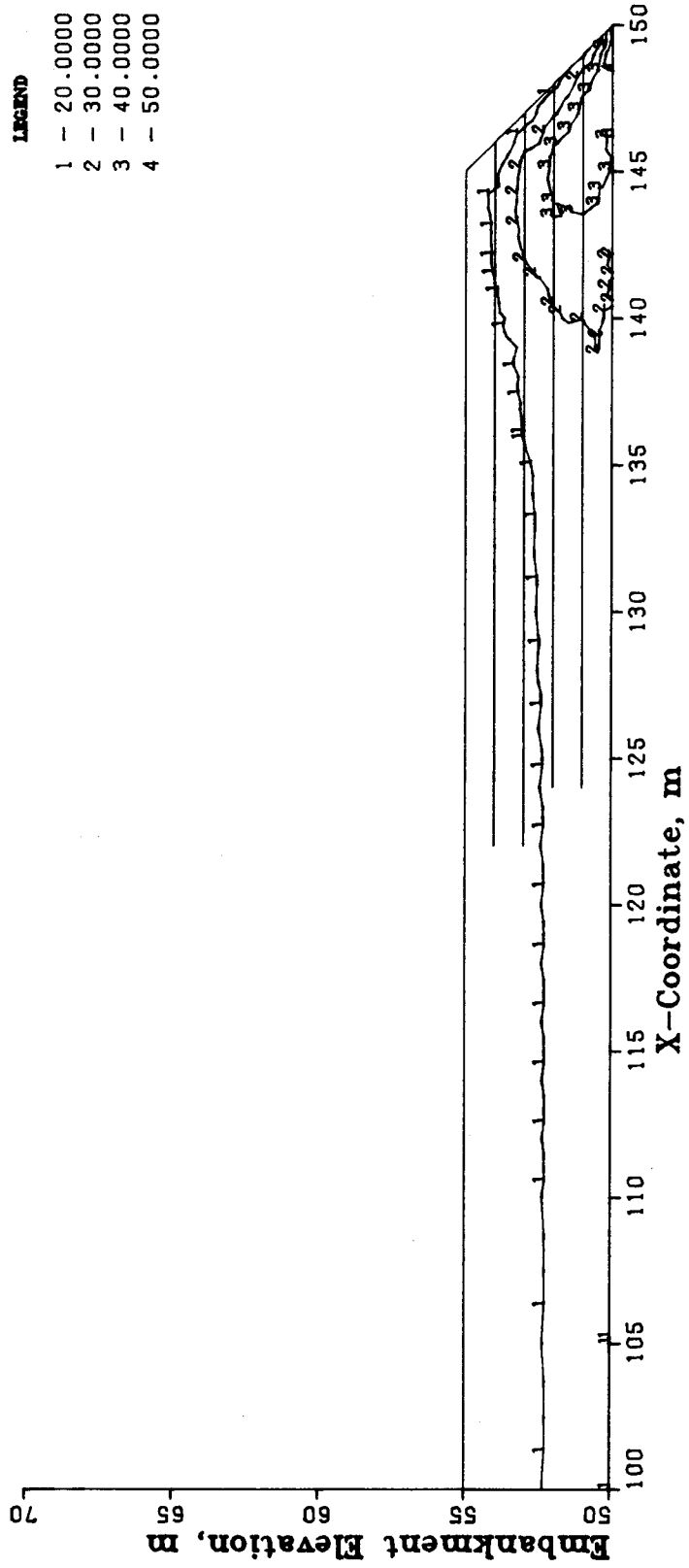


Figure D.1 Mobilized Soil Strength (%), H = 5 m

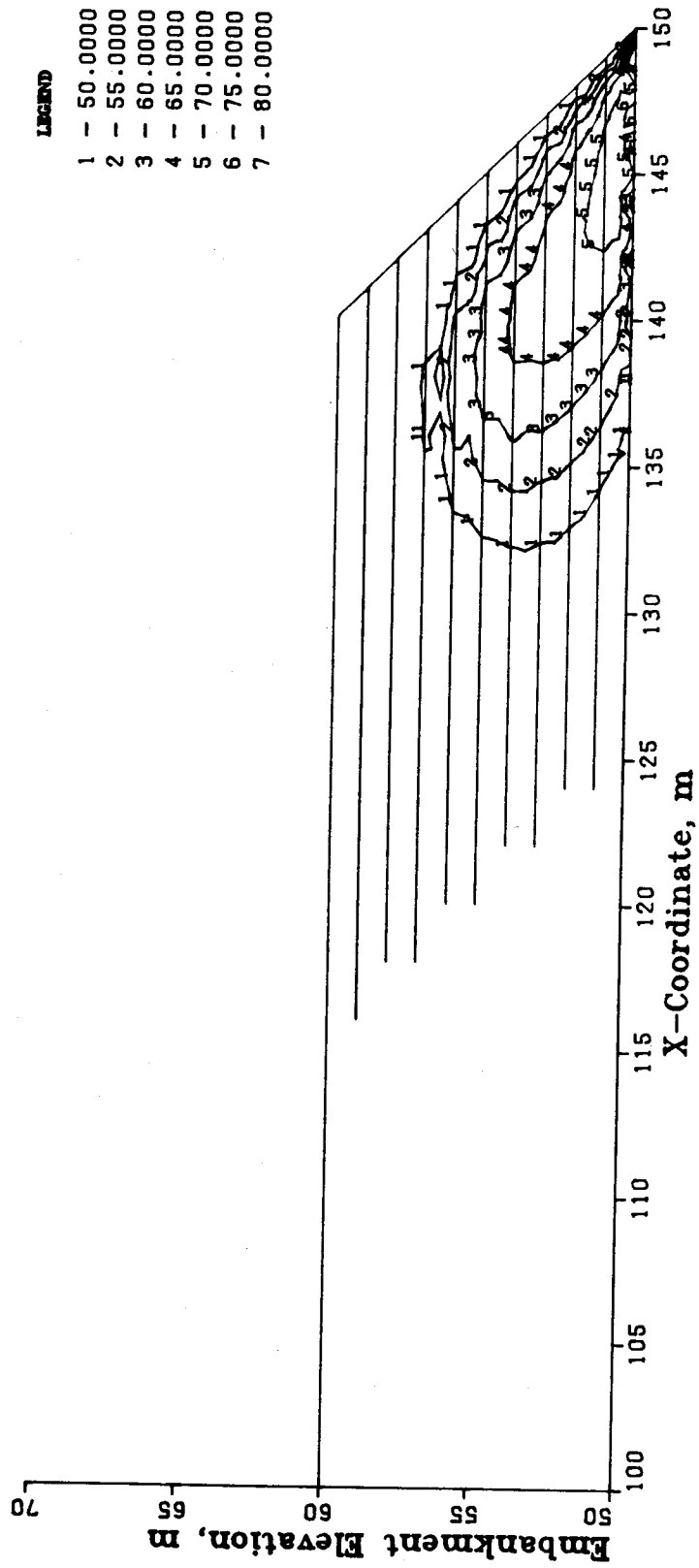


Figure D.2 Mobilized Soil Strength (%), H = 10 m

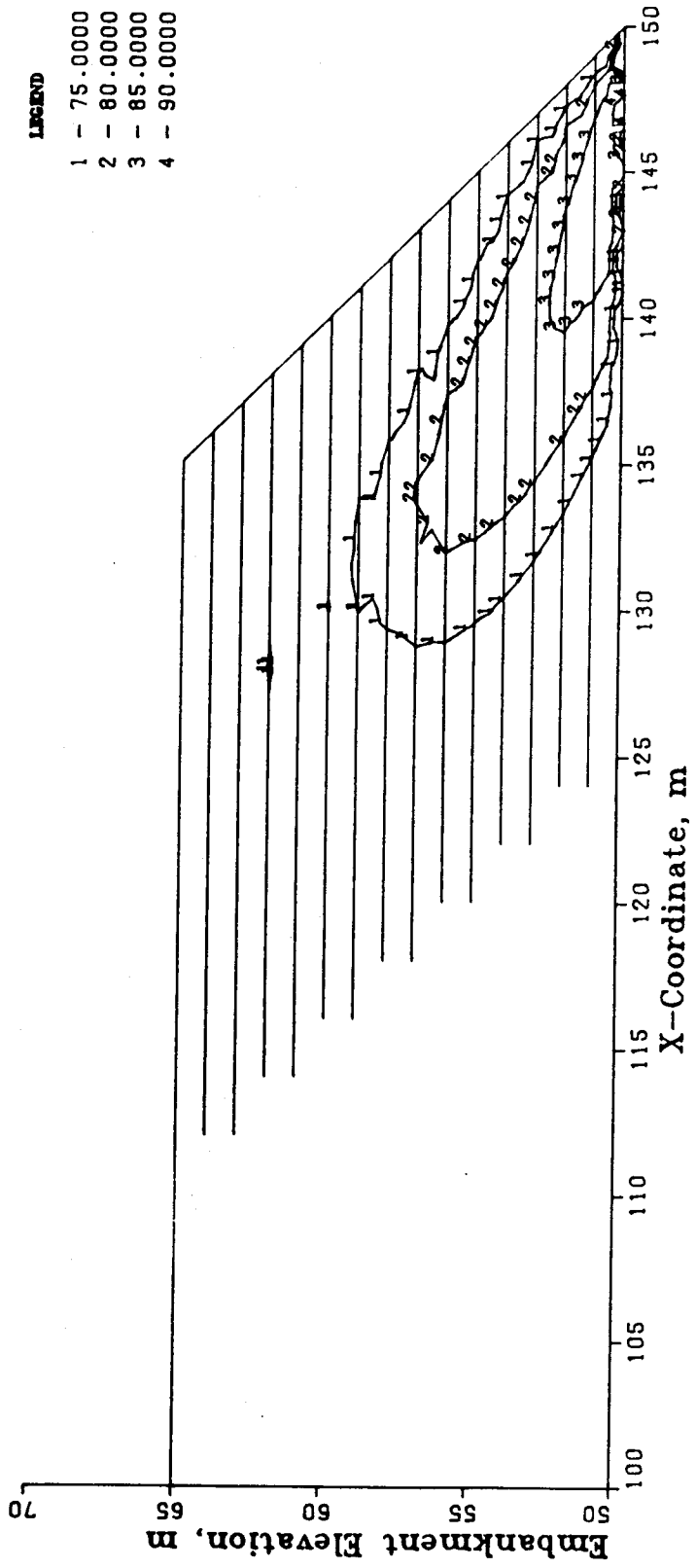


Figure D.3 Mobilized Soil Strength (%), H = 15 m

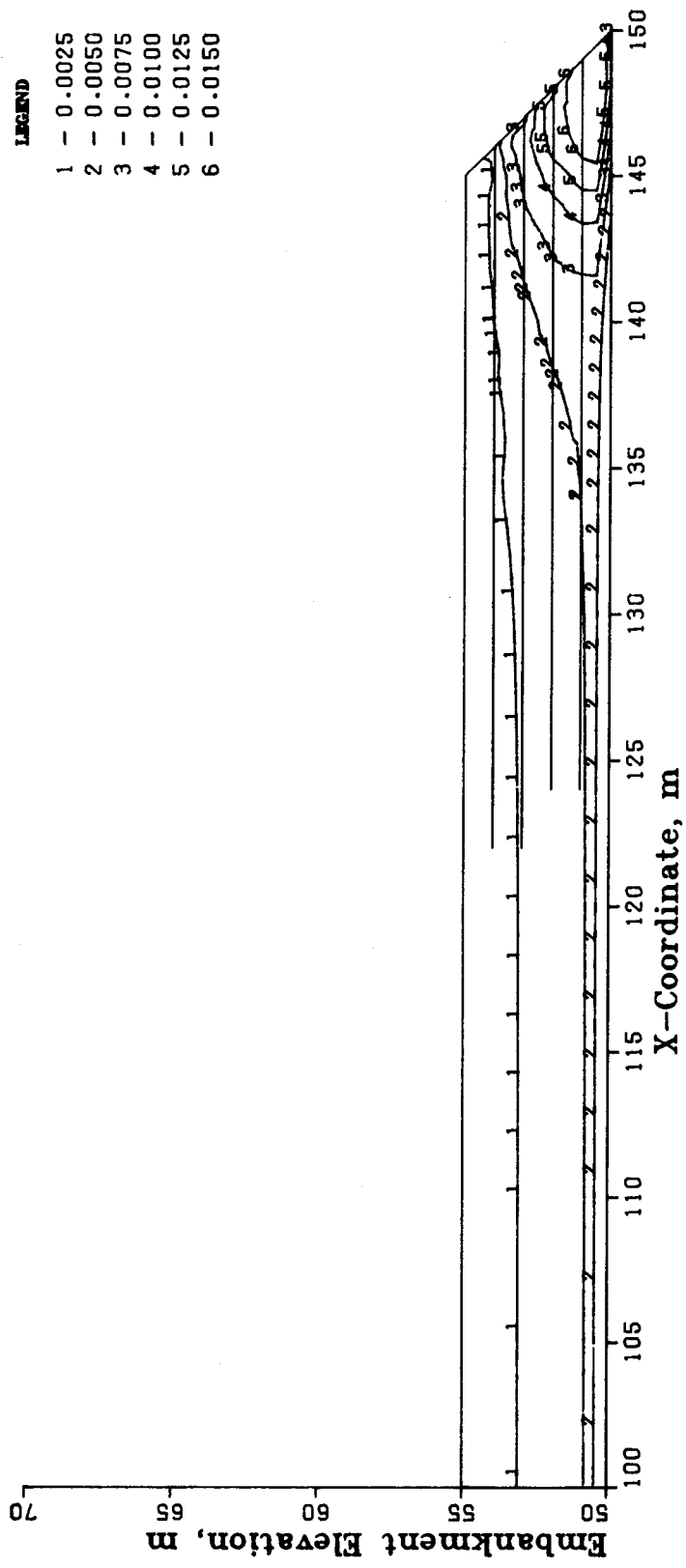


Figure D.4 Maximum Shear Strains, H = 5 m

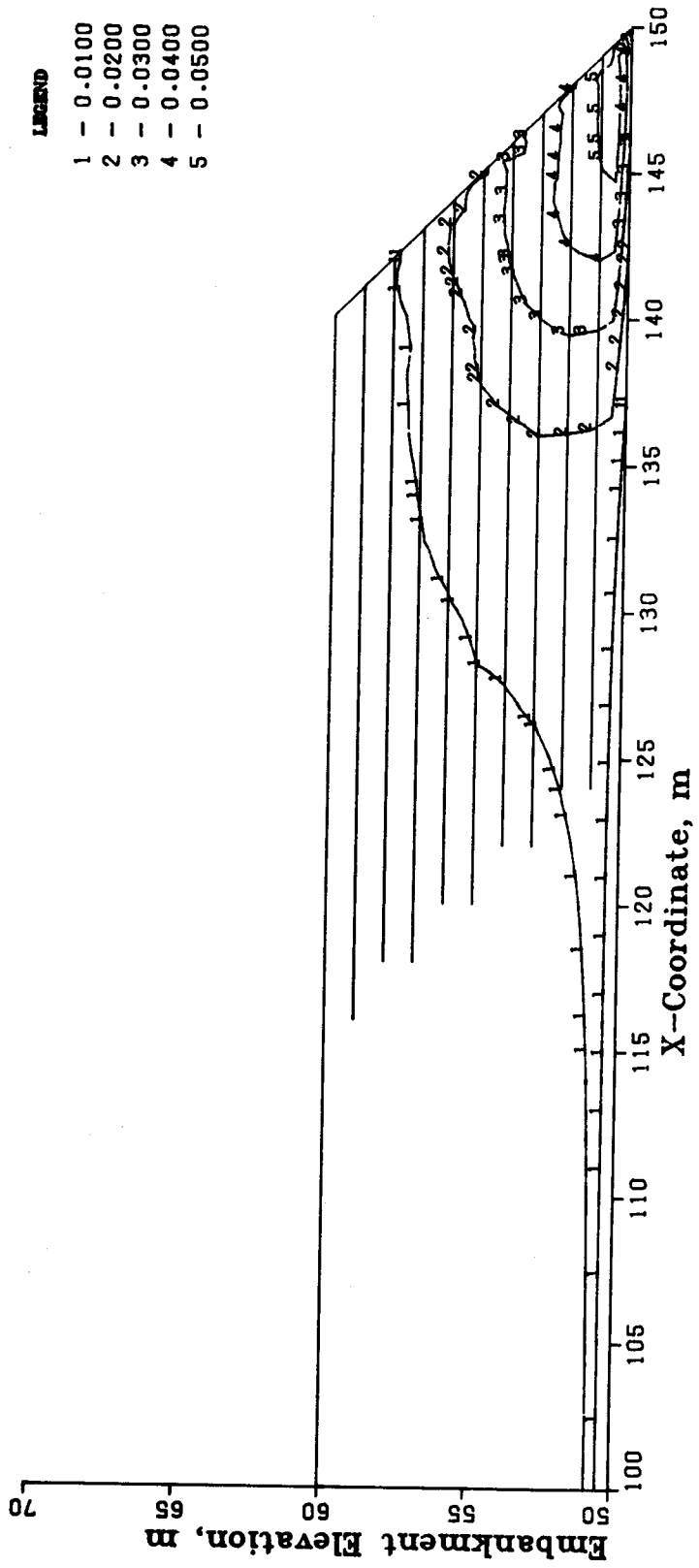


Figure D.5 Maximum Shear Strains, H = 10 m



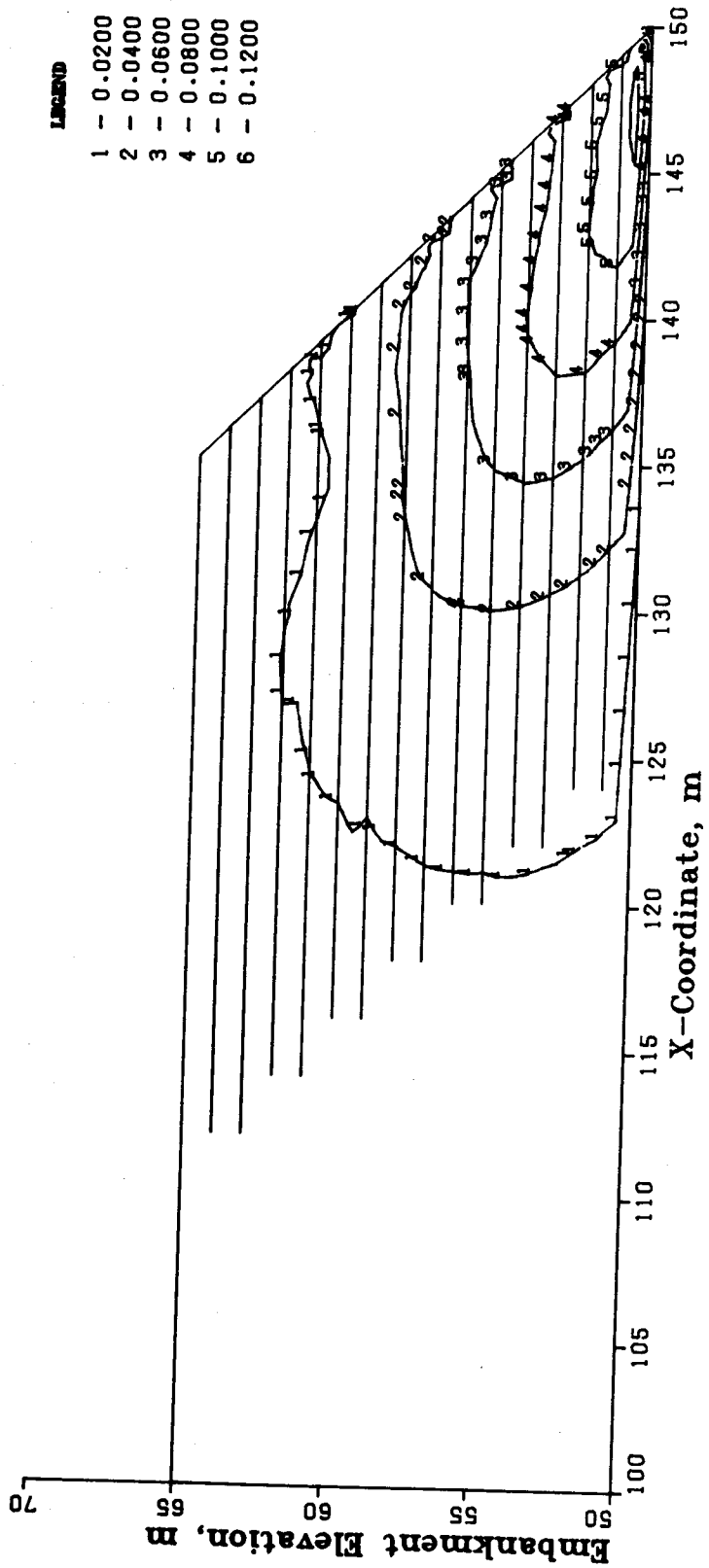


Figure D.6 Maximum Shear Strains, H = 15 m

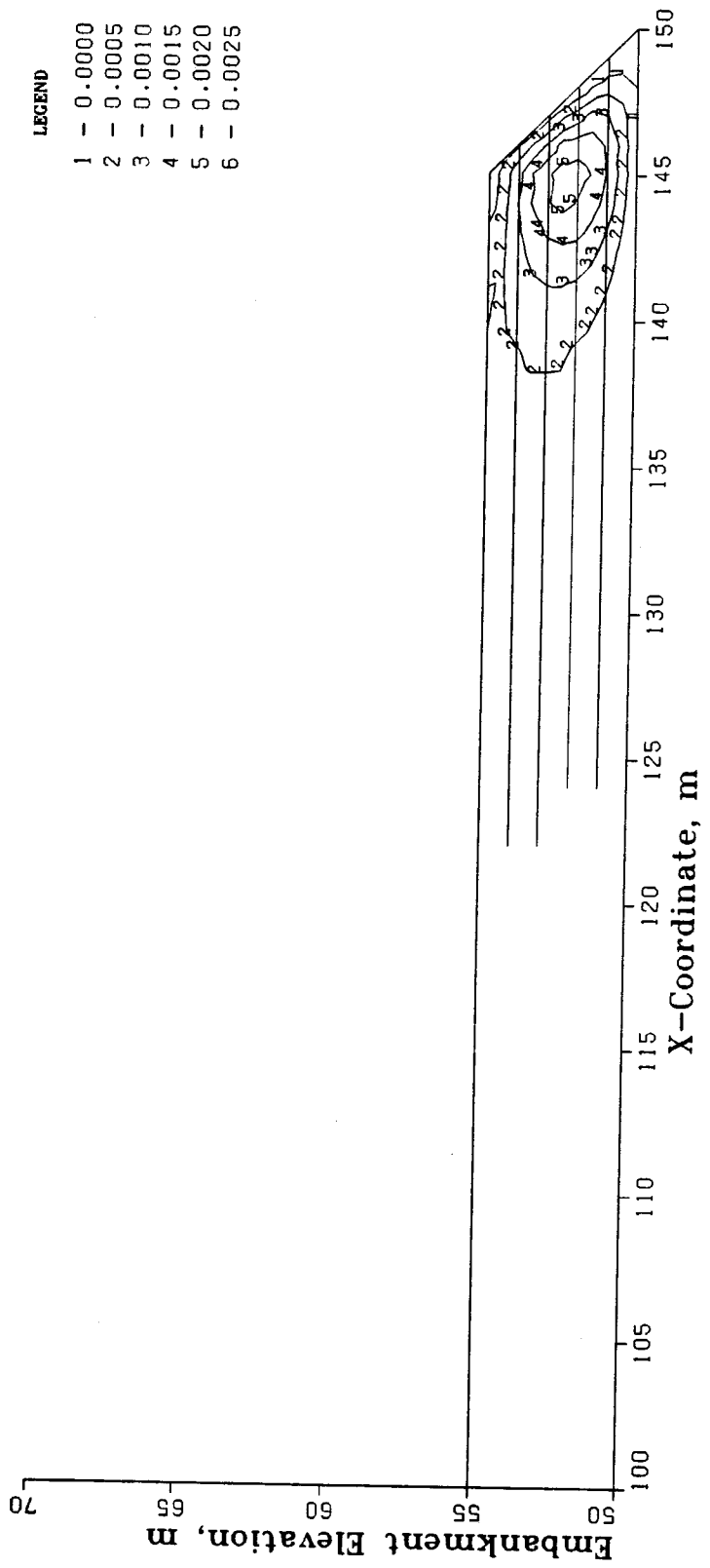


Figure D.7 Horizontal Strains, H = 5 m

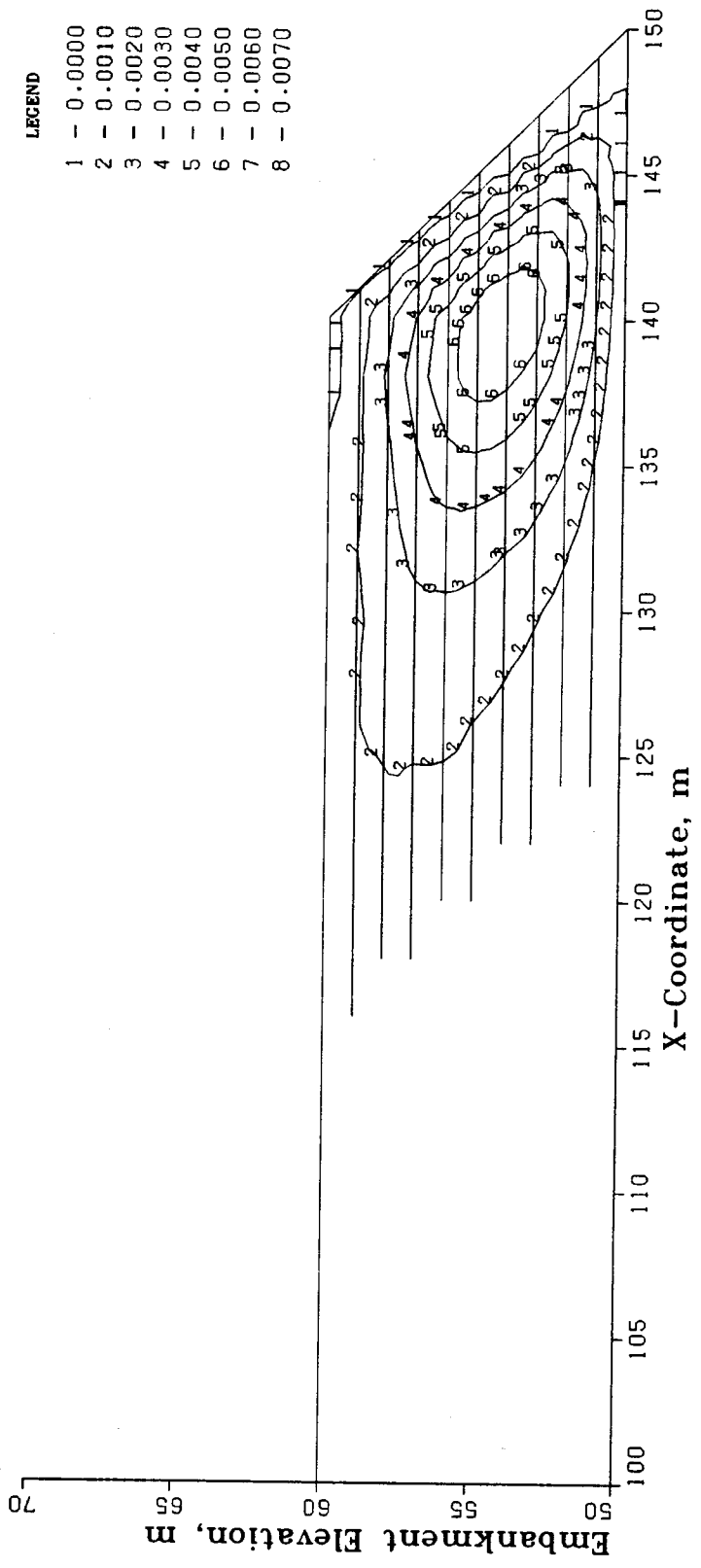


Figure D.8 Horizontal Strains, H = 10 m

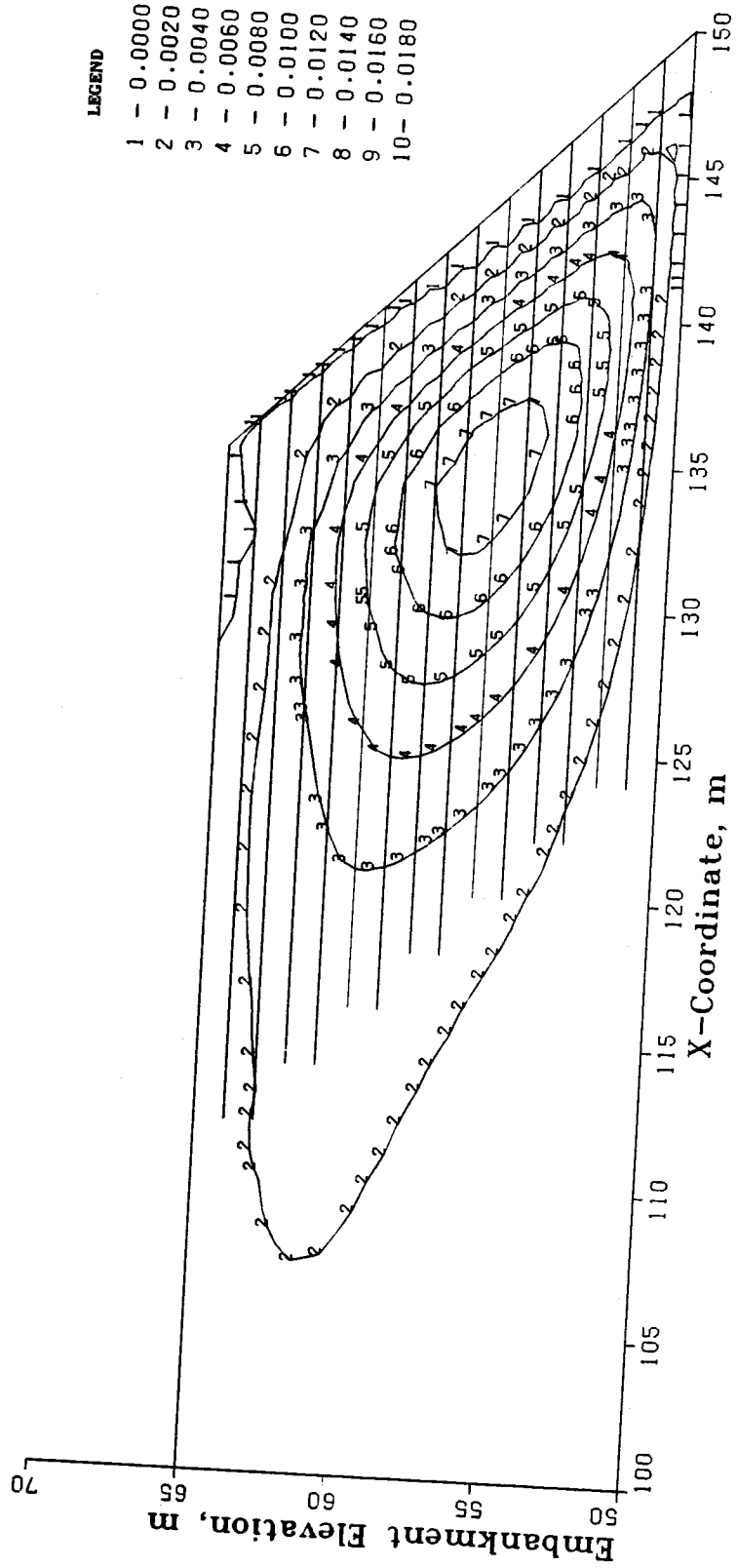


Figure D.9 Horizontal Strains, H = 15 m

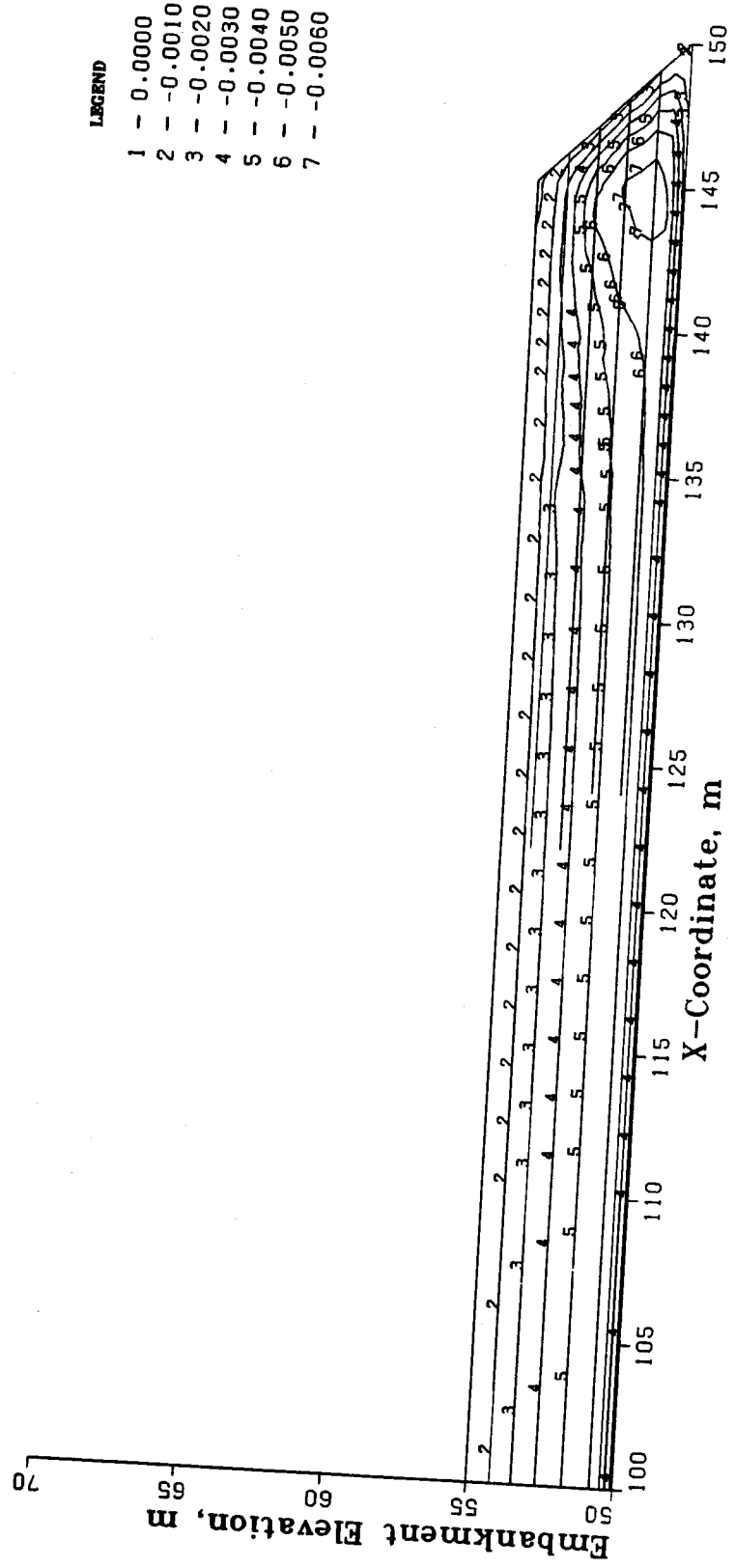


Figure D.10 Vertical Strains, H = 5 m

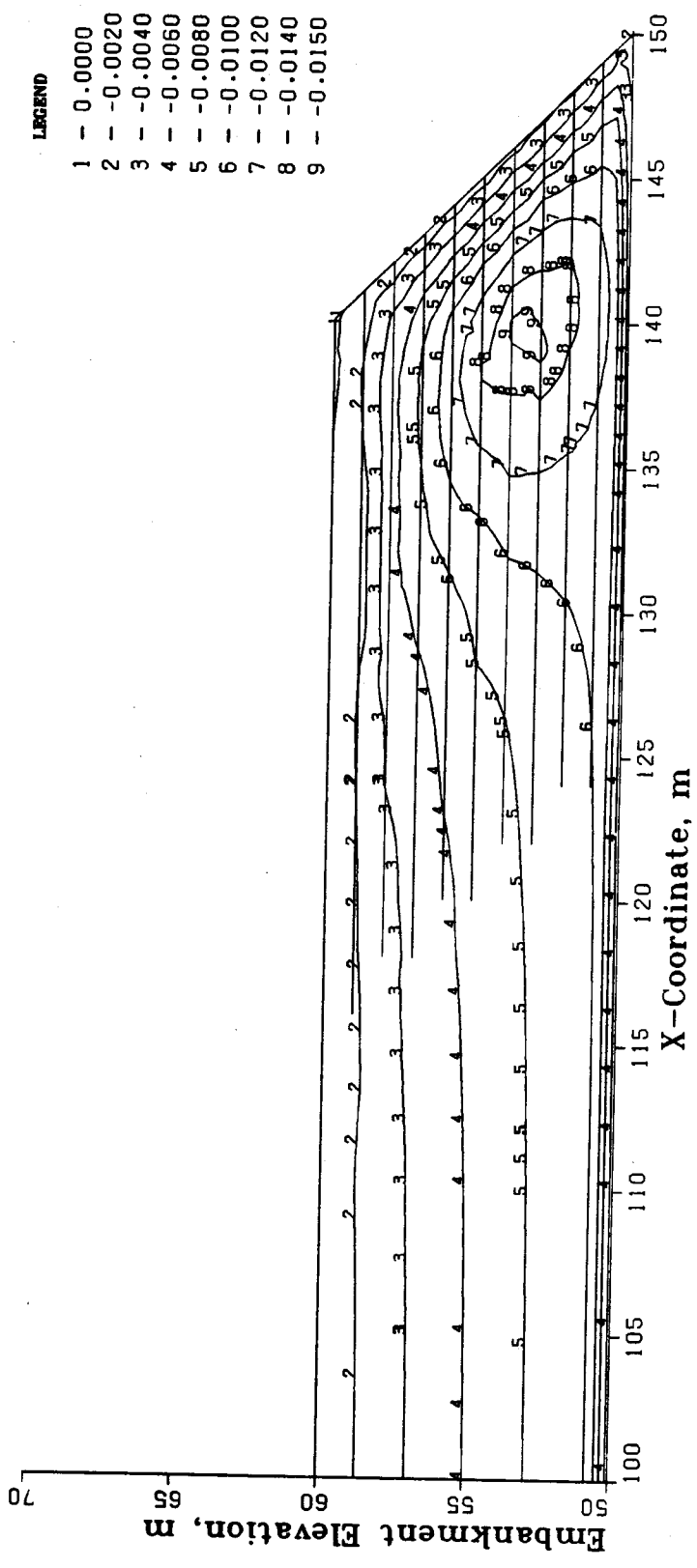


Figure D.11 Vertical Strains, H = 10 m

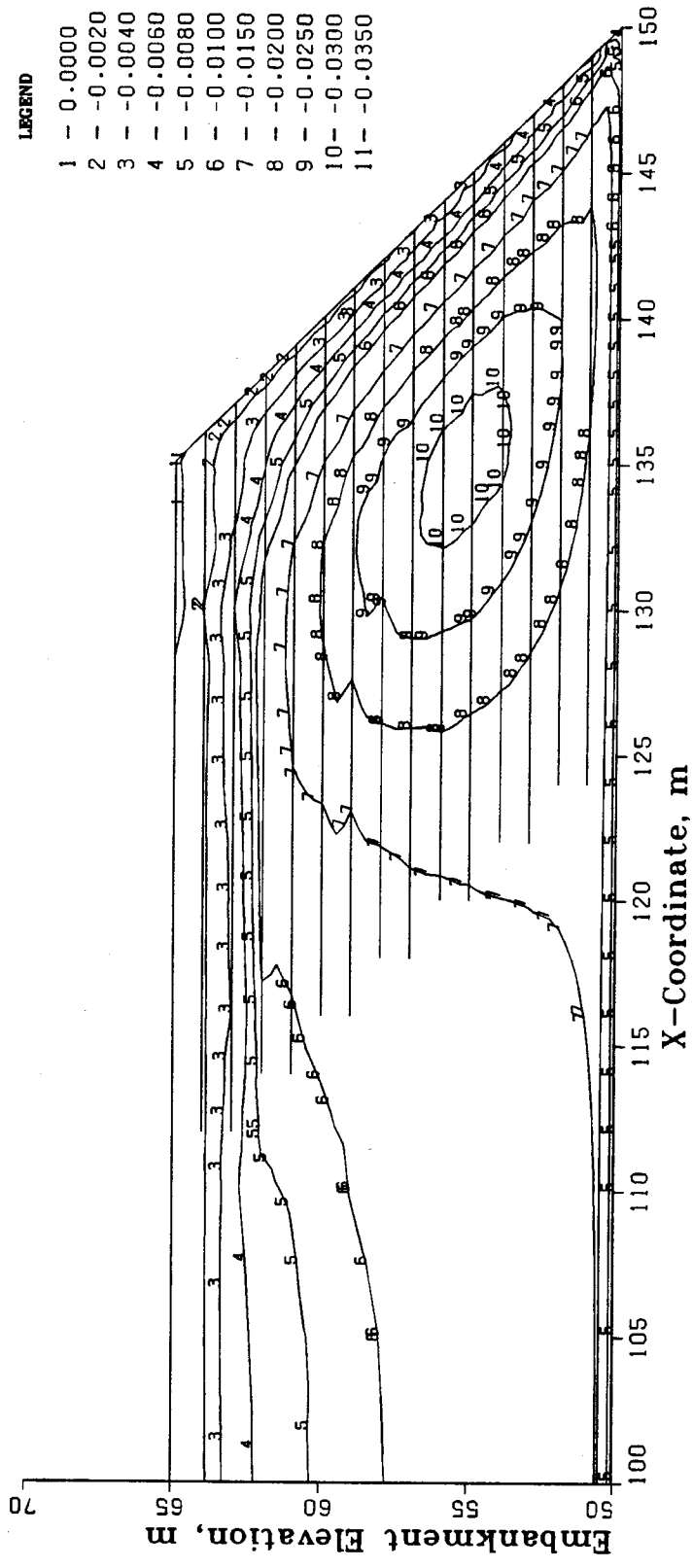


Figure D.12 Vertical Strains, H = 15 m

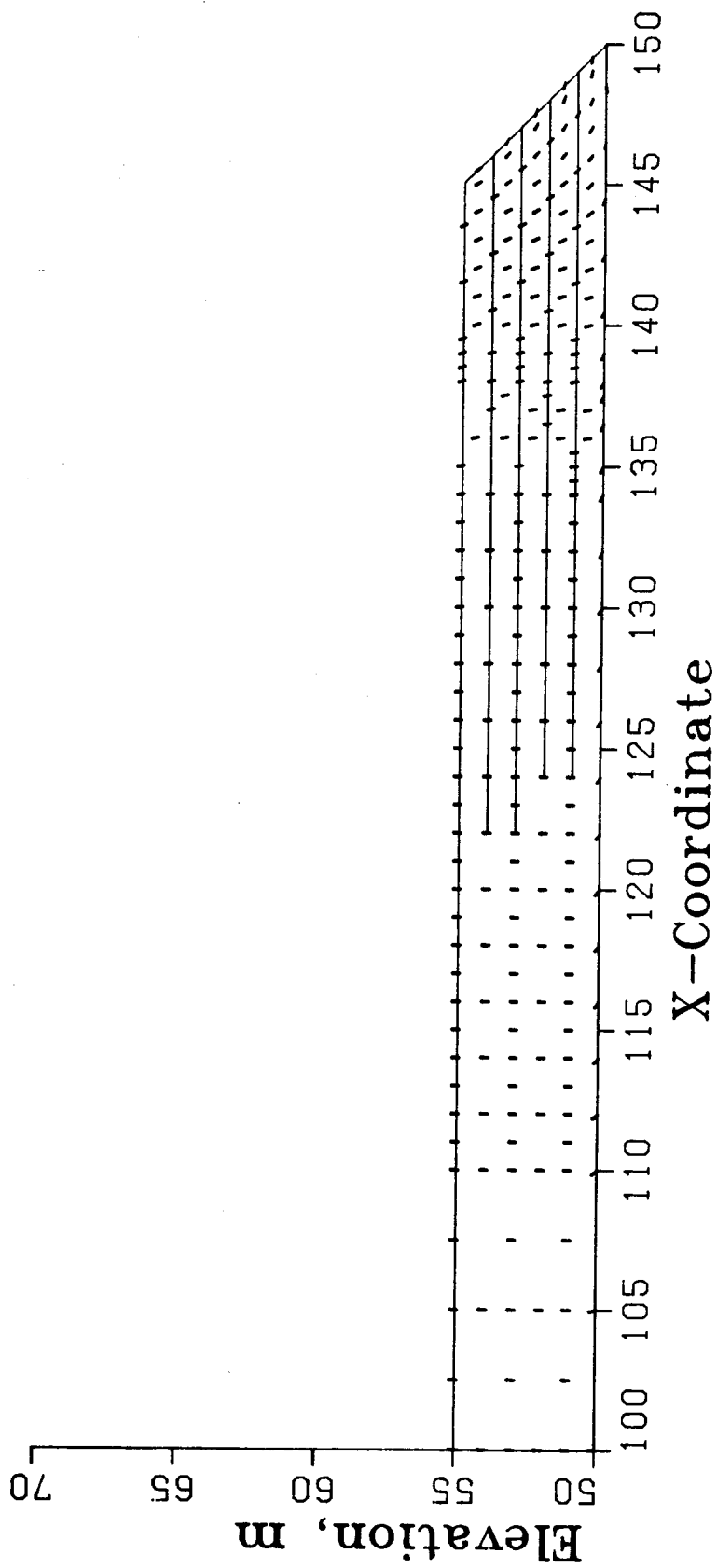


Figure D.13 Velocity Field,  $H = 5$  m, (Scale: 1 cm = .5 m)



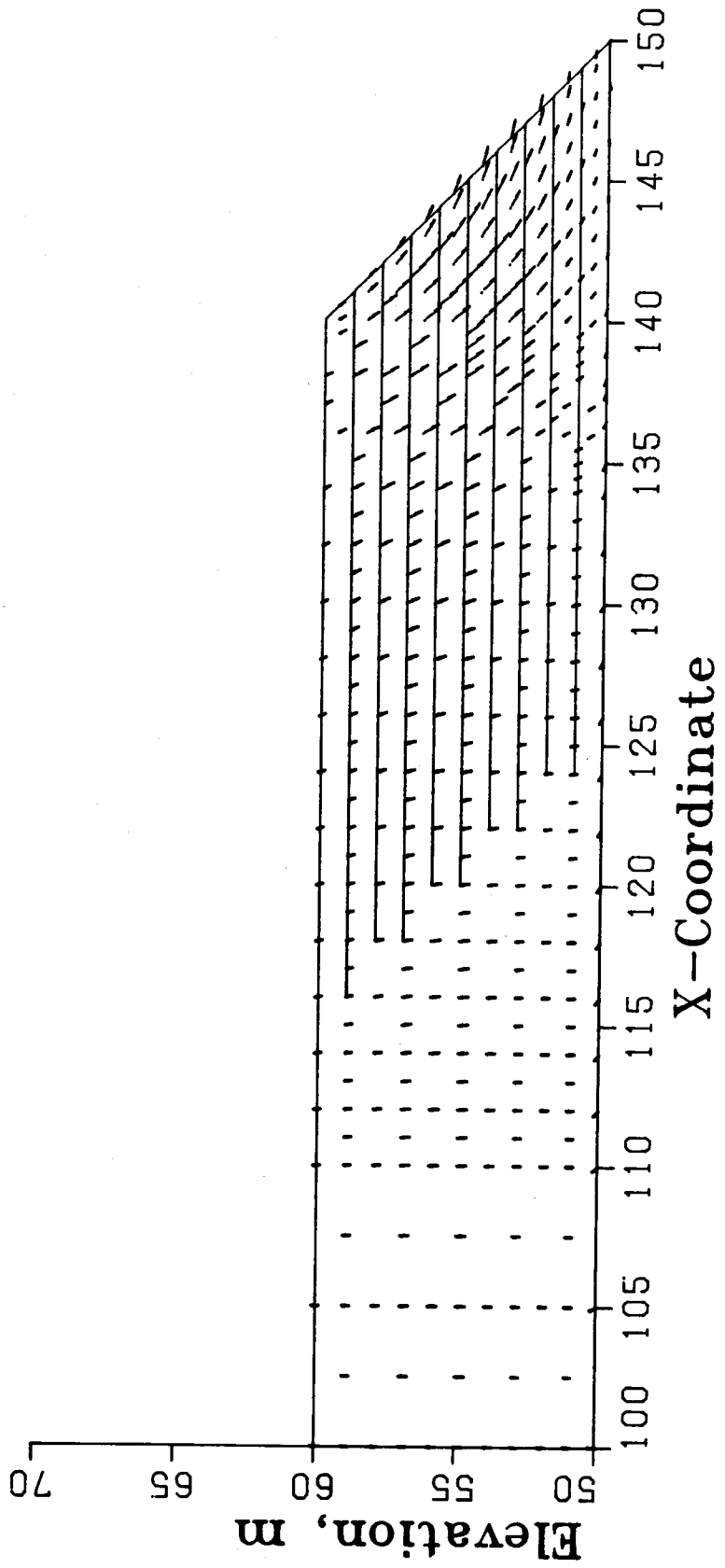


Figure D.14 Velocity Field,  $H = 10$  m, (Scale: 1 cm = .5 m)

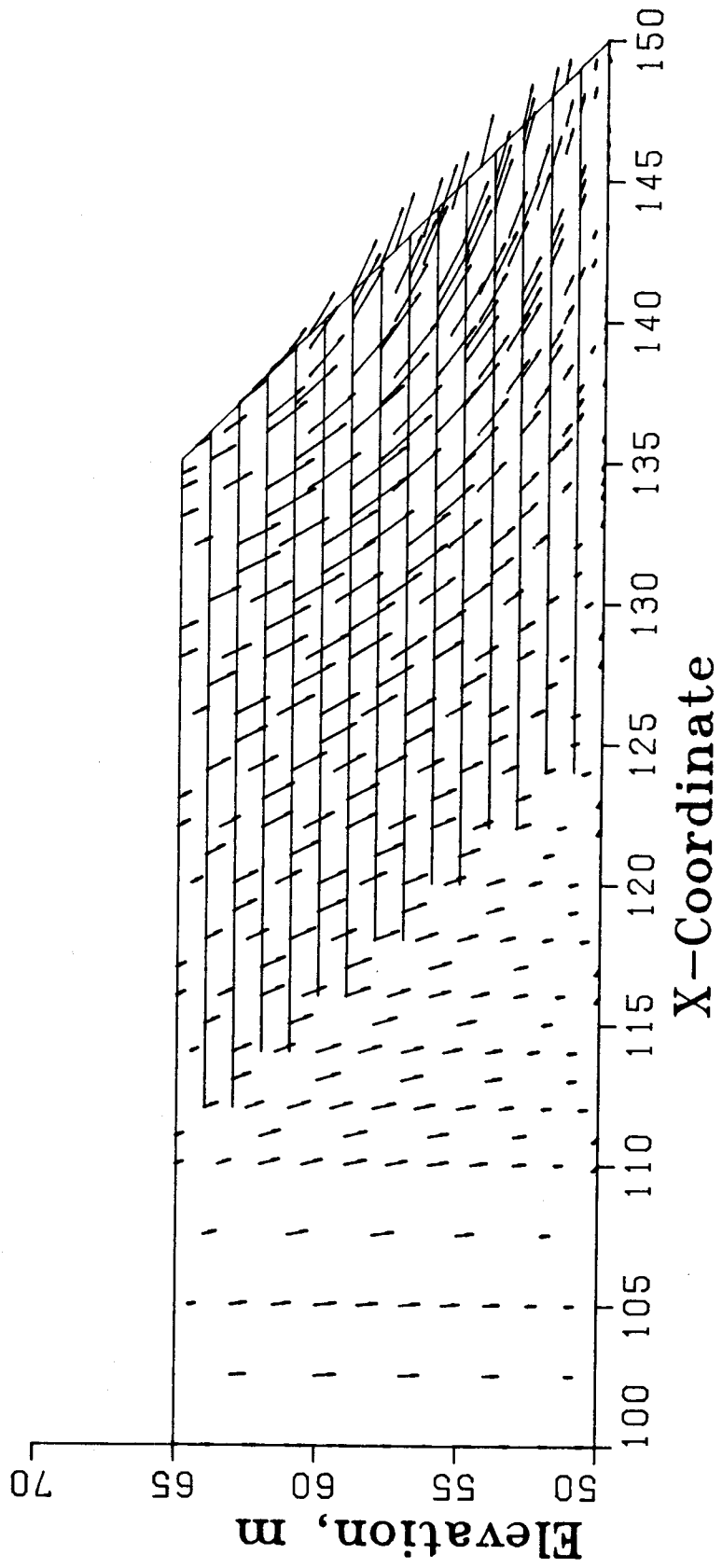


Figure D.15 Velocity Field,  $H = 15$  m, (Scale: 1 cm = .5 m)

**APPENDIX E: Reinforcement Load Distributions from Finite  
Element Analysis of the Reinforced Embankment**

The results of load distribution within each reinforcing layer as determined from the finite element analysis of the reinforced embankment are illustrated on the following figures for embankment heights of 5 m, 10 m, 15 m and 18 m.

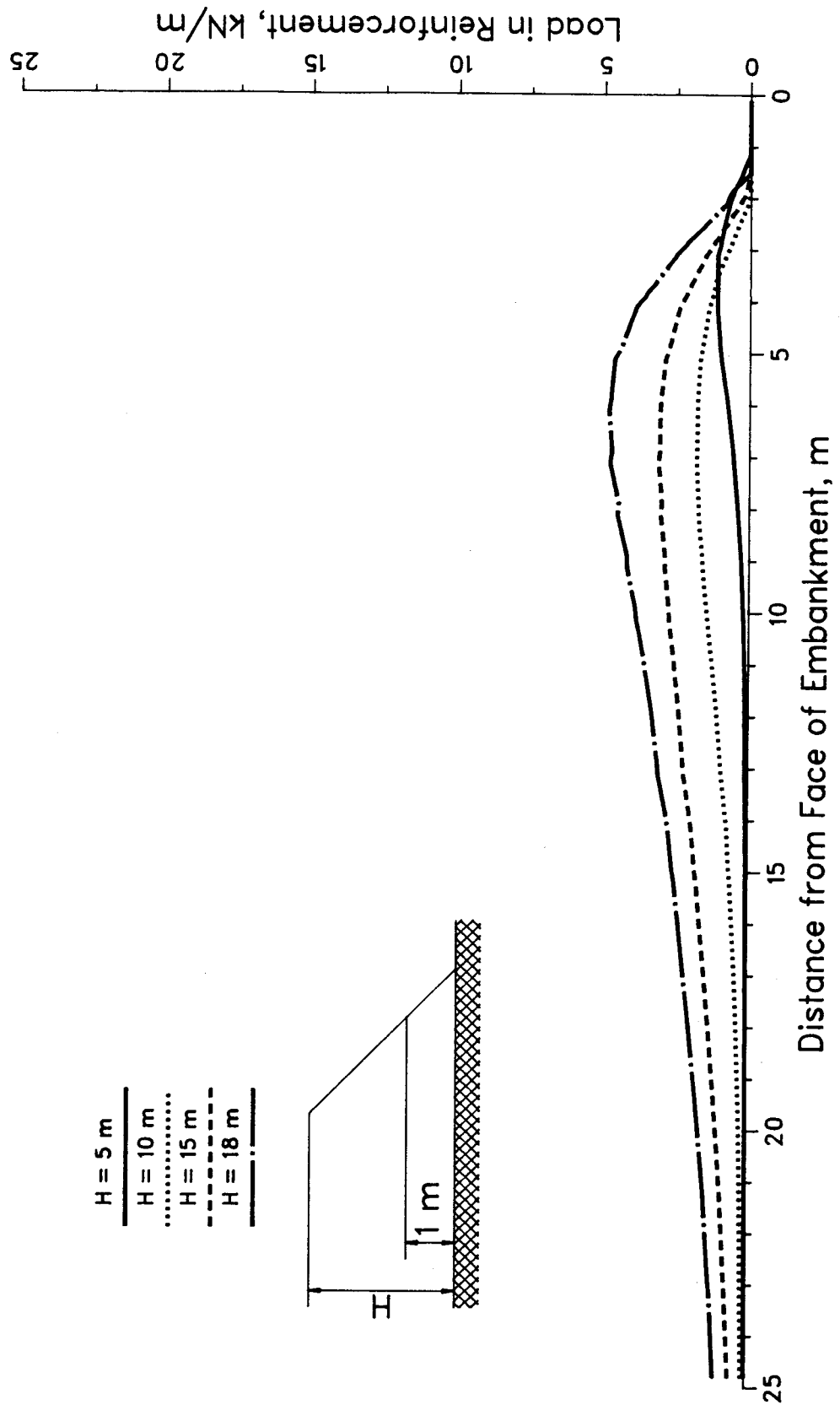


Figure E.1 Load in Reinforcing Layer 1 m Above the Foundation

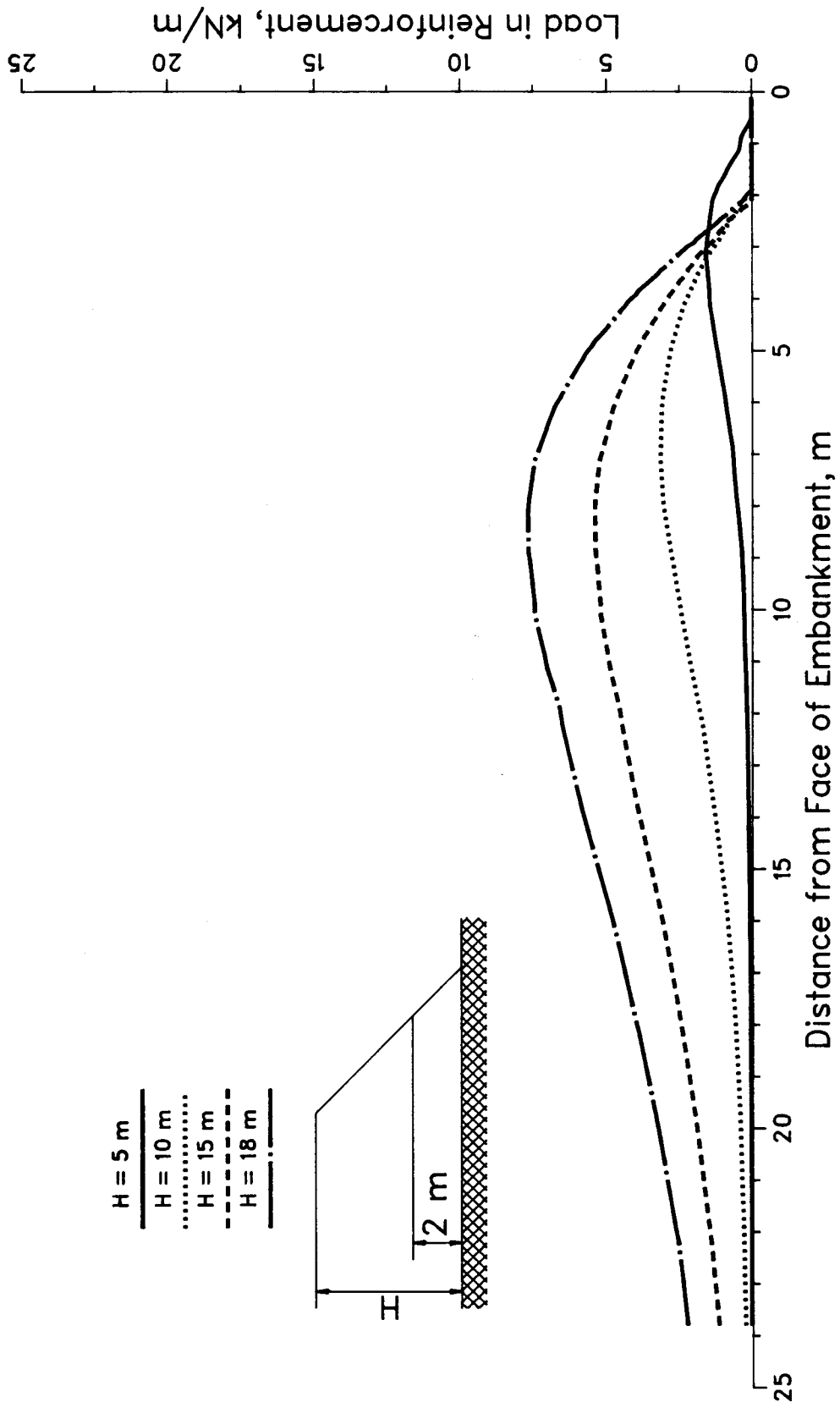


Figure E.2 Load in Reinforcing Layer 2 m Above the Foundation

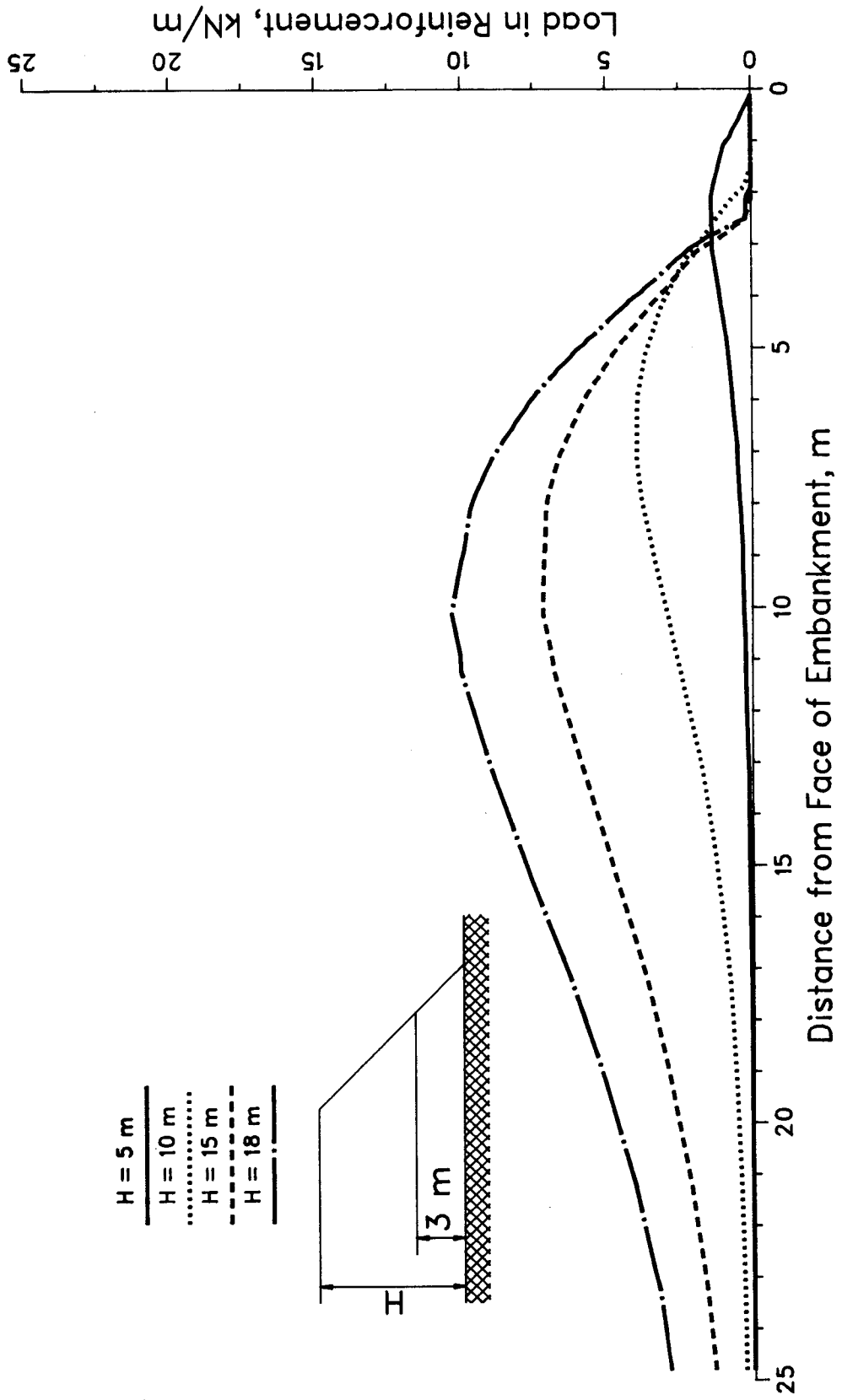


Figure E.3 Load in Reinforcing Layer 3 m Above the Foundation

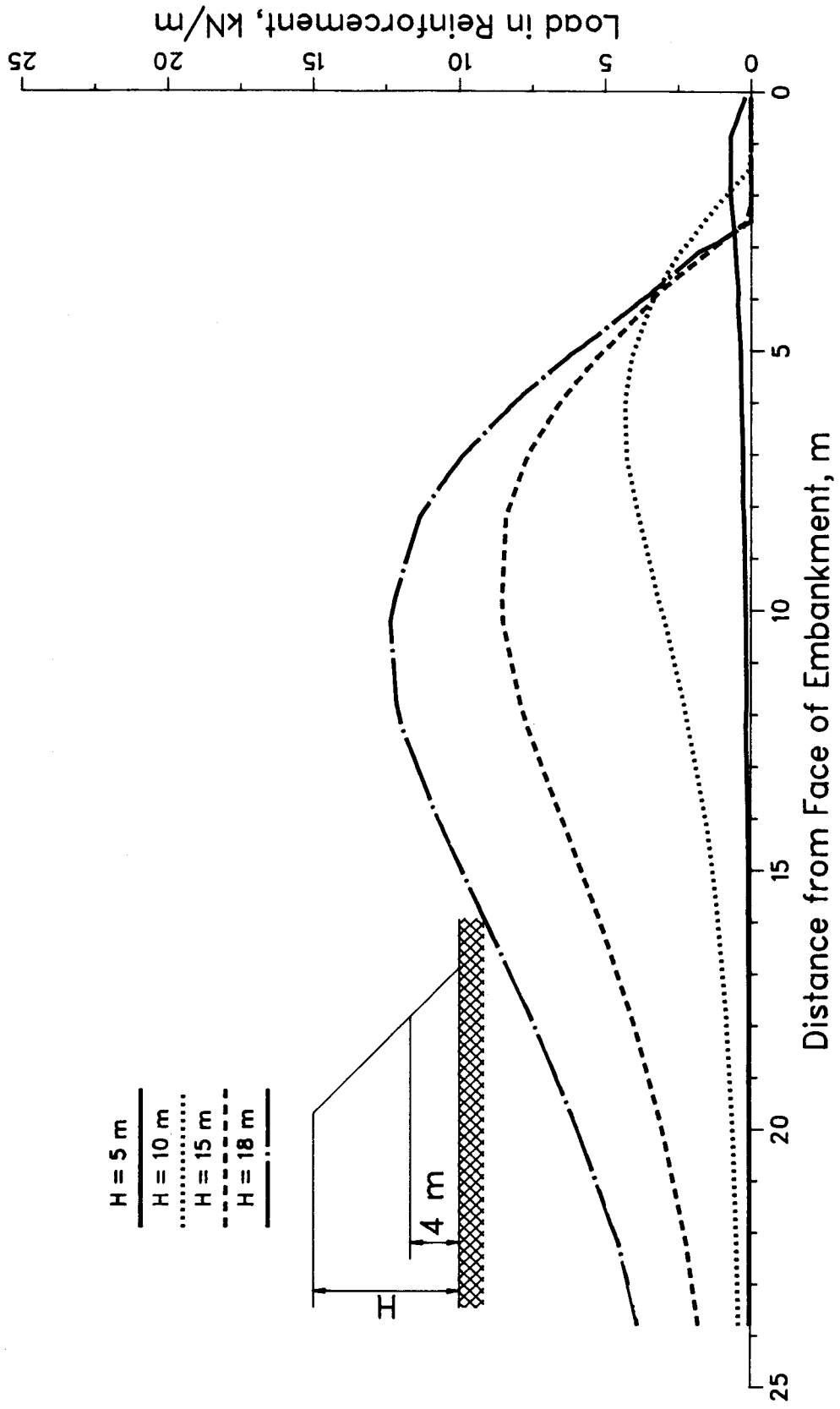


Figure E.4 Load in Reinforcing Layer 4 m Above the Foundation

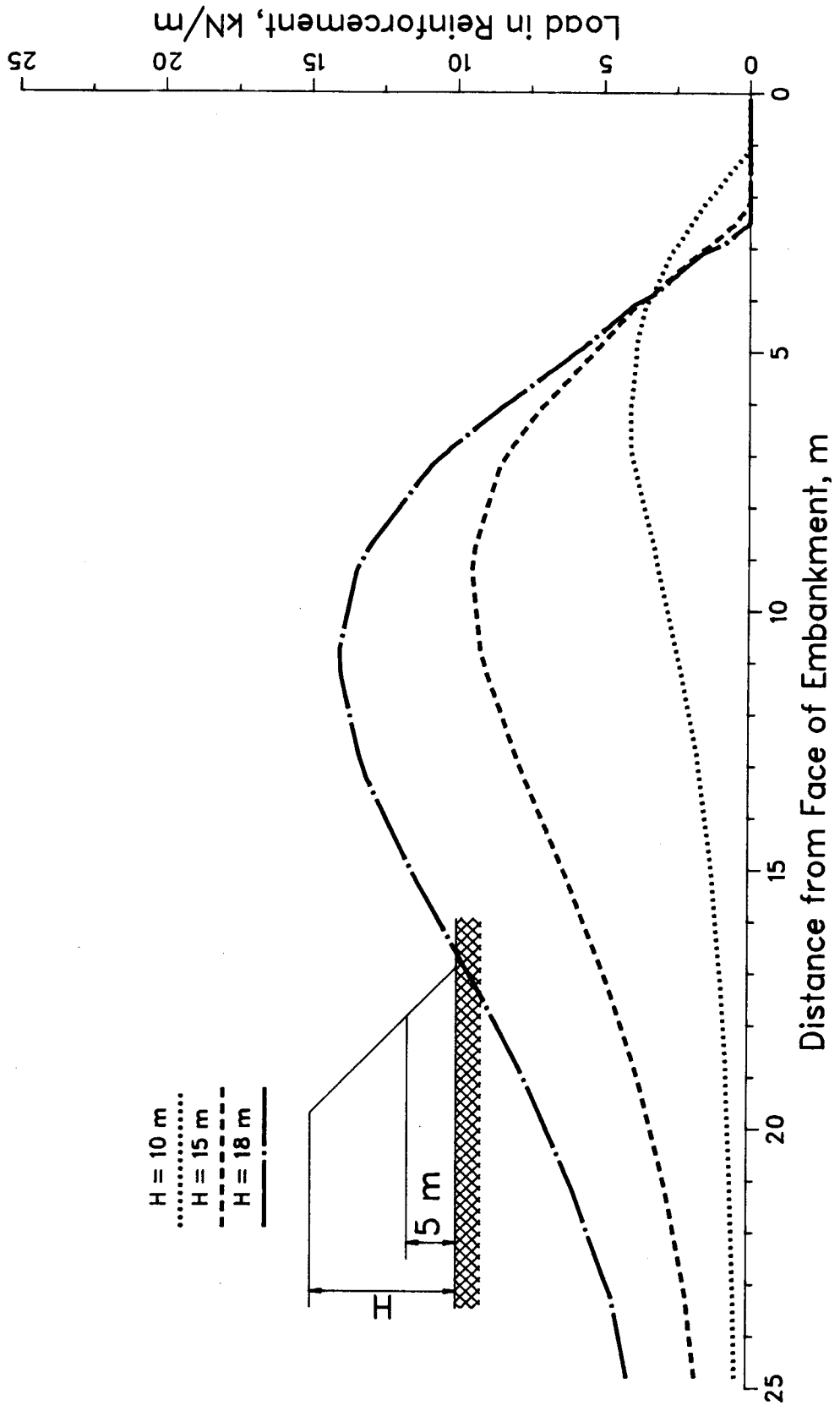


Figure E.5 Load in Reinforcing Layer 5 m Above the Foundation



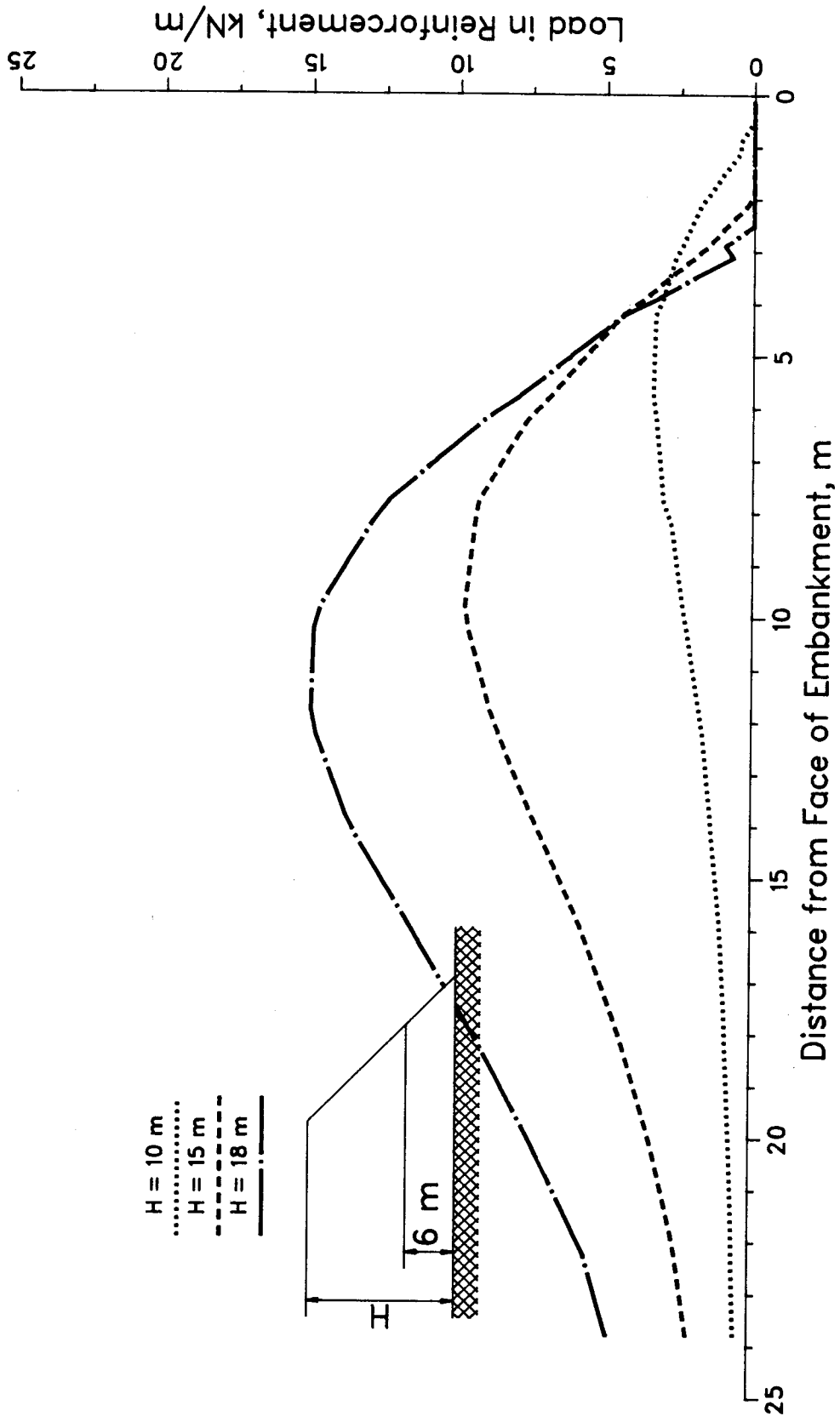


Figure E.6 Load in Reinforcing Layer 6 m Above the Foundation

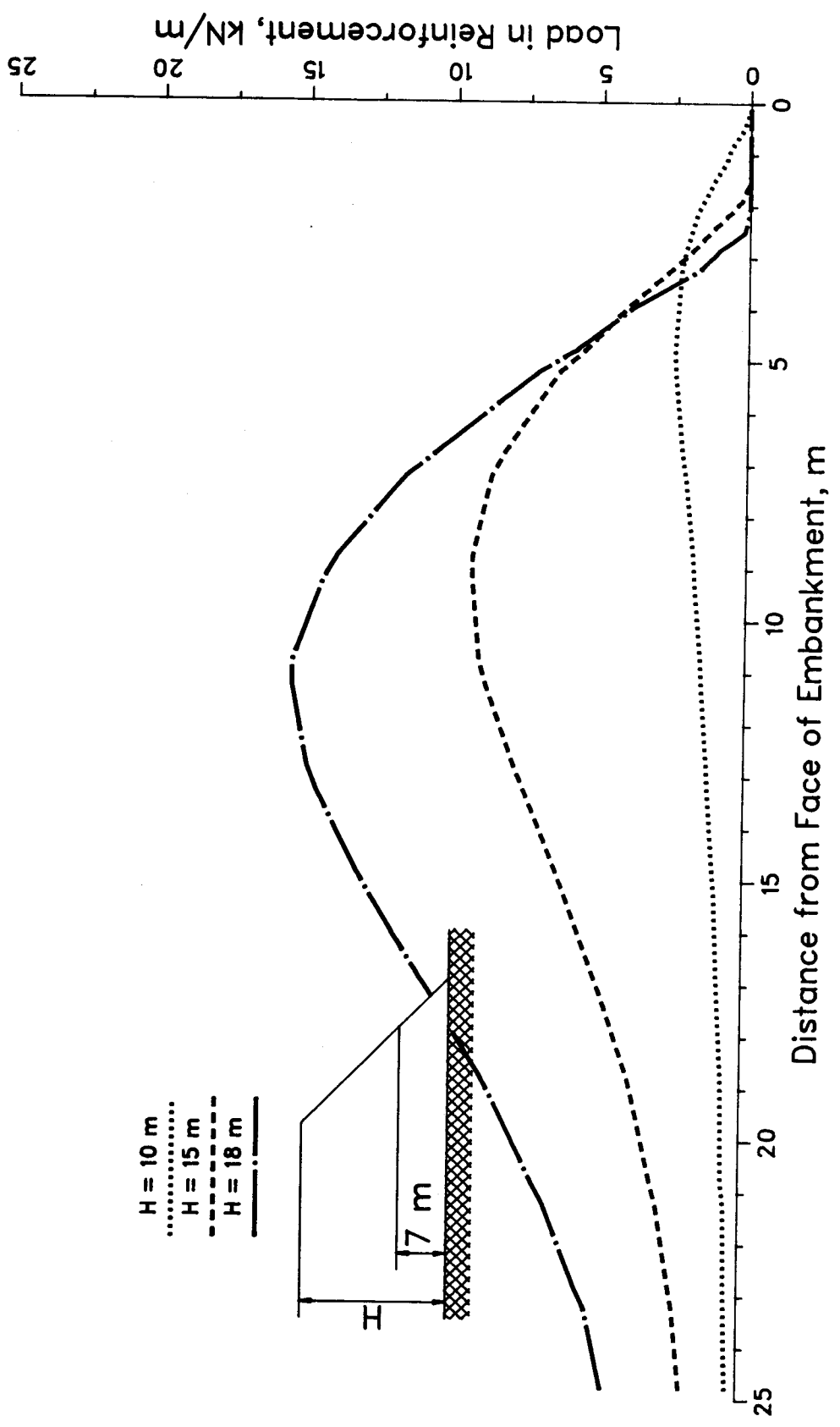


Figure E.7 Load in Reinforcing Layer 7 m Above the Foundation

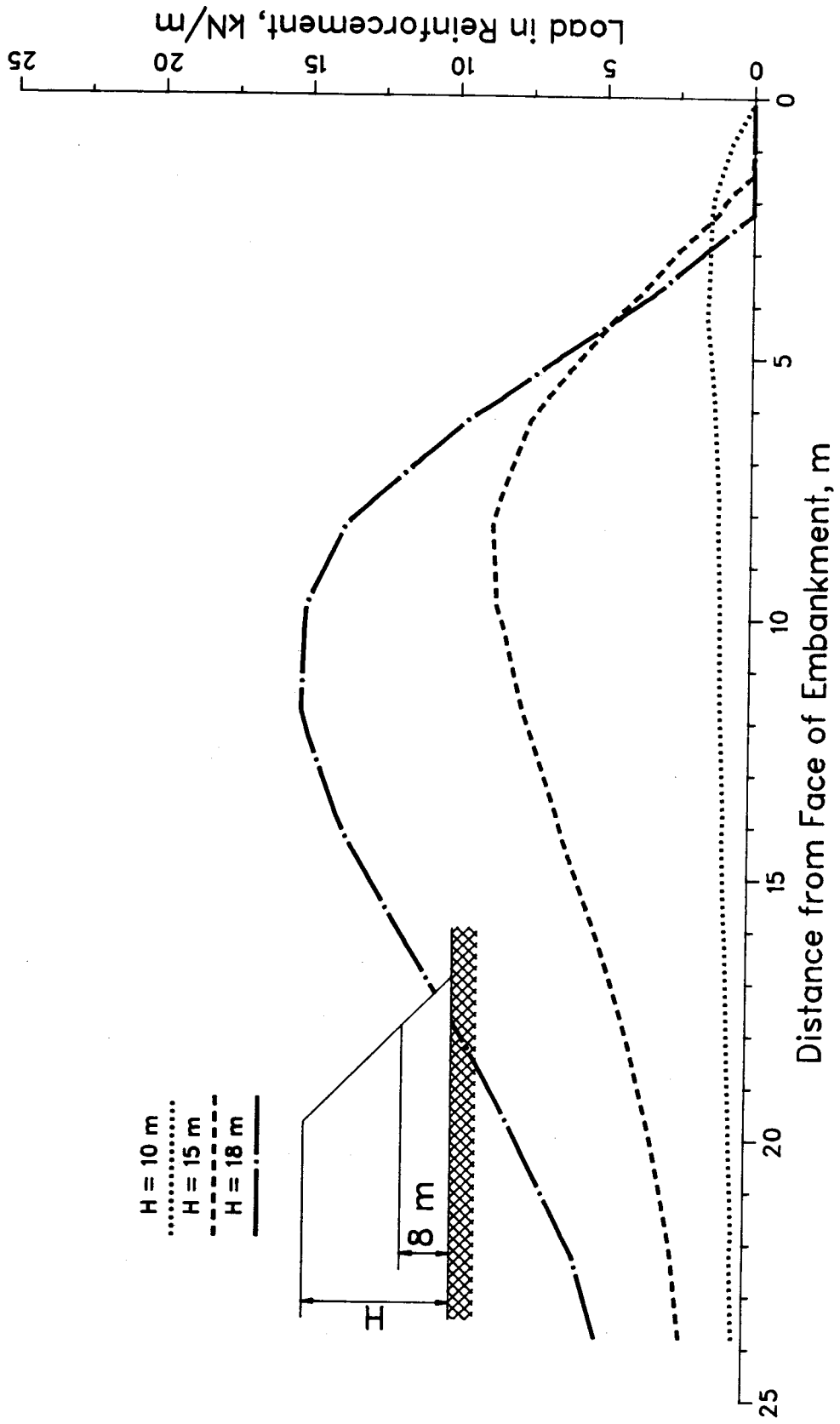


Figure E.8 Load in Reinforcing Layer 8 m Above the Foundation

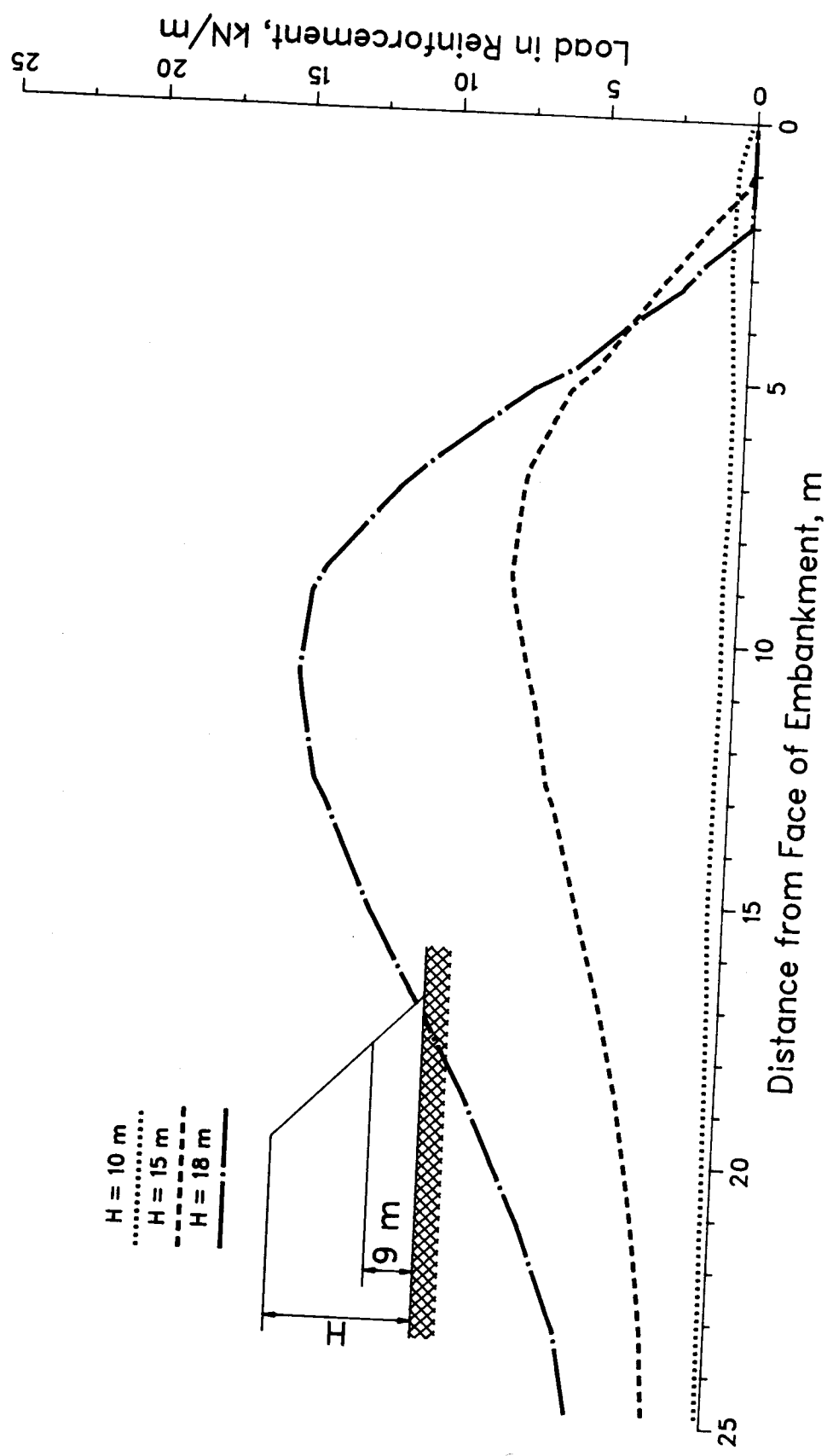


Figure E.9 Load in Reinforcing Layer 9 m Above the Foundation

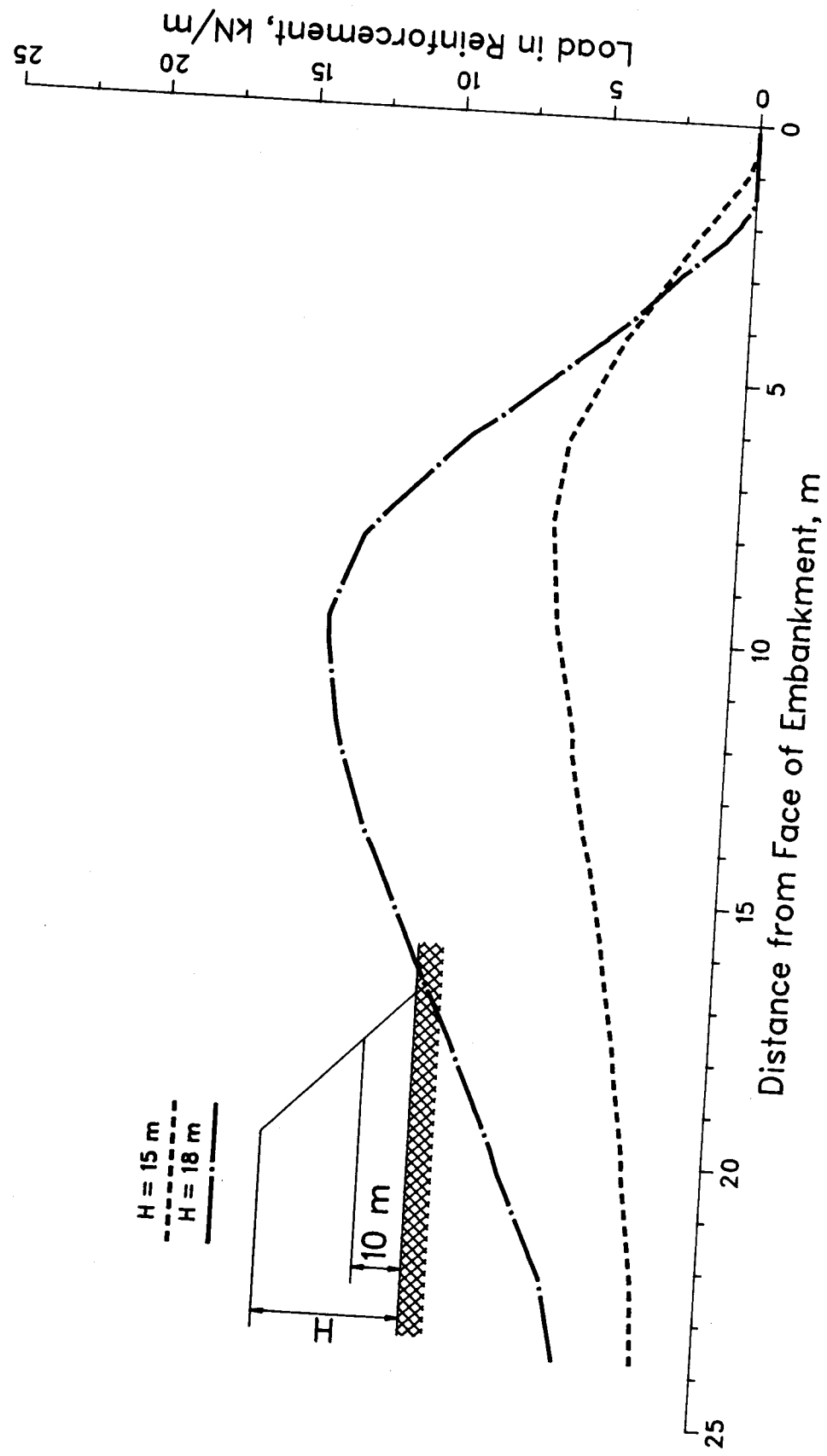


Figure E.10 Load in Reinforcing Layer 10 m Above the Foundation

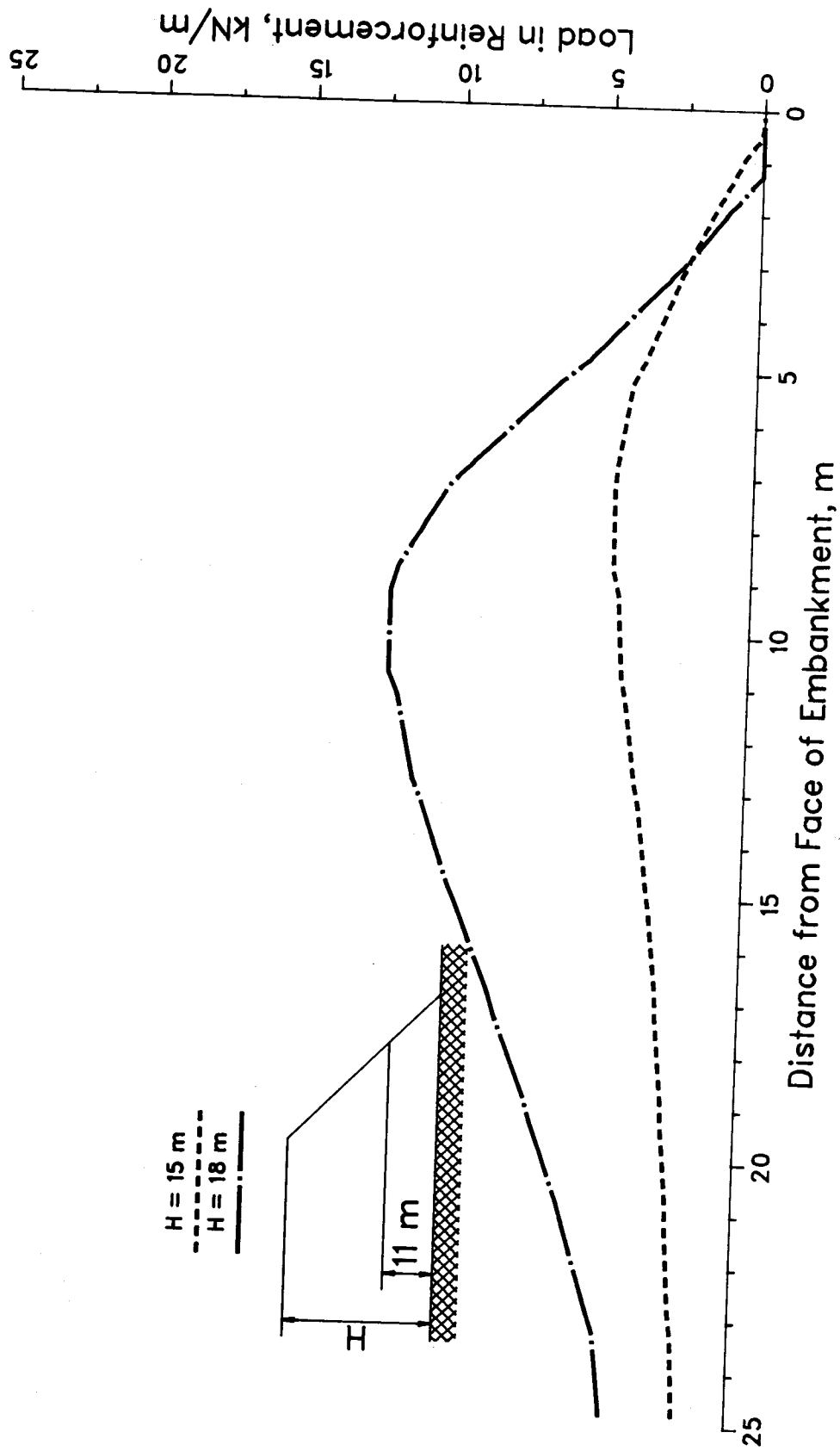


Figure E.11 Load in Reinforcing Layer 11 m Above the Foundation

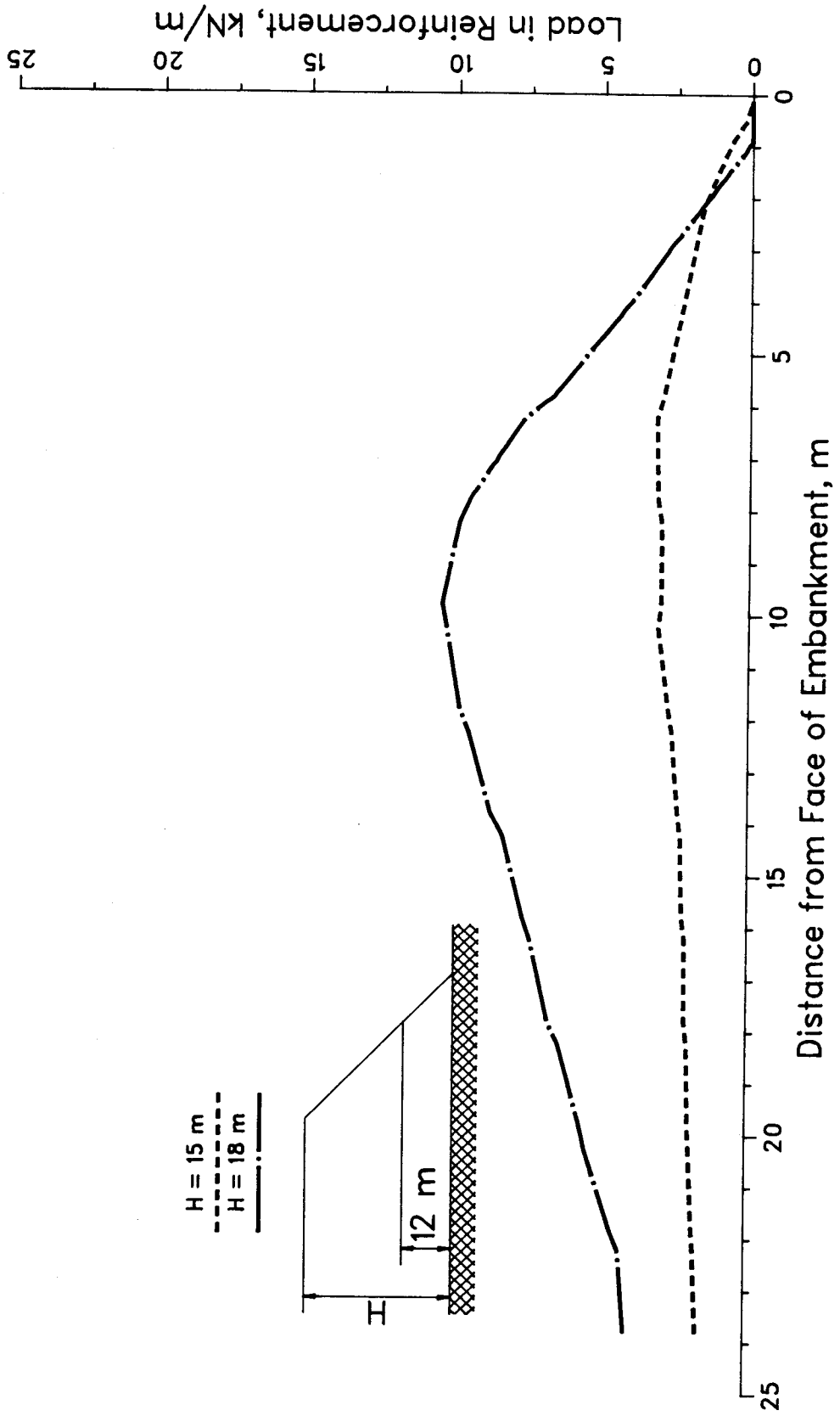


Figure E.12 Load in Reinforcing Layer 12 m Above the Foundation

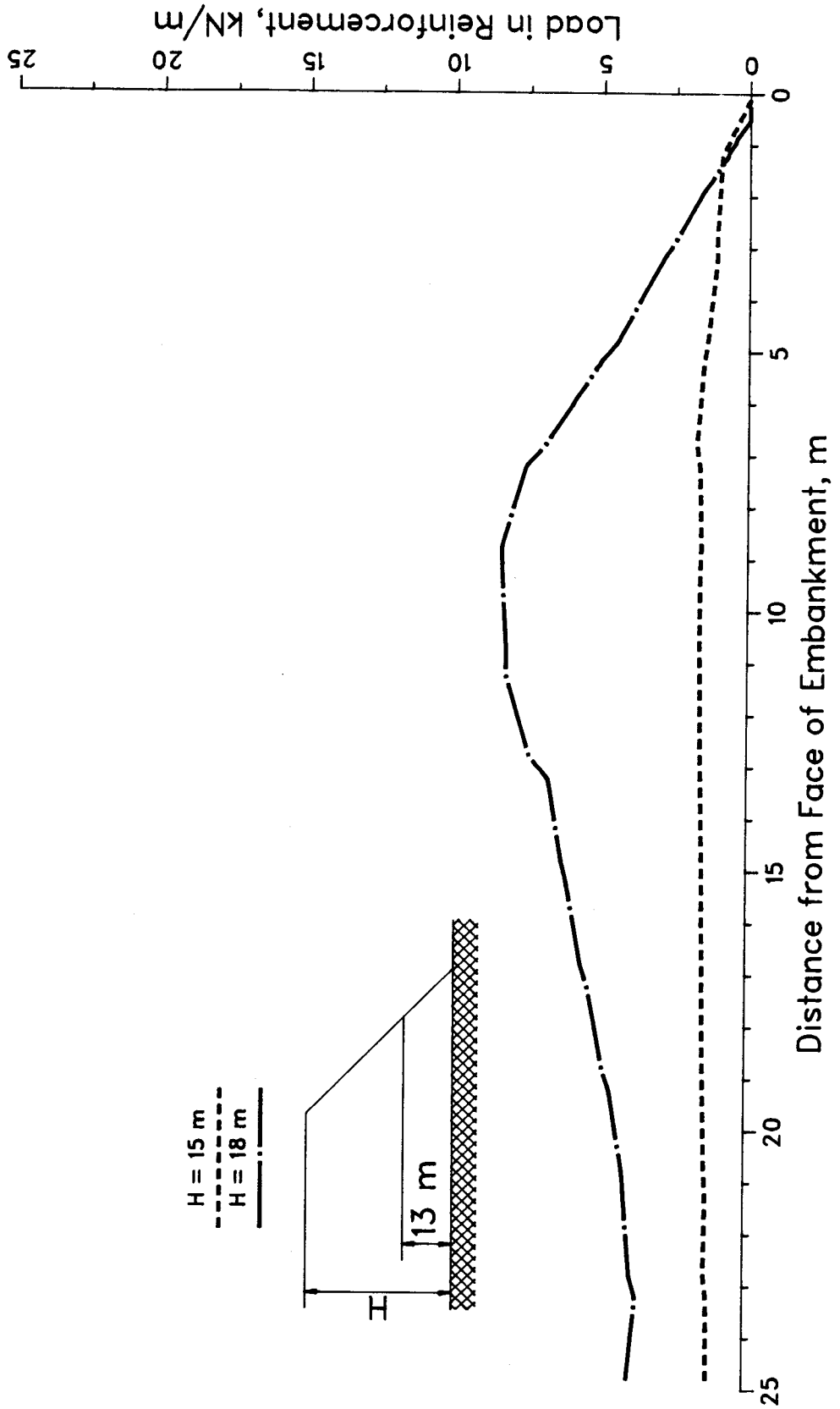


Figure E.13 Load in Reinforcing Layer 13 m Above the Foundation



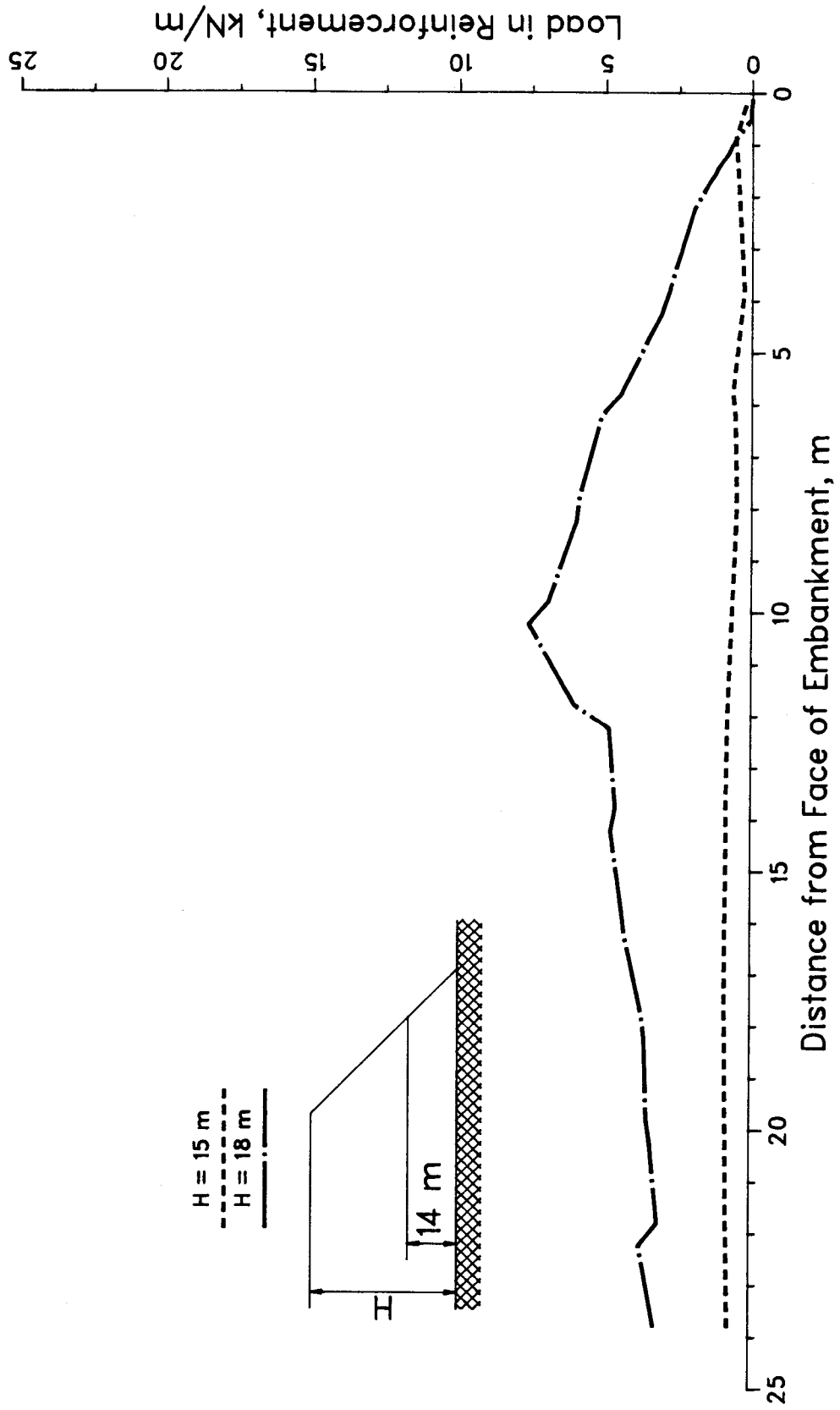


Figure E.14 Load in Reinforcing Layer 14 m Above the Foundation

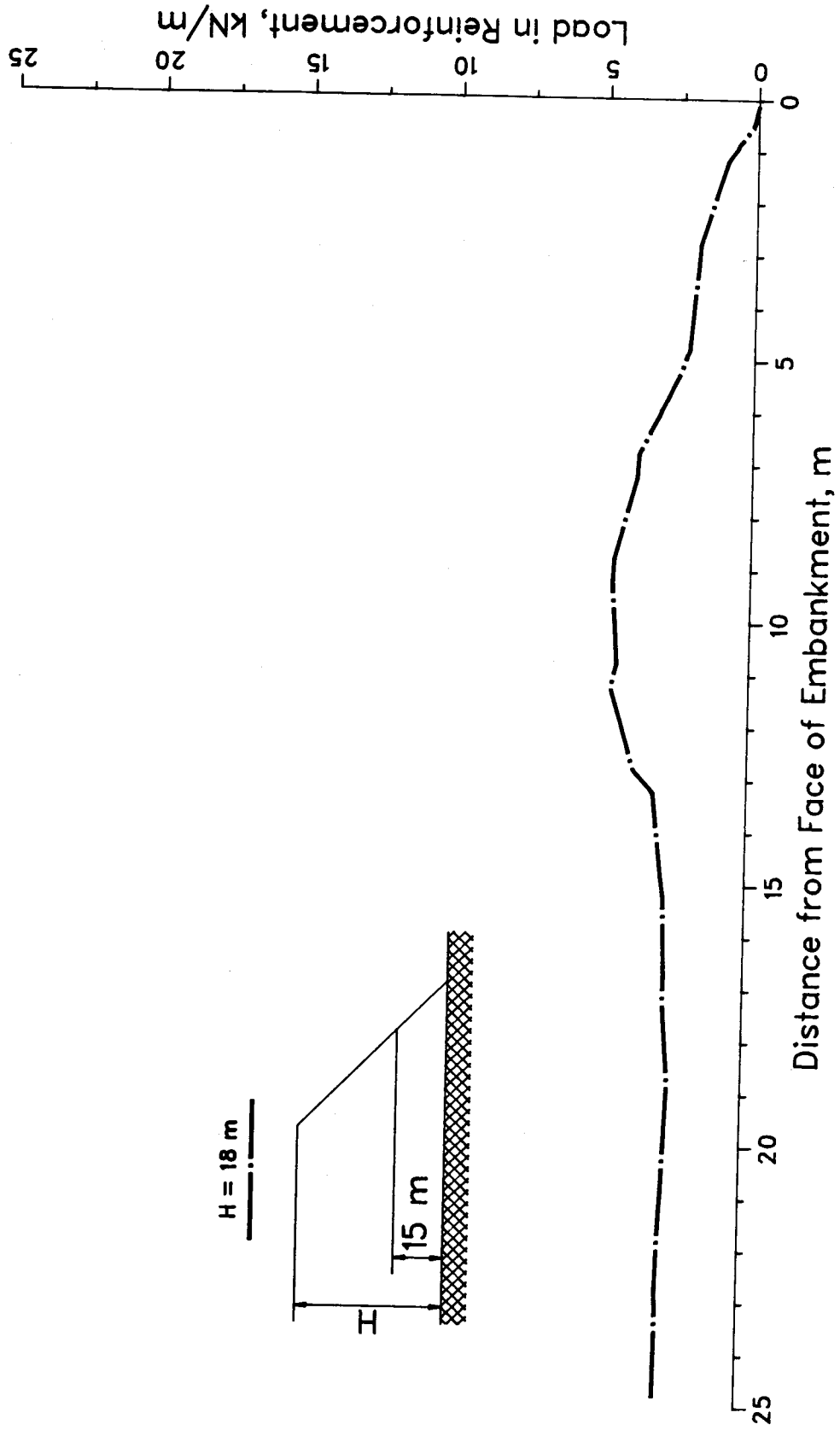


Figure E.15 Load in Reinforcing Layer 15 m Above the Foundation

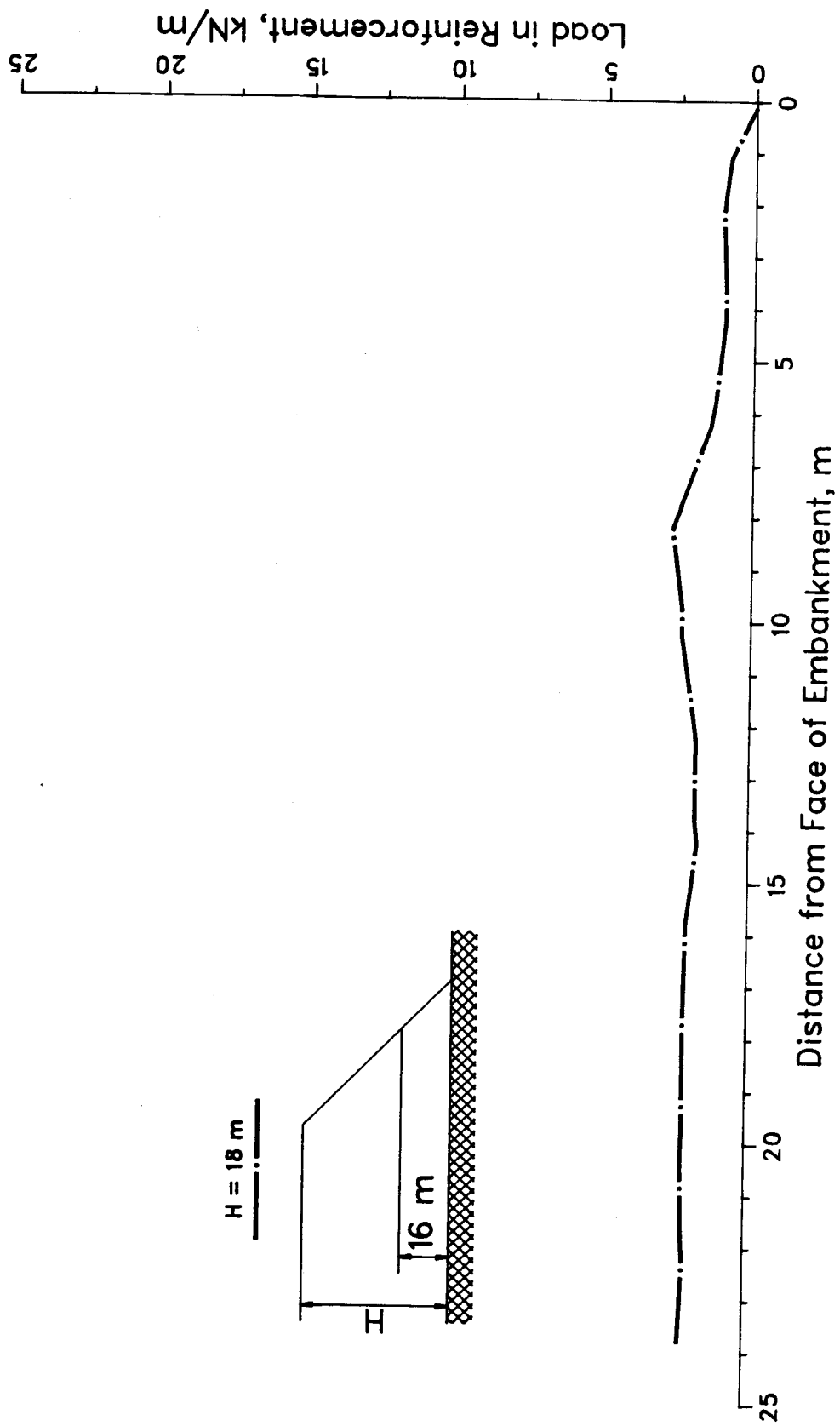


Figure E.16 Load in Reinforcing Layer 16 m Above the Foundation

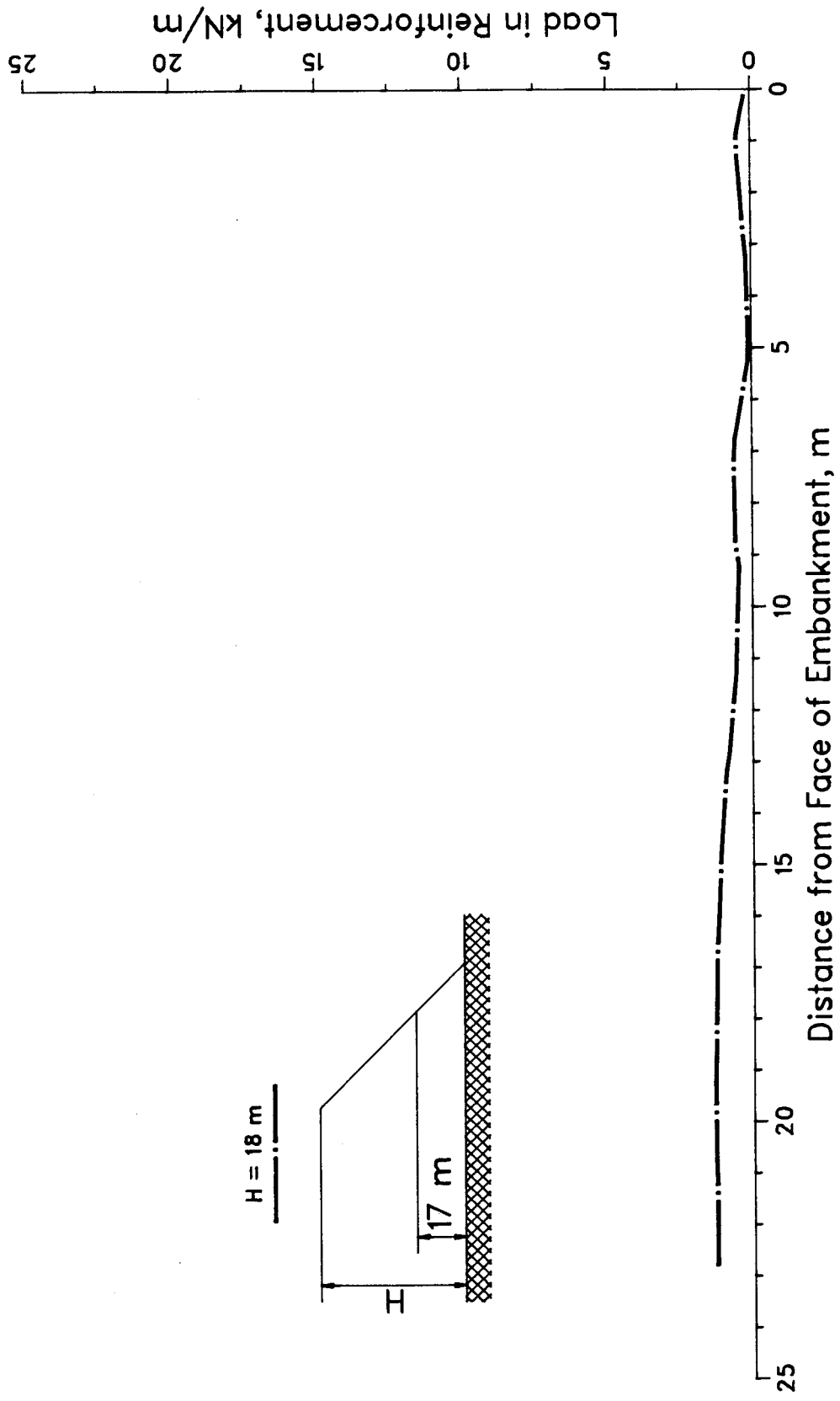


Figure E.17 Load in Reinforcing Layer 17 m Above the Foundation

## APPENDIX F: Factor of Safety Calculations using the Finite Element Results

The method used in calculating the factor of safety of both the nonreinforced and reinforced soil slopes from the finite element results is presented in this appendix. The procedure for determining the factor of safety consisted of obtaining the contours of  $\sigma_x$ ,  $\sigma_y$  and  $\tau_{xy}$  at each embankment height for both the nonreinforced and reinforced slopes. The critical slip surfaces determined by Bishop's Modified Method are superimposed on the stress contours and the  $\sigma_x$ ,  $\sigma_y$  and  $\tau_{xy}$  distributions along the slip surface are computed from the intersection of the slip surface with the stress contours. The normal and shear stresses along the slip surface are calculated using the following relationships:

$$\sigma_n = \sigma_x \cos^2 \theta + \sigma_y \sin^2 \theta + 2\tau_{xy} \sin \theta \cos \theta \quad [\text{F.1}]$$

$$\tau = \tau_{xy} (\cos^2 \theta - \sin^2 \theta) - (\sigma_x - \sigma_y) \sin \theta \cos \theta \quad [\text{F.2}]$$

The angle  $\theta$  refers to the angle of inclination of the slip surface at any point along the surface. The orientation of the slip surface ( $\theta$ ) can be calculated for each point as well as the distance of each point along the slip surface. The beginning of each slip surface begins at the top of the slope and ends at the toe of the slope. Once the normal and shear stresses are determined along the slip surface, their distributions along the slip surface can be plotted and

integrated to find the factor of safety. The equation used in determining the factor of safety from the finite element results is:

$$F_r = \frac{\int_L (c + \sigma_n \tan \phi) dL}{\int_L (\tau) dL} \quad [F.3]$$

The following section presents the determination of the factor of safety for the nonreinforced and reinforced embankment height of 15 m. The tables following this section give the information on the remaining embankment heights of 5 m, 10 m and 18 m for both the nonreinforced and reinforced embankment cases.

### F.1 Nonreinforced Slope

Figures F.1, F.2 and F.3 illustrate the  $\sigma_x$ ,  $\sigma_y$  and  $\tau_{xy}$  contours respectively for a nonreinforced embankment height of 15 m. The slip surface drawn in these figures is the critical slip surface determined by BMM ( see Table 5.2 ). The "tick" marks along each slip surface represent sampling points where the stress values were determined. From these values, distributions of  $\sigma_x$ ,  $\sigma_y$  and  $\tau_{xy}$  along the slip surface can be drawn. Figures F.4, F.5 and F.6 illustrate these stress distributions. Using Figures F.4 to F.6, the stresses at equal length intervals along the slip surface were selected. Table F.1 lists the values of these stresses along with the slip surface inclination,  $\theta$ , and the  $\sigma_n$  and  $\tau$  values at each length interval. Figures F.7 and F.8 show the

29\*

distribution of  $\sigma_n$  and  $\tau$ , respectively, along the slip surface. Using these stress distributions in Equation F.3, the factor of safety can be computed. The integral expressions in Equation F.3 were evaluated using Reimann Sums.

The following calculations are done to compute the factor of safety:

$$F_r = \frac{\int_L (c + \sigma_n \tan \phi) dL}{\int_L (\tau) dL}$$

$$\begin{aligned} \int_L (c + \sigma_n \tan \phi) dL &= c \times L + \tan \phi \times \sum_{i=1}^n (\sigma_{ni} \Delta L_i) \\ &= 33(27.3) + \tan(17^\circ) \{ 7.5(1.0) + 2[ 26.4 + 51.4 + \\ &\quad 67.2 + 82.7 + 99.1 + 110.2 + 115.1 + 117.1 + 115.8 \\ &\quad + 110.6 + 101.2 + 86.6 + 62.7] + 15.0(.3) \} \\ &= 1605.4 \text{ kN/m} \end{aligned}$$

$$\begin{aligned} \int_L (\tau) dL &= 11.0(1.0) + 2 \{ 23.1 + 34.5 + 38.5 + 44.7 + \\ &\quad 49.7 + 53.6 + 56.2 + 57.2 + 56.3 + 54.1 + \\ &\quad 51.8 + 49.4 + 43.0 \} \\ &= 1235.2 \text{ kN/m} \end{aligned}$$

$$\therefore F_{fe} = \frac{1605.4}{1235.2} = 1.3$$

## F.2 Reinforced Slope

The finite element results from the analysis of the reinforced slope provides an opportunity to calculate the factor of safety of the reinforced slope based on the strength of the soil alone,  $F_{r_0}$ . The value of  $F_{r_0}$  is computed using the same procedure explained in Section F.1 for the nonreinforced slope so no additional details will be provided here. Figures F.9, F.10 and F.11 illustrate the contours of  $\sigma_x$ ,  $\sigma_y$  and  $\tau_{xy}$  for the reinforced embankment height of 15 m. The slip surface drawn on these figures is the critical slip surface determined by BMM based on a horizontal force assumption. Figures F.12, F.13 and F.14 show the distribution of  $\sigma_x$ ,  $\sigma_y$  and  $\tau_{xy}$  along the slip surface. Table F.2 lists the values of these stresses which are used to determine the  $\sigma_n$  and  $\tau$  values along the slip surface. Figure F.15 and F.16 illustrate the distributions of the  $\sigma_n$  and  $\tau$  along the slip surface which are used in calculating  $F_{r_0}$  for the reinforced slope.

The determination of the overall factor of safety of the reinforced soil slope,  $F_r$ , is based on the following equation

$$F_r = F_{r_0} + \Delta F_r \quad [F.4]$$

The parameters in Equation F.4 are fully explained in



Chapter 6. Briefly however,  $F_{r0}$  is calculated by the procedure explained above and  $\Delta F_r$  is computed assuming the reinforcement force is a free body force acting at the intersection of the slip surface and the reinforcement.

Table F.1 Stress Distribution Values Along Slip Surface in Nonreinforced Embankment, H = 15 m

NONREINFORCED SLOPE  
 Radius of Slip Surface = 21.0 m

H = 15 m  
 Length of Slip Surface = 27.3 m

Slope Angle = 45 deg

L ( m )	Slip Surface Inclination ( degrees )	Horizontal Stress (kPa)	Vertical Stress (kPa)	Shear Stress (kPa)	Normal Stress (kPa)	Mobilized Shear Stress (kPa)
2	68	11	-39	-8	26.4	23.1
4	62.6	-6	-75	-11	51.4	34.5
6	57.1	-17	-96	-6	67.2	38.5
8	51.7	-26	-118	0	82.7	44.7
10	46.2	-40	-140	7	99.1	49.7
12	40.8	-51	-155	15	110.2	53.6
14	35.2	-59	-162	23	115.1	56.2
16	29.8	-66	-161	32	117.1	57.2
18	24.4	-73	-156	38	115.8	56.3
20	18.9	-77	-140	44	110.6	54.1
22	13.5	-77.5	-121	47	101.2	51.8
24	8	-73	-100	47.5	86.6	49.4
26	2.5	-59	-74	42.5	62.7	43

Table F.2 Stress Distribution Values Along Slip Surface in Reinforced Embankment, H = 15 m

**REINFORCED SLOPE**  
 Radius of Slip Surface = 18.0 m      H = 15 m      Slope Angle = 45 deg  
 Length of Slip Surface = 28.1 m

L ( m )	Slip Surface Inclination ( degrees )	Horizontal Stress (kPa)	Vertical Stress (kPa)	Shear Stress (kPa)	Normal Stress (kPa)	Mobilized Shear Stress (kPa)
1	77.8	-5	-19	-3	17.1	5.6
3	71.4	-13	-56	-6	48	17.8
5	65.1	-24	-88	-5	72.8	27.7
7	58.7	-35.5	-118	0	95.7	36.6
9	52.3	-51	-149	5.5	117.7	46
11	46	-66	-170	14	133.8	51.5
13	39.6	-77	-183	22	141.7	56.2
15	33.2	-85	-188	31	144.3	59.6
17	26.9	-90.5	-184	39.5	141.5	61.1
19	20.5	-96	-172	46	135.5	59.6
21	14.1	-101	-156	50.5	128.1	57.5
23	7.7	-90.5	-130	52	105	55.4
25	1.4	-70	-104	48	72.4	48.8
27	-5	-40	-65	39	33.4	36.2

Table F.3 Stress Distribution Values Along Slip Surface in Nonreinforced Embankment, H = 5 m

NONREINFORCED SLOPE  
 Radius of Slip Surface = 8.0 m      H = 5 m      Slope Angle = 45 deg  
 Length of Slip Surface = 9.91 m

L (m)	Slip Surface Inclination (degrees)	Horizontal Stress (kPa)	Vertical Stress (kPa)	Shear Stress (kPa)	Normal Stress (kPa)	Mobilized Shear Stress (kPa)
0.5	64.4	-1.5	-1.1	-2	7.7	5
1	60.8	-5	-2.1	-1.5	15.9	7.6
1.5	57.3	-9	-3.1	-0.5	24.1	10.2
2	53.7	-11.5	-4.0	0	30	13.6
2.5	50.1	15.5	-4.6	1	34.4	14.8
3	46.5	-19	-51.5	2.5	38.6	16.1
3.5	42.9	-22.5	-5.6	5	43	17.1
4	39.4	-2.5	-59.5	6.5	45.3	18.2
4.5	35.8	-2.8	-62.5	9	48.3	19.2
5	32.2	-3.1	-64.5	11	50.4	19.9
5.5	28.6	-34.5	-6.5	13.5	52.8	20.1
6	25	-3.6	-64.5	15	52.6	20.6
6.5	21.5	-38.5	-6.2	17	53.3	20.4
7	17.9	-39.5	-5.8	19	52.4	20.8
7.5	14.3	-4.0	-52.5	20	50.3	20.6
8	10.7	-39.5	-4.7	20	47.1	20
8.5	7.1	-37.5	-40.5	19.5	42.3	19.3
9	3.5	-3.1	-3.0	17.5	33.1	17.3
9.5	0	-14.5	-14.5	12.5	14.5	12.5

Table F.4 Stress Distribution Values Along Slip Surface in Nonreinforced Embankment, H = 10 m

**NONREINFORCED SLOPE**  
 Radius of Slip Surface = 14.0 m      H = 10 m      Slope Angle = 45 deg  
 Length of Slip Surface = 18.9 m

L ( m )	Slip Surface Inclination ( degrees )	Horizontal Stress (kPa)	Vertical Stress (kPa)	Shear Stress (kPa)	Normal Stress (kPa)	Mobilized Shear Stress (kPa)
2	65.3	-10.5	-4.6	-3.5	37.1	15.8
4	57.1	-20	-7.6	-1	58.6	25.9
6	48.9	-31.5	-9.8	4.5	73.7	32.3
8	40.7	-43	-11.4	12.5	85.6	37
10	32.5	-53.5	-12.0	22	92.6	39.4
12	24.3	-59.5	-11.9	29.5	91.7	41.8
14	16.1	-60	-10.5	35	82.1	41.6
16	7.9	-54.5	-8.1	36	64.8	38.2
18	-0.3	-3.6	-3.6	29	35.7	29
18.9	-4	-26.5	-1.6	25	23	25.5

Table F.5 Stress Distribution Values Along Slip Surface in Nonreinforced Embankment, H = 18 m

NONREINFORCED SLOPE  
 Radius of Slip Surface = 25.5 m      H = 18 m      Slope Angle = 45 deg  
 Length of Slip Surface = 32.4 m

L ( m )	Slip Surface		Horizontal Stress (kPa)	Vertical Stress (kPa)	Shear Stress (kPa)	Normal Stress (kPa)	Mobilized Shear Stress (kPa)
	Inclination ( degrees )	Stress (kPa)					
2	68.4	9.5	-33	-11	19.7	22.6	
4	63.9	11	-61	-15	35.2	37.6	
6	59.4	-6	-85	-14	52.3	41.4	
8	54.9	-20	-105	-8	69.4	42.7	
10	50.4	-31	-132	-1.5	89.5	49.9	
12	45.9	-42	-155	5	105.3	56.3	
14	41.4	-51	-171	13	116.4	61.2	
16	36.9	-60.5	-182	22	125.4	64.5	
18	32.4	-69	-189	30	130.6	67.1	
20	27.9	-77	-188	37.5	132.3	67	
22	23.4	-83	-179	45	130.9	65.8	
24	18.9	-89.5	-165	51	128.7	63.4	
26	14.4	-95	-147	55	124.7	60.7	
28	9.9	-100	-122	56	119.6	56.4	
30	5.4	-102	-87	53	111.8	50.7	
32	0.9	-70	-20	20	70.6	19.2	

Table F.6 Stress Distribution Values Along Slip Surface in Reinforced Embankment, H = 5 m

**REINFORCED SLOPE**  
 Radius of Slip Surface = 7.5 m      H = 5 m      Slope Angle = 45 deg  
 Length of Slip Surface = 9.8 m

L ( m )	Slip Surface Inclination ( degrees )	Horizontal Stress (kPa)	Vertical Stress (kPa)	Shear Stress (kPa)	Normal Stress (kPa)	Mobilized Shear Stress (kPa)
1	62.7	-4	-21	0	17.4	6.9
2	55	-12.5	-37.5	0	29.3	11.7
3	47.4	-19.5	-50	3	39	14.9
4	39.8	-25	-61.5	6	45.9	19
5	32.1	-33.5	-65	11	52.3	19
6	24.5	-39.5	-64	15	55	19.1
7	16.8	-40.5	-59	18.5	52.3	20.5
8	9.2	-35	-51.5	20	41.7	21.6
9	1.6	-22.5	-34.5	19	23.6	19.3
9.5	-2.3	-10	-20	15	8.8	14.6

Table F.7 Stress Distribution Values Along Slip Surface in Reinforced Embankment, H = 10 m

**REINFORCED SLOPE**  
 Radius of Slip Surface = 13.5 m      H = 10 m      Slope Angle = 45 deg  
 Length of Slip Surface = 19.0 m

L (m)	Slip Surface Inclination (degrees)	Horizontal Stress (kPa)	Vertical Stress (kPa)	Shear Stress (kPa)	Normal Stress (kPa)	Mobilized Shear Stress (kPa)
2	66.5	-11	-40	-3.5	32.8	13
4	58.4	-28	-76	-1	61.9	21.9
6	50.2	-38	-104	5	81.9	31.6
8	42.1	-47	-120	12.5	92.2	37.6
10	33.9	-57.5	-124	22	98.6	39.1
12	25.8	-65	-120	30	98.9	40.2
14	17.6	-70	-108	35.5	93.9	40
16	9.4	-67	-80	36	78.9	36.2
18	1.3	-31	-43	30	32.4	30.2



Table F.8 Stress Distribution Values Along Slip Surface in Reinforced Embankment, H = 18 m

**REINFORCED SLOPE**  
 Radius of Slip Surface = 25.0 m      H = 18 m      Length of Slip Surface = 33.3 m      Slope Angle = 45 deg

L (m)	Slip Surface Inclination (degrees)	Horizontal Stress (kPa)	Vertical Stress (kPa)	Shear Stress (kPa)	Normal Stress (kPa)	Mobilized Shear Stress (kPa)
1	71.7	-8	-20	-2.3	17.4	5.4
3	67.1	-5	-5.7	-10.5	41.6	26
5	62.5	-9.5	-8.8	-1.1	62.3	38.5
7	57.9	-2.4	-11.3	-8	80.7	43.5
9	53.3	-3.5	-14.0	-3.4	99.2	51.3
11	48.7	-5.1	-16.5	2.4	117.7	56.2
13	44.1	-6.5	-18.5	10.1	133.2	60.3
15	39.5	-7.6	-20.0	18.5	144.6	64.4
17	34.9	-8.5	-20.5	27.7	150.3	65.9
19	30.5	-9.0	-20.1	35	149.2	65.5
21	25.9	-9.4	-19.6	42.2	146.6	66.2
23	21.3	-9.5	-18.5	48	139.4	65.8
25	16.7	-9.6	-17.0	52.2	130.8	63.9
27	12.1	-9.5	-15.2	54.6	119.9	61.5
29	7.6	-85.5	-11.7	53.5	100.1	55.8
31	3	-5.5	-8.8	47.1	60	48.6
32.6	-0.7	-20	-50	38	19.1	37.6

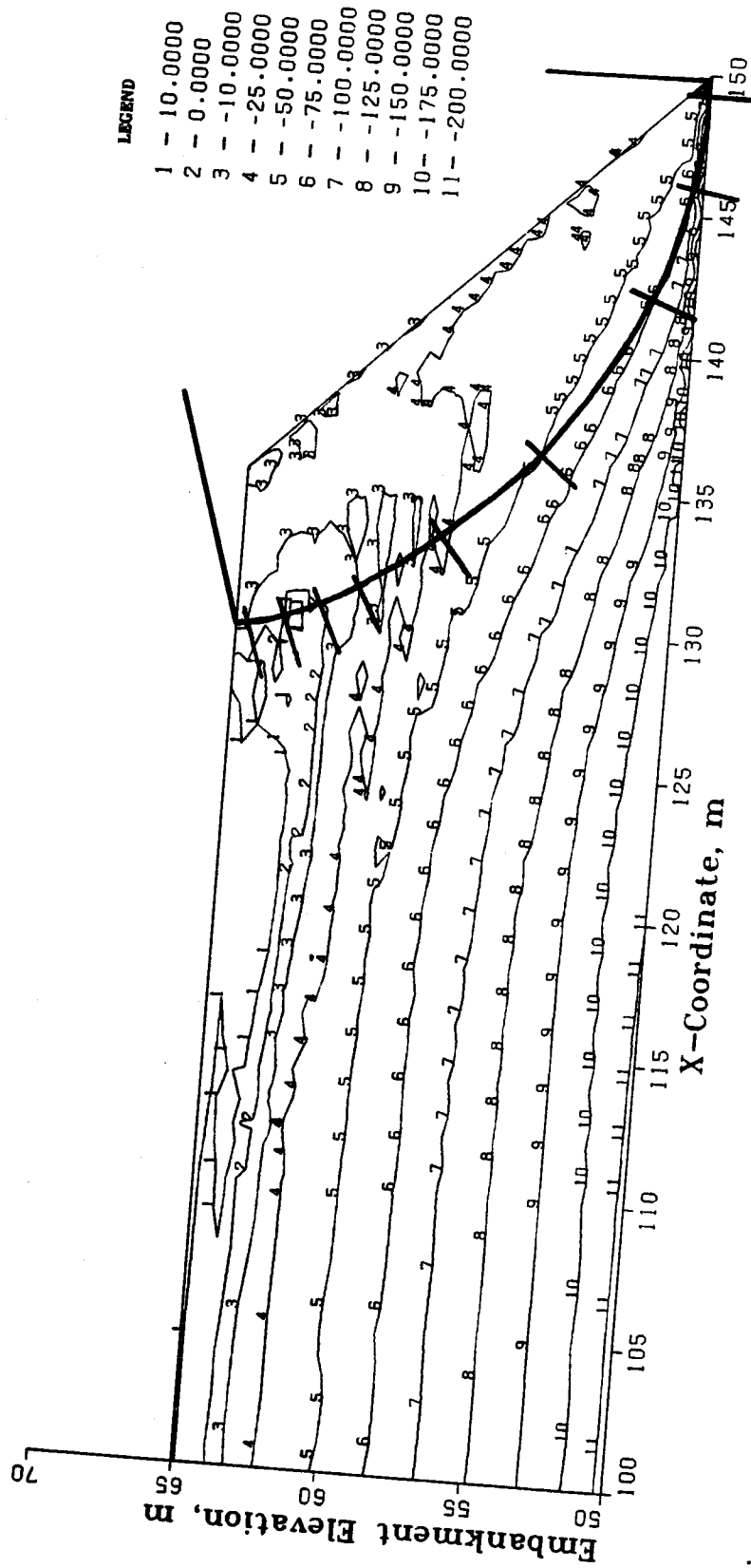


Figure F.1 Horizontal Stress,  $\sigma_x$  (kPa), Contours Within the Nonreinforced Embankment, H = 15 m

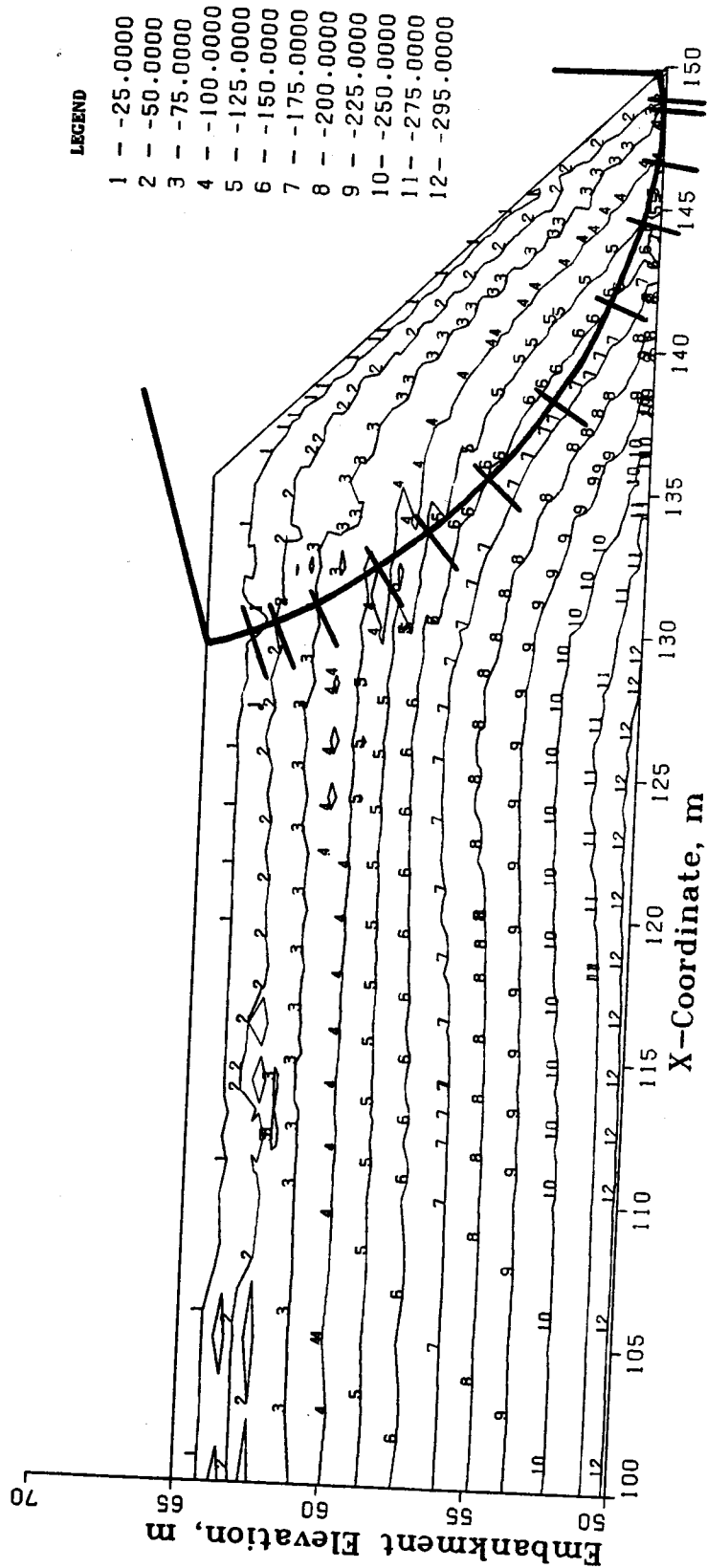


Figure F.2 Vertical Stress,  $\sigma_y$  (kPa), Contours Within the Nonreinforced Embankment,  $H = 15$  m

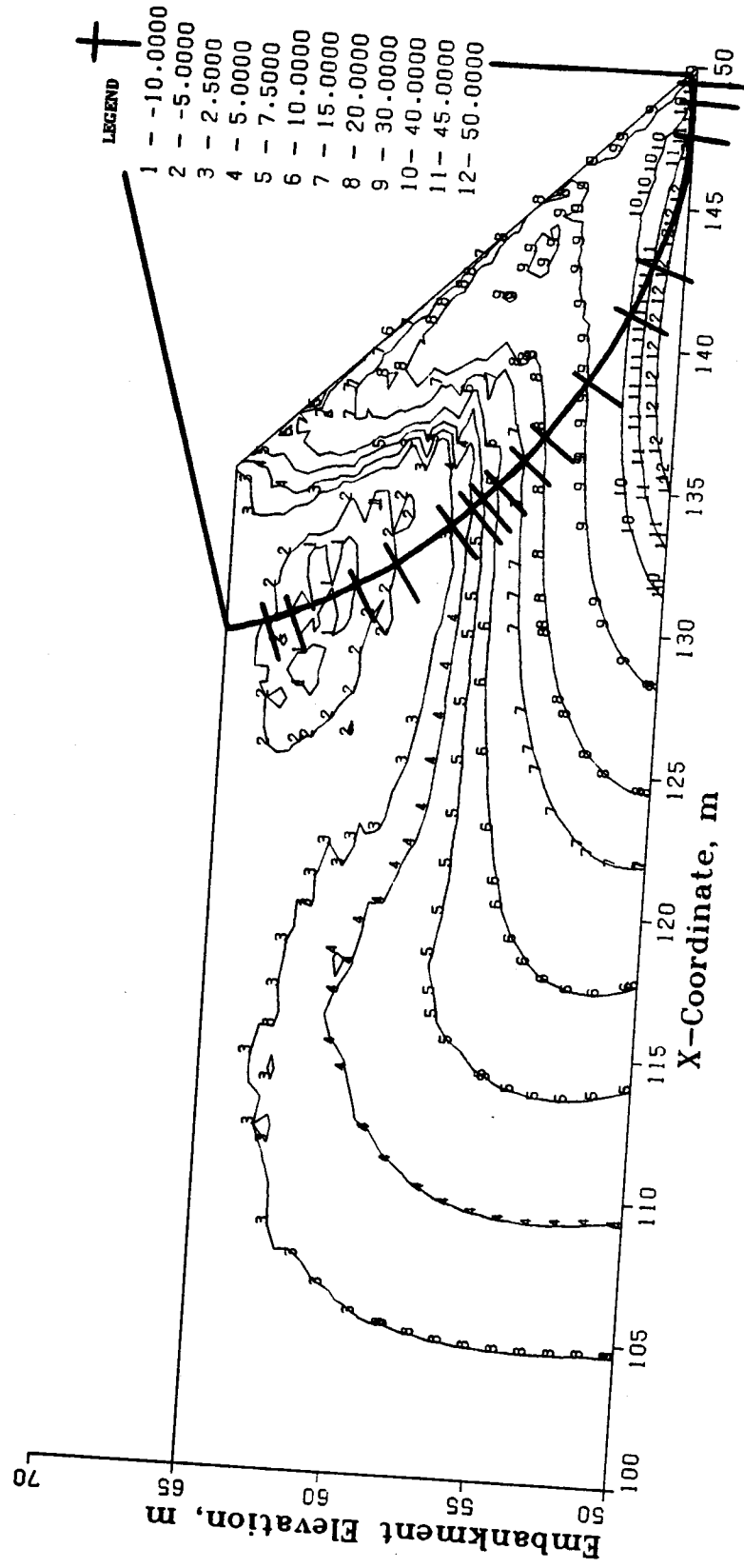


Figure F.3 Shear Stress,  $\tau_{xy}$  (kPa), Contours Within the Nonreinforced Embankment,  $H = 15$  m

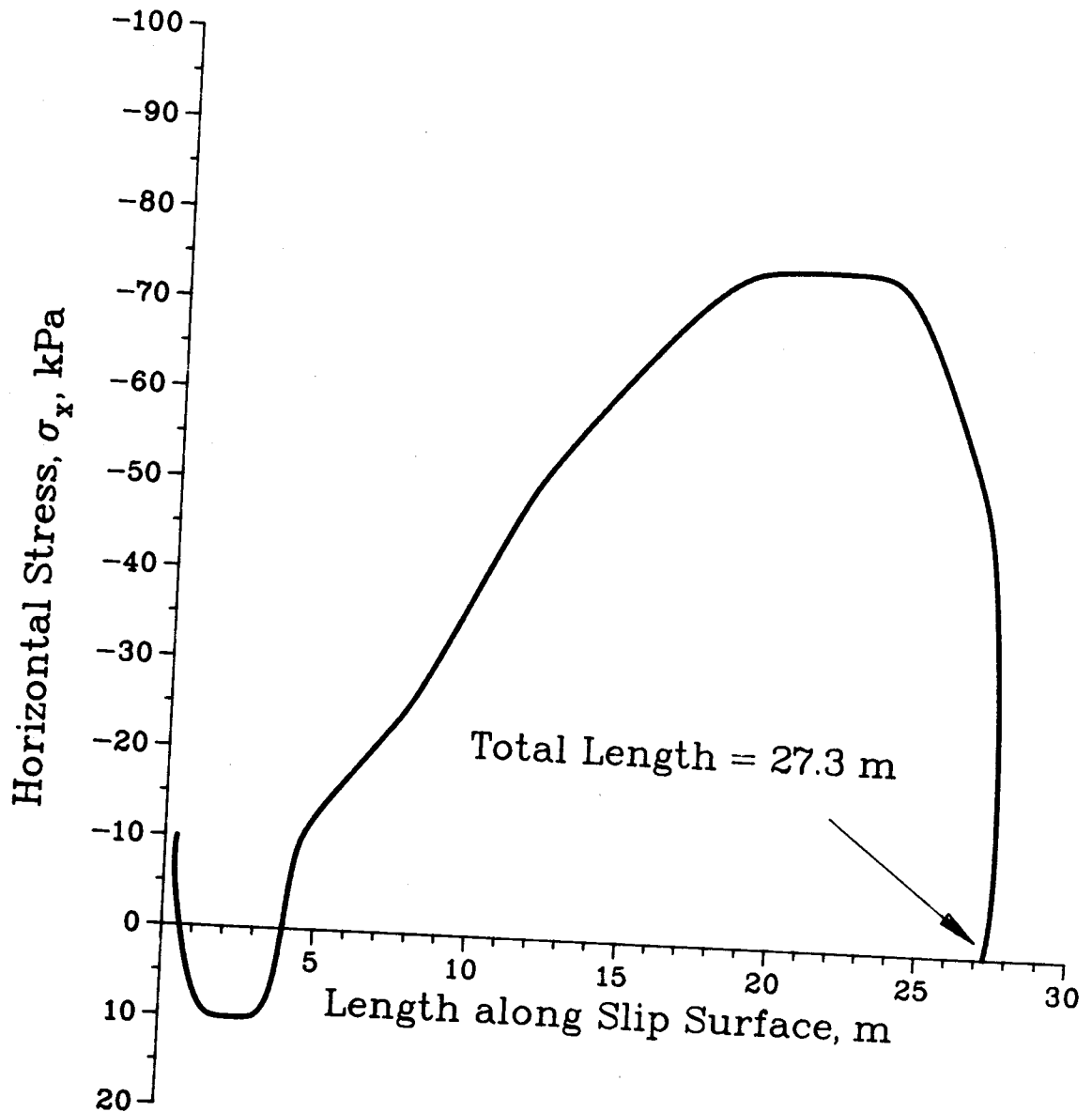


Figure F.4 Horizontal Stress,  $\sigma_x$  (kPa), Distribution Along the Slip Surface in Nonreinforced Embankment,  $H = 15$  m

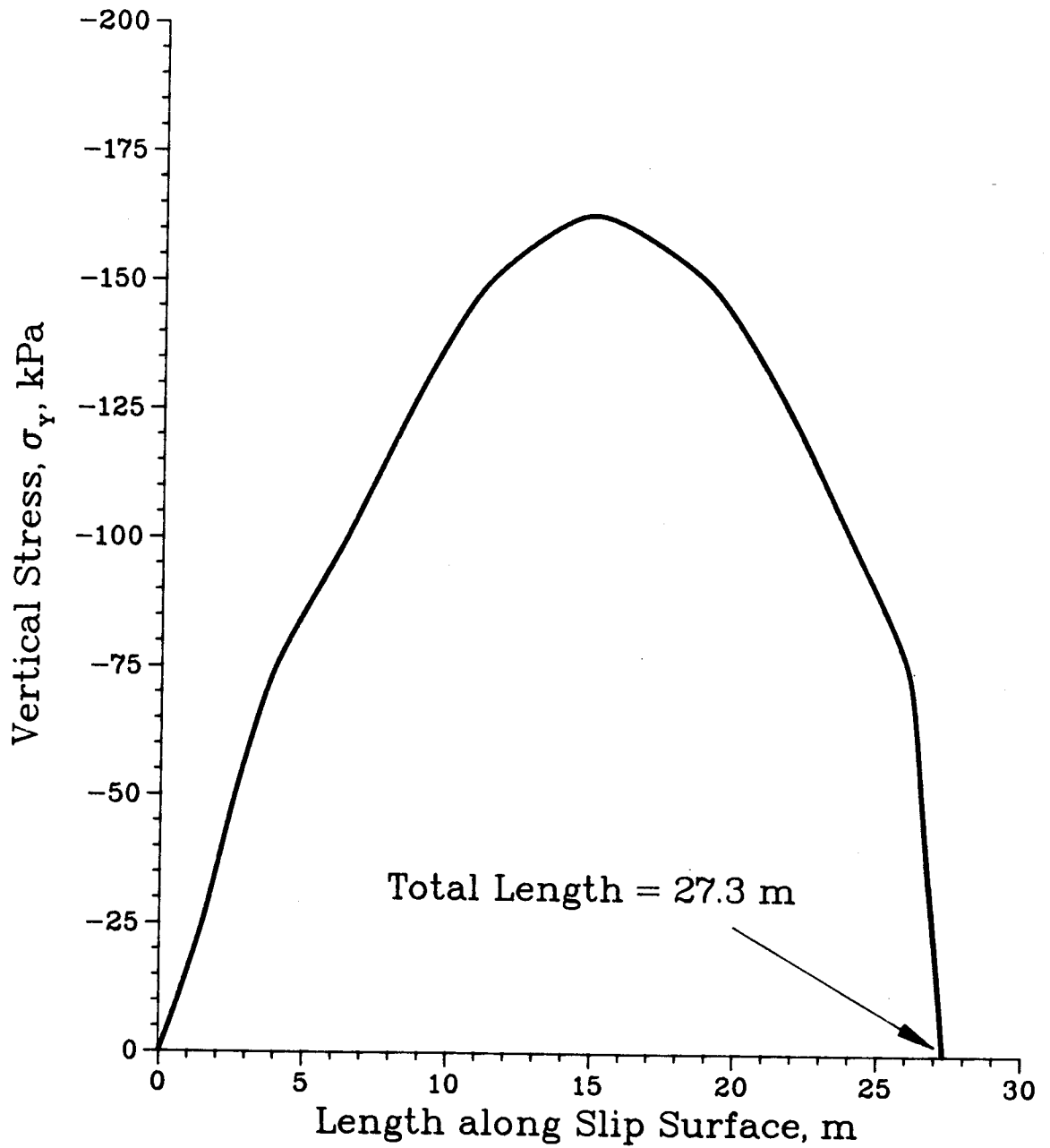


Figure F.5 Vertical Stress,  $\sigma_y$  (kPa), Distribution Along Slip Surface in Nonreinforced Embankment, H = 15 m

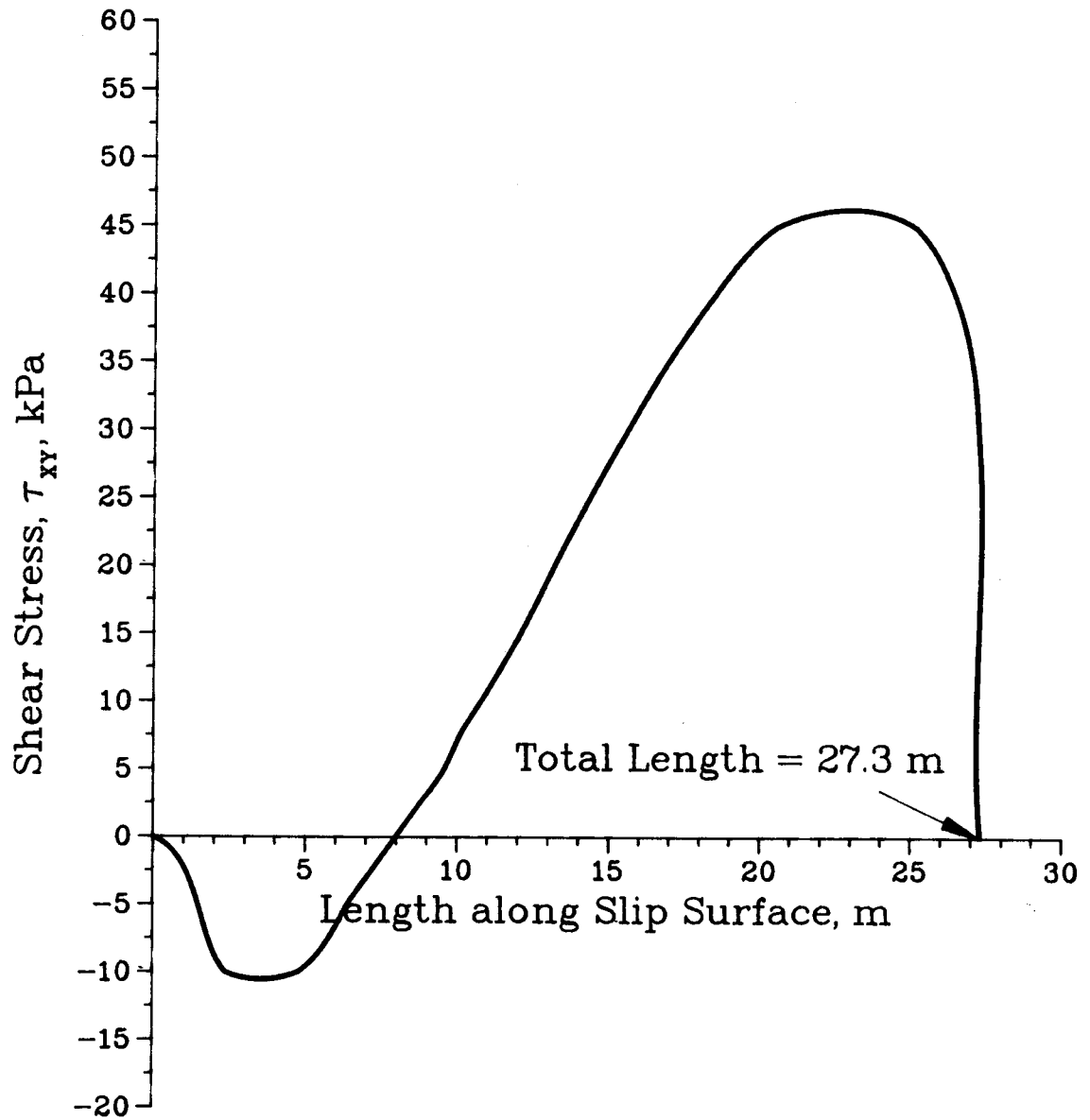


Figure F.6 Shear Stress,  $\tau_{xy}$  (kPa), Distribution Along Slip Surface in Nonreinforced Embankment,  $H = 15$  m

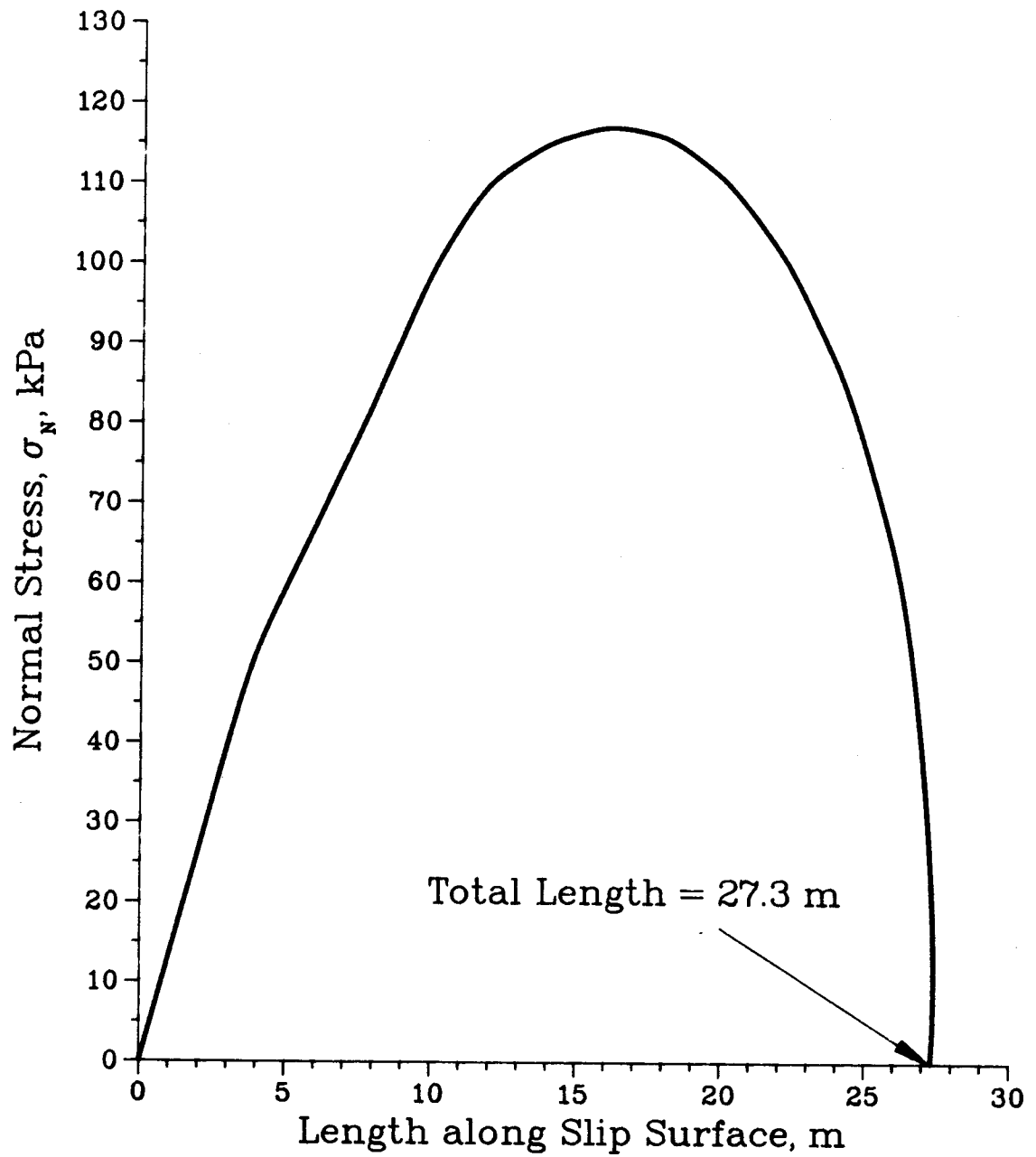


Figure F.7 Normal Stress,  $\sigma_n$  (kPa), Distribution Along Slip Surface in Nonreinforced Embankment, H = 15 m



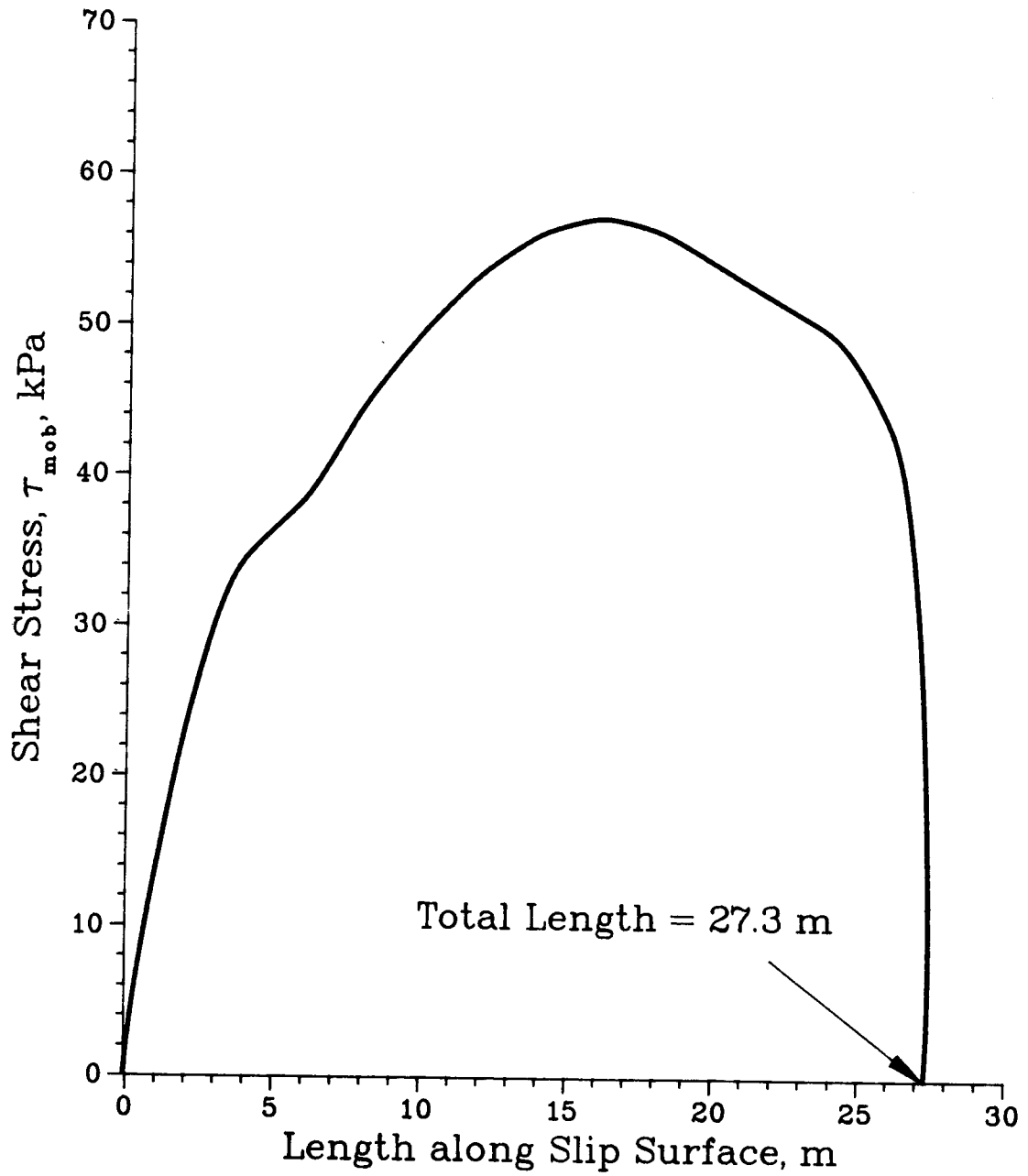


Figure F.8 Mobilized Shear Stress,  $\tau$  (kPa), Distribution Along Slip Surface in Nonreinforced Embankment,  $H = 15$  m

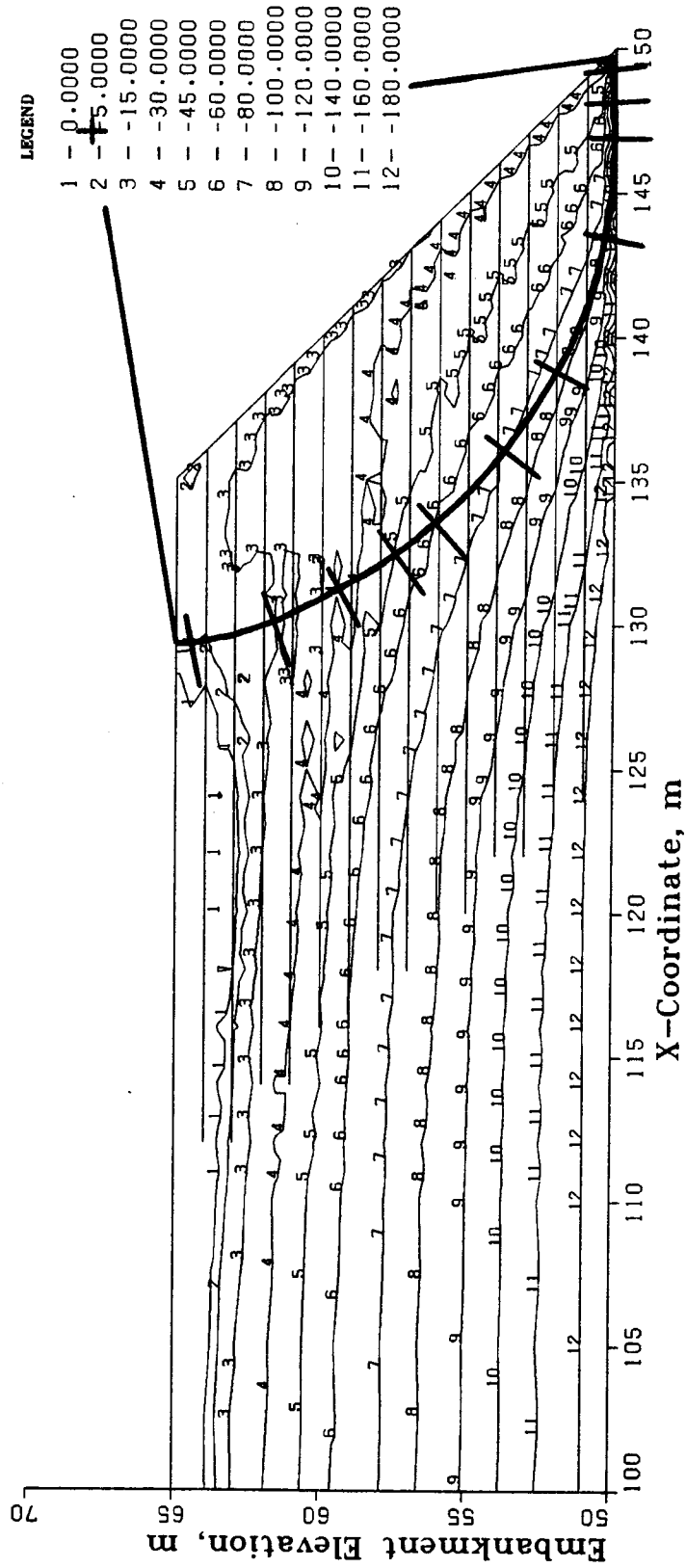


Figure F.9 Horizontal Stress,  $\sigma_x$  (kPa), Contours Within the Reinforced Embankment,  $H = 15$

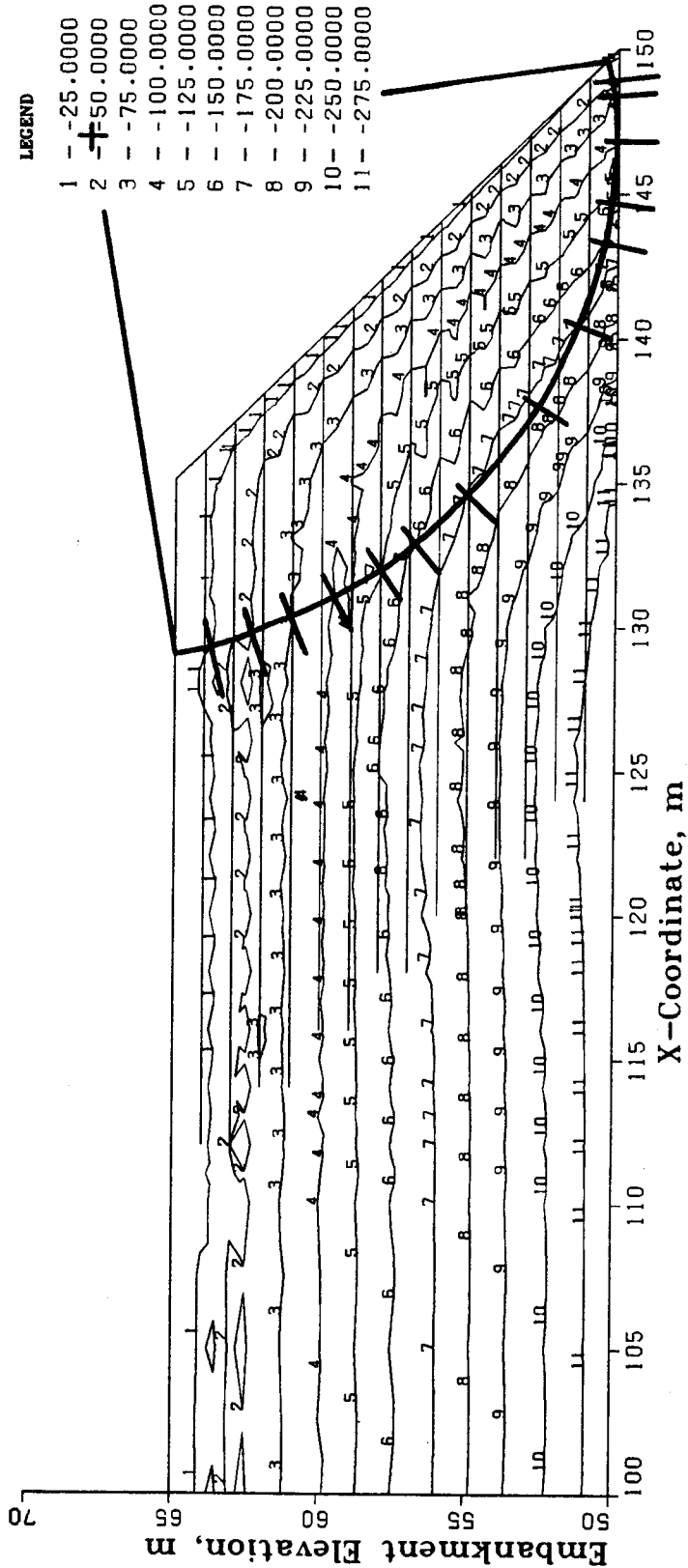


Figure F.10 Vertical Stress,  $\sigma_y$  (kPa), Contours Within the Reinforced Embankment,  $H = 15$  m

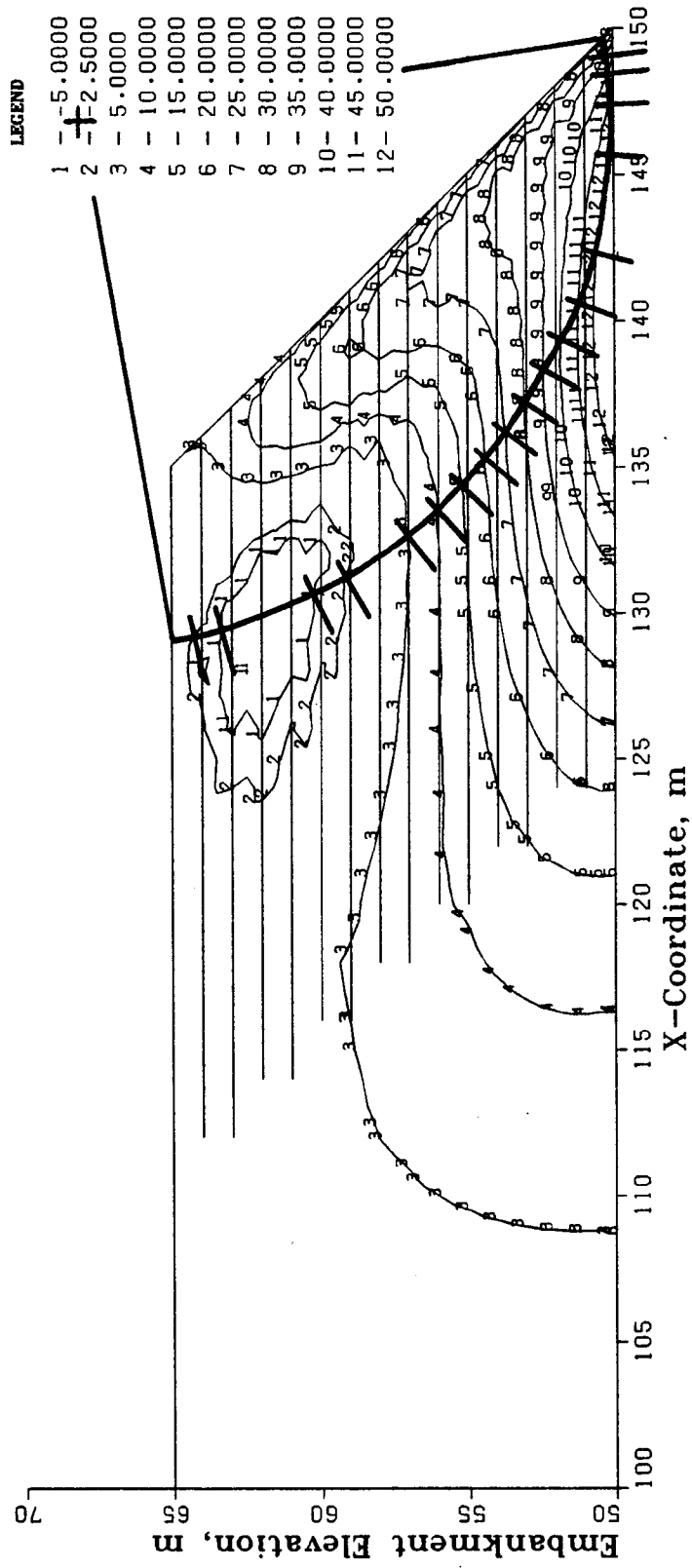


Figure F.11 Shear Stress,  $\tau_{xy}$  (kPa), Contours Within the Reinforced Embankment,  $H = 15$  m

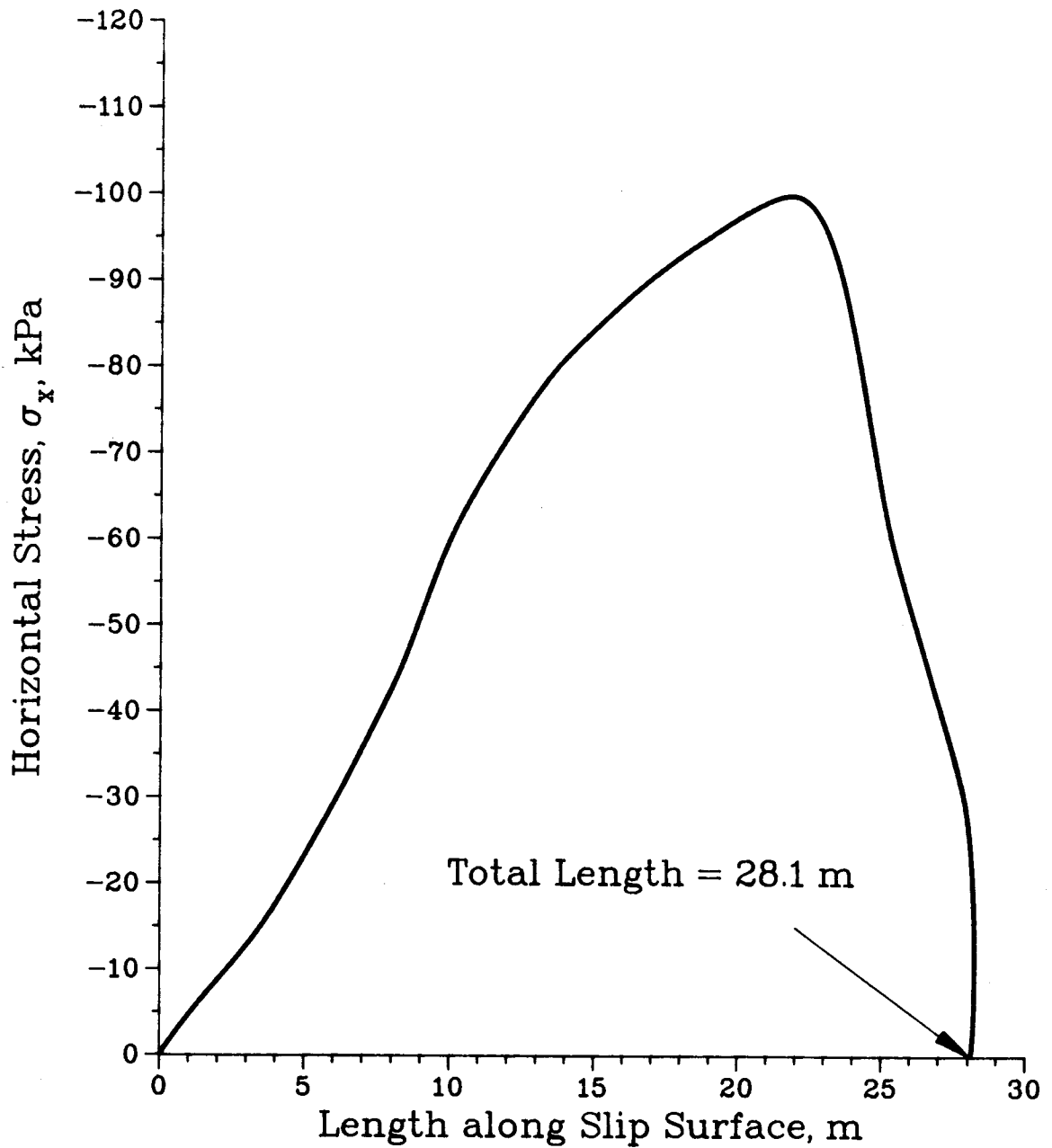


Figure F.12 Horizontal Stress,  $\sigma_x$  (kPa), Distribution Along the Slip Surface in Reinforced Embankment, H = 15 m

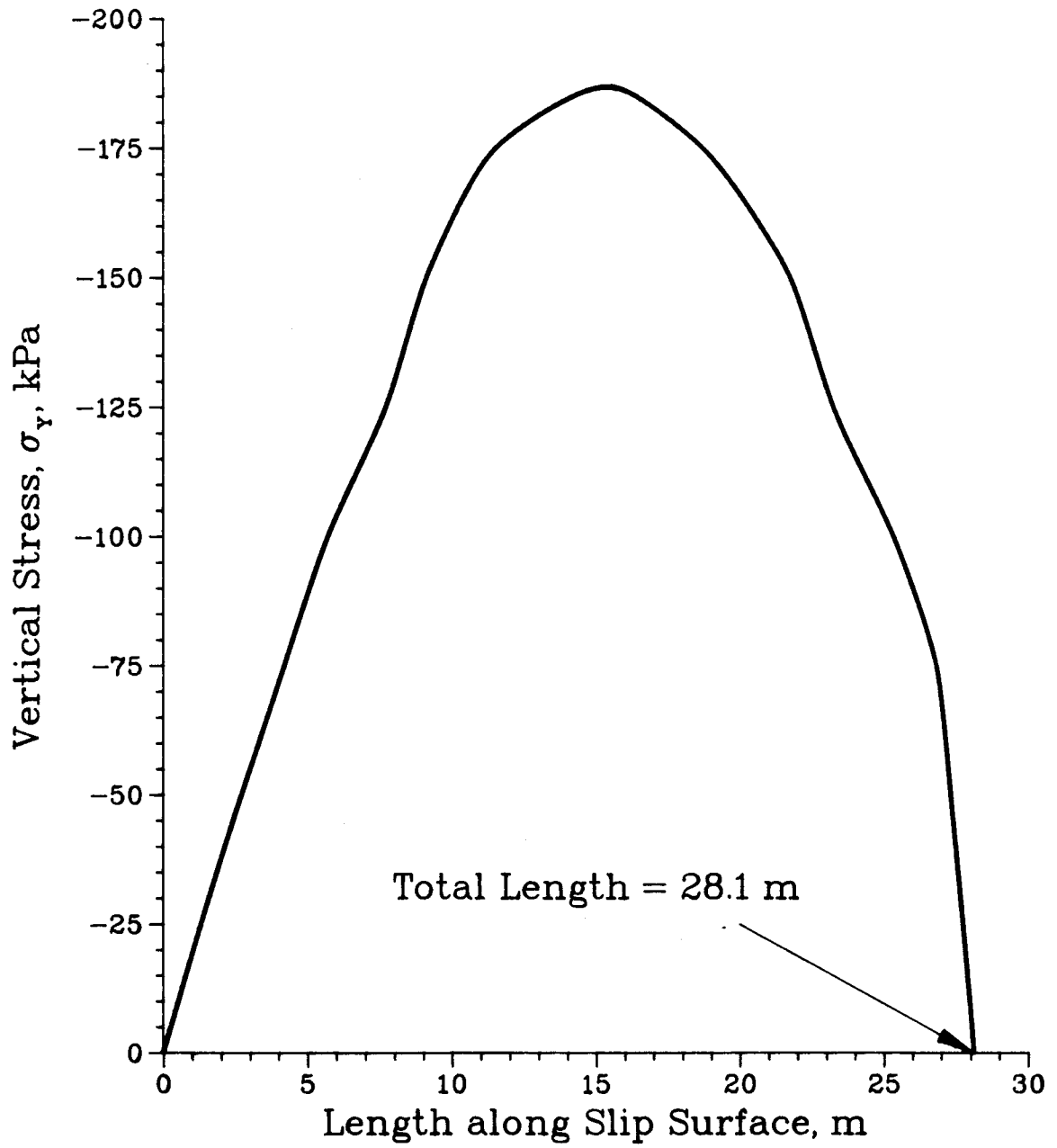


Figure F.13 Vertical Stress,  $\sigma_y$  (kPa), Distribution Along Slip Surface in Reinforced Embankment, H = 15 m

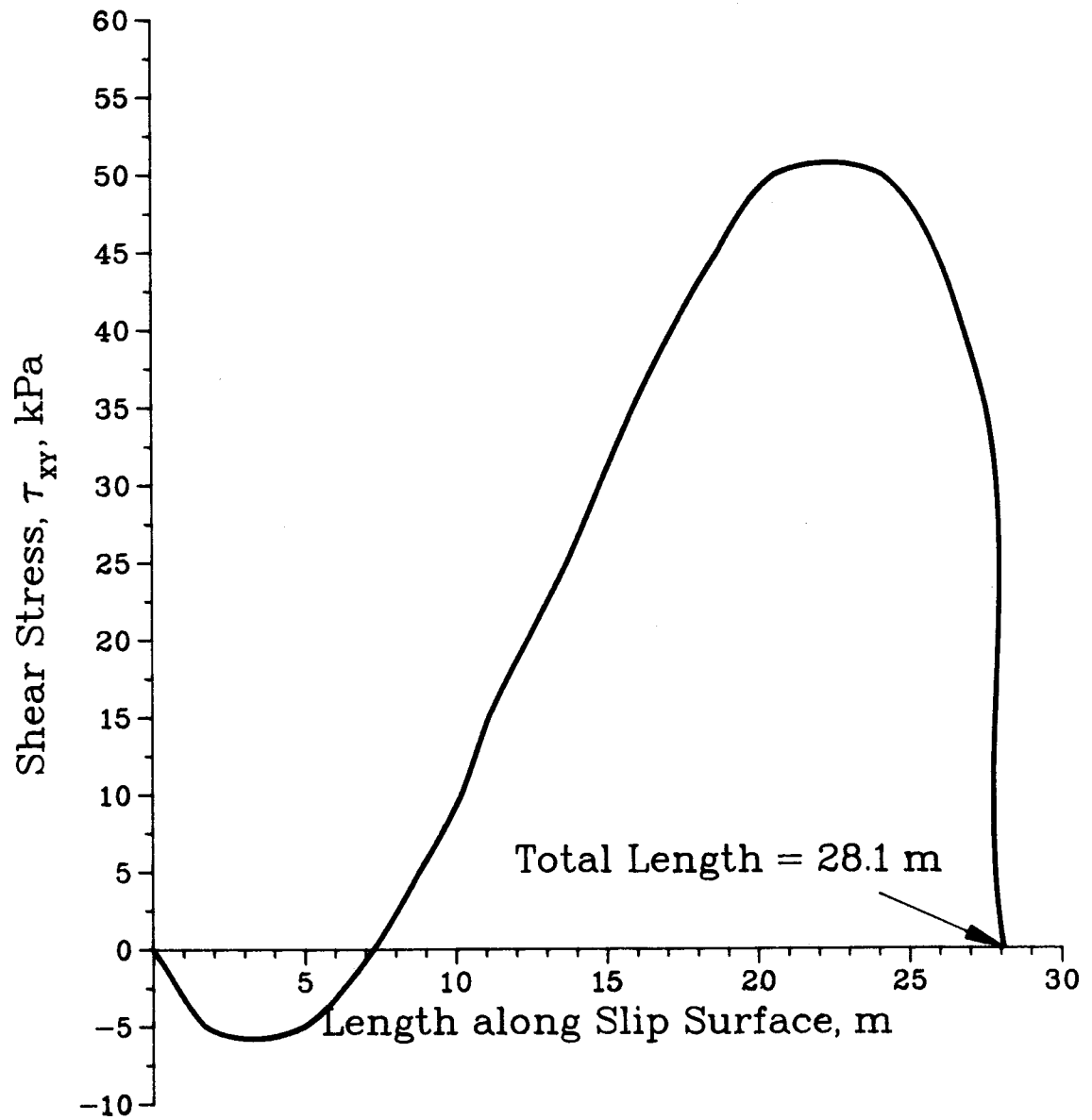


Figure F.14 Shear Stress,  $\tau_{xy}$  (kPa), Distribution Along Slip Surface in Reinforced Embankment, H = 15 m

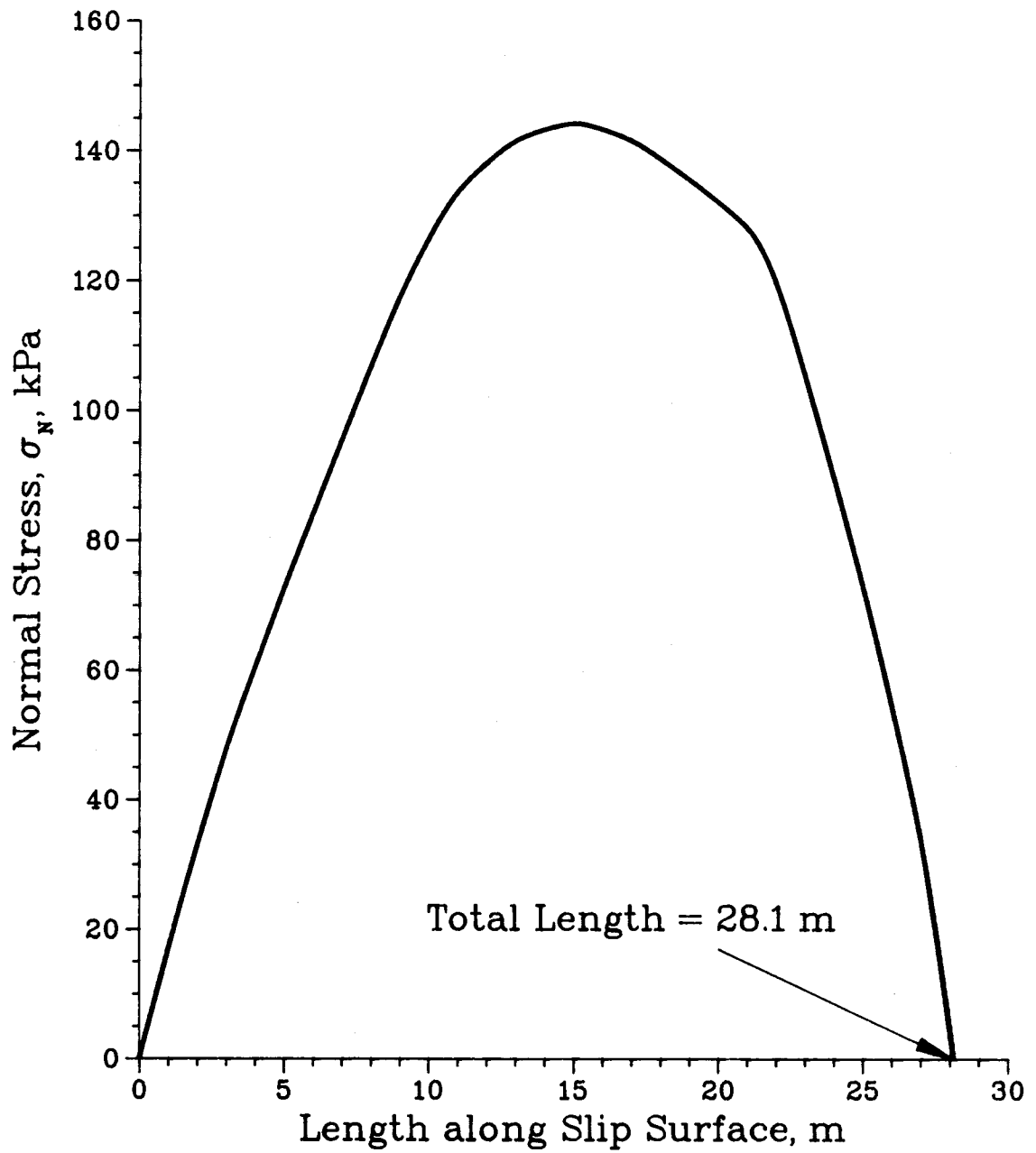


Figure F.15 Normal Stress,  $\sigma_n$  (kPa), Distribution Along Slip Surface in Reinforced Embankment, H = 15 m



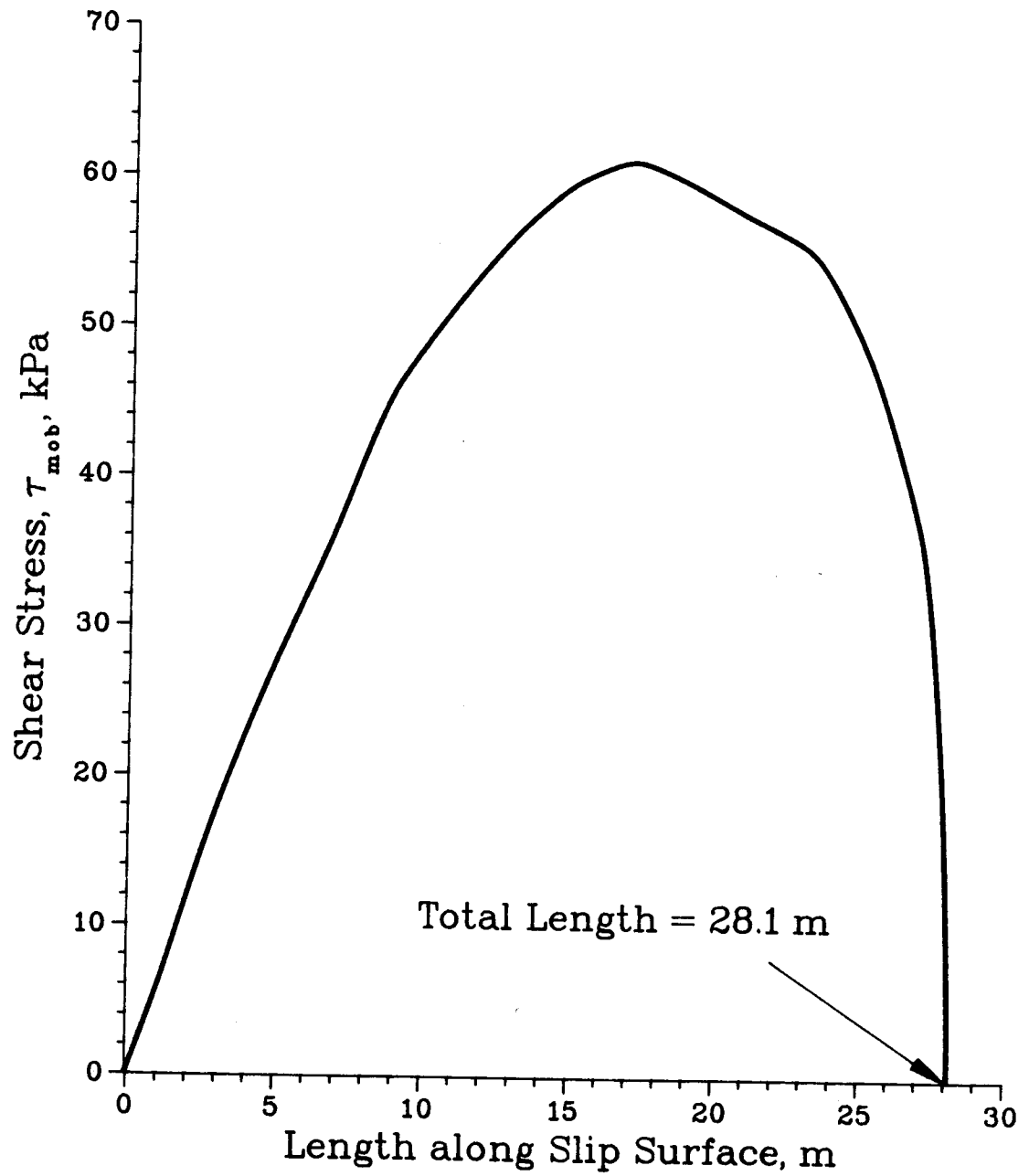


Figure F.16 Mobilized Shear Stress,  $\tau$  (kPa), Distribution Along Slip Surface in Reinforced Embankment,  $H = 15$  m